2020

Development of flexible, durable and ionic materials based on poly(acrylamide) hydrogels for soft conducting and sensing applications

Khalid Waleed Younus Zainulabdeen Zainulabdeen
University of Wollongong

UNIVERSITY
OF WOLLONGONG
AUSTRALIA

Development of flexible, durable and ionic materials based on poly(acrylamide) hydrogels for soft conducting and sensing applications

Khalid Waleed Younus Zainulabdeen

Supervisors:

Prof. Marc in het Panhuis

Dr Holly Warren

This thesis is presented as part of the requirement for the conferral of the degree:

Doctor of Philosophy (Ph.D.) in chemistry and molecular bioscience

The University of Wollongong

School of Chemistry and Molecular Bioscience

February 2020

Certification

I, Khalid Waleed Younus Zainulabdeen, declare that this thesis submitted in fulfilment of the requirements for the conferral of the degree PhD in chemistry and molecular bioscience, from the University of Wollongong, is wholly my own work unless otherwise referenced or acknowledged. This document has not been submitted for qualifications at any other academic institution.

Khalid W. Y. Zainulabdeen

7th February 2020

Acknowledgments

I would like to take this opportunity to thank my principal supervisor Prof. Marc in het Panhuis, for his guidance throughout the project. Working under him was a knowledgeable experience for me. Moreover, I would like to give my thanks to my co-supervisor Dr Holly Warren for her advisements and her theoretical and experimental support in this thesis.

Furthermore, I would express my appreciation to Keith Gregory for proofreading chapter 1 and 10 and I would like to give my sincere thanks to the PhD student Alex Keller for his support in proofreading chapter 5, 6 and 7 and for his valued assistance at the hard time during my PhD study. Moreover, I would like to thank my other peers Dr Ali Al-Nasrawi and Dr Reece Gateley who helped me to solve some technical issues during my project. Besides, I would like to express my deep gratitude to Prof. Jenny Beck and Prof. Paul Keller for their patience, continuous and unlimited encouregement and support to achieve this success. In addtion, I would like to introduce my sincere thanks to Christopher Richardson, Will Price, Monica Birrento; Catherine Brown and Todd Mitchell for their help and main role to make my thesis meet the high standareds. Moreover, I want to express my gratitude, respect and love to my wife and my three kids for their patience and support during my PhD study period. Also, I would like to express my deep gratitude to my parent who are always prayed for me continuously to meet them again with my PhD degree. Last but not least, I would like to give my thanks to the Higher Committee of Education and Development in Iraq for supporting me with this scholarship to study at prestigious Australian university such as the University of Wollongong. Finally, I would gratitude the University of Wollongong for providing all the type of support for the HDR students to facilitate all the challenges that might face the students.

Table of contents

List of Names or Abbreviations

μ Micro

AS After saturation

AAm Acrylamide

AP Ammonium persulphate

CAD Computer Aided Design

DN Double network

Eq. Equation

G′ Storage modulus

G″ Loss modulus

GPRS General Packet Radio Service

GPS Global Positioning System

g Gram

HEH Hydrogel-elastomer hybrid

ICE Network Ionic covalent entanglement network

IPN Interpenetrating Polymer Network

J Joule

kJ Kilojoule

kPa kilopascal

KPS Potassium persulfate

L Liter

LVE Linear viscoelastic region

M Molar

MBAAm N, N’, Methylene bisacrylamide

mg Milligram

mL Milliliter

PAAm Poly(acrylamide)

Pa Pascal

PDMS Polydimethylsiloxane

PEDOT Poly(3,4-ethylenedioxythiophene)

rGO Reduced graphene oxide

RT Room temperature

RVC Reticulated vitreous carbon

SDS Soft sensor device

TEMED N,N,N’,N’-Tetramethylethylenediamine

UV Ultra Violet

VHB Very high bonding tape

Abstract

Soft ionic hydrogels have garnered significant interest for their applications in soft electronics and tissue engineering. However, further demands are still on the rise for developing these materials to possess flexibility, durability, low cost, non-toxic and reliable conductivity. In this work, a poly(acrylamide) (PAAm) hydrogel containing salt was utilised for its significant features such as high flexibility and excellent conductivity. Therefore, several hydrogels were prepared from the polymerisation reaction of the mononer acrylamide (AAm) to produce different polymers networks of PAAm hydrogels by the use of different crosslinking materials and methods aiming to optimise their mechanical and electrical characteristics, with the aim of applying these hydrogels in different applications such as soft sensing and conducting devices.

Ionic-covalent entanglement hydrogels were prepared by mixing cross-linked gellan gum (GG) and $CaCl_2$ ionically with PAAm and methylenbis(acrylamide) (MBAAm) covalently. The mechanical behaviour was modified by altering the ionic and the covalent polymers ratio. The electrical properties were investigated with varying hydrogel ratios which displayed optimised mechanical properties for use in conducting and sensing applications. It was observed that gels prepared with 0.1 M $CaCl_2$ and 1.11 % (w/v) GG with PAAm consisting of 4.44 % (w/v) and AAm with 3 % (w/v) MBAAm exhibited optimum mechanical characteristics reporting 216±12 kPa (compressive stress to failure) for the compression test analysis and 264±5kPa (shear modulus) for the oscillatory rheology demonstration. The electrical conductivity and the water content for the optimised ICE gel displayed a noticeable increase from 3.3±0.5 $mS.cm^{-1}$ to 127±15 $mS.cm^{-1}$ and from 78 % to 85 %, respectively, after it was immersed in 2.7 M NaCl solution.

In a parallel aim of this thesis, PAAm containing 6 M LiCl hydrogel was hybridised with cellulose kitchen sponge using a novel method for producing a soft, cheap, conducting and non-toxic strain gauge. The hybrid form of cellulose sponge/PAAm hydrogel structure was attached to two carbon fiber electrodes on both ends of the hybrid structure sealed by two acrylated very high bonded tape (VHB) layers. The gauge displayed a consistent response over multiple cycles after stretching to 15 % strain recording a gauge factor of 0.38±0.04. The same hydrogel was utilised for fabricating a novel ionic PDMS/PAAm electrode after it was embedded within a PDMS substrate to improve its mechanical characteristics. The mechanical and electrical performances of the PDMS/PAAm electrode were characterised revealing a maximum tensile

stress of 39±3 kPa and a conductivity of 35±1 $mS.cm^{-1}$.

A PAAm containing 9 M LiCl hydrogel was subjected to an in situ UV light source to develop a durable, flexible and soft wearable sensor device (SSD) which could send a SOS signal remotely even after one year of the device at room temperature (RT). This distinctive feature of the hydrogel stimulated investigation of this material in 3D printing technology. Two techniques were tested: the direct-ink writing technique and the hand-held printing technique. The rheological properties of the prepared PAAm containing NaCl and LiCl materials were studied, i.e. starting materials and inks for the potential of 3D fabricating soft electronic devices or soft sensory gauges. The rheological analysis showed that controlled UV-crosslinking while cooling to -6 °C, enabled 3D printing of the PAAm without the need for any additional rheological modifiers. The 3D printed hydrogel materials exhibited conductivity values of 117±13 $mS.cm^{-1}$ for the PAAm with 9 M LiCl and could be stretched up to four times their length. These data, to the best of our knowledge, are considered to be the highest conductivity of any 3D printed hydrogel stretched by this amount currently reported. A second extruding technique was implemented for extruding PAAm containing 4 M LiCl using the hand-helding technique on a VHB tape substrate to fabricated hydrogel-elastomer hybrid (HEH) as a durable soft strain gauge device. The device exhibited a robust interface between the printed hydrogel with an elastomeric matrix using a simple interpenetration polymerisation method. The mechanical and the electrical properties of the HEH devices were examined before and after one year of storage in a plastic Petri-dish at RT (21-23 ^{o}C).

The HEH displayed near identical mechanical behaviour after one year of storage. It was shown that the HEH devices were able to be stretched up to 215 % repeatedly with no issue both initially and after one year of storage. The gauge factor for the HEH was determined and compared to the as-prepared device before and after one year of examination giving a sensitivity of 0.7±0.1 and 0.74±0.01, respectively.

Furthermore, the sensing investigations revealed stable R/Ro data after 1000 cycles of stretching during finger bending, giving a change ratio of 1.3±0.1. It was observed that the R/Ro difference for both periods, before and after one year of storing, was only 0.05.

Finally, a conducting soft, durable bridge was fabricated from PAAm containing CsCl for developing spontaneous bifunctional oxygen and hydrogen evolution by composite poly(3,4-ethylenedioxythiophene) (PEDOT)/nano-Ni/reduced graphene oxide (rGO) films. This study demonstrated that PAAm containing CsCl hydrogel could be an effective salt bridge device for water splitting applications for at least fourteen hours of operation which is considered to be the longest time of an operating water splitting system using

soft conducting stretchable hydrogel currently reported.

This project demonstrates the potential that PAAm hydrogel containing various salts are a promising material for the fabrication of devices that are non-toxic, low cost, possess excellent mechanical performance, electrical conductivity and long-life durability. These characteristics make ionic PAAm hydrogels a remarkable candidate for use in different technologies such as 3D printing technique and other fabrication methods for developing a wide range of both soft conducting and sensing applications.

List of Figures

List of tables

Overview of chapters

Chapter 1: A general introduction.

This introduction is a general overview of all current hydrogels, preparations, theoretical measurements, characterisations and application of soft conducting and sensing devices.

Chapter 2: Experimental techniques.

This chapter is an overview of all the procedures, instruments and the techniques that were used in this thesis.

Chapter 3: Electrical investigations for optimised mechanical properties of ionic-covalent entanglements hydrogels.

This chapter describes the characterisation of the electrical properties of the optimised mechanical properties of ionic-covalent entanglements hydrogels.

Chapter 4: Preparation, characterisation and 3D printing of ionic PAAm hydrogels.

This chapter is based on the following published manuscript:

Khalid Zainulabdeen, Marc in het Panhuis, and Holly Warren, "Preparation, Characterisation and 3D Printing of Ionic Poly(acrylamide) Hydrogels", Proceedings of the first MoHESR and HCED Iraqi Scholars Conference in Australasia, 2017, Melbourne, *https://researchbank.swinburne.edu.au/file/b083d58b-327d-464f-906e-57530405c7c5/1/proceedings_ISCA2017.pdf*

This chapter describes preparations of hydrogels consisting of PAAm containing either NaCl or LiCl using different concentrations. The water content stability, mechanical and electrical performances were characterised. Furthermore, three hydrogels were selected for their excellent properties, and 3D printed using specific experimental technique after examining their rheological characteristics. The electrical and the mechanical performance for the printed hydrogels were characterised and compared to the casted one.

Chapter 5: Wearable remote soft sensor device development from ionic PAAm hydrogel.

This chapter is based on an oral presentation contribution at the International Conference on Emerging Advanced Nanomaterials (ICEAN), Newcastle from 30th of October to 2nd of November 2018.

https://www.newcastle.edu.au/research-and-innovation/centre/gican/icean-2018.

Khalid Zainulabdeen, Ali Al-Nasrawi, Marc in het Panhuis, and Holly Warren, "Wearable remote soft

sensor device development from ionic poly(acrylamide) hydrogel".

This chapter including innovating and operating a soft sensor device (SSD). The mechanical and the electrical performance were examined after applying multiple cycles of compression stress before and after one year of the initial examination. Furthermore, the SSD was connected to an Arduino device to supply a power current from either a Li battery or a solar cell power bank to send a Bluetooth signal to a mobile phone which had a specific application called 'UOW data sender'. This application sends two types of information to the database including coordination and text message help to another mobile phone (relative to the SSD holder or service centre) to receive this information.

I declare that my role in this project was finding the concept of the project, preparing the hydrogel, fabricating the SSD, operating the SSD, connecting the SSD to an Arduino device with all the SSD characterisations and analysis (mechanical and electrical), all the figures, designing and 3D printing the Arduino container box and writing the details of these processes. However, the mobile application set, the communications between the database and the mobile phone application experiment and writing the details of these steps were performed by Ali-Al-Nasrawi.

Chapter 6: Handheld printing of soft, stretchable conductive component for a strain gauge device.

This project describes fabricating a durable soft strain gauge device as we called HEH composed of a printed soft, stretchable conductive hydrogel. The device was produced by extruding an ionic AAm ink solution over a VHB tape substrate and then cured using UV light to initiate the photopolymerisation reaction. The mechanical and the electrical performance were carried out while applying multiple cycles of the tensile test before and after one year of the initial assessment. Furthermore, the resistance sensitivity for the HEH over a finger bending was examined and compared after one year of the initial characterisation.

Chapter 7: Preparation, characterisation and application of cellulose sponge-PAAm material as a strain sensing element.

This work describes producing a non-toxic strain gauge device from ionic PAAm/cellulose sponge hybrid electrode sealed by two VHB tape layers using a novel method. The mechanical and the electrical characteristics, as well as water content study, were examined for all the device components. Furthermore, the resistance sensitivity for the fabricated device was conducted after applying tensile test analysis.

Chapter 8: Designed conducting polymer composites that facilitate long-lived, light-driven Oxygen and Hydrogen evolution from water in a photoelectrochemical concentration cell (PECC)

This chapter has been adapted from the manuscript "Designed conducting polymer composites that facilitate long-lived, light-driven Oxygen and Hydrogen evolution from water in a photoelectrochemical concentration cell (PECC)" which is published by the Journal of Composite Science and I was listed as a second author for this manuscript as shown in the following link: https://www.mdpi.com/2504-477X/3/4/108/htm

The participants' names of this manuscript, were:

Mohammed Alsultan, Khalid Zainulabdeen, Pawel Wagner, Gerhard F. Swiegers and Holly Warren.

(Published December 2019).

This project demonstrates a novel, mechanically durable, highly electrically conductive, and flexible PAAm containing CsCl hydrogel. The water content stability, mechanical and electrical assessments were established and the anionic and soft bridge was produced using the same hydrogel. The fabricated hydrogel was applied as a separator for two water splitting half-cells (cathode and anode). The cells split water upon connection with the hydrogel for up to fourteen hours of continuous operation.

I declare that my role in this project was preparing the PAAm containing CsCl hydrogel and characterising its mechanical properties such as compression and tensile test analysis. The hydrogel water content study was also investigated over two weeks. Furthermore, the electrical studies were carried out for the prepared hydrogel bridge before and after use. Finally, all data, figures from 8.2-8.5 and tables from 8.1-8.3 of the hydrogel studies were analysed, discussed and written after these characterisations. Otherwise, all the other experiments related to the electrocatalytic and photoelectrocatalytic study in Appendix 2 section, the figures (8.1, a2.1, a2.2. a2.3) were prepared, analysed, discussed and written by author Mohammed Alsultan.

Chapter 9: Development of reinforced polyacrylamide electrodes with customizable mechanical properties

The participants' names of this chapter were: Alex Keller, Khalid Zainulabdeen, Holly Warren, Marc in het Panhuis.

This chapter describes fabricating an electrode using an optimised PDMS sponge with $CaCl_2$ after assessing the different salts (NaCl, LiCl, $CaCl_2$) and sugars (white and brown) removal efficiency and mechanical

properties. PDMS/PAAm containing 6 M LiCl hydrogel electrode was produced. The mechanical and electrical properties were investigated and displayed significant values.

My role in this project was collaborating in the PDMS sponge fabrication after fabricating sacrificial templates from different salts and sugars such as NaCl, LiCl, $CaCl_2$, white and brown sugar, respectively based on observations made by Alex Keller. I analysed the mechanical properties via tensile testing of the different PDMS sponges after removal of the templates by water as shown in table 9.1 and figure 9.1. Lastly, I constructed the PDMS/PAAm electrodes as shown in figure 9.2 A and B. The mechanical and electrical characterisations of the PDMS sponges after embedding PAAm containing 6 M LiCl hydrogel sealed by VHB tape were also assessed and analysed as shown in table 9.2. The porosity sizes data of the PDMS sponges were collected using an optical microscope as shown in table 9.1.

Alex Keller contributed to the PDMS sponge preparation after adding different fillers. He analysed the porosity size data as shown in table 9.1.

Figures contribution in chapter 9:

Figures prepared by Khalid Zainulabdeen in this chapter: Figures 9.1 A experiment and 9.1 B experiment and data analysis and 9.2 A and B experiment and pictures and 9.3 experiment and analysis.

Figures prepared by Alex Keller in this chapter: Figures 9.2 A analysis.

Tables' contribution in chapter 9:

Tables prepared by Khalid Zainulabdeen in this chapter: Tables 9.1 mechanical tensile parameters experiment and analysis and pore size study experiment, 9.2 mechanical tensile parameters analysis and experiment and conductivity analysis and experiment of PAAm/PDMS electrode.

Tables prepared by Alex Keller in this chapter: Tables 9.1 pore size analysis.

Chapter 10:

This chapter describes the conclusions of each chapter in this thesis as well as the future directions.

List of Publications and Presentations

- **Chapter 4: Preparation, characterisation and 3D printing of ionic PAAm hydrogels.**

  This chapter is based on the following published manuscript:

  Khalid Zainulabdeen, Marc in het Panhuis, and Holly Warren, "Preparation, Characterisation and 3D Printing of Ionic Poly(acrylamide) Hydrogels", Proceedings of the First MOHESR and HCED Iraqi Scholars Conference in Australasia, 2017, Melbourne, *https://researchbank.swinburne.edu.au/file/b083d58b-327d-464f-906e-57530405c7c5/1/proceedings_ISCA2017.pdf*

- **Chapter 5: Wearable remote soft sensor device development from ionic PAAm hydrogel.**

  This chapter is based on an oral presentation contribution at the International Conference on Emerging Advanced Nanomaterials (ICEAN), Newcastle from 30th of October to 2nd of November 2018.

  https://www.newcastle.edu.au/research-and-innovation/centre/gican/icean-2018

  Khalid Zainulabdeen, Ali Al-Nasrawi, Marc in het Panhuis, and Holly Warren, "Wearable remote soft sensor device development from ionic poly(acrylamide) hydrogel".

- **Chapter 8: Designed conducting polymer composites that facilitate long-lived, light-driven Oxygen and Hydrogen evolution from water in a photoelectrochemical concentration cell (PECC).**

  This chapter has been adapted from the manuscript "Designed conducting polymer composites that facilitate long-lived, light-driven Oxygen and Hydrogen evolution from water in a photoelectrochemical concentration cell (PECC)" which is published by the journal of Composite science and I was listed as a second author for this manuscript as shown in the following link: https://www.mdpi.com/2504-477X/3/4/108/htm

  The participants' names of this manuscript, were:

  Mohammed Alsultan, Khalid Zainulabdeen, Pawel Wagner, Gerhard F. Swiegers and Holly Warren.

  (Published December 2019).

Chapter 1

Introduction

Critical overview

This chapter provides an outline of the preparation of different types of hydrogel and highlights their mechanical and electrical characteristics in order to demonstrate their possible use in several applications such as soft conducting devices, tissue engineering, 3D printing, sensor devices and soft robotics.

The recent advances in smart soft materials have led to wide popularity in the use of soft materials in robotics, which have advanced remarkably in the last half-century and recently allowing very strong, fast, reliable, and accurately controlling robot motion. Together these have progressed the development of soft, flexible, durable, and conductor materials based on PAAm containing salt hydrogels for promising soft conducting and sensing applications.

1.1 History of Hydrogels

Hydrogels have acquired a considerable reputation in the last few decades. Their exceptional properties are considered to be promising in a broad range of applications which has led to innovative designs and new materials that have revolutionised this field. [1, 2] Hydrogels have been utilised in many biomedical applications; in medicine as eyes lenses, and stitches, as well as in a plethora of different areas of clinical treatment, i.e. heart disease, diabetes mellitus, and osteoporosis. In the 1950s Prof. Wichterle and Lim of Prague, [3] synthesised the first hydrogel with the possibility of biomedical use. This was poly-2-hydroxyethyl methacrylate, and was quickly exploited with the first use in contact lenses. [3-7] The main characteristic of this inventive biopolymer compound was its tolerance to changing pH and temperature. Three decades later, hydrogels were produced for other new applications: Lim and Sun created calcium alginate micromolecules for engineering biological cell, [8] and the Yannas' group developed hydrogels with other non-toxic materials, i.e. collagen and cartilage extracted from sharks, to produce novel bandages presenting the best burns treatment at that time. [9] Today, hydrogels continue to impress with the latest hydrogel products utilised in advanced applications, for example in tissue engineering and regeneration, where they are monitored as a result of their non-invasive behaviour, especially in the treatment of cartilage. They can also be used in the prevention of post-surgery formation drugs delivery, biosensors coatings, and transplanting biological cells. [8-11]

Hydrogels are materials that are characterised by their softness and wetness. They consist of cross-linked polymers that are hydrophilic and capable to accommodate large volumes of water. [12, 13] In a typical hydrogel, the quantity of absorbed water is not less than 20 % of the total weight of the hydrogel. However,

if the absorbance percentage increases beyond 95 % of the entire hydrogel weight, then the hydrogel is classified as a super-absorbent hydrogel. [14-18] Figure 1.1 shows a typical picture of a hydrogel.

Figure 1.1 A picture of a typical synthetic hydrogel. Photo produced by the candidate.

One of the most significant features of a hydrogel is its swelling behavior. This depends on factors such as the nature of the polymer chain (i.e. hydrophilic or hydrophobic), as well as the density of entanglements within the polymer network. [19, 20] The swelling ratio Q is calculated using equation 1.1:

$$\mathbf{Q = (W_s - W_d) / W_d} \quad \textbf{(Eq. 1.1),}$$

Where Ws is the swollen hydrogel weight, and W_d is the dry hydrogel weight. [21] Hydrogel swelling is a complicated process consisting of multiple steps. In the first step, water molecules mix with the hydrogel, with its hydrophilic behavior attributed to the presence of polar substituents (e.g. alcohols). The final step includes the absorbance of an excess amount of water, and is due to the resistance of the osmotic driving force of the polymer chains towards infinite dilution by the covalent or physical cross-links. The water fills the holes between the polymer chains and the centres of larger macro-pores. [22] The amount of the absorbed water by a hydrogel is reliant on the interactions between water molecules with polymer network and temperature, as described by the Flory-Huggins solution theory. [23]

Three-dimensional polymer networks are produced through chemical or physical cross-linking. [24, 25] There are a number of processes for this:

1.1.1 Radiation

Cross-linking between two hydrogel polymers occurs upon radiation, for example by a focused electron beam, by using either gamma-ray or X-ray, or by using UV light. [26-30] The radiation activates a free radical reaction for the polymer to produce cross-linking to form a new polymer (Figure 1.2).

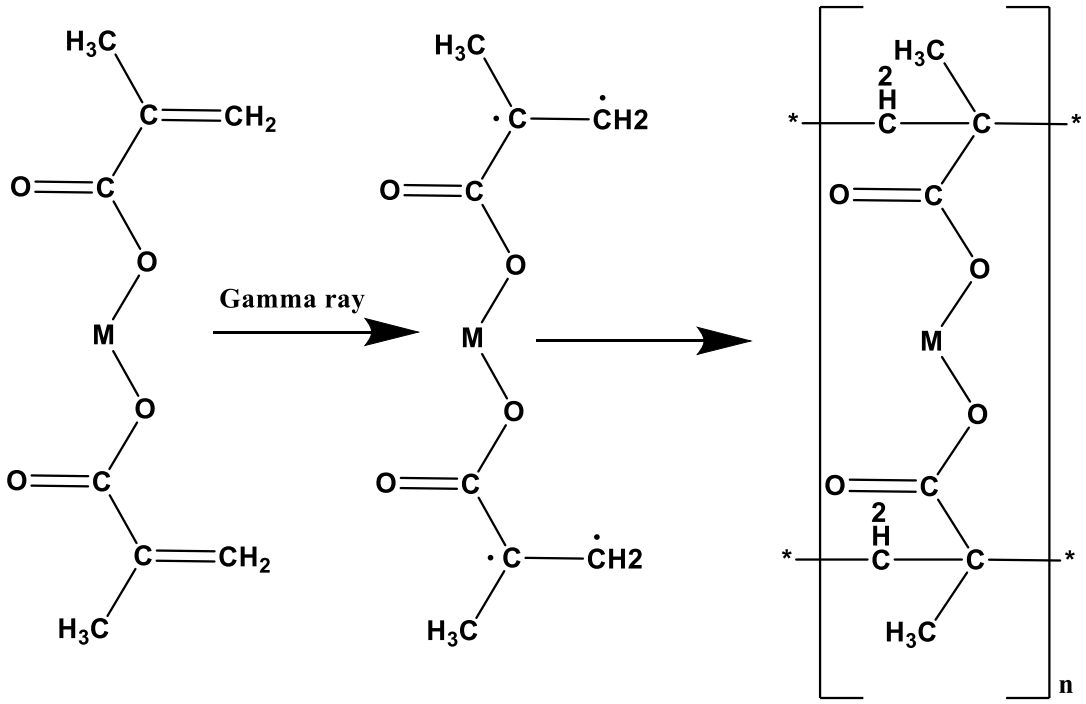

Figure 1.2 polymerisation of metal methacrylates using gamma radiation. Illustration adapted from reference [26].

1.1.2 Chemical cross-linking

The chemical cross-linking of polymer networks occurs by linking monomer units using covalent bonds. [31] There are several common processes for chemical bonding of hydrogels. The first is copolymerisation of a monomer with a cross-linker. [32] The monomer is a molecule with functionality to allow the formation of three different bonds resulting in branching in the polymer backbone. Alternatively a polymer network [33] can be produced using monomers containing a vinyl group, acrylic acid, AAm, hydroxyl-ethyl methacrylate, or a pyrrolidone vinyl and can be polymerised using polymerisation addition method. They can be cross-linked with monomers that have divinyl groups as cross-linking handles. [34] However, cross-linking reagents possess active terminal functional groups (*e.g.* amino acids containing primary amines, or thiols) which can be used in this case as nucleophiles in these cross coupling reactions. Cross-linkers can be conveniently utilized to modify drugs, nucleic acids, and solid surfaces. [35] Cross-linking reagents have been utilised to develop the characteristics of three-dimensional structures of proteins, heptane protein conjugation carrier, and molecular associations in the biological cell membranes. Cross linking agents also are convenient for immune-toxins and producing other kinds of protein components. [35]

Moreover, cross-linkers are selected for their chemical reactivity (i.e. specific functional groups) and

suitability of the reaction to the specific application. The best chemical cross-linker to use for a particular application must be identified empirically. Cross-linkers are nominated depending on the following features: Chemical specificity, water solubility, spacer arm length, and permeability of the cell membrane, same (homo-bifunctional) or various (hetero-bifunctional) reactive groups, spontaneously reactive or photo-reactive groups and cleavability. An example of a chemical cross-crosslinking is shown in figure 1.3. [35]

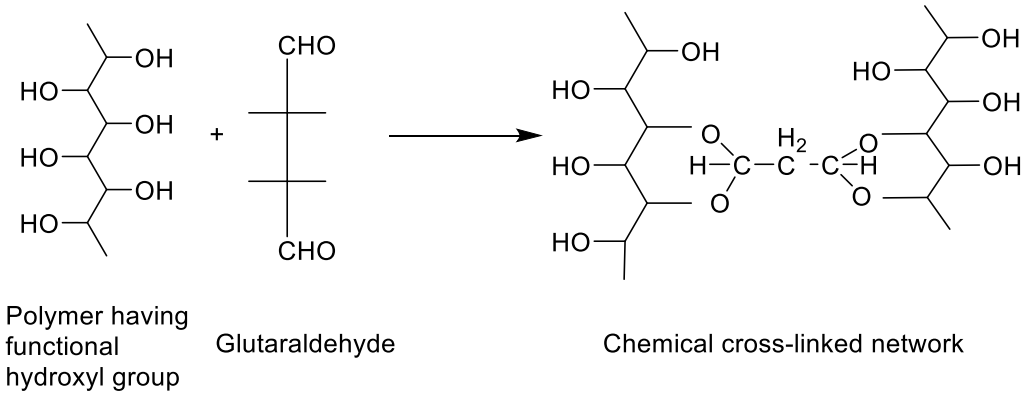

Figure 1.3 An example of polymerisation by using a covalent bond. Adapted and modified from reference. [35]

1.1.3 Physical cross-linking:

Physical cross-linking can be created by joining the polymer chains with a non-covalent bond including ionic interactions, Van der Waals interactions, hydrogen bonds, and hydrophobic interactions (Figure 1.4). [20]

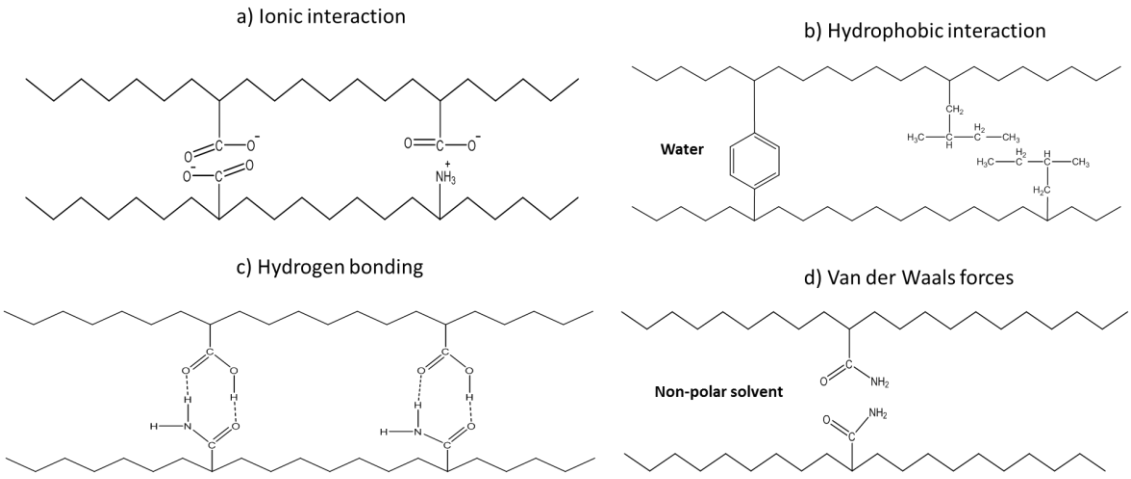

Figure 1.4 The main four types of physical cross-linking hydrogel represents a) ionic interaction, b) hydrophobic interaction, c) hydrogen bonding and d) Van der Waals forces. Reconstructed and adapted from reference. [20]

The material classification of hydrogels can be divided into two main groups; synthetic hydrogels and natural hydrogels. [36] Polymerisation reactions of organic chemicals produce synthetic hydrogels and are generally stronger and form more uniform matrices than natural hydrogels, [37, 38] which are renowned for their biocompatibility having greater cell recognition and adhesion than most synthetic hydrogels. [39] Natural hydrogel materials can be sourced by the fermentation of some species of bacteria or by extraction from plant and animal tissues. The formation of the hydrogel can be classified according to the following types: 1) blend hydrogels, 2) IPN and semi-IPN hydrogels, 3) polyelectrolyte complex hydrogels, 4) counterion induced hydrogels, 5) thermally induced hydrogels and 6) specific interaction induced hydrogels, as discussed below. [40]

1.1.3.1 Blend hydrogels

Blend hydrogels are polymers prepared by the participation of two different polymer solutions. The new blend hydrogel possess features that are different from the individual polymers and have an affinity to water with an enhanced level of water absorption. Other gels are prepared by blending, e.g. mixing chitosan with poly(vinyl oxide). [41]

1.1.3.2 IPN and semi-IPN gels

The interpenetrating polymer network (IPN) and the semi-interpenetrating polymer networks (semi-IPNs) initiation were a solution for the common low mechanical strength and toughness of the soft materials. [42]

They include two or more polymer chains physically overlapping and interlocking together and/or interpenetrating both synergistically. [43] The semi-IPN is formed by the meshing of filaments or branches without the presence of covalent links. [44] An example of this type of formation of semi-IPNs is the chemical and physical crosslinking between Salecan which is a novel water-soluble β-glucan with PAAm as shown in figure 1.5.

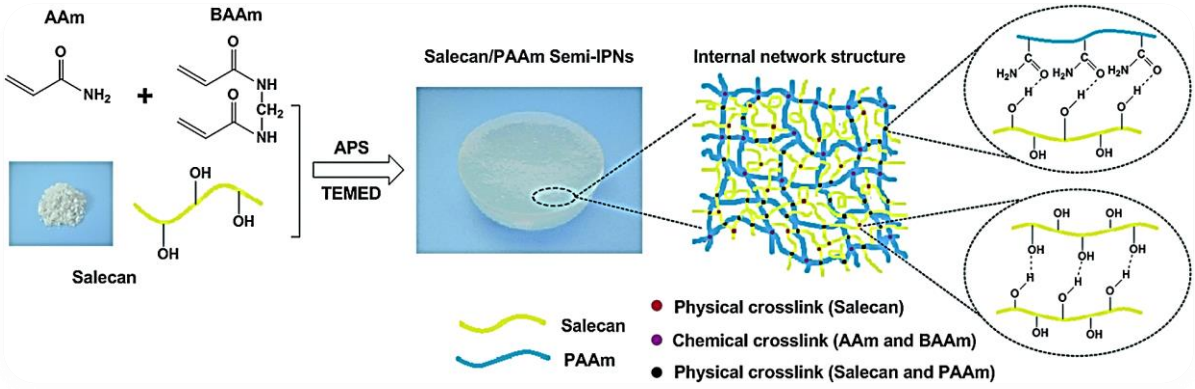

Figure 1.5 An example of physical and chemical cross-linking for the Selecan/PAAm Semi- IPN. Adapted from reference [45]

1.1.3.3 Polyelectrolyte Gels

A polyelectrolyte hydrogel is a polymer chain that contains charged macro-ions, polymer networks, and micro counter ions that are concentrated in the frame of the polymer network. Polyelectrolyte hydrogels display the capability to absorb a large amount of water within the network structure and can reach up to 2000 times the polymer weight, but without dissolving in it. [46] Polyelectrolyte gels reveal different unique electrical responses that vary from those of linear polyelectrolyte solutions. [47, 48] Polyelectrolytes that contain amine and carboxylate functional groups promote specific interaction; examples include chitosan, sodium alginate [49] and membranes of poly (methacryloyl ethyl trimethyl ammonium methyl sulfate) (PMETMMS) [50] (Figure 1.6).

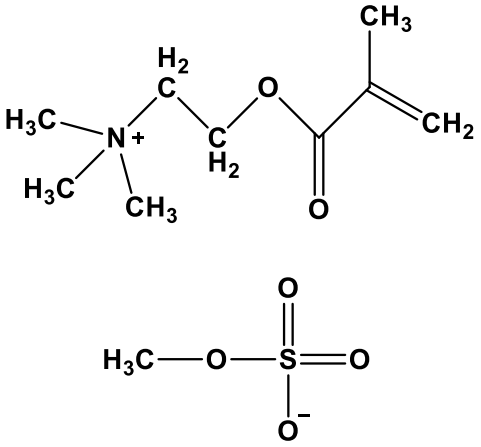

Figure 1.6 Poly (methacryloyl ethyl trimethyl ammonium methyl sulfate) (PMETMMS) structure. Adapted and reconstructed from reference [50]

1.1.3.4 Counterion induced hydrogel

Polyelectrolytes can form gels in the presence of the counterion due to the ability of the ionic polymer to cross-link by using di or tri-valent counterions. An example is the process of gelation for sodium alginate by adding calcium ion Ca^{2+}; [51, 52] and the dissolving lithium perchlorate in ethylene carbonate solution with poly (methylmethacrylate). [53] Figure 1.7 illustrates the gelation of sodium alginate by adding Ca^{2+} ions.

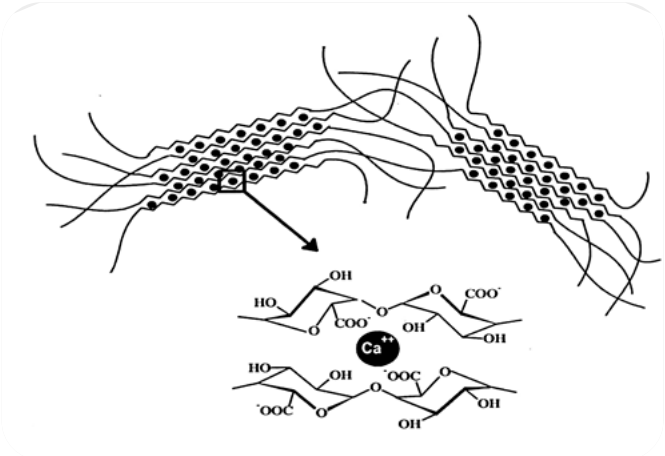

Figure 1.7 The Gelation of sodium alginate by the addition of Ca^{+2} ions. Adapted from reference [52]

Moreover, binding counterions plays a crucial role in collapsing the charged gel [54-58] with cationic hydrogels commonly displaying significant counter ion specificity for the collapse. [43], [59] It was

reported that higher concentrations of the charging groups attached to the polymer crosslinker chains results in higher collapsing amplitudes. [54] Furthermore, the swelling ratio of polyelectrolyte hydrogels would be affected substantially by adding low molecular weight salts. This effect is due particularly to the decrease in the osmotic pressure of counterions. [54]

1.1.3.5 Thermally-induced hydrogels

This type of thermoresponsive gel occurs when thermal energy changes the composition of the polymer in liquid, or it changes the balance between the hydrogen bonds and hydrophobic interactions. A typical example of this type of gel is the gelation of a gelatin solution by a reduction in temperature. [61]

Agarose gels have also been prepared in this way behaving like liquids at higher temperatures but become gels when the temperature is lowered. [62]

1.1.3.6 Specific interaction induced Gels

In gels of this type, sensitive hydrogels that undergo swelling changes in response to specific biomolecules can be modified to design smart hydrogels that could degrade in response to increase in concentration of specific biomolecules. [63] For example, the widely researched glucose–sensitive hydrogels have the ability to sense the levels of blood glucose and release insulin in accordance with the glucose levels. The polymeric networks can form by specific interactions between glucose and concanavalin A [63, 64] as shown in figure 1.8.

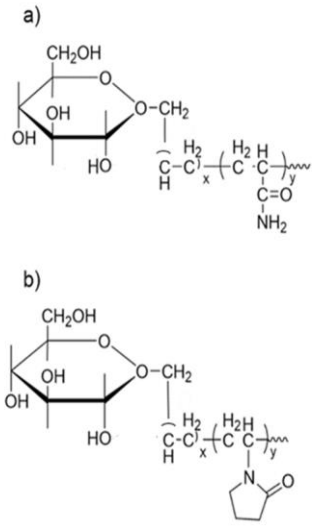

Figure 1.8 Structure a) allyl glucose – AAm Copolymer and structure; [48] b) allyl glucose – vinyl pyrrolidone Copolymer. Reconstructed and adapted from [49]

1.2 Hydrogel toughness

Hydrogels resist and dissipate stress by stretching the polymer network. Under low to medium strains, the polymer chains uncoil to dissipate energy. At high strains, the covalent bonds along the backbone of the polymer chain can be stretched significantly until one of the bonds is cleaved open and the chain cracks in two. Generally, long polymer chains are tougher than short chains because of having more bonds for energy to be dissipated through. Furthermore, polymers made of long chain molecules have higher melting points than those made of short chains. In addition, stiff chains can pack together and stick to each other. [65] A consequence of this is those lightly cross-linked hydrogels are stiffer than highly cross-linked hydrogels due to the greater length between cross-links. Most hydrogels are composed of heterogeneous networks that desrease toughness. [66] A heterogeneous network has cross-links that are not of a uniform length, an issue common in all gelation procedures, but regularly takes places when the hydrogel is synthesised by the method of polymerisation of a monomer with a cross-linker. [66] In these reactions, tightly cross-linked microgels are initially prepared, which are subsequently connected by longer, loosely cross-linked polymer chains to yield a macro gel as illustrated in figure 1.9.

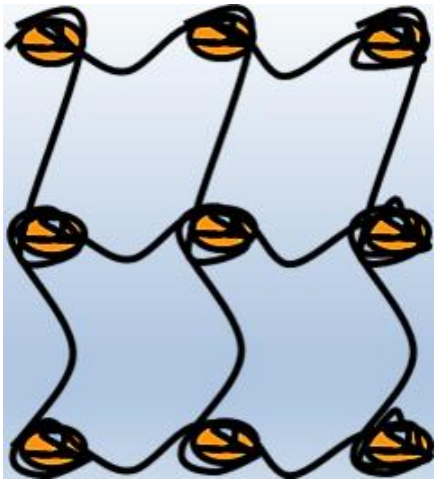

Figure 1.9 A two-dimensional representation of a heterogeneous polymer network, revealing tightly cross-linked microgels that are a linkage by longer, cross-linked polymer chains. The figure was modified and adapted from. [67]

There are two possible reasons identified why heterogeneous networks yield brittle hydrogels. The first is that in the loosely cross-linked regions of the polymer network, there are very few polymer chains that are required to be fractured for crack propagation. [67] The densely cross-linked microgels could also

contribute to the brittle nature of heterogeneous networks since micro-cracks can form within the tightly cross-linked clusters. The shorter polymer strands within these microgel clusters require little energy to fracture. [68] This results in the formation of a micro-crack that serves as a stress-concentrator. As stated above, hydrogels have the ability to absorb and hold a large quantity of water. This swells the polymer network to an expanded state that lowers the polymer chains number per unit cross-section area of the material. Furthermore, the toughness of the network is lowered as there are fewer polymer chains that need to be broken for crack propagation. Additionally, it is less likely for crystallisation to occur under stress in the swollen state because of chain separation. The effect of water content on a hydrogel is considered similar to the effect of temperature on polymers. Raising the temperature in plastic, or increasing the water content in a hydrogel, results in lowering the stiffness and strength of the materials. [69, 70] Swelling alone can be enough to cause some single network hydrogels to fail.

1.3 Single Network Hydrogels

Single network hydrogels are the easiest type of hydrogel material to synthesise. As suggested by their name, single network hydrogels are prepared by the polymerisation of a single network of polymer chains. Traditionally these have been the most favoured form of hydrogels applied for engineering applications. Single network hydrogels are polymer compounds with unusually low toughness, [71] with fracture energies less than 10 Jm^{-2} (tear test). [72, 73] Single network hydrogels are particularly brittle when compared to other polymer network systems. This is because they are deficient in the hardening mechanisms (strain hardening) that many natural tissues reveal when dissipating energy under strain. [73] Single network hydrogels are soft with elastic moduli that can easily mimic those of soft tissues. Furthermore, these materials have low strength and low toughness; consequently, they would be incapable of resisting external strains and stresses. Therefore, these materials are not considered for use in medical implants. Researchers consequently have designed a number of novel hydrogel materials, such as DN hydrogels, which significantly improve the poor mechanical behaviour observed for most single network hydrogels. [74]

1.4 DN Hydrogels

A new method for producing tough hydrogel materials was developed in 2003 by the Gong group. [72] It established that forming a second polymer network that mixes or merges throughout the first network structure, as shown in figure 1.10, increases the strength and toughness of the hydrogel materials. It was

noticed that by synthesising an interpenetrating PAAm network, the mechanical toughness of the copolymer hydrogel poly(2-AAm-2-methyl propane sulfonic acid) and 2,2,2-trifluoromethyl acrylate increased 700 times and the strength of poly(2-AAm-2-methyl propane sulfonic acid) (PAMPS) hydrogel increased 42.5 times. This new type of tough hydrogel is referred to as a DN hydrogel, which is a subset of IPN hydrogels. [74]

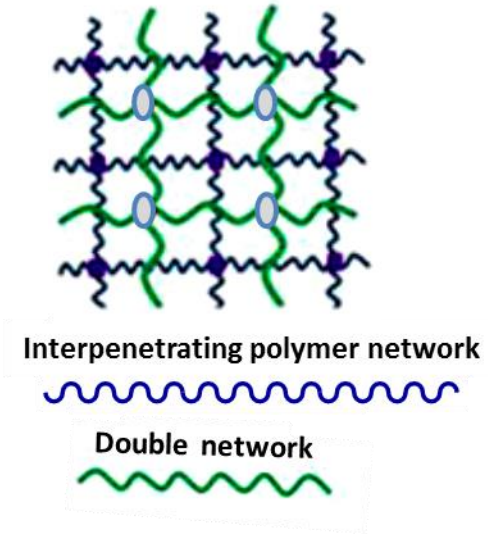

Figure 1.10 A schematic of a DN hydrogel where the second blue polymer network is interpenetrating within the other polymer network in yellow. Reconstructed after adaption from reference. [74]

The two-step approach is one of the most prevalent methods for producing a DN gel. Initially, a single network hydrogel is produced with the second network sequentially formed by submerging the gel in a second solution with monomers of the second network. The addition of an initiator or irradiation with ultraviolet light can be utilised to polymerize the monomers to produce the second network. [38], [75] A single step method can be utilised when preparing DNs with polysaccharides or other polymers. [76-77] The hydrated natural polymer and the monomer solution of the second network are soaked together and cooled. The polymerisation reaction of the monomer solution is started by the initiator. After polymerisation, the second polymer network is formed by the cooling of the natural polymer. It is essential to mix two polymers that have different mechanical characteristics. There are three main guidelines for maximising the toughening assistance of hydrogels when forming a DN hydrogel: The first network consists of a stiff and brittle polymer network such as a polyelectrolyte with several cross-links. The second

network is a soft and ductile polymer chain, i.e. a neutral polymer chain exhibits the same behavior to a reinforcing fiber through the matrix as does the first network. The molar concentration of the second network is greater than the molar concentration of the first network. Finally, the first polymer network is tightly cross-linked whilst the second polymer network is only loosely cross-linked. [69], [78-80].

The enhanced stiffness of DN hydrogels is because of the stability afforded by the second network on the micro-cracks that may form in the first network. When subject to stress, cracks propagate throughout the first network due to the high crosslinking of the heterogeneous brittle polymer network. The micro-cracks that are produced in the first network of a DN hydrogel are immobilized by the ductile second network chains of the polymer. The second polymer network enhances the stabilisation of the micro-cracks so that they do not easily propagate and combine into macro-cracks. [70] When a macro-crack is produced and propagates throughout a DN, a damaged area of the gel will form in front of the crack tip. [81, 82] This results in fracturing the polymer chains from the first network that absorbs energy. As the number of polymer chains that need to be fractured for crack propagation to occur increases, the toughness of DN hydrogels is increased. The stiffness of DN hydrogels under cyclic loading is described by the irreversible nature of the damage zone. [83] DN hydrogels are predicted to be exciting materials for soft robotic tissue implant usages [84] in which both single network hydrogels and DN hydrogels have elastic moduli in the range of soft tissues and reveal good biocompatibility. [84]

Recent developments in non-linear modelling, compliant mechanisms, and smart soft materials have led to the increased popularity in using soft materials in robotics. Robotics studies have advanced remarkably in the last 50 years [85] with the technologies being robust and solid, fast, reliable, and accurate in controlling robot motions. Almost all the techniques for fabrication, robot control and sensing are based on a conventional definition and fundamental assumption for robotics: a kinematic chain of rigid links. [85, 86] Soft material can help to provide functionality that is beyond the capacities of recent hard robotics technology. The high robustness and adaptability of soft robotics highlight their importance as body parts in natural organisms. For instance, the skin has the ability to be deformable and soft, while it is robust and waterproof at the same time. [87] The soft interactions of the hydrogel actuators are skin mimics. These can be utilised for physical therapy that can be controlled with interaction control design. The stiffness can be regulated in line with the forces applied by the patients [88] Nevertheless, there is an assumption that robotics theory and robotics techniques must be managed in order to achieve an outcome whereby the device works in an efficient and sustainable manner. [89]

1.5 Soft robotics

Soft, stretchable electrodes are a significant example of the application of soft robotics, which exhibits a broad range of human life usages and can be applied in both clinical and non-clinical fields. Furthermore, they can be designed to be biocompatible, biodegradable, [90] and responding to external stimuli, such as electrical or environmental modification (Figure 1.11). [1]

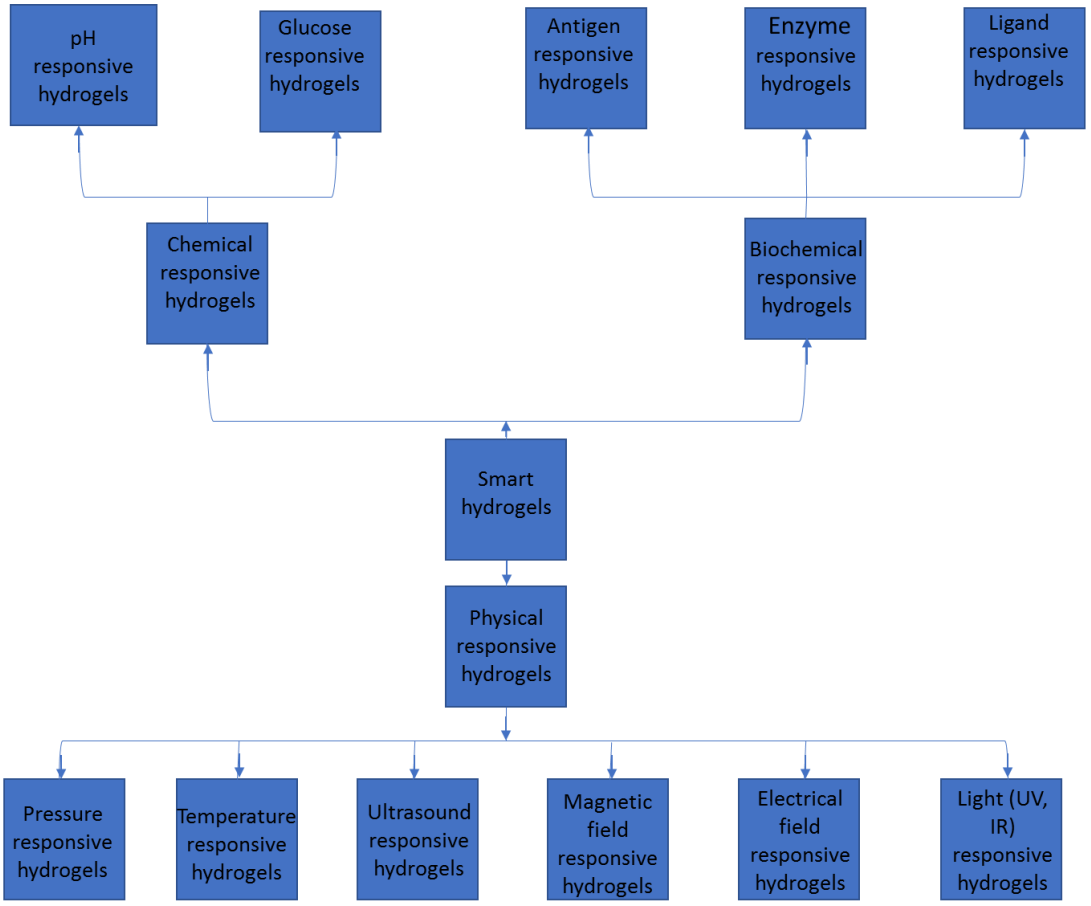

Figure 1.11 Specific sensors types of smart robotics. Reconstructed after adaption from reference. [91]

Specific soft biotics composed of soft or/and elastic materials mimic the human skin but have a different level of sophistication. Soft robots show great potential to benefit human life in areas such as health and wellness, home rehabilitation, entertainment, and safety. Soft, stretchable electronics can be used in multiple functions such as feedback sensors utilising strain in soft robotics during a stretching activity as shown in figure 1.12.

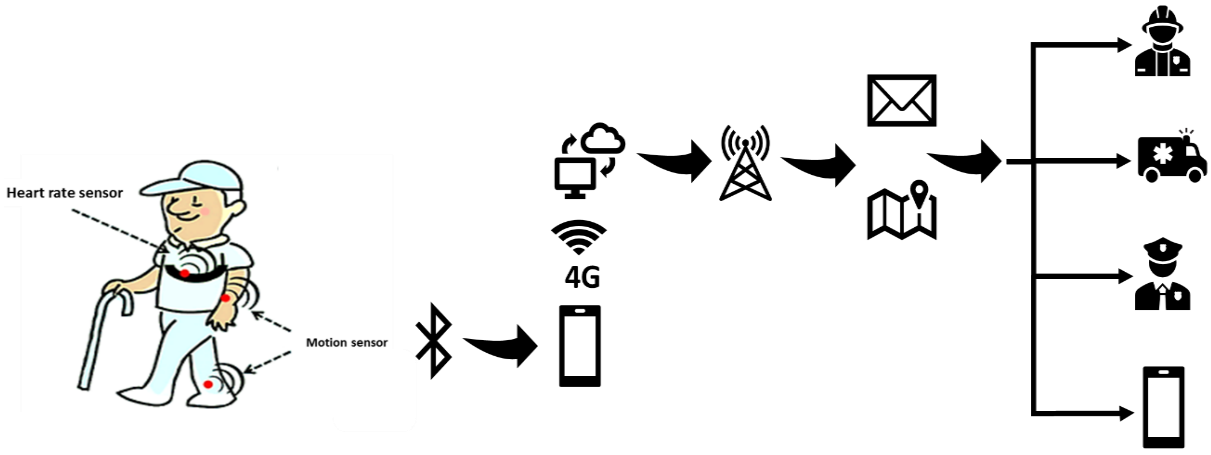

Figure 1.12 Motion sensors applications. Illustration modified after adaption from reference. [100]

1.6 Hydrogel sensor devices

The rapid developments in constructing electrodes on flexible substrates have broadened the horizon of future generations of electronics [92, 93] involving implantable [94–96] and wearable [97–100] devices. However, some challenges remain including the production of electrodes that maintain their electrical features when they are stretched. [100] Current techniques for material printing have been reported, e.g. the application of nanomembranes, nanoribbons or other complex patterns, [92, 93] that have been developed to achieve metal electrode stretchability. These electrodes are not suitable for biological applications due to their high stiffness, which can be detrimental to *in vitro* cellular differentiation. [101] and may cause inflammation and fibrosis *in vivo* resulting in signalling disappearance in long-term use [102, 103] This increases the need for polymers having a lower stiffness than metals for developing biocompatible organic devices. [104]

However, to commence development in the tissue engineering field with integrated electronics, it is critical to develop all-polymeric soft and stretchable patterns that exhibit biocompatibility and have favourable electrical properties, in particular, to have charge storage capacity. [105] Although various studies have achieved the printing of conducting polymer–hydrogel precursors for tissue engineering use [106], these exhibited low conductivity and unreliable mechanical property in high-stress environments. This limited their applicability, especially for muscle tissue engineering and long-term *in vivo* use. [107]

Several ionic conducting soft materials have been described by their stretchability and transparency including hydrogels and iono-gels. [108–110] These are soft materials composed of polymeric networks

that have the ability to swell when they soaked in any hydrophilic liquid. However, although most soft materials dry out in the open environment, soft materials containing hydrogels have the ability to retain water in a low humidity environment, and iono-gels are non-volatile when they are vacuumed. [108–110] Furthermore, many soft materials are biocompatible and can be fabricated to be used as biometric sensor monitors. Jeong-Yun Sun et al. [108] utilised ionic conductors, such as PAAm containing NaCl, as a strain gauge to investigate possible sophisticated sensory device that were highly stretchable, transparent, and biocompatible. The sensor device wasconnected to a multimeter that can report the signal from stretching the device when attached to a finger as in figure (1.13 a, b, c and d). Figure (1.13 d) displays the capacitance signal change resulting from stretching the device as the finger is bent. The (B) peak on the hydrogel sensor device represents the finger bent position. The S areas represent the strain released state. The transparency permits the sensory devices to be conducted without hindering optical signals.

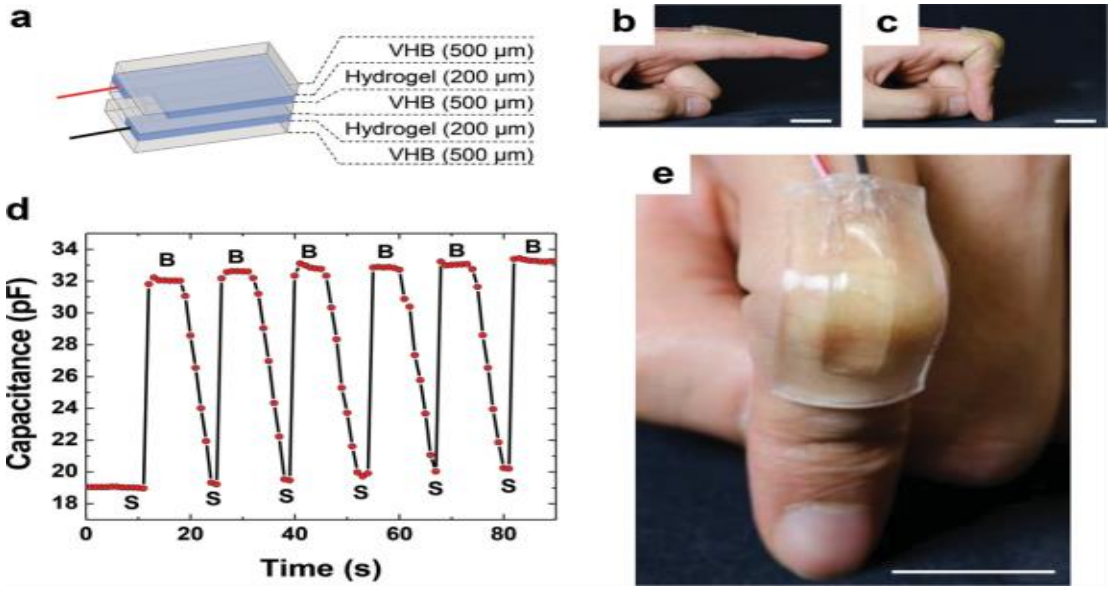

Figure 1.13 Fabricated ionic skin. a) Ionic skin sensor fabricated by sandwiching VHB tape layer between two layers of conducting, flexible ionic hydrogels. The whole components are sealed with the other two layers of VHB tape. b) Attaching the ionic skin device to a finger. c) The finger and the ionic skin device in the bending state. d) The capacitance measurements over multiple cycles of finger straightening 'S' and bending 'B'. e) Transparent ionic skin device over a bending finger. Illustration adapted from reference. [108]

A strain sensory device can be 3D fabricated by utilising a PAAm containing salt hydrogel. [111] Accordingly, LiCl was used instead of NaCl [108] to improve the water retention efficiency of a hydrogel by a selection of the appropriate concentration.

Based on this, PAAm containing salt hydrogel exhibited conductivity, stretchability and transparency. Therefore, it was intended to be used to fabricate soft, conducting and stretchable electrodes or sensors in this thesis using different techniques. Various materials have been selected to be included within the hydrogel for its low price, non-toxicity such as VHB tape, cellulose sponge and PDMS sponge. VHB tape was utilised in the projects described in this thesis either as a strain gauge substrate component for the extruded hydrogel or to cover the device to isolate the hydrogel from any environmental changes such as temperature and humidity or direct contact with any foreign materials. Furthermore, one thesis chapter describes how the conducting hydrogel's contact was controlled by sandwiching two layers of fabricated conducting hydrogels either side of a perforated VHB tape layer. Cellulose sponge was cross-linked with conducting hydrogel thermally to produce a stretchable strain gauge. Furthermore, the same hydrogel emerged within an optimised PDMS sponge to fabricate a stretchable electrode.

Direct ink writing and handheld printing technique were also used to 3D print conducting, flexible and durable hydrogels using a photo-polymerisation process which suggests the potential for this class of material in applications such as a soft sensing element or as soft robotics. Hybrid 3D printing is a new fabrication method for producing soft electronics. Within an integrated additive manufacturing platform, the direct ink writing of conductive and dielectric elastomeric materials can be combined with the automated pick and- place of surface mount electronic components. Using this approach, insulating matrix and conductive electrode inks were directly printed in specific layouts. Passive and active electrical components were then integrated to produce the desired electronic circuitry by using an empty nozzle (in vacuum-on mode) to pick up individual components, place them onto the substrate, and then deposit them (in vacuum-off mode) in the desired location. The components are then interconnected via 3D printed conductive traces to yield soft electronic devices that may find potential application in wearable electronics, soft robotics, and biomedical devices. The mechanical and electrical stability of some of the fabricated devices were examined before and after one year to investigate their durability.

In conclusion, this unique collection of features could widen prospects for innovative applications in implantable or wearable electronics. Therefore, to determine if a hydrogel is suitable for sensor devices, it is crucial to investigate its characteristics.

1.7 Mechanical properties of hydrogels

Soft polymer materials are increasingly used in various sectors of human activity. However,their low mechanical strength and toughness limit their applications. The mechanical behaviour of the hydrogel may be studied by carrying out compression tests for compressive failure strain (ε), compressive secant modulus overstrains (E), compressive failure stress (σ), and compressive strain energy to failure (U). Stress is a measure of the internal force for an object per unit cross-sectional area as shown in equation (1.2). Therefore, the formula for calculating stress is the same as the formula for detecting pressure:

$$\sigma = \frac{F}{A} \quad \text{,…….} \quad \textbf{(Eq. 1.2)}$$

Where σ is stress (Newtons per square meter or, Pascals), F is a force (in Newtons, with symbol N), and A is the sample cross-sectional area and represents the point that corresponds to the maximum stress in figure 1.14. The application of stress causes strain. Putting pressure on an object causes it to stretch. The strain is a measure of how much an object is being stretched. The formula for strain is shown in an equation (1.3):

$$\epsilon = \frac{\Delta l}{l_0} = \frac{l - l_0}{l_0} = \frac{l}{l_0} - 1 \quad \text{,……..} \quad \textbf{(Eq. 1.3)}$$

Where l_0 is the original gauge length of an object to be stretched, and l is its length after it has been stretched. Δl is the extension of the object, the difference between these two lengths. Meanwhile, a compression secant modulus is a measure of the stiffness of a material. It specifies how much a material will stretch (i.e., how much strain it will undergo) as a result of a given amount of stress, represented by the tangent slope value or by the formula of equation (1.4):

$$\boldsymbol{E} = \frac{\sigma}{\epsilon} \quad \text{,…….} \quad \textbf{(Eq. 1.4)}$$

The values for stress and strain must be taken at as low a stress level as possible, providing a difference in the length of the sample can be measured. The strain is unitless, so compression secant modulus has the same units as stress, i.e. N/m² or Pa. Stress (σ) can be plotted versus strain (ε). The toughness of a material (i.e. how much it resists stress, in J m^{-3}) is equal to the area under the curve, between the y-axis and the fracture point. [112] In a tensile experiment, the elastic or Young's modulus of the hydrogel is calculated from the slop of the initial point of the stress-strain curve as shown in figure 1.14, whereas in compression experiments, the secant modulus of the elastic region is more arbitrary due to the J-shape of the stress-strain curve.

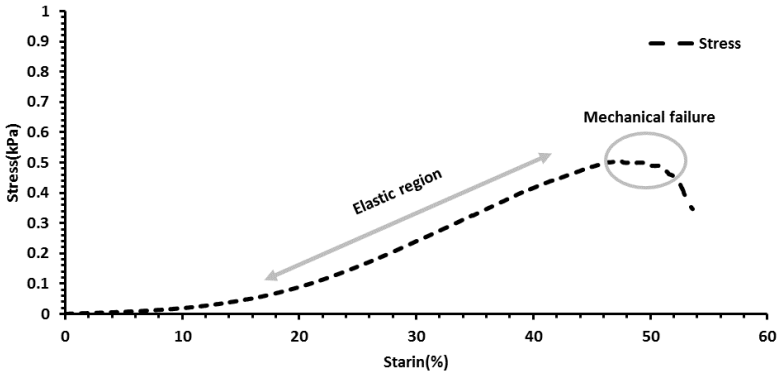

Figure 1.14 Stress vs strain diagram after the tensile test for a hydrogel revealing elastic region and the mechanical failure region. This graph was generated by the candidate.

Conventionally produced synthetic hydrogels typically reveal low Young's modulus range (1 – 100 kPa), low tensile and compression strength range (1 – 100 kPa) and low fracture energy value (< 10 J m^{-2}). [113] Different procedures have been used recently to structure more robust hydrogels permitting their functionalization in load-bearing applications. Amongst the available methods for fabricating tough hydrogels are slip-link networks, [114] nano-composite gels [115], DN gels, [72] multifunctional cross-linked hydrogels, [116] homogeneous hydrogels, [117, 118], and IPN gels. [119] These preparation techniques have been shown to enhance hydrogel strength and toughness. One approach to positively alter the mechanical properties of a hydrogel is adopting an IPN system [120], which are prepared using a covalent cross-linked network, and an ionic cross-linked network. This is a crucial criterion that controls to costumise the mechanical and physical properties of an IPN hydrogel. Covalently cross-linked PAAm networks were synthesised in the presence of GG and calcium chloride that was ionically cross-linked to synthesis the IPN hydrogels. [121] Preparing IPN with optimum mechanical properties can be obtained by the blending of two cross-linked networks, interpenetrating within each other at the molecular level. IPNs usually display a significant physical and mechanical properties in between other networks, so the mixing of a less swellable, stiffer hydrogel with a more-swellable, softer hydrogel can be used to regulate the IPN modulus and swellability. The extra benefit of such IPNs is the noticeable increase in toughness that it often improves the mechanical properties which is typical of yield in IPNs as DN hydrogel networks. [122] The first network is more tightly cross-linked than the second network and the molar ratio of the second network to the first network is more than 5. [81], [123, 124] As explained previously in section 1.4 there is a

sequential two-step of polymerisation process for the preparation of DN hydrogels. However, a one-pot preparation method for producing IPNs in which at least one of the networks is a biopolymer have been known for some time [125-127] and have recently been revealed to present significant toughness. [119,128] These hydrogels are synthesised using a one-step method by dissolving the biopolymer in a solution of the monomer that is then cross-linked to produce a covalent polymer network. The mechanical and physical features of these hybridised hydrogels can be modified mainly by changing the ratio of the two networks and the degree of cross-linking in each network. [121]

Brown [67] and Tanaka [129] have suggested that the large value of fracture energy (G_c) in hydrogels is due to the DN hydrogel heterogeneity. Moreover, they considered that there are two major roles for the presence of void and entanglement at the crack tip. The first one occurs by the high curvature barring stress concentration, and the other by the resistance or energy dispersion of fracture energy, which contributes to decreasing the stress around the leading edge of the crack, thus prohibiting crack extension and inhibiting the crack growth at the microscopical scale. In particular, Brown referenced his model to illustrate the failure process in the DN gel using the Lake-Thomas concept [130] that considered the degree of energy dissipation on the failure of a polymer strand and he focused on the importance of the particular double microstructure, the tightness of the first polymer network and the looseness of the second polymer network. The model explained that a substantial increase in the number of strands would exist in the second network after the formation of the crack within the first network. The crack expansion exists in two stages, the first initiated by the creation of many cracks in the first network, with a high crosslinking density, through the formation of the damaged zone near the main crack tip. External stress could yield multiple cracks formed in the first network, leading to extension of the damaged zone.

Meanwhile, the second network is involved in crack expansion by forming a yield strip around the crack. This region of material can be considered to be elastic with low modulus. The energy that typically exists to break the chains and extend the crack is called elastic energy. Hence, the excellent mechanical performance of the DN gel is probably caused by the local yielding of the DN hydrogel to obtain a soft material, and the energy dissipation by the resulting structure consolidates the reliable fracture energy (G_c). [131] Many studies on DN hydrogels have revealed that there is a significant chance to produce strong and stiff gels. Preparing hydrogels with high strength and toughness should promote the use of hydrogels in a wide range of applications that could be related to biomedical or non-biomedical areas. This nominated DN hydrogels could be developed to enhance the hydrogel networks and then to improve the mechanical

properties. [132]

There has been recent interest in engineering hydrogels to enhance the mechanical properties by creating a high swelling ratio in water. [133] The swelling ratio can be of the order of 100−1000 for many gels and are termed super swelling or superabsorbent materials and are used in products such as disposable diapers. [134−137] The swelling ratio depends on the fraction of ionizable groups along the polymer backbone; i.e. ionic gels swell considerably more than non-ionic gels. [136, 137] The swelling ratio also depends on the density of cross-links within the gel, with the lower the cross-link density, the higher the swelling. [136, 137] However, gels with low cross-link densities tend to be soft and floppy. Thus, the synthesis of gels with an ideal combination of water absorbency and mechanical properties remains a challenge.

The mechanical properties of synthetic hydrogels usually fall in one of two extremes, depending on the cross-link density. [138, 139] If the gels are weakly cross-linked, they tend to be soft (low elastic modulus) and may be difficult to handle, as they may be slippery and difficult to grasp by hand or with tweezers or forceps. In contrast, highly cross-linked gels tend to be stiff (high elastic modulus), but are generally also quite brittle. These gels are easy to handle but have a low strain and their tensile strength, toughness, and resiliency tend to be quite low. [140, 141] This weakness in the mechanical properties is attributed to the inhomogeneous distribution of the cross-linkers within the polymer networks due to the free-radical polymerisation of the gel nanostructures. For example, there are many looped chains present, and a dangling end is created in this type of hydrogel. When stress is applied, the gel will deform, and the polymer segments will deform creating zones of high stress in the polymer resulting in irreversible breaks at low deformation. Recently, some naturally occurring soft materials have been explored, such as aquatic creatures, which showed remarkable resilience and robustness when compared to other synthetic hydrogels. [140, 141] The low strength was attributed to the nanostructure that typically exists in gels made by conventional free-radical polymerisations. [140, 141] In particular, cross-links tend to be distributed in homogeneously; i.e. there is a wide distribution in segment lengths (molecular weights) between adjacent cross-links. When such a gel is deformed, some chain segments tend to deform much more than others, which creates zones of high stress in the gel. Consequently, the gel suffers irreversible rupture at low deformations. As a result, more studies were undertaken to improve the toughness and the stretchability of a dense cross-linking polymer network. [142−150] For example, Tew *et al*. pioneered hydrogels using particular end-functionalized monomers for producing uniform cross-linking distribution. Haraguchi *et al*. [142, 143] developed hydrogels with high elongations at break (~1200%) by utilising nanoparticle cross-linkers

instead of the conventional multifunctional monomers. [134] Gong *et al*. [151] innovated the interpenetrating or "DN" gels concept to optimise the mechanical performance. Generally, alternate methods are needed to devise hydrogels that swell greatly and remain reasonably tough even in the swollen state. [134] Tensile testing has been suggested to study the mechanical properties of the prepared hydrogel by extension up until the rupture point. Additionally, compression testing is necessary to study the viability of the prepared hydrogel to bear external forces before breaking. This test could also be undertaken under multiple cycles to examine the durability of the prepared hydrogel against exposure to constant external stress. Oscillatory shear rheological measurements are also required with a controlled strain rheometer to identify the flow properties of the material, and to study the elastic and viscous characteristics. It is also interesting to make predictions for mechanical properties of PAAm (on a continuum mechanics scale) based on the micro- or nanostructure of the material. [152]

The primary aim of this project was to develop some perception of the optimisation of the mechanical properties of the ionic PAAm hydrogel or the ionic-covalent entanglements in GG/PAAm hydrogel by synthesis using different concentration ratios of salts, and the covalent cross-linkers.

1.8 Rheology

Rheology is the study of the flow of matter, mainly in a liquid state. However, the plastic flow of soft solid materials can be examined in response to an applied force. [153] Furthermore, this characterisation technique enabled the investigation of the flow that substances possess in a complex microstructure such as muds, sludges, suspensions, polymers as well as many edibles and additives, biological fluids (e.g. blood) or other materials which belong to the class of soft matter. [154]

The term rheology was pioneered by Professor Eugene C. Bingham in 1920 [155] and was derived from the aphorism of simplicius (often attributed to Heraclitus), and Panta rhei; "everything flows". [156, 157]

Technically, rheology is an interesting principle dealing with continuum mechanics to study the materials flow by combining elasticity and (Newtonian) fluid mechanics. In particular, this study showed that rheology is a combination of elasticity and viscosity features. [158] In the last decades of 20th century, researchers were interested in involving PAAm for building a better understanding of the mechanical properties for investigating the micro- or nanostructure of the material, for instance, the particle or the molecular size and the architecture of polymers in a solution or in a stable suspension. Furthermore, materials with fluid features normally flow when pressure is applied. Correspondingly, different forms of

stress (e.g. shear, torsional, etc.) and materials will produce variant responses of stress. Much of theoretical rheology is undertaken in association with external forces and torques with internal stresses and internal strain gradients and velocities. [153], [159, 160]

An additional aim of this study was to create a correlation between deformation and stress by applying further measurements using the technique of rheometry. This device functions by determining distinct rheological material relationships which are then compliant to mathematical analysis by the specific technique of continuum mechanics. [161]

The examination of flow or deformation yielding from a specific shear stress domain is known as shear rheometry (or shear rheology) and the study of extensional flows is extensional rheology. [161] Rheological properties of composites based on different ratios of GG /PAAm were studied as functions of crosslinking density, which determine the structure of the three-dimensional network of the formed polymer as described in chapter three. The rheological parameters are described in the plot of both storage modulus G′ and Loss modulus G″ versus strain; Figure 1.15 describes rheological parameters where the plateau refers to the linear viscoelastic (LVE) region, in which, a high value of G′ is a good indication for the presence of a cross-linked polymer network. However, the end of the LVE region corresponds to a shear strain of the hydrogels after which inelastic deformation occurs. Moreover, the sol-gel transition represents the transformation of the hydrogel state from solid to liquid. [162]

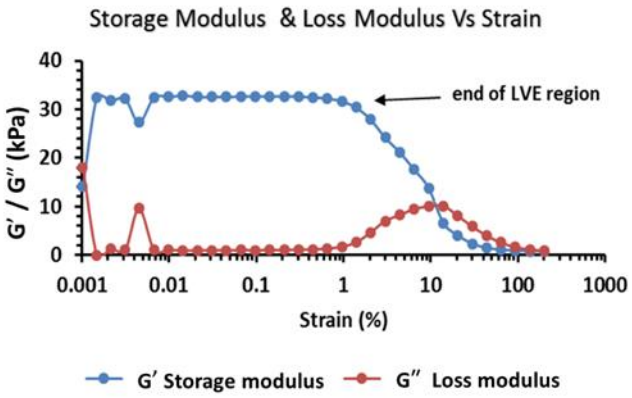

Figure 1.15 Shows storage modulus and loss modulus versus strain. This illustration created by the candidate.

The rheological analysis was also performed to investigate the viscoelastic characteristics as a function of temperature and time at a constant shear rate to achieve optimum viscosity to form a uniform and stable

filament during extrusion for developing 3D printing of conducting, flexible and durable hydrogel (Chapter 4).

1.9 Electrical characteristics

A range of applications has been studied involving pressure sensors for soft robotics [163, 164], stretchable conductors [108], foldable actuators, [165, 166] and interfaced neural prosthetic. [167] Soft conducting hydrogels are considered to be significant solutions to a plethora of current problems in soft robotics such as electrical and mechanical compliance matching. [168] It is known that non-ionic hydrogels exhibit no electrical conductivity and therefore, there is interest in developing suitable methods to boost the electrical conductivity of hydrogels by doping with strong acids, adding salts, [163, 164], [169] or incorporating conducting fillers. [170–172] In order to achieve this, it is essential to characterise the electrical properties of prepared hydrogels by calculating the conductivity from the measured impedance. The actual conductivity (σ) for prepared hydrogels was taken from the plot of total resistance against hydrogel length [168], as shown in figure 1.16.

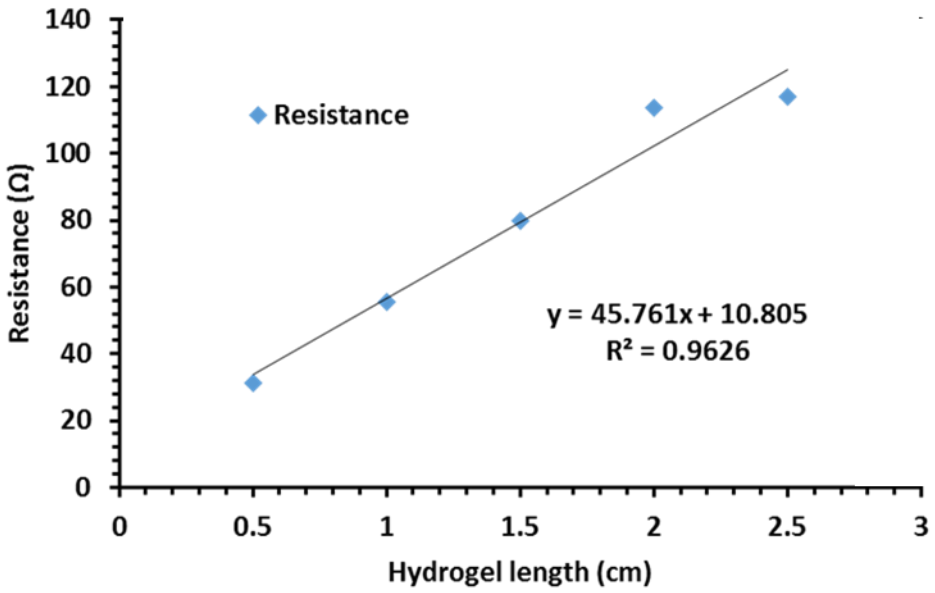

Figure 1.16 Typical plot of resistance (RI) versus gel length. Figure produced by the candidate.

The plot behavior revealed a linear relationship that enhanced the calculation of the contact resistance (R_c) from the *y*-intercept, and the sample conductivity from the slope. The total resistances of hydrogel

samples were calculated by equation (1.5) describing a geometric object sample shown in figure 1.17. [172]

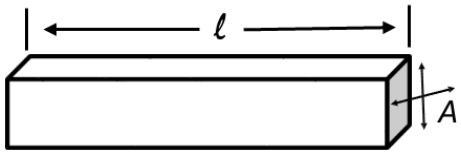

Figure 1.17 Uniform specimen object having length l, and area A. Reconstructed after adaption from. [172]

$$R_T = \frac{l}{\sigma \times A} + R_C \quad \text{..... (Eq. 1.5)}$$

Where A is the cross-sectional area of the hydrogel sample (in cm^2), and σ is the conductivity (in S/cm). The hydrogel mould item has 10 sample moulds with five lengths which range between 0.5-2.5 cm, with the width of each sample mould 0.5 cm while the height is 0.6 cm. R_C (in Ω) is the resistance at the contact points. Since the slope of equation above is 1 / (σ *A*), then σ = l / (slope × *A*). [172]

The contact resistance, R_C values are measured and expressed as impedance that describes the interfering between gel and electrodes (porous RVC). The impedance behaviour revealed an obvious increase (at an independent frequency) with hydrogel length increase [172] as shown in figure 1.17.

Measuring conductivity is crucial for studying the ability of the prepared hydrogel to conduct after the addition of different salts to the PAAm and ICE hydrogels, including NaCl and LiCl, and $CaCl_2$ with ICE gel. These salts were previously used with Polyacrylamide (PAAm) hydrogel to produce conductive stretchable and durable hydrogels. However, these hydrogels were synthesized using Thermo-initiator such as ammonium persulphate, while our hydrogels were prepared using photo-initiator such as α-Ketoglutaric acide. The aim of using photo-initiation reaction in synthesising our hydrogels is to ultimately extrude these material to design a 3D soft structure device. In particular, salts like NaCl was selected broadly to produce conductive hydrogels and stretchable hydrogel. While LiCl was selected in the hydrogels preparation in this thesis as it has been used previously in several studies for its, conductivity, stretchability high water retention capabilities. On the other hand, $CaCl_2$ was seleceted for its capapbilty to produce tough ICE hydrogel. The conductivity of ionic hydrogels has been calculated using different techniques including both alternating and direct current measurement devices, i.e. electrical impedance, conductivity meters, and four-point probe techniques. [170-172]

Hydrogels containing ionic groups within their polymer networks can form fixed charges along their polymer chains when they swelled and are called polyelectrolytic gels. These fixed charges can be stabilised by adding cations to the polymer chains to form ionic bonds that cross-link the polymer network. [173-177] Furthermore, these cations can be used to create ionic conductive hydrogels [163], [173-179] and can transport charges through the water-filled micro-pores of the polymer network [180-182]. Therefore, factors that affect the ionic conductivity are the water content, the concentration of cations, ion-polymer interactions, crosslinking, and hydrodynamic radii of the ions [182-185]. In general all these parameters such as crosslinking, ion-polymer interactions, hydrodynamic radii of the ions having an impact on the diffusion properties of water molecules and the ions mobility inside the hydrogel and hence will effect on the conductivity. Therefore, an increase in the concentration of the ions will lead to higher conductivity.

The electrical impedance study of gel samples was carried out for frequencies between 1 Hz and 100 kHz using a custom-designed instrument or by using a potentiostat (Gamry Reference 600) instrument and sample compartment. The sample compartment held the gels which were casted into a rectangular shape with a width of 0.5 cm, height 0.6 cm, and length from 0.5 to 2.5 cm. Reticulated vitreous carbon (RVC, an ERG Aerospace, foam structure with 20 pores per inch, relative density 3% or void volume 97%, resistivity 0.323 Ωcm) pieces were placed in the ends of the sample compartment to act as electrodes. Impedance analysis was performed by applying a 1 V peak voltage (alternating current signal) using a waveform generator (Agilent U2761A), across the circuit consisting of a known resistor (R_k, 100 Ω) and the gel sample. The impedance was obtained by measuring the voltage drop across the known resistor with an oscilloscope (Agilent U2701A). The impedance values measured in this manner include a contact resistance, R_C, owing to the interface between gel and electrodes (porous RVC). Figure 1.18 shows the schematic representation of the custom-built electrical impedance analyzer for the PAAm hydrogel mould with carbon foam electrodes. [168]

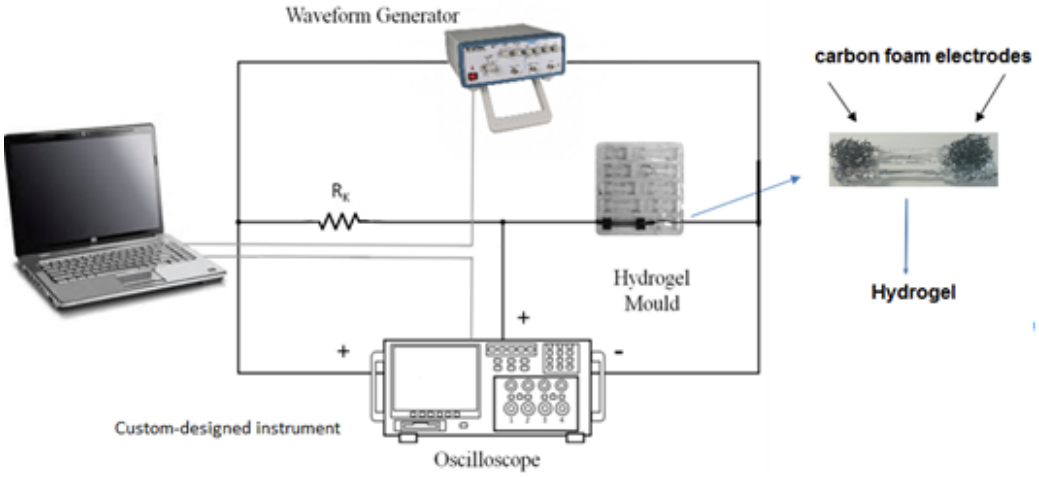

Figure 1.18 Schematic figure to present the custom-built electrical impedance analysing system for the PAAm hydrogel meld with carbon foam electrodes. Reconstructed after adaption from reference. [168]

We hypothesise that the calculated conductivity of the fabricated hydrogel using the direct-write assembly technique and the moulded hydrogel may be investigated by measuring the impedance and the dimensions of the hydrogel samples. This investigation could lead to building a better understanding of the electrical reliability of the fabricated hydrogel compared to the moulded one as shown in the studies described in chapter four.

1.10 Resistance sensitivity

The electrical resistance sensitivity of a sensing material can be characterised by measuring the electrical resistance changes due to applied strains or stress. Pressure sensors using piezoresistive elements in silicon as the stress-sensitive element were invented in the 1960s, and are now among the most successful micro-machined sensors. Since then, the performance of piezoresistive pressure sensors has been improved by the introduction of new microfabrication technology [186] and have been implemented in advanced applications placing high demands on both precision and stability, such as medical and automotive applications and applications for the avionics market. There are several different pressure sensing units used in the electronic industry on the application. [187]

Recently developed soft sensors have been implemented to investigate the possibility of identifying the location and pressure of touch based on capacitance change**.** [188**]** However, most of these developments have been applied to applications that operate at low mechanical stress. As a result, a wearable soft sensor

device (SSD) was developed consisting of two lithium chloride conducting PAAm electrodes separated by a perforated elastomeric very high bonded (VHB) tape as shown in chapter five. The novel perforation of the elastomeric material separating the electrodes enables the creation of a sensor with an inbuilt threshold of operation. The device allowed for the detection of mechanical stress via a change in resistance within the electrodes, which enabled the device to operate at a much higher range of stress than was used in previous sensors that utilised a change in capacitance. The SSD was shown to be durable, to exhibit reliable electrical sensitivity and mechanical recovery over 50 cycles of compressive stress for over one year. This SSD was combined with an Arduino device [189] to send a signal to a mobile phone, creating a custom-built remote sensor. This work has the potential to enable better data collection for enhanced logistical decision making and emergency response via applications such as elastic sensors for use in remote areas.

This thesis used the SI-unit Pascal (Pa). The electrical sensitivity has been calculated as shown in equation (1.6)

Resistance sensitivity= $\Delta R/\Delta\sigma$,…….. **(Eq. 1.6)**

Where ΔR is the magnitude of resistance change between loading and unloading resistance state values in ohm, while $\Delta\sigma$ represents the magnitude of stress change between loading and unloading states in Pa. Therefore, the calculated resistance sensitivity unit would be ohm/Pa. [190]

Other areas of this thesis have utilised the resistance change resulting from stretching the fabricated soft sensory device to work as a strain gauge as described in chapters six and seven. Strain gauges are an engineered sensor pattern that have the ability to react when the pattern has been deformed or stretched in one direction. When the sensor is distorted, there is a modification in the physical structure of the sensor pattern (surface area, track length), and this alteration results in measurable property changes, such as capacitance [191, 192] or, more commonly, resistance. [193, 194] Strain gauges are of raised attention for human-sensing actuator for the field of soft robotics [193] due to their ability to easily sense human-motion. The sensitivity of the device is evaluated by calculating the gauge factor.

Fundamentally, all types of strain factors illustrate the conversion of mechanical motion into an electrical signal. This means that alterations in capacitance, inductance, or resistance directly corresponds to the strain experienced by the sensor. If a hydrogel is held under tension, it gets slightly longer, and its cross-sectional area is reduced. This changes its resistance (R) in proportion to the strain sensitivity (S) of the hydrogel resistance. When a strain is produced, the strain sensitivity, which is also called the gauge factor (GF), is revealed given by equation (1.7):

$$GF = \frac{(\frac{\Delta R}{R})}{(\frac{\Delta L}{L})} = \frac{(\frac{\Delta R}{R})}{\varepsilon} \quad \text{..... (Eq. 1.7)}$$

Where ΔR is the resistance change between the status of the deformed and undeformed sponge-hydrogel device, R is the resistance magnitude for the undeformed device, ΔL is the change in the deformation length in mm, and L is the undeformed length of the device. Sometimes the strain ($\frac{\Delta L}{L}$) is designated by (ε) as shown in figure 1.19. [195]

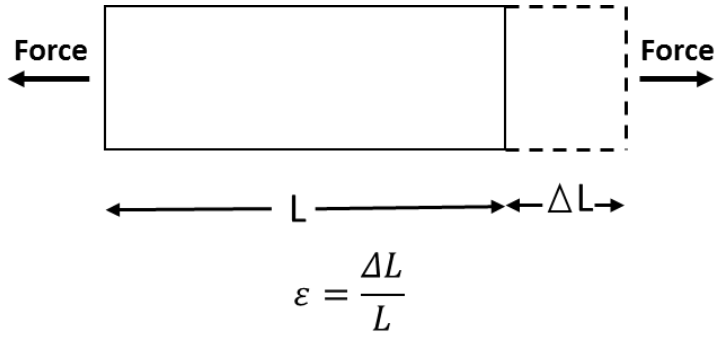

Figure 1.19 Description of the device strain. Reconstructed after adaption from reference. [195]

1.11 3D Printing

1.11.1 Direct ink-writing technique

Numerous attempts to develop 3D fabrication processes to reach the micro or even the nanoscale filament sizes for the fabricated hydrogels have been reported. [196, 197] The direct-write assembly technique was chosen for its ability to pattern 1D and 3D micro periodic scaffolds with an extensive range of hydrogel materials. AAm solution was combined as a based ink with *in situ* photopolymerisation using UV as a light source to produce hydrogel scaffolds with micrometre dimensioned properties. [196] The direct ink writing technique extrudes the AAm ink layer by layer with lateral feature dimensions smaller than those that are performed by using ink-jet printing [198-200]. Thus, the direct-write assembly technique was used to construct 3D hydrogel scaffolds by extruding the thick ink through a fine-tipped nozzle, depositing a filamentary pattern. This pattern solidified rapidly in the air using a UV light source to obtain layers of a fixed shape. This technique is different from previous techniques as it does not need reservoir induced coagulation to enable the 3D extrusion of the polyelectrolyte inks as others did. Robert and his co-workers produced a 3D printed hydrogel structure composed entirely of a mixture of PAAm and glycerol. [201] This, and several previous studies, focused on 3D fabrication for the hydrogel containing PAAm mixed

with various materials, e.g. glycerol, sodium alginate, etc. for increasing the ink viscosity and hence, improving the extrusion process. [196], [202] Fabricating pure PAAm containing salt hydrogel became a challenge that needed to be overcome. Therefore, one of the aims of this project was to develop a 3D fabrication process for pure PAAm containing salt hydrogel, by using a direct-write assembly technique to enable the printing of microscale sized scaffolds as described in chapter four.

3D Printing is a technique used for achieving laying down multiple layers of material to build up three-dimensional structures that are designed using CAD (Computer Aided Design) software as a 3D modelling program or by using a 3D scanner (copying an existing item). [203] Each layer can be recognised "as a thinly sliced horizontal cross-section of the eventual object" such as figure 1.20. [204]

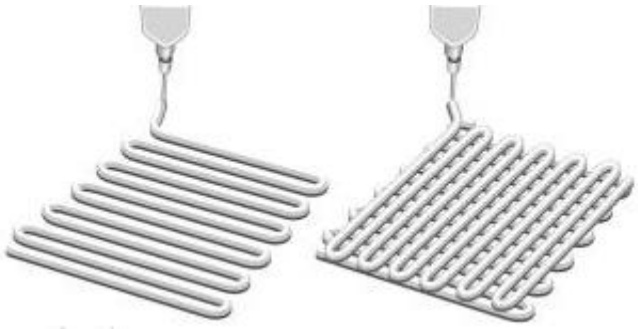

Figure 1.20 Shows the bilayer extrusion concept. Adapted from reference. [204]

3D Printing is receiving attention from a wide range of fields because of the capability to rapidly produce 3D object materials. Hydrogels were one of the nominated materials to be utilised in the application of tissue engineering due to its ability to form a gel with a defined shape. [204-207] This gel can be solidified by using a photo, chemical or thermal initiator. [208] Moreover, the 3D printing technique was harnessed to design soft materials in the desired form by either extrusion or inkjet process. [207] Recently, electrically conducting materials were being developed to introduce electronic functionality to fabricated polymer-based objects. Hydrogels are considered to be promising materials to enable the provision of new utilities by the introduction of printable sensing and actuating devices. [208] In this project, we hypothesised that the parallel development of hydrogel materials like PAAm containing salt, with the application of suitable 3D fabrication techniques such as direct-write assembly would stimulate the advancement of several applications including sensors, soft robotics and bionic implants.

PAAm hydrogels containing salt as the electrolyte have been used as highly robust transparent hydrogels

in stretchable electronics. For instance, a PAAm hydrogel containing sodium chloride (NaCl) has been reported to be fully transparent, highly stretchable and as being ionic conductive. [209] Water plays two leading roles in hydrogels containing salt. While the salt provides the conducting ions, water molecules operate as the solvent. A hydrogel containing salt possesses conductivity on the proviso that it includes water, but the less water it contains, the stiffer and more brittle it will be. Therefore, the water retention capacity of a hydrogel is fundamental. [210] Previous reports have noted that if the hydrogel has a poor water retention capacity, it usually fails to work after a few hours due to drying out. [108] Thus, a primary goal of this thesis is to prepare, and 3D fabricate a tough, durable and transparent hydrogel sensor device. Additionally, studying the rheological characterisation for the AAm solution with UV curing is crucial to providing a better understanding of the gelation features of the gel before and after adding NaCl and LiCl by demonstrating the complex viscosity behaviour or the storage modulus behaviour to facilitate the process for hydrogel fabrication. Furthermore, measuring rheology is necessary for establishing the optimal conditions for extrusion printing for the PAAm gel precursor solution (the ink) at different temperatures. The prepared solution could be exposed to cooling to increase the viscosity of the gel which could enhance the extrusion process depending on the change in the viscosity of the prepared solution (ink). This can be measured at different temperatures during cooling using a rheometer. The hydrogel precursor solution will pattern and extrude into a defined shape by using a custom-built 3D printer based on a Sherline 1820 Machinery and Linex CNC-EMC software. The Dymax BlueWave 75 Rev 2.0 U Light Curing Spot Lamp System using a 19+ W cm^{-2} UV source with a 1 meter light guide was utilised to enhance the photo polymerisation reaction and hence, to cure the extruded ink. The ability of the precursor solution to construct by extrusion is dependent on viscosity. [211] The gelation is typically a crosslinking reaction initiated by UV light [208]. The gelation time can be identified either by crossing of G’ and G’’ or by reporting the time when the values of the complex viscosities became steady and stable. This technique will be adopted to 3D fabricate hydrogel strain sensor devices. These have potential useful applications since they mimic skin characteristics.

1.11.2 Hand-held printing

The development of skin mimic robotics involves a series of technologies that combine conventional fabrication processes such as microelectromechanical systems (MEMS) technology, complementary metal-oxide-semiconductor (CMOS) processes, and mechanical milling with submerging techniques such as

printable electronics, additive manufacturing, and a laser process. Different materials can be processed using these fabrication techniques, to produce structures in flexible sensors that are similar to the skin. [212] The 3D printing of stretchable soft robotics, with their ability to mechanically mimic skin, has been utilised in the manufacture of various devices including biomedical devices, [213–216] electronics, [217, 218] artificial tissues, organs, [219–221] and soft sensors. [111], [222–224] Current studies by Vlassak *et al*. [111] and Robinson *et al*. [225] enabled flexible ionogel and hydrogel extrusion respectively with an elastomer silicone using a direct ink extrusion printer. The direct ink writing technique offered easy printing of multiple materials including hydrogels at high resolution. [202], [226] However, there are several challenges with using this technique since it requires spatial planning to set up the computer and specific software as well as the cost of the devices. In this project, one of the goals was to introduce a straightforward extrusion system by using a hand-held printing device (Chapter six). The precursor solution uncross-linked ionic AAm is controllably driven out of a steel nozzle using physical or pneumatic pressure as an acrylate elastomer tape in a 2D shape. The nozzle head is directly connected by a transparent tube to the installed syringe in the syringe pump device. This type of printing employs an easy, quick and mobile system and could remove the need for high-cost printing devices for fabricating simple patterns of flexible materials to make soft strain gauge devices.

1.12 Hydrogel-forming materials

Preparing PAAm containing salt and PAAm with GG are examples of a wide range of hydrogel-forming materials. By changing the salt concentration or mixing PAAm with GG tough, strong, stretchable, conductive, and durable hydrogels could be developed to meet application demands especially in electronics, [92, 93] involving implantable, [94–96] and wearable [97–100] devices.

1.12.1 Gellan gum

Gellan gum (GG) is a water-soluble linear anionic polysaccharide formed by the fermentation of *Sphingomonas elodea*, a bacterium that exists on some varieties of lily pad. [84] The bacterium uses the GG to produce a biofilm which encapsulates the bacterium to host cell defences and antibiotics. [227] Recently many commercial applications have been found for this natural hydrogel. It is approved by the U.S. Food and Drug Administration and European Union (E418) as a food additive and an emulsifier in skin care products and medicine [228]. GG is currently applied in controlled drug delivery systems [229, 230] and interestingly, is being studied as a material for cellular scaffolds for tissue engineering. [231, 232]

GG is known as a viable gelling agent for solid culture media and has been utilised for plant tissue culture, [233, 234] bacterial culture, [235] and more recently to enhance mammalian cells. [236] The molecular structure is a tetra saccharide repeated unit made up of two glucose residues, a rhamnose residue and a glucuronic acid residue (Figure 1.21). [237] When fermented it becomes in a high acyl gels that forms two acyl units, acetate and glycerate localised on the same glucose molecule. On average, there is one glyceride unit per repeat, and the acetate group is on every second repeat. [238] The hydrogels produced by this form of GG are soft and elastic, but by eliminating the acyl groups with an alkali treatment, stiffer hydrogels are formed. [239]

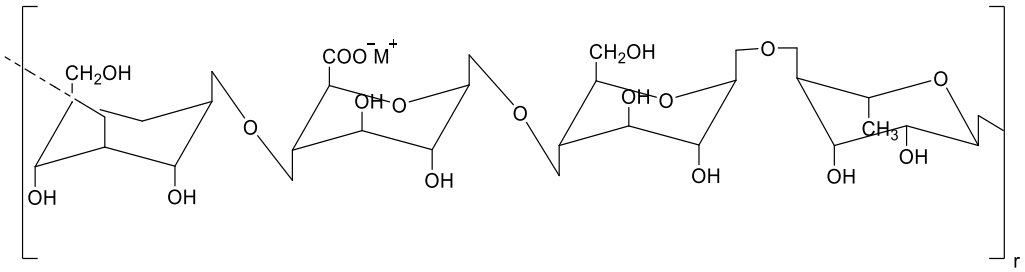

Figure 1.21 The molecular structure of a low acyl GG repeat unit. Reconstructed after adaption from reference [240]

The heating of a solution of GG results in polymer chains adopting a random coil conformation. This allows the polymer chains to transit into a double helix structure upon cooling of the solution. [241] A thermally reversible process occurs at low concentrations, so although the ordered state reveals a weak gel this is called a pseudo-gel. The formation of a true hydrogel is dependent upon the aggregation of helical sequences that are achieved by the addition of cross-links that present as bridges between the two polymer chains. [242] The addition of divalent cations (Ca^{2+} or Mg^{2+}) to the solution results in the formation of true gels. A crosslink is formed when a divalent cation is oxidised by the carboxylic acid groups on the glucuronic acid residue. A divalent cation can bind to two glucuronic acid residues, to form an ionic cross-link. [243, 244]

By breaking and reforming its cross-links, GG hydrogels can dissipate energy. A chemical hydrogel consists mostly of covalent bonds, so once they are cleaved, they will not reform. On the other hand, in hydrogels with ionic cross-links, such as GG, stress will create fractures at one of the ionic cross-links of the polymer network. The network is left with a free cation that is capable of cross-linking back into the network at another anionic site. [245] A consequence of the stress relaxation properties of ionic hydrogels

is that they will show plastic deformation when the hydrogels are strained. Plastic deformation occurs because new ionic bonds are formed in the stressed design. [246]

Although GG is exhibiting promise, it is not convenient for use in soft tissue medical implants due to its poor strength and toughness caused by its brittle, anionic, heterogeneous network structure. If the mechanical properties of GG could be improved, it would be a potential material for this application. It is hypothesised that the toughness of GG will be increased by combining it with PAAm. Low acyl GG is preferred over high acyl GG for the first network of a DN hydrogel system because it is stiff and brittle. [237]

1.12.2 PAAm

PAAm is identified using various names, including PAAm, polyacrylic amide, poly(1-carbamoylethylene); acronyms include Pam, PAAm, and PAM, while trade names include Cyanamer (American Cyanamid), Hercofloc (Hercules Chemical), Percol (Allied Colloids), Purifloc (Dow Chemical), and Separan (Dow Chemical). PAAm is significant in having an extremely high molecular weight (e.g. 3 to 15 million, average molecular weight) and has an excellent hydrophilic properties while also being nonionic. Its solubility in non-aqueous solvents is limited to those that are very polar (e.g., glycerol, formamide, and ethylene glycol). It is not soluble in many organic solvents including diethyl ether and aromatic hydrocarbons, and those that are otherwise miscible with water, e.g. methanol, ethanol, and acetone. This property forms the basis of many schemes of formulation analysis, i.e. via extracting unreacted AAm monomer from the polymer. [247] PAAm gel networks can be prepared in an aqueous medium and are broadly utilised in electrophoresis [248] for protein separations or as membranes [249] for protein isolations or blood purifications. Because these hydrogels are used in some applications where human contact is involved, the products are required to be non-toxic and biocompatible. PAAm is most often used to increase the viscosity of water (acting as a thickener), to encourage flocculation of particles present in water, [250-253] as a soil conditioning agent, [254-257] as hydrogels [258] including contact lenses, and in many biomedical applications. [259-262] Although the AAm monomer is toxic, it is generally agreed that PAAm is not. [263] Consequently, the ability to purify of PAAm gels by removing residual monomers and then keeping the gels in a stable form becomes an important issue. PAAm is a water-soluble polymer formed from AAm compound with the subunit molecular formula of (C_3H_5NO) [264] (Figure 1.22). PAAm is a synthetic chemical that can be developed to fit a wide range of applications. [265] It is synthesised by the polymerisation of AAm and a

low concentration of MBAAm which acts as a cross-linker with the functionality to make bonds to 4 different monomers. The reaction is a vinyl addition polymerisation initiated by the attack of free radicals [266] that can be created from persulfate ions. The rate of formation of the persulfate free radicals are accelerated by *N*,*N*,*N*',*N*'-tetramethylethylenediamine (TEMED). [36] This branching reaction forming a chemical hydrogel is randomly caused by MBAA while the linear AAm polymer chains elongate. PAAm hydrogels that are produced in this free radical polymerisation method have a heterogeneous network structure. MBAAm is highly reactive because of its high functionality. [36], [267]

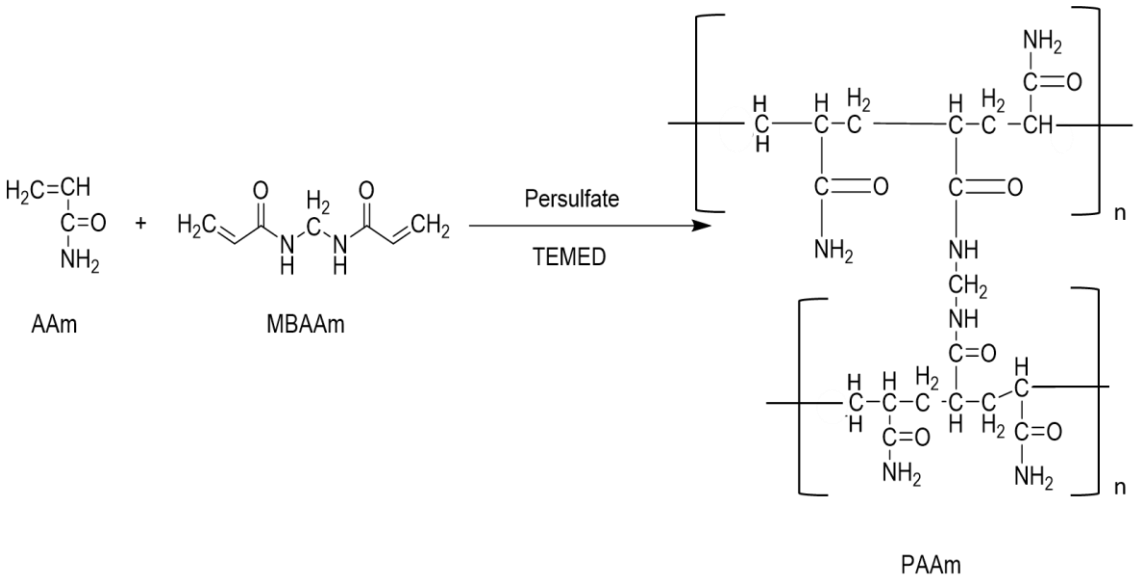

Figure 1.22 AAm polymerisation reaction. Reconstructed after adaption from reference [267]

Two forms of PAAm are commercially available; the first is a straight-chain, water-soluble PAAm and the second is cross-linked PAAm which is insoluble in water but absorbs huge quantities of water. The cross-linked PAAm polymer utilised in these studies was a cross-linked anionic copolymer, [268] the macromolecular and molecular structure of which is shown in figure 1.23.

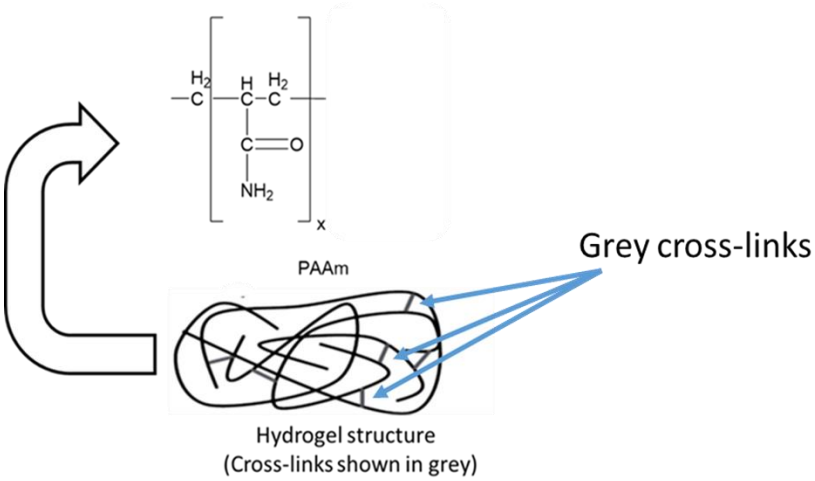

Figure 1.23 Macromolecular structure of cross-linked PAAm. Reconstructed after adaption from reference [269]

The mechanical properties of PAAm hydrogels are heavily influenced by the cross-linker concentration, which affects the hydrogel's heterogeneity. Tightly cross-linked PAAm hydrogels are brittle due to the formation of microgels. In contrast, loosely cross-linked PAAm hydrogels are soft and ductile. [229] The polymeric networks swelling behaviour is influenced by the polymer composition, i.e. by the synthetic conditions such as the AAm/MBAAm in polymeric networks and by the swelling media. It is a result of the presence of specific functional groups, these hydrogels have the potential to be utilised as colon-specific drug delivery devices, and also they can be implemented for water absorption from oil-water emulsions. [270–272]

1.12.3 PAAm containing salts

PAAm hydrogels containing salts possess fully transparency, remarkable stretchability, low cost, ionically conducting, and can fabricate easily. Hydrogels containing water and salts could be ionized into cation (C^+) and anion (A^-), that are responsible for conducting ions. Salt and water have two critical roles: salt offers the conducting ions while water serves as the solvent. [273]

The conduction behavior of an anionic hydrogel depends on the presence of two important factors, namely salt and water. However, the less water it contains, the stiffer it will be. Therefore, the water retention efficiency of a hydrogel is an essential factor affecting directly both mechanical and electrical properties. The hydrated ions are formed from bonding ions with water molecules. Ionic hydration, having salt and pure water gives significant variations in other properties including resistivity, volume, and freezing point.

[274-276]

For instance, a hydrogel comprising of water and NaCl ionised into sodium cations (Na^+) and chloride anions (Cl^-), forms conducting ions within the hydrogel. The hydrogel has been utilised as an electrode in a transparent loudspeaker. [108] However, this hydrogel has limited water retention efficiency, thus, it usually fails to work after a few hours due to drying out [273] One way to control the rate of water evaporation is to encapsulate the hydrogel; however, there are still some limitations that need to be resolved. The concept of binding the ions with water molecules in the ionic gel is explained by the correlation of water molecules binding to ions and the need to break these bonds to evaporate, while free water molecules evaporate naturally as shown in figure 1.24. [273] A higher degree of ionic hydration of the dissolved salt gives a stronger bond strength between the cation/anion-water molecule pairs and more bonded water molecules. [273]

Therefore, the water retention efficiency of a hydrogel can be improved by choosing the dissolved salt accurately such as LiCl or CsCl and using it at a specific concentration that gives optimum hydration, mechanical, and electrical performance. [273]

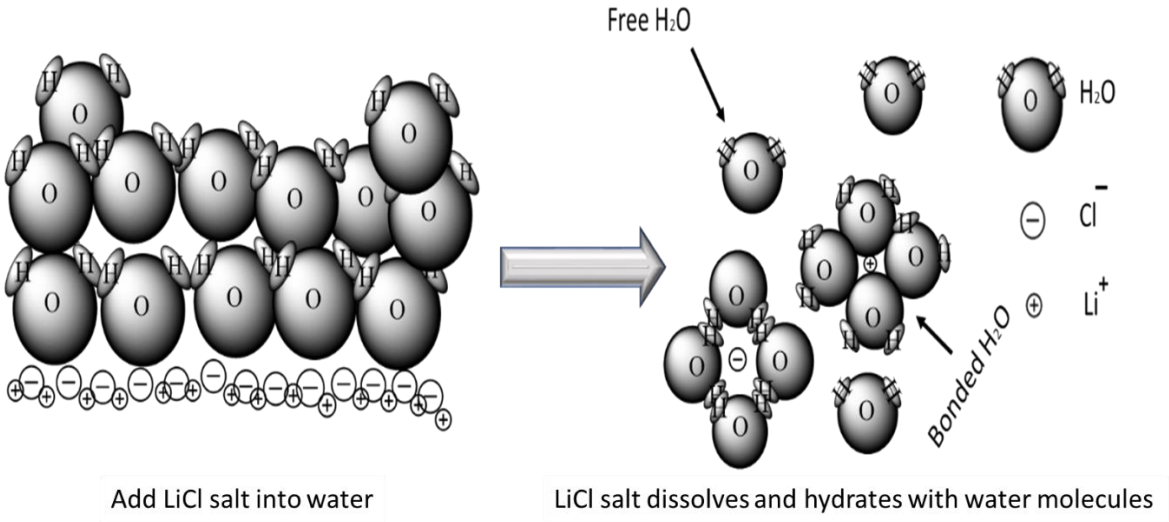

Figure 1.24 Schematic of the hydration of LiCl in water. Reconstructed after adaption from reference. [273]

1.12.4 Cellulose sponge

There is an intense interest to include porous materials derived from biopolymers to be utilised in different fields, such as separation, filtration, and load-bearing [277-280] as well as the potential applications as

water flow manipulators. An example of these biopolymers with these capabilities are sponges made of polysaccharide materials, which have been widely used for coupling the distinct properties of high porosity, low density, and high specific surface area, with the distinct characteristics of biodegradability, non-toxicity, low cost, easy modification, and abundance in nature. [281, 282]

One of these popular polysaccharides is the cellulose molecule, considered as a classical highly biocompatible biomaterial. [283] It is biosynthesised by various organisms and can be manufactured in continuous elementary microfibrils, having 5–10 nm diameter and 100 nm to several micrometres in length [284]. Cellulose is a polymer having chains cross-linked by hydrogen bonding, and water molecules that participate in the binding sites, causing the polymer volume to increase. Cellulose is composed of repeated units of glucose molecules bonded by (1,4)-β-glycosides which forms a repeating monosaccharide, and has six hydroxyl groups to form hydrogen bonding and intra and intermolecular bonding as shown in figure 1.25. These hydrogen bonds are the reason why cellulose has a physicochemical interaction with water and forms a porous structure; the process is known as hygroscopic expansion, conventionally observed in the detergent [285] and paint industries. [286]

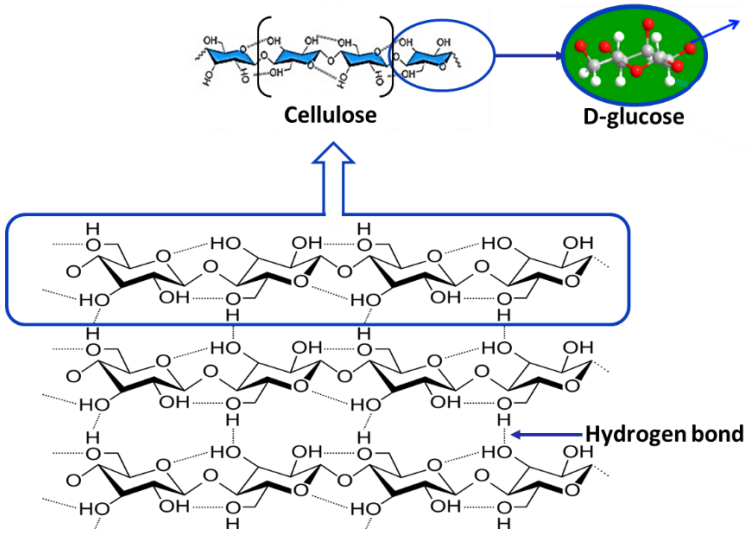

Figure 1.25 Cellulose molecules strands, bonded by hydrogen bonds (dashed) within and between cellulose molecules with a simple description to the hydrophilic site in glucose monosaccharide molecule. Reconstructed after adaption from reference [277-279]

Several recent studies reported cellulose in different applications such as tissue engineering and smart materials due to its promising features including cell attachment and proliferation and their similarities to the extracellular matrix. [277-290]

Cellulose sponges could also be used to fabricate ‘‘smart” materials after a suitable developmental process with a stimuli-responsive polymers. Some stimuli-responsive polymers such as hydrogels have been used for developing smart, responsive polymers composed of cellulose and other components using different hydrogels for their capability to reflect any reaction to external stimuli such as light, [291, 292] temperature, [293] pH [294, 295] and stress or strain. [188] These features were a topic of this thesis aims: to fabricate a hybridised cellulose sponge-hydrogel (as illustrated in chapter 7) responsive polymers as a strain gauge by crosslinking an ionic conductive hydrogel inside porous cellulose microsphere fibres in kitchen sponge and to prepare the hybrid in a relatively simple, cost-effective, and green approach. PAAm containing lithium chloride hydrogel was chosen for its high water retention capacity, conductivity and stretchability. Therefore, it has been used in this project as the main hydrogel component to be cross-linked within the cellulose sponge. The mechanical and the electrical properties of the PAAm-LiCl/Cellulose matrix were assessed and compared with the same properties of both dry and wet cellulose sponges. Furthermore, the water percentages, surface areas, volumes were determined for all sponge samples to study the effect of grafting the hydrogel and water molecules with the kitchen sponge on the mechanical and the electrical properties of the PAAm-LiCl/Cellulose matrix components.

Finally, a hybridised cellulose sponge-hydrogel strain gauge was fabricated after characterising the mechanical and electrical hysteresis as well as determining its gauge factor under multiple cycles.

1.12.5 PDMS sponge

Polydimethylsiloxane is a polymeric organosilicon compound also known as dimethicone or dimethylpolysiloxane. It is the simplest member of the silicone polymer family. PDMS, compared with other materials, has advantageous properties including typically optically transparent, chemically inert, non-toxic, is durable, and elastic [296-301]. PDMS is one of the most widely utilised silicone-based polymers and it refers to the group of silicones, which are produced from silicon, carbon, hydrogen and oxygen, and sometimes other elements as well as shown in figure 1.26. [302]

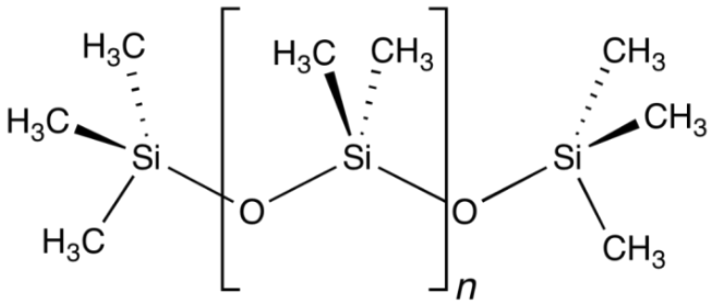

Figure 1.26 PDMS structural formula. Reconstructed after adapted from reference. [302]

PDMS molecular formula is $CH_3[Si(CH_3)_2O]nSi(CH_3)_3$, where n is the number of repeating monomer $[SiO(CH_3)_2]$ units. [302] the industrial synthesis proceeds from dimethyldichlorosilane and water producing hydrochloric acid from the polymerisation reaction as shown in the following net reaction: [303]

$$n\mathrm{Si(CH_3)_2Cl_2} + (n+1)\mathrm{H_2O} \longrightarrow \mathrm{HO[-Si(CH_3)_2O-]_nH} + 2n\mathrm{HCl}$$

PDMS was pioneered by both Dow Corning and General Electric Company in the middle of the 20th century.

Based on application needs, alterations to the viscoelastic properties can be accomplished by cross-linking the polymer. [304], e.g. cross-linking vinyl groups, or by adding fillers, such as silicon dioxide, to the polymer network. [305] Two methods have been reported for curing PDMS; either thermally [306] or by radiation. [307-309]

After the curing process, robust PDMS templates will have an external shiny hydrophobic surface. [310] The surface chemistry of this compound has a hydrophobic moiety making it difficult for the hydrophilic solvents to wet the PDMS surface. Plasma oxidation techniques and laser treatment were utilised to modify the surface hydrophobicity of the PDMS by adding silanol groups to the surface. This technique coats the PDMS surface with polar groups, enabling it to be miscible with water. [310]

PDMS does not swell with many chemical solvents. However, this material swells when treated with hydrophobic solvents. Most hydrophilic solvents such as water, nitromethane, acetonitrile, dimethylsulfoxide, and ethylene glycol, commonly utilised in analytical chemistry, swell the PDMS matrix the least. [311] This enables PDMS to be used in extracting analytes from water for quantitative analysis. However, many hydrophobic solvents such as pentane, diisopropylamine, triethylamine, and xylene can make a PDMS sponge swell significantly. [311] This phenomenon is frequently utilised for extraction the analytes from the PDMS sponge.

PDMS was widely involved in several electronic devices such as the stretchable soft materials for application in energy devices, and biomedical treatments. [312] PDMS electrodes have significant advantages over traditional electrodes in continuous health care monitoring. [312, 313] Current studies have determined that fabricating porous elastomeric polymers enhances their ability to deform and their failure strain dramatically exceeds that of their solid (i.e. nonporous) state. [314-316] Therefore, some studies were interested in increasing the PDMS porosity for oil/water separation [317, 318] by using either sugar [319-321] or NaCl [322] or even citric acid monohydrate. [319] Other studies focused on making porous PDMS sponges to fabricate conductor devices using brown [323] or white sugars [324] to synthesise porous templates saturated with carbon fibres. Also, other PDMS electronic devices were made by a conductive metal such as Au, [325, 326] Pt, [327] or Ti [328] film inside the PDMS sponge to make it acquire conductivity without reducing the PDMS porosity. Herein, chapter nine in this thesis investigated a new process for the preparation, characterisation and customization of a robust and conductive PDMS sponge electrode. Different PDMS/filler sponge templates were produced by mixing NaCl, LiCl and $CaCl_2$ as well as white and brown sugars, with uncured PDMS material. Porous PDMS templates were produced after curing then washing in water to remove the salts or the sugars fillers. The water removal efficiency was characterised for the produced washed PDMS/filler templates. Furthermore, the mechanical properties were examined and correlated to the microscale porosity. Furthermore, a PDMS/PAAm electrode was fabricated to initiate a novel conducting stretchable electrode. The mechanical and the electrical characteristics were conducted after encapsulating PAAm containing 6 M LiCl hydrogel sealed by VHB tape.

1.13 Aims

1.13.1 The aims of this project

Develop soft, flexible, durable, and conductive materials based on PAAm hydrogel for promising soft conducting and sensing applications.

1.13.2 The specific aims of this project

- To develop materials that have excellent mechanical and electrical properties achieving high flexibility, transparency, and reliable conductivity using PAAm containing different salts such as NaCl, LiCl or CsCl.
- To develop new methodologies for 3D printing soft conducting stretchable material that mimics the human skin. Furthermore, to optimise the durability as well as the mechanical and electrical features of this material to be approximately identical to the properties of that non-printing material. This aim can be achieved by preparing PAAm hydrogel after adding different concentrations of soluble salts such as LiCl and NaCl.
- To employ PAAm polymer compound to synthesis variant materials after either cross-linking it with different materials such as GG/calcium chloride and cellulose sponge or encapsulating it within porous PDMS sponge.
- To study water retention capacity of each prepared hydrogel during sequential intervals to demonstrate the mechanical and the electrical durability of these types of hydrogels.
- To fabricate a wearable soft sensing device after characterising its mechanical and electrical characterisations under various conditions aiming to innovate a wearable device that has the ability to transmit the signal coded using Bluetooth device to the mobile phone with a specific app.
- To fabricate stretchable electrodes, consists of PAAm containing LiCl or CsCl hydrogel composites for the potential application as stretchable conducting devices.
- To investigate the mechanical and electrical durability of some of the fabricated soft sensor devices such as in SSD and HEH after simultaneous *in situ* characterisation initially and after one year in response to multiple cycles of different kinds of stresses such as tensile or compressive test.

Chapter 2

Experimental Techniques

2.1 Materials & Methods

Acrylamide monomer (AAm) (99.9 %), *N,N′*-methylenebis(acrylamide) (MBAAm), α-ketoglutaric acid, ammonium persulfate (APS), potassium persulfate (KPS), sodium chloride (NaCl) (≥99.9%), calcium chloride ($CaCl_2$) (≥99.9 %), lithium chloride (LiCl) (≥99.9 %), cesium chloride (CsCl) (≥99.9 %) and tetramethylethylenediamine (TEMED) were purchased from Sigma Aldrich, Australia. Cellulose kitchen sponges, white and brown sugar were purchased from Aldi, Australia. Sylgard 184 Silicone Elastomer kit which contains the silicone elastomer base and silicone elastomer curing agent was purchased from Dow Corning Australia. Low acyl gellan gum (GG) was received as a gift from CP Kelco (Gelzan). Very high bonded (VHB) tape (22 mm width x 0.5 mm height) double sided transparent foam tape made from high performance acrylic adhesives was purchased from 3M.

2.2 Sample preparation:

2.2.1 Preparation of PAAm

PAAm hydrogel-forming solutions were synthesized as follows: A solution of 16 % (w/v) of AAm in Milli-Q water at room temperature (21-23 ^{o}C) was added 0.1 % (w/v) MBAAm and 0.014 % (w/v) α-ketoglutaric acid as the cross-linking co-polymer and photoinitiator, respectively. The gel solution was stirred and degassed in a vacuum desiccator for 20 minutes under 0.1 bar pressure, at room temperature (21-23 ^{o}C). AAm solutions were poured into plastic moulds depending on the required characterisation i.e mechanical or electrical examinations and cross-linked using a Dymax BlueWave 75 Rev 2.0 UV Light at 1.15 W/cm^2 intensity.

Thermally cross-linked PAAm hydrogels were synthesised as previously, however, 0.05 % (w/v) APS was used to replace α-ketoglutaric acid. The gelation process was carried out by adding 80 µL of TEMED as an accelerator.

2.2.2 Preparation of PAAm containing salt hydrogel

The hydrogels were synthesized using 16 % (w/v) AAm powder monomer and 15.7 % (w/v) (2.7 M) or 23.3 % (w/v) (4 M) NaCl or 16.9 % (w/v) (4 M), 25.4 % (w/v) (6 M), 33.9 % (w/v) (8 M), 38.2 % (w/v) (9 M) or 42.33 % (w/v) (10 M) LiCl or 50 % (w/v) (2.97 M) CsCl into deionized water at room temperature RT. Then 0.1 % (w/v) of MBAAm and 0.014 % (w/v) of α-ketoglutaric acid were added. The gel solution

was stirred using a magnetic stirrer (Stuart) and degassed in a vacuum desiccator (Robinair) for 20 minutes under 0.1 bar at RT. After the degassing process, the AAm solution was poured into sample mould suited to the required characterisation technique such as mechanical and electrical testing of the resultant hydrogel. These hydrogels were cured via UV irradiation.

For mechanical tensile testing, solutions were poured into a 13 cm × 13 cm box, cured and cut into "dog-bone" shapes (conforming to JIS – K625060). Compression testing was carried out on gels which were cast and cured in cylindrical moulds (diameter = 18 mm, height = 10 mm). For electrical characterisation, hydrogel samples (height = 6 mm, width = 5 mm) of varying length between 5 and 25 mm were cast in plastic moulds with reticulated vitreous carbon foam 1 cm ×1 cm ×2 cm (RVC, ERG Aerospace, 20 pores per inch) at each end. Wires were connected directly to the RVC electrodes above the height of the gel samples.

2.2.3 Preparation of ICE hydrogel:

Hydrogels were prepared by combining hot solutions of the biopolymer GG and the monomer AAm, which were cross-linked simultaneously through the addition of the relevant cross-linking agents, i.e. $CaCl_2$ and MBAAm. GG/PAAm hydrogels were synthesized by a simultaneous network formation technique. Prior to producing any hydrogels, the following solutions were prepared: A stock solution of TEMED (0.5 M) was prepared as an accelerator by dissoving TEMED (0.24 mL) in water (4 mL). A stock solution of 0.1 M calcium chloride was prepared and was heated to 70 °C for the preparation of the hydrogels. A stock solution of the initiator KPS was also prepared by dissolving KPS (25 mg) in water (2 mL).

2.2.3.1 Preparation of ICE network hydrogels with different ratios of covalent and ionic cross-linkers

The preparation of ICE network hydrogel to study the effect of covalent cross-likers on the mechanical performance required the following compounds: adding 300 mg of GG with 2.4 mg of $CaCl_2$. 3 % (w/v) AAm has been used with different concentrations of MBAAm ranged between (0.5-5) % (w/v).

The preparation of ICE network hydrogels to study the effect of ionic cross-linkers on the mechanical behaviour required the following compound: GG (300 mg) was added to nine different $CaCl_2$ solutions (0.00, 0.01, 0.05, 0.08, 0.10, 0.25, 0.50, 0.70 and 1.00 M, 600 µL) followed by the addition of AAm (50 mL, 3% w/v) and MBAAm (50 mL, 4.44% w/v) solution to each.

2.2.3.2 Preparation of ICE network hydrogels with different ratios of covalent and ionic polymers and keeping the total amount of the polymer constant.

To study the influence of changing the ionic and covalent polymer ratio on the mechanical characterisations for the ICE network hydrogels, the following compounds were used with different concentrations ratios for both GG and AAm ranged from (3.774 GG+1.776 AAm) % (w/v) to (0.33 GG+5.22 AAm) % (w/v) with 4.44 % (w/v) MBAAm and 2.4 mg $CaCl_2$. For each hydrogel prepared, 22.5 mL of Milli-Q (resistivity 18.2 MΩ cm) water was added to a beaker and heated to 70 ^{o}C. KPS was added followed by a 60 µL of TEMED and the solution quickly poured the hot solution into a cylindrical plastic mould 10 mm high and 17 mm in diameter. The resulting hot solution was transferred to a mould in a desiccator, which was then evacuated (to 0.100 bar) and held for two hours after which the formed hydrogels were removed from moulds. [239]

2.2.4 Preparation of cellulose sponge-hydrogel hybrid samples

The cellulose sponge samples were cut depending on the characterisation type as shown in table 2.1.

Table 2.1 shows the sponge samples name with their dimensions for compression and tensile test analysis and impedance characterisations.

Cellulose sponge sample name	Sponge dimension for compression test (mm)		Sponge dimension for Tensile test (mm)		Sponge dimension for Impedance test (mm)	
Cellulose sponge	Length	12	Length	40	Length	25
	Width	12	Width	11	Width	10
	Height	13	Height	12	Height	10
Dry sponge	Length	12	Length	40	Length	25
	Width	12	Width	11	Width	10
	Height	12	Height	11	Height	10
Wet sponge	Length	12	Length	40	Length	25
	Width	12	Width	12	Width	10
	Height	12	Height	11	Height	10
Sponge-PPAm hydrogel composite	Length	16	Length	40	Length	25
	Width	12	Width	12	Width	10
	Height	12	Height	9	Height	10
Sponge-PPAm containing 6M LiCl	Length	12	Length	40	Length	25
	Width	12	Width	11	Width	10
	Height	13	Height	12	Height	10

The dry sponge samples were prepared by placing them in the oven at 70 °C for one hour. However, the wet sponges were prepared by immersing them in RO water at room temperature for 5 seconds and then squeezed until no dripping water come from the sponges. All the sponge samples were weighed using the electronic balance before characterisation. Some tensile and compression samples of dry and wet sponges displayed slightly different dimension. This is due to the shrinking or swelling after treating them with heat or water. Moreover, the sponge-hydrogel composite revealed a small difference compared to other sponges

due to the cross-linking between the hydrogel and the sponge.

The PAAm hydrogel was prepared by adding 16 % (w/v) AAm, 0.2 % (w/v) APS, 0.05 % (w/v) MBAAm to RO water and 0.1 % (v/v) of TEMED and poured all mixed solution directly into a sample moulds with diameter: 10 mm height and 16 mm diameter for compression test analysis and length: 40 mm, width 14 mm, height 4 mm for tensile test analysis and length: 25 mm, width 10 mm, height 10 mm for impedance analysis allowing 2 minutes for gelation process at room temperature. All hydrogels were degassed in a vacuum desiccator (Robinair) for 20 minutes to draw the oxygen from the sample prior to characterisation. PAAm-sponge hybrids were prepared by cutting 100% natural Cellulose kitchen sponge and soaking cellulose sponge samples in 16 % (w/v) AAm, 0.2 % (w/v) APS, 0.05 % (w/v) MBAAm. TEMED 0.1 % (v/v) was added by pouring directly on the sponge samples and allowed to gel at room temperature. The prepared samples were cut in specific dimensions as described in table 2.1. PAAm containing 6 M LiCl was also prepared and characterised mechanically and electrically before and after soaking the cellulose sponge in the gel making the PAAm LiCl salt containing hydrogel. Accordingly, PAAm containing salt-sponge hybrids were prepared by soaking samples of sponge cellulose in the PAAm containing salt solution mixture in specific dimensions as described in table 2.1 and figure 2.1b. For electrical characterisation two 50 mm carbon fibre ribbons were attached at each end as electrodes as shown in figure 2.1c.

For electrical, mechanical compression and tensile testing of prepared hydrogels, AAm precursor solutions were poured into a 15 cm x 15 cm box, cured and cut into cubic and rectangular shapes as shown in table 2.1 and figure 2.1d.

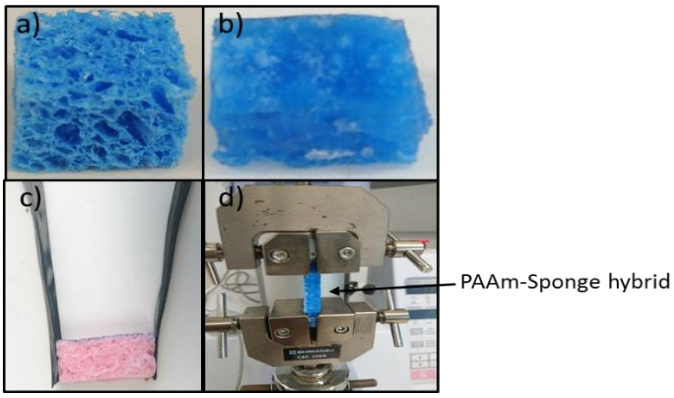

Figure 2.1 Typical photo for a) cellulose sponge sample for compression test b) cellulose sponge and ionic hydrogel hybrid sample for compression test c) cellulose sponge sample with carbon fibre ribbon electrodes for impedance test d) cellulose sponge and ionic hydrogel hybrid sample for tensile test.

2.2.5 Preparation of PDMS samples

Porous PDMS sponge templates were fabricated by adding 1 g of Sylgard 184 Silicone Elastomer to 3 g of LiCl, $CaCl_2$, NaCl, white sugar or brown sugar. PDMS cross-linker silicone elastomer curing agent was added 0.1 g and stirred for 5 minutes. The mixture was cast, poured into a mould, and heated at 70 ^{o}C in the oven for 30 minutes before the cross-linked PDMS was removed from the mould and placed into a 120 ^{o}C oven for another 30 minutes to process the cross-linking. The PDMS cylinder templates were cut from these PDMS samples using a hole-punch to produce PDMS samples of approximately 15 mm diameter and 4 mm height for the hydrophilicity test and dog bones of approximately 4 mm thickness, neck width of 3 mm and a gauge length of 14 mm for tensile testing as shown in figure 2.2. These samples were soaked in milli-Q water (resistivity, 18.2 MΩ cm) for 6 hours to remove the hard filler templates. The remaining water was removed from the sponge by repeatedly squeezing the sponges in a paper towel and oven drying for 30 minutes at 120 ^{o}C.

Figure 2.2 Photos of PDMS samples for both a) the hydrophilicity test and b) tensile test.

2.3 Device preparation:

Different devices were prepared after each preparation and characterisation.

2.3.1 Wearable remote soft sensor device:

2.3.1a Soft sensor device preparation

The hydrogel sensor device was prepared by using a perforated VHB acrylic tape (3M) 1 cm height having 5 cm^2 area. This VHB perforated layer sandwiched between two slides of PAAm+9 M LiCl hydrogels each layer 2 mm height and 30 mm diameter that was contacted to two wired electrodes. All components were covered by VHB tapes to electrically isolate the devices as shown in figure 2.3 (a and b).

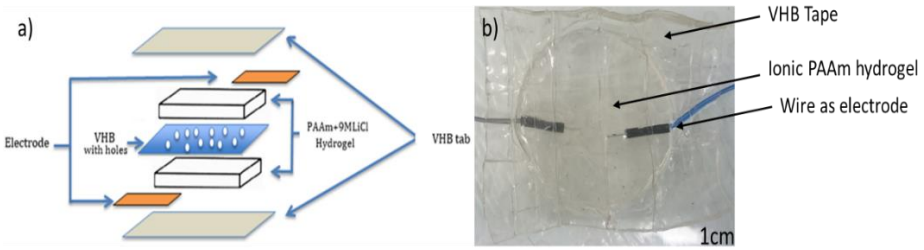

Figure 2.3 a) A typical figure of PAAm+9 M LiCl hydrogel sensor device components with b) a typical photo for the soft sensor device.

2.3.1b Wireless sensor device connection

The SSD was attached to the Arduino device that contained three slots (RFD 22102, RFD 22122, and RFD22128) as shown in figure 2.4.

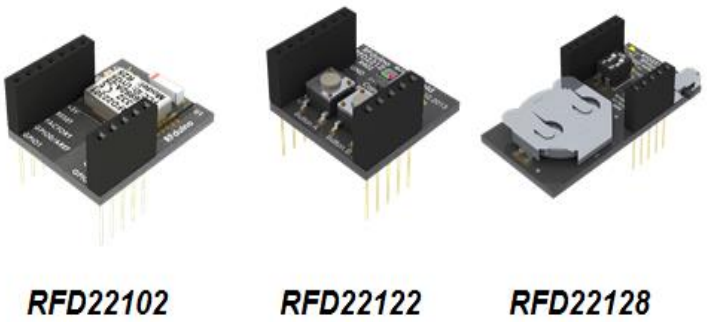

Figure 2.4 Three pictures of Bluetooth pressure sensor device kit (RFD 22102, RFD 22122 and RFD128). This figure is modified after adaption from reference [189].

Each circuit device has a specific role and can be illustrated as the following: The RFD22128 CR2032 coin battery shield, which has the ability to provide electrical charges from a 3 V battery connected to the

hydrogel sensor device via electrodes. The RFD22122 RGB LED / pushbutton shield plugs onto the RFduino; it has two button inputs with a 10 k resistor; it has the ability to transfer the electrical signal from the prepared SSD after the hydrogel sensor is pressed. Meanwhile, RFD22102 RFduino is a Bluetooth 4.0 low energy BLE RF module with built-in ARM cortex M0 microcontroller for rapid development and prototyping projects which has the ability to transfer and upload the created signal to a Bluetooth formed/framed/extension signal ready to be received by any Bluetooth mobile phone application via Bluetooth compatible devices such as mobile phones and then sending it to the database center through internet IP connection technology. [189]

The device was paired with a mobile phone wirelessly; Li battery power supply was substituted with a solar cell power bank, connected to the Arduino slots.

A box was fabricated to contain the Arduino slots that would be connected to the SSD and to be wearable as shown in figure 2.5:

Figure 2.5 Shows images of a) and b) 3D fabricated plastic box with its lid c) Arduino device inside a fabricated box connected to the SSD over a surf board d) A covered Arduino device inside a fabricated box connected to the SSD bonded by a rubber band over a helmet and e) an Arduino device inside a 3D fabricated box with solar cell power bank connected to the SSD and bonded on a bicycle helmet.

2.3.2 Cellulose sponge-hydrogel hybrid strain gauge preparation

The hydrogel/sponge hybrid gauge was prepared by sandwiching two VHB layers on a piece of PAAm containing salt-sponge hybrid having dimensions 70 mm length 12 mm width x 11 mm height. Two of 10 cm carbon fibres ribbons were connected to each end of hydrogel/sponge piece as shown in figure 2.6 a and b:

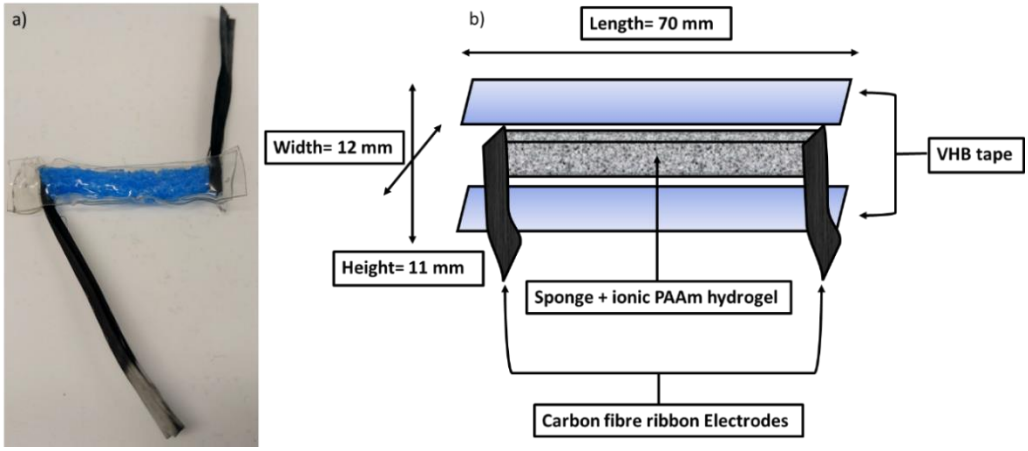

Figure 2.6 a) A photo of a soft strain gauge device made from cellulose sponge and PAAm with LiCl hydrogel. b) The typical figure describes the soft strain gauge device components. This figure was produced by the candidate.

2.3.3 PDMS/PAAm electrode preparation

The PAAm containing LiCl hydrogel was prepared by mixing 16% (w/v) acrylamide, 25.4% (w/v) lithium chloride and 0.05 % (w/v) MBAAm in 100 mL of milli-Q water in a beaker. After a homogenous mixture was formed 0.2 % (w/v) AP was added. The mixture was poured into a weighing boat having length by the width of 13 cm by 13 cm and a height of 2 cm. The solutions were left to cure for 24 hours at room temperature and cut into dimensions: 40 mm length, 5 mm width, and 5 mm height. The patterned hydrogel samples were sealed in two layers of VHB tape. The hydrogel was cast in a 10 mm wide, 10 mm high and 45 mm long mould with 4 grams of a 1:3 mixtures of PDMS and $CaCl_2$, respectively. Samples were cured in an oven and any salt filler present washed off as described in section 2.2.5 giving a device as shown in figure 2.7.

Figure 2.7 PAAm containing LiCl hydrogel embedded within PDMS.

2.3.4 Conductive hydrogel bridge for oxygen and hydrogen evolution reaction preparation

PAAm hydrogel-forming solution was synthesized by adding 20 % (w/v) CsCl to milli-Q water at RT. AAm monomer powder was added to yield a 4 % (w/v) AAm concentration. Then 0.1 % (w/v) of MBAAm and 0.014 % (w/v) of α-ketoglutaric acid were added as cross-linking co-polymer and photo-initiator, respectively. The gel solution was stirred and degassed in a vacuum desiccator for 20 minutes under 0.1 bar pressure, at room temperature. The AAm solution was poured into a U-shaped glass mould (diameter = 20 mm, length = 130 mm) as shown in figure 2.8. Solutions were cross-linked using UV Light at 1.15 W/cm^2 intensity.

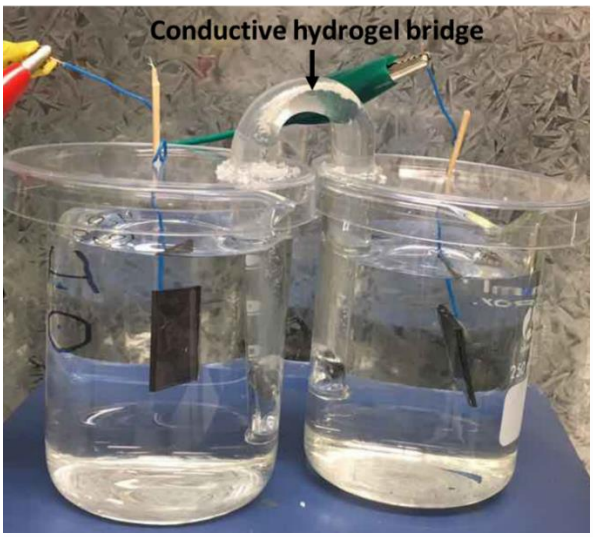

Figure 2.8 H_2 and O_2 production experiment by water splitting process using conductive hydrogel as a salt bridge.

2.4 3D printing:

2.4.1 Extrusion printing

3D extrusion printing was performed using an adapted CNC milling machine (Sherline Products, 5400) which acted as an x-y positioning stage. An independent linear actuator (Zaber Technologies, T-LA60A) was mounted onto the z-axis of the milling machine and used as a syringe pump. PAAm lines were direct-

written by depressing the syringe at a constant speed of 28 µm.sec^{-1}, with stage jog speed of 134-162 mm. minute^{-1} and syringe-tip height of 0.39 mm. The extruded ink was cross-linked by UV photopolymerisation during the extrusion process and between each printed layer (10 minutes) as illustrated in figure 2.9a. Layers were dried with nitrogen gas for 2 minutes prior to addition of the following layer. Dog-bone (width 1.5 cm, thickness 0.5 cm, length 4 cm) and rectangular (width 2.5 cm, thickness 0.5 cm) patterns (Figure 2.9b) were printed for mechanical and electrical characterisation, respectively.

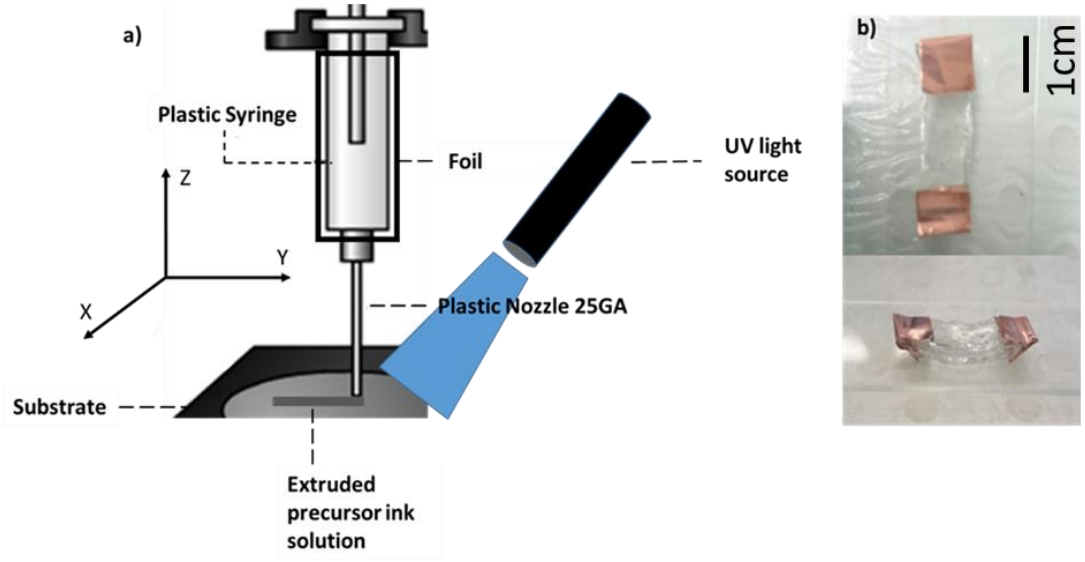

Figure 2.9 a) A schematic figure of an extrusion printer having 5 mL syringe with a 25GA tip used in extruding the precursor ink solution; the syringe set in the extrusion device covered by foil using Sherline device to extrude AAm ink solution on the substrate slide then curing the extruded ink solution by direct focusing UV light source on the extruded position b) A typical image of 3D fabricated hydrogel sample bonded with cupric electrodes. This figure was produced by the candidate.

2.4.2 3D printing by hand-held printing technique for strain gauge fabrication

The ionic AAm ink solution was prepared by adding 4 M of LiCl to fabricate ionic PAAm hydrogel in U and/or zigzag shape patterns having length 60 mm, 0.75 mm width and 0.8 mm height (Figure 2.9c). KDS Scientific LEGATO 100 Syringe Pump was used for employing the hand-held extrusion technique to extrude the ionic AAm ink solution on a VHB elastomeric substrate layer allowing for preparing a soft elastomer hybrid for as shown in (Figure 2.10 a). The UV light was set directly and applied to the extruded position in order to cure the ink solution (Figure 2.10 b and d). A steel syringe with 21 GA tips were used in extruding from a 5 mL syringe having 13 mm inside diameter. The extruding process was performed at

0.5 mL. min.$^{-1}$ extrusion rate.

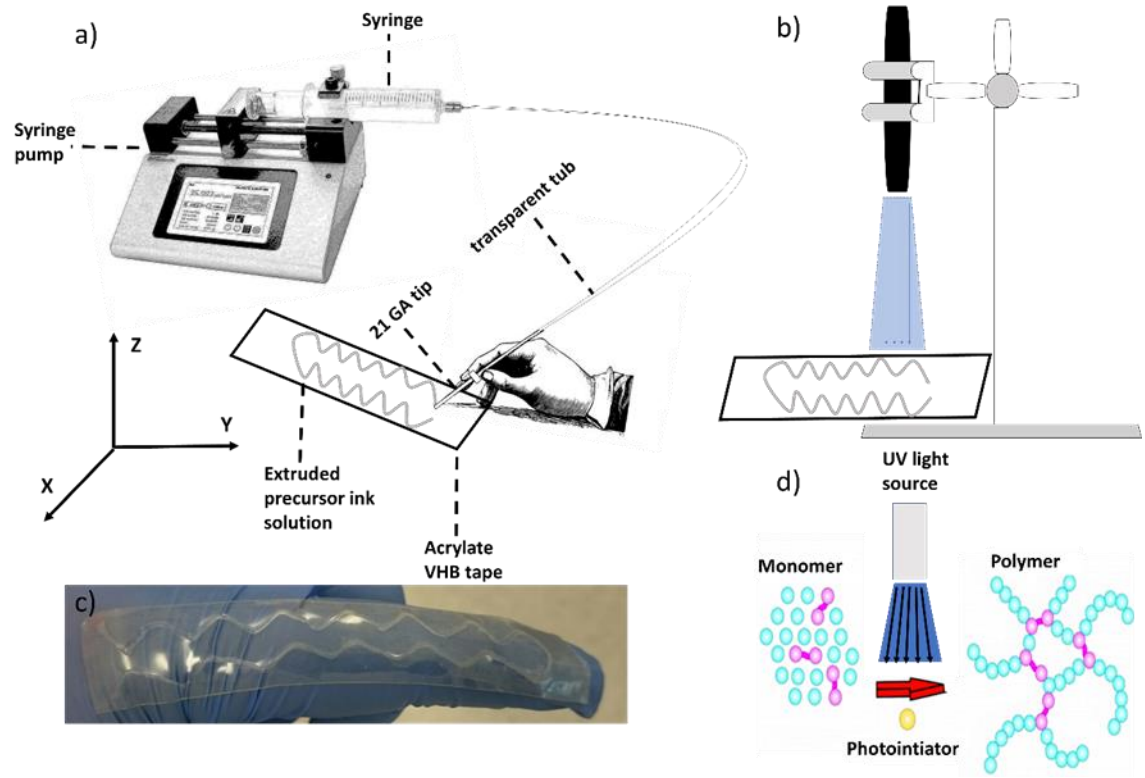

Figure 2.10 Typical figures describing a) the hand-held extrusion technique on an elastomeric substrate b) focusing UV lamp on the extruded solution for gelation process c) a typical photo for a printed gel over elastomeric substrate (VHB) d) illustrating the photo-initiation process to form the hydrogel polymer by focusing UV light source. This figure was produced by the candidate.

2.5 Characterisation Techniques:

Different instruments were used to characterise the mechanical, electrical, rheological, stability and morphological properties for the prepared samples and devices.

2.5.1 Mechanical analysis:

Two different types of mechanical characterisations were performed to assess the mechanical properties of the samples and the devices using Shimadzu mechanical tester (Figure 2.11).

2.5.1a Compression testing

Testing was conducted in the compression analysis mode using steel compression plates, diameter 12 cm (Figure 2.1) and 2 cm diameter. A 500 N load cell was used for all samples. Data were collected using the Trapezium X software. Samples were compressed at a rate of 10 m.min^{-1} for all the prepared samples. All

the samples either compressed until failure or under multiple cycles. Stress-strain data were collected for determining the compression strain to failure (ε_c), compression secant modulus at different strain percentages (E_c), compression stress to failure (σ_c) and work of compression (W_c) : [128]

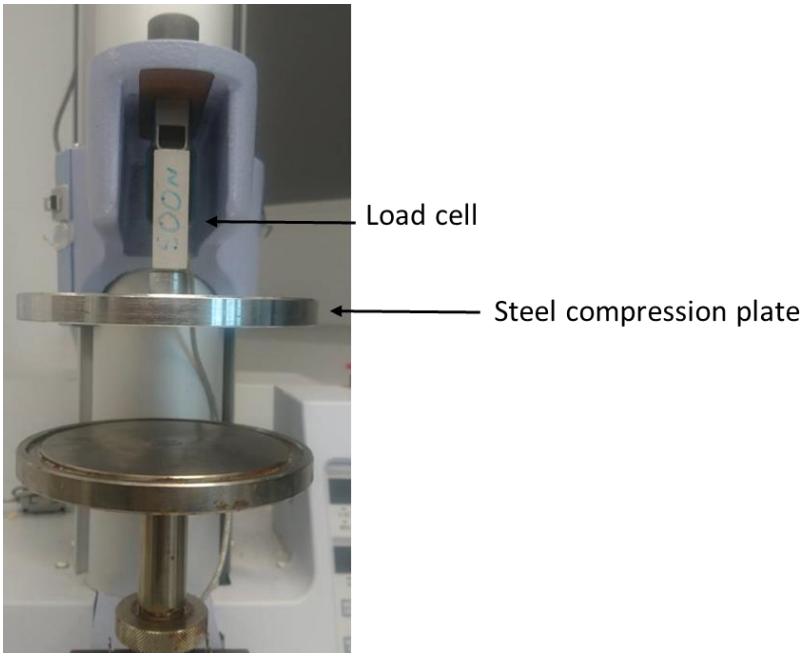

Figure 2.11 Picture of Shimadzu EZ-S universal mechanical tester.

2.5.1b Tensile test analysis

Tensile testing was carried out with a 50 N load cell at an extension rate of 4 mm.min^{-1} until failure and/or under multiple cycles for all samples at RT except the PDMS specimens were extended at 10 mm.min^{-1}. Testing was conducted in the tensile analysis mode using four steel clamps. The resulting stress-strain data was utilised for determining the elongation to failure (ε_t), Young's modulus at different strain percentages (E_t), tensile fracture stress (σ_t), work of extension (W). [329]

2.5.2 Rheological Testing

Oscillatory shear rheological measurements were conducted with a digital rheometer (Anton Paar, Physica MCR 301, parallel plate) with a Peltier temperature-controlled stage as shown in figure 2.12. Viscoelastic characteristics were measured as a function of temperature and time at a constant shear rate of 100 s^{-1}, using a cone and plate measuring system with 49.97 mm diameter, angle 0.992 °, 0.55 mL sample volume and a heat controlled sample stage at a temperature range between 16 to -6 °C.

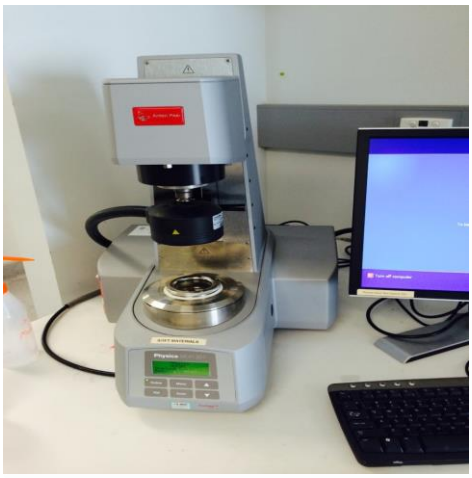

Figure 2.12 Typical picture of the rheometry instrument.

2.5.3 Electrical characterisation

The impedance measurements were obtained using a custom-built setup, described in previous studies. [173] Briefly, a 1 V peak voltage was applied using a waveform generator (Agilent U2761A), through the circuit with a known resistor (R_k, 10 kΩ) in series with the hydrogel sample. The circuit current was calculated across the known resistor with an oscilloscope (Agilent U2701A) and applied to the unknown samples or devices to measure the electrical impedance as shown in figure 2.13.

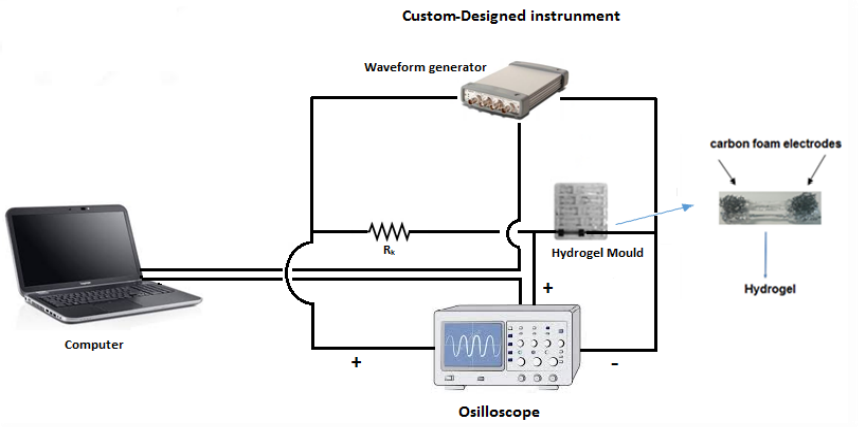

Figure 2.13 Schematic of custom-built electrical impedance analyser with hydrogel mould containing conducting carbon foam electrodes. This figure was modified after adaption from [173]

However, the impedance behaviour of the cellulose sponge and the PDMS sponge samples were characterised using a potentiostat (Gamry Reference 600). The electrical analysis was performed by applying 10 mV (AC rms) and 0.1 V (DC) between frequencies of 1 Hz and 100 kHz. The impedance

measurements were conducted on all samples with a cross-sectional area of 1 cm^2 except cellulose sponge samples which was described in table 2.1. All samples were examined at five different lengths (0.5 cm - 2.5 cm).

Furthermore, the resistance was characterised for the fabricated devices before and/or after applying DC voltage source from a 3 V battery. Strain-gauge devices were tested with the mechanical analyzer instrument (Shimadzu EZ-S, Japan) and a multi-meter device (Keysight) with Keysight Bench View software (Figures 2.14a and b).

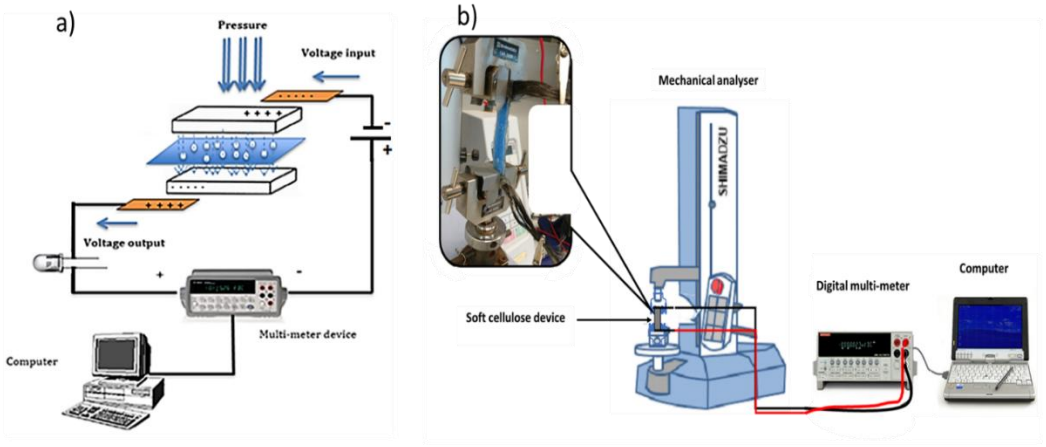

Electrical examination during compression test Electrical examination during tensile test

Figure 2.14 Schematic figure that describes the electrical characterisations during both a) compression test and b) tensile test on the samples. This figure was produced by the candidate.

Some devices such as soft strain gauge and hydrogel-sponge hybrid strain gauge devices were electrically characterised by sticking the devices over the finger joint as displayed in figure 2.15 a and b.

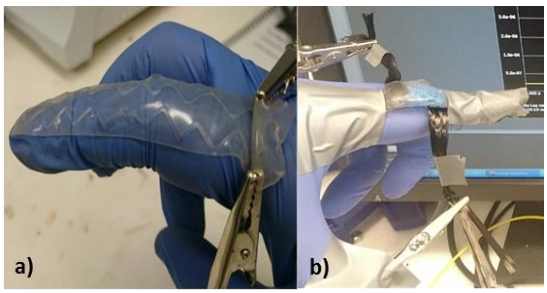

Figure 2.15 Two photos describing a) a printed hydrogel on an elastomeric substrate connected to two alligator clamps electrodes bonded over the finger joint and b) hydrogel-sponge hybrid strain gauge device attached to two carbon fibre ribbons on each end and covered by two VHB layers bonded over the finger joint.

2.5.4 Characterising durability testing

The samples and devices characterised for water retention by measuring the weight change of the samples during the storage period or by characterising the device mechanical and electrical properties as mentioned previously after storing it for a period. The weight of the samples was determined using a digital lab balance at RT.

2.5.5 Morphology characterisations

The morphological properties were characterised either by taking a photo for some samples and devices using Sony digital camera and to determine the pore size for the fabricated PDMS samples. Leica Z16 microscope system (Figure 2.16) was used for taking photos for sponge samples while the pore sizes of the PDMS sponge samples were obtained using a Leica DM4000–6000 optical microscope. The average pore sizes were determined using an image-processing program Leica Application Suite (LAS) software.

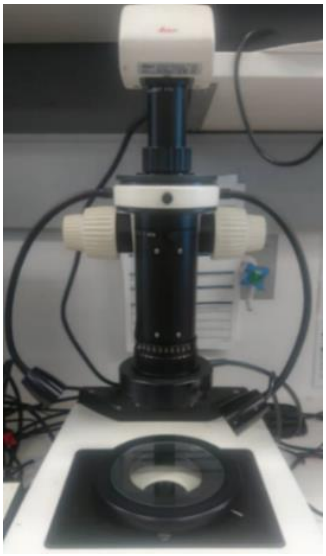

Figure 2.16 Leica Z16 microscope system

Chapter 3

Electrical investigations for optimised mechanical properties of ionic-covalent entanglements hydrogels

3.0 Introduction

The main aim of this project is to examine the electrical and mechanical behavior for the optimized mechanical properties of ionic-covalent entanglement GG/PAAm hydrogels. The hydrogels are characterised using compressive stress-strain testing and oscillatory shear rheological measurements. The specific aims are as follows: Firstly, assess the effect on the mechanical characteristic of changing the Ca^{+2} ionic cross-linker concentration. Secondly, assess the effects on mechanical characteristics of changing the MBAAm covalent cross-linker concentration. Thirdly, studying the effects on mechanical characteristics of changing the ratios of the GG and PAAm with keeping the amount of the polymer constant (1:4). Fourthly, investigating the mechanical features of the synthesized hydrogels by using two techniques, these are compression stress-strain test by determining compressive failure strain (ε), compressive tangent modulus overstrain (E), compressive failure stress (σ) and compressive strain energy to failure (W) and examining the oscillatory rheology test by determining the storage modulus or the linear viscoelastic region LVE.

Fifthly, comparing the findings from both techniques could enhance the conclusion of this study to select the exact concentrations ratios for the hydrogel chemical components that shows optimum mechanical properties for the synthesized ICE network hydrogels. Finally, characterizing the mechanical properties using compression test analysis and the electrical properties before/after soaking the optimized ratio of the ICE hydrogel in 2.7 M NaCl for 24 hours.

3.1 Compression strain stress measurements:

Different concentrations of ICE network hydrogels of GG/ PAAm hydrogels were synthesised using the simultaneous network formation technique. Parameters such as compressive failure stress **(σ)**; compressive failure strain **(ε)**; compressive tangent modulus **(Ec)** and work of compression **(W)** were adopted to demonstrate the mechanical behaviours for different ratio concentrations of the hydrogel components. Figure 3.1 illustrates a typical example of an ICE hydrogel sample during a compression test.

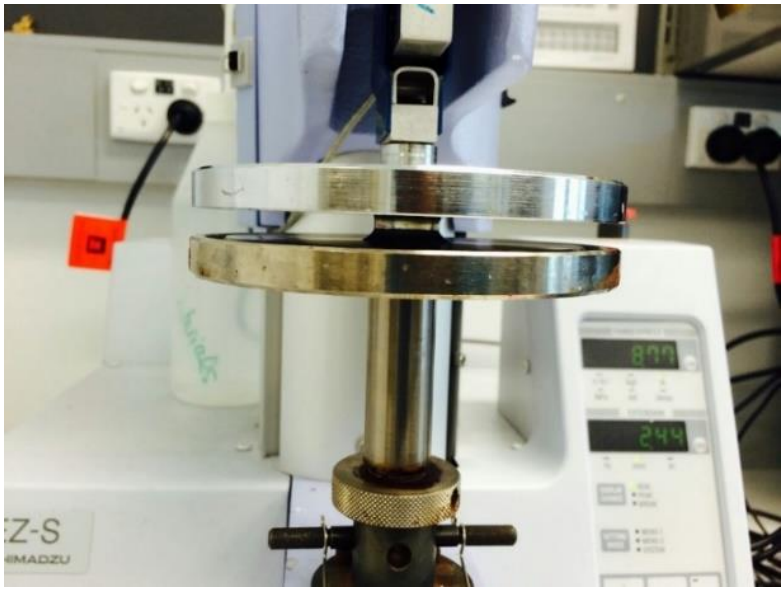

Figure 3.1 A typical picture of ICE hydrogel during a compression test.

3.1.1 Effect of the covalent crosslink density

To investigate the impact of the covalent cross-links of PAAm on the overall gel characterisations, hybrid gels with different concentrations of the cross-linker MBAAm were prepared. The ICE network hydrogels were prepared as follows: To solutions of MBAAm (0.5, 0.8, 1.0, 2.0, 2.7, 3.0, 3.1, 4.0 and 5.0% w/v, 50 mL each) was added a solution (50 mL) prepared by adding GG (300 mg), and CaCl2 (2.4 mg), to AAm solution (50 mL, 3% w/v). These gels (Figure 3.2 and table 3.1) showed an optimum value for stress failure, compression tangent modulus, and work of compression with values of 216±12 kPa, 141.0±0.1 kPa and 46.8±0.5 J m^{-3} respectively, as well as a strain failure of 55.2±7.2 % which was a high value, but not the optimal example. Generally, the overall trends for the mechanical properties parameter values increased as the ratios of (MBAAm/AAm) increased until 1. The continuous increase in these ratios resulted in a noticeable decrease in the value of the mechanical parameters. The concentrations for the hydrogel components associated with the maximum mechanical properties with GG, AAm and MBAA were 1.11 % (w/v), 4.44 % (w/v) and 3 % (w/v) respectively. This shows that the ICE hydrogel with a ratio of (MBAAm/AAm) (1) exhibited optimum mechanical properties, i.e. it withstands stress many times more when compared to other concentration ratios. The mechanical properties are optimum at a ratio of 1 and enhance the stiffness and strength of the hydrogel. This is likely arising from the best cross-linking network configurations of the covalent bonds of the PAAm chains, strengthened by the ionic cross-linking of Ca^{2+}/GG, allowing the energy stored in the entire chain to be dissipated. This energy dissipation enables

deformation stability when these gels are subjected to compression stress as shown earlier in Fig.1.10. This also explains why the mechanical properties of the prepared hydrogel decreased when the ratio increased above 1 which changed the cross-linking configuration, destabilising the chain cross-linking network distribution that dissipate energy after the application of external mechanical pressure. There is a high percentage of error in the stress and strain values when compared to the compressive tangent modulus and energy to failure values as shown in tables (Table 3.1), due to these values (stress and strain parameter values) being recorded from the average last data readings before the hydrogel breaking point for three different samples. The low rate percentage of errors of both compressive modulus and energy to failure values are due to calculating the slope between (0-5) % strain and calculating the integration values of the stress and strain readings between (0-strain at failure point) %, respectively, as shown in figure (a1.4)

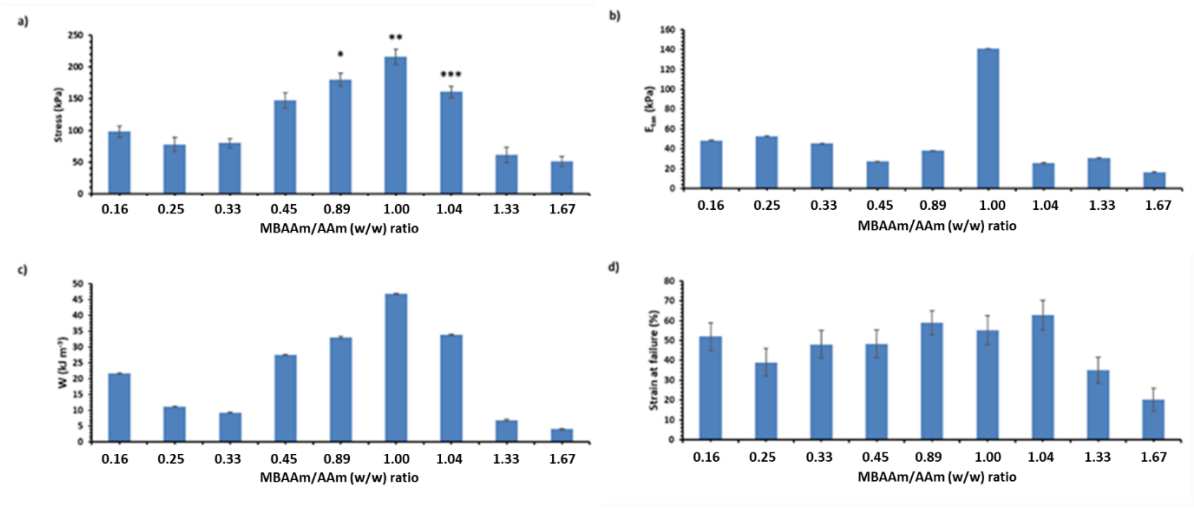

Figure 3.2 shows the trends in a) Compressive mechanical stress at failure, b) compressive tangent modulus, c) compressive strain energy to failure, d) compressive strain to failure of typical ICE network hydrogels as a function of MBAAm /AAm ratio. The stress versus strain curve for the three different points (*, **, *) in figure 3.2 (a) which represents the prepared ICE hydrogels with the ratios 0.89, 1 and 1.04 (MBAAm/ AAm), respectively. This experiment was repeated three times from three different samples. Uncertainty values associated with data in these graphs are shown in table 3.1. All the data analysis of this figure are located in appendix 1a pages 205-213.**

Table 3.1 Summary of the mechanical properties of the ICE network hydrogels with different ratios of (MBAA)/(AAm) and constant ratio of Ca^{2+}/ GG described by compressive tangent modulus (Etan), compressive stress to failure (σ), compressive strain to failure (ε), compressive strain energy to failure (W). This experiment was repeated three times using three different samples. All the data analysis of this figure are located in appendix 1a pages 205-213. The stress versus strain curve for the three different points (*, **, *) in this table represents the prepared ICE hydrogels with the ratios 0.89, 1 and 1.04 (MBAAm/ AAm) in figure 3.2 (a) as shown above.**

MBAAm % (w/v)	MBAAm/AAm (w/w) ratio	Stress (kPa)	Strain (%)	Compressive tangent modulus to failure (kPa)	Compressive strain energy to failure (W) ($J\ m^{-3}$)
0.5	0.16	98±9	52±7	48.2±0.2	21.7±0.3
0.75	0.25	78±11	39±7	52.6±0.2	11.1±0.2
1	0.33	80±7	48±7	45.1±0.2	9.3±0.2
2	0.45	147±12	48.3±7	26.9±0.1	27.5±0.3
2.66	0.89	*180±10	59±6	37.9±0.4	33.0±0.4
3	1.00	**216±12	55.2±7.2	141.0±0.1	46.8±0.5
3.108	1.04	***161±9	62.8±7.3	25.6±0.2	33.8±0.4
4	1.33	61.6±11.8	35.1±6.6	30.6±0.2	6.9±0.2
5	1.67	51.3±7.6	20.1±5.8	16.2±0.3	4.03±0.14

3.1.2 The effect of the ionic crosslink density:

The ICE network hydrogels were prepared to study the effect of ionic cross-linkers on the mechanical behaviour required the following compound: GG (300 mg) was added to nine different $CaCl_2$ solutions (0.00, 0.01, 0.05, 0.08, 0.10, 0.25, 0.50, 0.70 and 1.00 M, 600 µL) followed by the addition of AAm (50 mL, 3% w/v) and MBAAm (50 mL, 4.44% w/v) solution to each.

The mechanical properties of the synthesised ICE network hydrogels were examined by changing the concentrations of the ionic cross-linkers and keeping the other hydrogel components constant as shown in figure 3.3 and table 3.2. The data reveals an optimum value for the stress failure, compression tangent

modulus, and work of compression with values of 216±12 kPa, 141.0±0.1 kPa and 46.8±0.5 J m^{-3} respectively, as well as the strain failure of 55.2±7.2 %. Similar trends were observed for the ratio of Ca^{2+} cross-linker to GG. The optimum mechanical properties show a dramatic increase in the stress to strain failure, compressive tangent modulus and work of compression for the GG/PAAm hydrogel at the ratio 0.8 Ca^{2+}/GG. Hence, the stress needed to deform the gel increased with increasing the concentrations of Ca^{2+} reaching a plateau peak at 0.1 M Ca^{2+} or the ratio 0.8 of the Ca^{2+}/GG. However, the mechanical properties for the notch to heal any created crack decreased as the Ca^{2+}concentration increased. This could indicate that the mechanical properties of ICE hydrogel were optimised at the ratio 0.8 of Ca^{2+}/GG. This is because the polymer chain cross-linking network configurations enhance the stiffness and strength of the hydrogel for the ionic bonds of Ca^{2+}/GG chains. This would be strengthened by the covalent cross-linking of PAAm/MBAAm chains, allowing the energy stored in the entire chain to be dissipated, and hence enabling stabilisation of the deformation when these gels are subjected to breakable compressing stress as shown previously in figure 1.10. This also explains why the mechanical properties of the prepared hydrogel decreased when increasing the ratio above 0.8 which is changing the crosslinking configuration that destabilize the chain network distribution to dissipate the energy after applying mechanical stress.

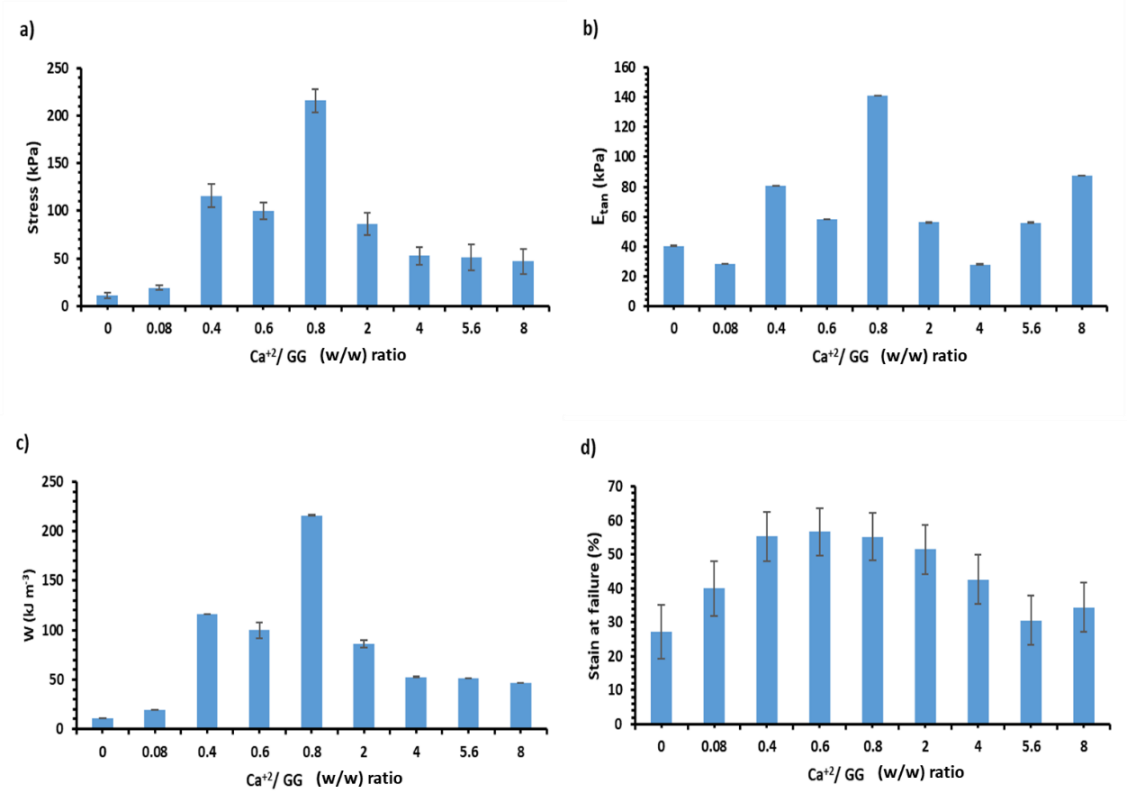

Figure 3.3 Compressive mechanical stresses at failure (a), compressive tangent modulus (b), Compressive strain energy to failure (c) and compressive strain to failure (d) of typical ICE network hydrogels as a function of Ca^{2+}/GG ratio. This experiment was repeated three times using three different samples. Uncertainty values associated with data in these graphs are shown in table 3.2. The lines are for guidance only. All the data analysis of this figure are located in appendix 1b pages 213-222.

Table 3.2 Summary of the mechanical properties of the ICE network hydrogels with different ratios of Ca^{2+}/ GG at a constant ratio of (MBAAm)/ (AAm) as described by compressive tangent modulus (E_{tan}), compressive stress to failure (σ), compressive strain to failure (ε) and compressive strain energy to failure. (W). This experiment was repeated three times using three different samples. All the data analysis of this figure are located in appendix 1b pages 213-222.

Ca^{2+} (M)	Ca^{2+}/ GG (w/w) ratio	Stress (kPa)	Strain (%)	Compressive tangent modulus (kPa)	Compressive strain energy to failure (W) ($J\ m^{-3}$)
0	0	11±3	27.3±7.9	40.40±0.06	0.96±0.06
0.01	0.08	19.2±2.3	40±8	28.30±0.07	2.10±0.08
0.05	0.4	116±12	55.3±7.2	80.80±0.05	28.7±0.3
0.07	0.6	100±9	56.7±7	58±0.1	39±8
0.1	0.8	216±12	55.2±7	141±0.1	46.8±0.5
0.25	2	86±12	51.5±7.2	56.1±0.1	35.1±3.5
0.5	4	52.6±9	42.6±7.3	27.9±0.2	7.3±0.4
0.7	5.6	51.1±13.3	30.6±7.3	56.0±0.1	6.8±0.1
1	8	46.7±13.3	34.4±7.2	87.4±0.1	8.5±0.14

3.1.3 The effect of changing the ionic covalent entanglements ratio for the (MBAAm/AAm) and (Ca^{2+}/ GG) hydrogel:

To study the influence of changing the ionic and covalent polymer ratio on the mechanical characterisations for the ICE network hydrogels, the following compounds were used with different concentrations ratios for both GG and AAm ranged from (3.774 GG+1.776 AAm) % (w/v) to (0.33 GG+5.22 AAm) % (w/v) with 4.44 % (w/v) MBAAm and 2.4 mg $CaCl_2$. Changing the concentrations of the ionic polymer (Ca^{2+}/ GG) and a polymer possessing a covalent bond (MBAAm/AAm) while keeping the total ratio of the hydrogel polymer constant (1:4) resulted in a typical change in the mechanical properties. Figure 3.4 and table 3.3

reveal a significant increase for the mechanical parameters at the ICE network ratio (1.11 GG+ 4.44 AAm) % (w/v) recording an optimum values for the stress failure value, compression tangent modulus, and work of compression with values of 216±12 kPa, 141.0±0.1 kPa and 46.8±0.5 J m^{-3} respectively, as well as the strain failure of 55.2±7.2 %, displaying a high magnitude values.

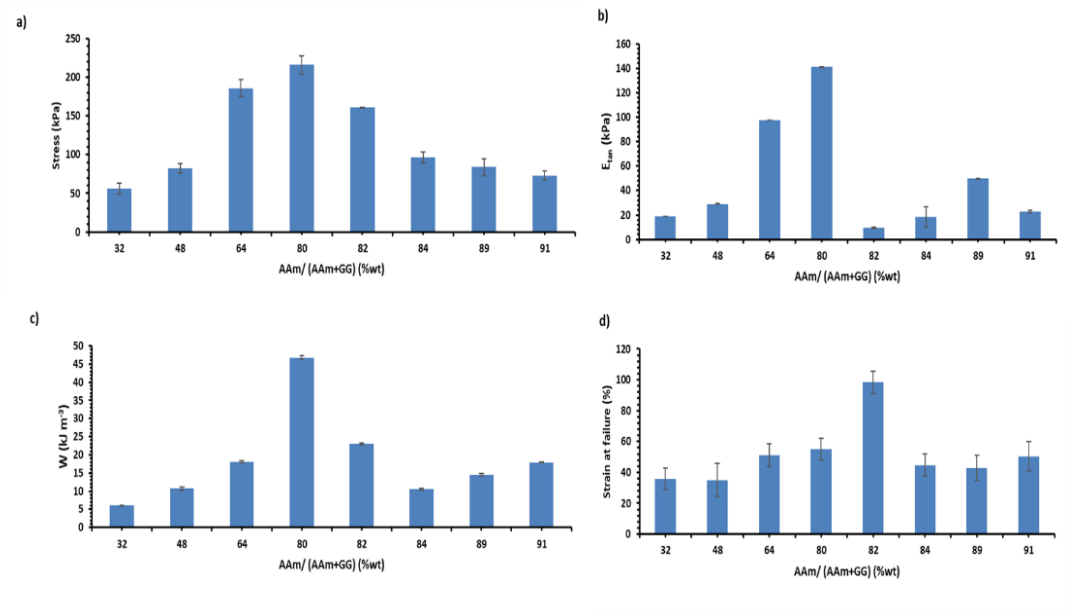

Figure 3.4 Compressive mechanical stresses at failure (a), compressive tangent modulus (b), Compressive strain energy to failure (c) and compressive strain to failure (d) of typical ICE network hydrogels as a function of GG-AAm ICE network hydrogels. This experiment was repeated three times using three different samples. Uncertainty values associated with data in these graphs are shown in table 3.3. The lines are for guidance only. All the data analysis of this figure are located in appendix 1c pages 223-230.

Table 3.3 Summary of the mechanical properties of the ICE network hydrogels with different ratios of GG and AAm described by compressive tangent modulus (E_{tan}), compressive stress to failure (σ), compressive strain to failure (ε), compressive strain energy to failure (W). This experiment was repeated three times using three different samples. All the data analysis of this figure are located in appendix 1c pages 223-230.

Hydrogel ICE network ratio % (w/v)	AAm/ (AAm+ GG) (%wt)	Stress (kPa)	Strain (%)	Compressive tangent modulus (kPa)	Compressive strain energy to failure (W) ($kJ\ m^{-3}$)
3.774 GG+1.776 AAm	32	56±7	35.8±7.2	18.9±0.2	6.05±0.12
3.4 GG+ 2.15 AAm	48	82.4±6.5	35.1±10.8	29.0±0.2	10.7±0.5
1.998 GG+3.552 AAm	64	186±11	51.1±7.3	97.5±0.1	18.1±0.3
1.11GG+4.44 AAm	80	216±12	55.2±7	141±0.1	46.8±0.5
0.88 GG+ 4.66 AAm	82	161±0.4	98.4±7.2	9.35±0.65	23.0±0.3
0.66 GG+ 4.89 AAm	84	96±7	44.6±7.2	18.5±8.3	10.5±0.3
0.44 GG+ 5.11 AAm	89	84±11	43±8	49.7±0.2	14.5±0.4
0.33 GG+ 5.22 AAm	91	73.1±5.8	50.4±9.5	22.8±0.9	17.9±0.1

The main output from these data corresponds to establishing the maximum values of each mechanical parameter of the ICE hydrogel polymer at the ratio 80 (%wt) and indicates that as the concentration of the AAm increases the mechanical parameters of the ICE hydrogels increases significantly. This is due to the crosslinks formed between the amine functional groups positioned on PAAm chains and the carboxyl substituents on GG chains that enhance the robustness of the ICE hydrogel. Accordingly, the mechanical behaviour shows a remarkable decrease when the ICE polymer ratio increases to more than 80 (%wt). This suggests that establishing the mechanical properties of an optimised ICE network hydrogel requires inclusion of exact concentrations for both covalent bonding polymers such as PAAm and the ionic bonding polymer such as GG. On the other hand, the reason for the unexpected increase in the strain failure of the hybrid hydrogel polymer at a ratio of 82 (%wt) compared to 80 (%wt) was not clear.

3.2 Rheology measurements:

Oscillatory shear rheology measurements were conducted with a controlled strain rheometer. Strain amplitude sweeps (frequency 10 Hz) revealed that all gels exhibited a clear plateau of storage (G′) and loss (G″) moduli as shown in figure 3.5. This plateau is commonly referred to as the linear viscoelastic LVE region, and the high values of (G′ /G″) are symbol of the cross-linked polymer network(s). [128] The end of the LVE region corresponds to the shear strain that the hydrogels can withstand before the polymer network starts to breakdown. Amplitude sweeps have been used to examine the mechanical properties of the synthesised ICE network hydrogels by comparing the properties described by LVE with different concentrations of ionic and covalent entanglements hydrogels in order to obtain gels with optimised mechanical performances.

In addition to the compression test, the effect of the covalent crosslink density of PAAm was also examined using a rheology test. Figure 3.5 shows a significant increase in the mechanical properties of GG/ PAAm hydrogel with GG, AAm and MBAAm concentrations of 1.11 % (w/v), 4.44 % (w/v) and 3 % (w/v) respectively, when compared to other concentration ratios of MBAAm/ AAm. Table 3.4 shows all rheological measurements data using different concentrations ratios of MBAAm/AAm. Changing the MBAAm quantities while keeping the concentration of AAm constant reveals a significant increase in (G′**)** in the LVE region. The mechanical characteristic reached an optimum value of (G′ /G″) (68.7±0.6 kPa) at a MBAAm/AAm ratio of 1.

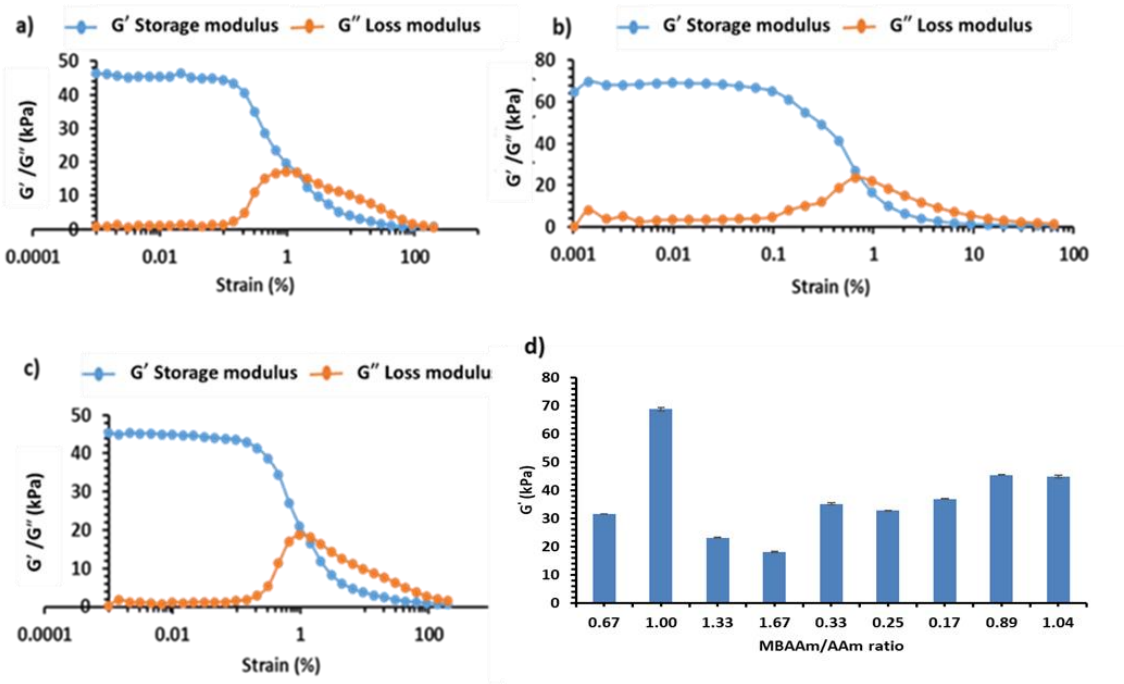

Figure 3.5 Storage modulus LVE region vs (MBAAm/AAm) ratio concentrations of the ICE network hydrogel, (a, b and c) respectively show 3 optimum points present which refers to the values of the LVE regions, while Figure 3.5 (d) represent the LVE versus MBAAm/AAm ratio. This experiment was repeated three times using three different samples. Uncertainty values in (Figure 3.5 d) associated with the data in these graphs are shown in table 3.4. All the data analysis of this figure are located in appendix 1 pages 231-235.

Table 3.4 Storage Modulus (G′) for different concentrations of ratios of MBAAm/AAm. This experiment was repeated three times using three different samples. All the data analysis of this figure are located in appendix 1 pages 231-235.

MBAAm/AAm ratio	**Storage Modulus** (G′)/ **kPa**
0.16	36.8±0.6
0.25	32.7±0.1
0.33	35.1±0.3
0.45	31.53±0.09
0.89	45.4±0.2
1	68.7±0.6
1.04	44.8±0.4
1.33	23.1±0.2
1.67	18.0±0.2

Data from the rheological measurements of the MBAAm/AAm ratios exhibited the same trend as shown from the data from the compressive stress-strain testing for MBAAm/AAm ratios in describing the mechanical properties for the synthesised hybrid gels. This trend illustrated an optimisation of the mechanical properties for the ICE networks gel by changing the concentration of the covalent cross-linker (MBAAm) while maintaining the concentration of AAm and all other hydrogel components constant to study the effect of the covalent crosslink density of PAAm on the mechanical behavior described within LVE region (G′).

Furthermore, the effect of the cross-linker density on GG hydrogels by changing the concentration of the Ca^{2+} ion while keeping the concentrations of GG and other hydrogel components constant was examined using rheology test as shown in (Figure 3.6 and table 3.5)

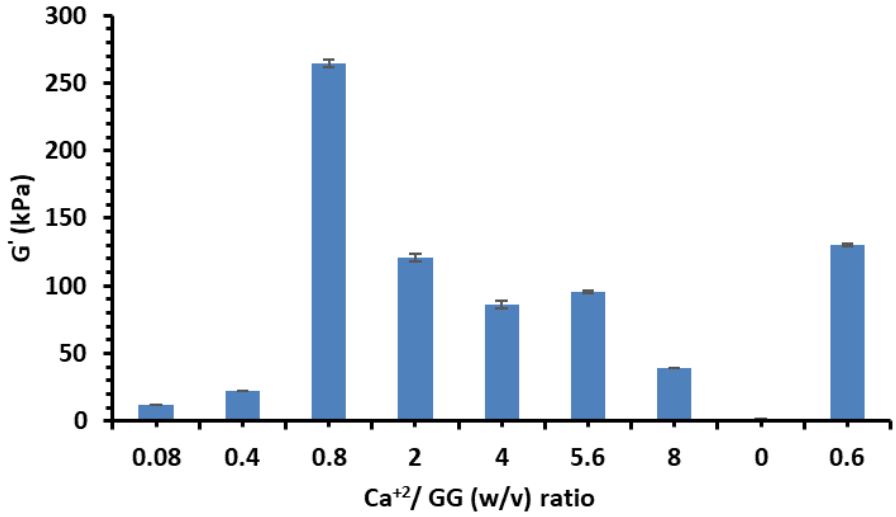

Figure 3.6 Storage modulus (LVE) region vs (Ca^{2+}/GG) ratio concentrations of the ICE network hydrogel. This experiment was repeated three times using three different samples. Uncertainty values associated with data in these graphs are shown in table 3.5. All the data analysis of this figure are located in appendix 1 pages 235-240.

Table 3.5 Storage Modulus (G′) for different concentrations of ratios of Ca^{2+}/GG. This experiment was repeated three times using three different samples. All the data analysis of this figure are located in appendix 1 pages 235-240.

Ca^{2+}/(GG) ratio	Storage Modulus (G′)/ kPa
0	1.92±0.01
0.08	12.2±0.2
0.4	22.14±0.04
0.6	131±1
0.8	264±3
2	12.1±2.6
4	86.2±2.6
5.6	95.4±0.7
8	39.60±0.01

The unexpected increasing values for the rheological measurements for this type of hydrogels could result from changing the reaction conditions *e.g.* increasing the time of the reaction. Despite this, the overall data are cohesive and logical as it enhances data from previous probes that used compressive stress-strain testing. Figure 3.6 shows that the highest value for the linear viscoelastic LVE region was 264±5 kPa resulting from using 0.1 M $CaCl_2$ and recorded a (Ca^{2+}/GG) ratio of 0.8. This value indicated the preparation at this specific ratio produced optimum mechanical properties when compared with preparation at other ratios that give lower mechanical properties. Finally, The effect of changing the ionic covalent entanglements ratio for the (MBAAm/AAm) and (Ca^{2+}/GG) hybrid hydrogel was studied by changing the concentrations of the ionic polymer (Ca^{2+}/ GG) and polymer that has covalent bond (MBAAm/AAm) with keeping the total ratio of the hydrogel polymer constant and indicated a typical change in the mechanical properties characterised by LVE region (G′). Figure 3.7 and table 3.6 reviews the storage modulus (G′) values or LVE region for different concentrations ratios of AAm/ (AAm+ GG):

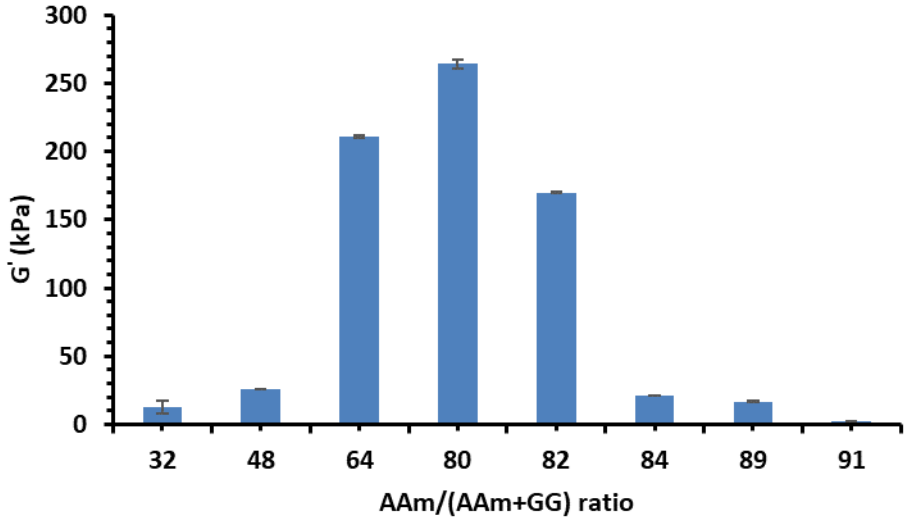

Figure 3.7 Storage modulus (LVE) region vs AAm/ (AAm+GG) ratio concentrations. This experiment was repeated three times using three different samples. Uncertainty values associated with data in these graphs are shown in table 3.6. All the data analysis of this figure are located in appendix 1 pages 240-244.

Table 3.6 Storage Modulus (G′) for different concentrations ratios of AAm/(AAm+GG). This experiment was repeated three times using three different samples. All the data analysis of this figure are located in appendix 1 pages 240-244.

Hydrogel/ ICE network ratio % (w/v)	AAm /(AAm+ GG)	Storage Modulus (G′)/ kPa
3.77 GG+1.78 AAm	32	13.0±5.0
3.4 GG+3.55 AAm	48	26.0±0.2
1.99 GG+3.55 AAm	64	211.0±2.0
1.11GG+4.44 AAm	80	264.0±3.0
0.88 GG+4.66 AAm	82	170.0±6.0
0.66 GG+4.89 AAm	84	21.0±0.1
0.44 GG+5.11 AAm	89	16.8±0.2
0.33 GG+5.22 AAm	91	2.6±0.1

Analysis of the data in figure 3.7 shows that increases in the quantity of AAm also increases the storage modulus until it reaches its maximum value at the concentration ratio 80 acting from (1.11 GG+4.44 AAm) % (w/v) recording storage modulus of the ICE network hydrogel 264±3 kPa. However, the continuous increase in the AAm concentration contributes to a decrease in the values in the LVE and consequently, the strength and stiffness of the hybrid hydrogel decreases. This could due to the decrease of ionic crosslinking polymer associated with the increase of AAm polymer in order to maintain the total ratio of the polymer to be constant. This reason can be sufficient to lower the stiffness and toughness of the prepared ICE hydrogel network. This is explained by the reformation of the ionic crosslinks, leading to the healing of the internal damage when it is under external stress. Furthermore, the findings of the rheological measurements mainly match the results from the compressive stress-strain test on the prepared ICE network hydrogel.

Therefore, the mechanical properties of the synthesised ICE network hydrogels have been optimised by studying the effect of ionic crosslinking as well as the effect of the covalent crosslinking and by studying

the effect of changing the ratios of AAm and GG while keeping the total amount of the polymer constant. Oscillatory rheological test and compressive stress-strain test have been performed to studying the mechanical behaviour of these prepared gels. Measuring the mechanical properties revealed that ICE hydrogel polymer components with the following concentrations: Ionic polymer: 0.1 M $CaCl_2$ and 1.11 % (w/v) GG with PAAm that consist 4.44 % (w/v) (AAm) with 3 % (w/v) (MBAAm) revealed optimum mechanical properties.

The mechanical and the electrical properties were examined for the optimised hydrogel after soaking it in 2.7 M NaCl to investigate the possibility of the ICE gel being utilised as a soft electrode or sensor. Compression test analysis was performed on the ICE gel before and after soaking it in the NaCl salt solution to study the mechanical properties (Figure 3.8).

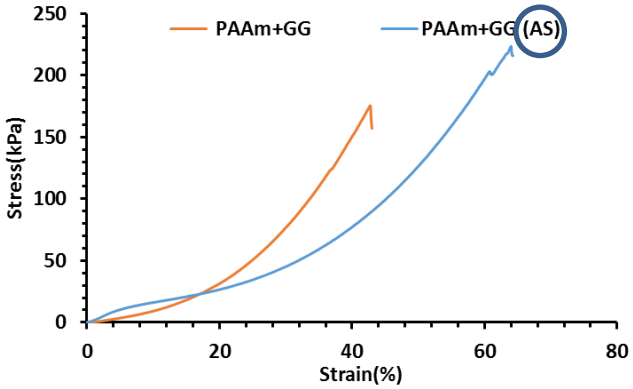

Figure 3.8 Shows stress versus strain plot for PAAm+GG hydrogel before and after soaking (AS) it in 2.7 M NaCl salt solution. This experiment was repeated three times using three different samples.

Soaking PAAm+GG hydrogel in 2.7 M NaCl salt solution reduced the mechanical properties with the stress at failure decreasing by more than 40 kPa, and this is attributed to the effect of the high-water percentage allowing the ICE gel to swell. The electrical conductivity was examined for the ICE gel and exhibited a significant increase from 3.3±0.5 $mS.cm^{-1}$ to 127±15 $mS.cm^{-1}$ after immersion in 2.7 M NaCl. This rise can be rationalised by the presence of Na^+ and Cl^- charge carriers in the soaking solution with significant immersion of these ions inside the ICE-hydrogel. Furthermore, the water content in the ICE hydrogel was increased from 78% to 85% after the hydrogel was soaked in 2.7 M NaCl salt solution for 24 hours. This change in hydrogel dimensions was determined using the stress/stress calculations.

3.3 Conclusions

The mechanical characteristics of the ICE network were investigated. Hydrogels were synthesised using various ratios of ionic Ca^{2+} cross-linked GG, and covalent MBAAm cross-linked PAAm concentrations and the effect of ionic and covalent crosslinking on mechanical behaviour was studied. In addition, the effect of varying the ratios of PAAm and GG on the mechanical characteristics was investigated.

Compressive stress-strain testing and oscillatory rheological testing were utilised to study the mechanical behaviour of these prepared gels. It was established that gels prepared with 0.1M $CaCl_2$ and 1.11% (w/v) GG with PAAm consisting of 4.44% (w/v) (AAm) with 3% (w/v) (MBAAm) exhibited optimum mechanical characteristics. The following optimum values were observed: 141.0±0.1 kPa (compressive tangent modulus), 216±12 kPa (compressive stress to failure), 55 ±7% (compressive strain to failure), and 46.8±0.5 $J.m^{-3}$ (compressive strain energy to failure). Oscillatory rheology demonstrated that increasing the overall polymer concentration (at constant polymer network ratio) increased the shear modulus from 68.7±0.6kPa to 264±5kPa. An ICE network hydrogel with optimised mechanical characteristics was prepared.

The electrical conductivity for the ICE gel that displayed optimum mechanical features was investigated before and after immersion in 2.7 M NaCl with its water content revealing a distinct increase of both conductivity from 3.3±0.5 $mS.cm^{-1}$ to 127±15 $mS.cm^{-1}$ and water content from 78% to 85%.

Further studies could include the recovery of hysteresis behaviour of swollen hydrogels and examining the homogeneity of the hydrogels using optical microscopy. In addition, the connectivity between GG and PAAm polymer networks in the hydrogels should be examined using the FTIR spectroscopy and finally, the ability to process these ICE hydrogels using additive manufacturing (3D printing) or fabricating soft sensors for potential applications in tissue engineering and soft robotics should be examined.

Chapter 4

Preparation, characterisation and 3D printing of ionic PAAm hydrogels.

This chapter is based on the following published manuscript:

Khalid Zainulabdeen, Marc in het Panhuis, and Holly Warren, "Preparation, Characterisation and 3D Printing of Ionic Poly(acrylamide) Hydrogels", Proceedings of the First MoHESR and HCED Iraqi Scholars Conference in Australasia, 2017, Melbourne, *https://researchbank.swinburne.edu.au/file/b083d58b-327d-464f-906e-57530405c7c5/1/proceedings_ISCA2017.pdf*

4.0 Introduction

The ability to print soft hydrogels is of significant interest for its potential application in the fields of soft robotics and tissue engineering. This project aims to 3D fabricate soft, transparent, conductive and stretchable material. Ionic PAAm has been prepared and characterised, before and after soaking in 6 M LiCl solutions, to assess its suitability for 3D printing. The rheological analysis was carried out under controlled UV-crosslinking, while cooling to -6 °C, to enable 3D printing of the PAAm without the need for any additional rheological modifiers. The electrical and mechanical characteristics of 3D printed PAAm containing LiCl or NaCl hydrogel materials were characterised and compared to the properties of casted hydrogel samples.

4.1 Water loss percentage

PAAm+6 M, 8 M, 9 M LiCl and PAAm+2.7 M NaCl have been chosen as representatives due to each hydrogel exhibiting the best water retention capacity among previously studied formulations of PAAm. [273] Cylindrical PAAm-salt hydrogels were prepared as described in chapter 2. A Sony digital camera recorded the morphological changes of the gels over time. Figures 4.1 (a-f) show the different hydrogel samples with varying concentration stored in the lab at room temperature (21 ^{o}C) for 30 days. After 30 days, all samples were seen to shrink to some extent; however, this took place at various shrinkage rates. The relationship of shrinkage effect and LiCl concentration between 6 M and 10 M is compared in Figure 4.2 (a-d). A decrease in volume change was observed with increasing salt concentration; however, higher salt concentrations resulted in slight turbidity of samples after 30 days. This may be attributed to the interstitial water being removed through evaporation, resulting in a higher salt concentration and, hence, undissolved salt crystals. This phenomenon was repeated when the NaCl concentration was increased from

2.7 M to 4 M (Figures 4.2 (e-f)), where salt crystals coat the surface of the 4 M NaCl sample. The small size of the Li^+ ion gives rise to properties not seen for other alkali metal chlorides, such as excellent solubility in polar solvents and hygroscopic properties. [273] These properties encouraged embedding LiCl in the PAAm hydrogel to improve the water retention capacity which in turn enhanced the hydrogel softness.

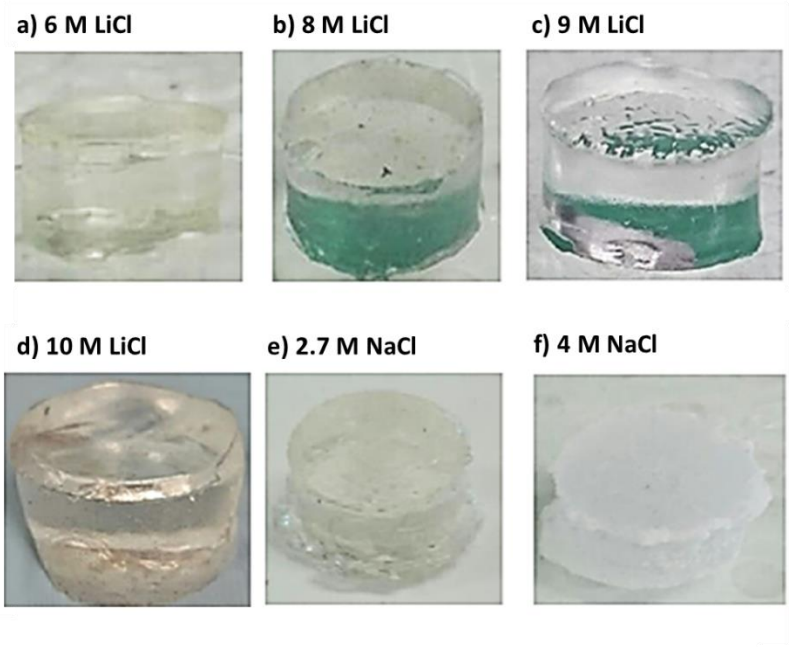

Figure 4.1 Typical photos for PAAm hydrogel samples (height 10 mm, diameter 18 mm) consisting of a) 6 M LiCl, b) 8 M LiCl, c) 9 M LiCl, d) 10 M LiCl, e) 2.7 M NaCl and f) 4 M NaCl after 30 days at room temperature.

The water loss percentages have been determined for each salt content using eq. 4.1. Their masses were recorded every certain time (i) using an electronic scale. Figure 4.2 shows the evolution of water loss percentages versus storage time in the lab for PAAm hydrogels containing each salt concentration.

$$Water\ loss\ \% = \frac{Mass\ of\ hydrogel\ (time{=}i) - Starting\ mass\ of\ hydrogel}{Starting\ mass\ of\ hydrogel}\ x\ 100 \quad \textbf{.....(Eq.4.1)}$$

A clear difference can be seen between the evaporation curves of PAAm containing NaCl and LiCl; the water loss continued to increase over the 30 days for PAAm-NaCl, compared to reaching a plateau, or a "steady-state" stage, at around 15 days for PAAm-LiCl samples. It was also noted that samples containing higher concentrations of LiCl exhibited a lower water loss percentage: 4% compared to 8% for 9 M and 6 M, respectively. This suggests that the water retention capacity is directly proportional to LiCl salt content.

Since PAAm-NaCl gels did not reach a steady-state stage, it was assumed that they do not possess water-retention capabilities. These results correspond with observations from (Figure 4.2) and are in agreement with the difference in ionic hydration, [273] where a higher degree of ionic hydration means stronger bond-strength between ion-water pairs and more bonded water molecules which hence, decreases evaporation rates. Due to these high water-retention capabilities, PAAm hydrogels containing high LiCl salt content may be suitable for applications such as soft sensing devices or soft robotics.

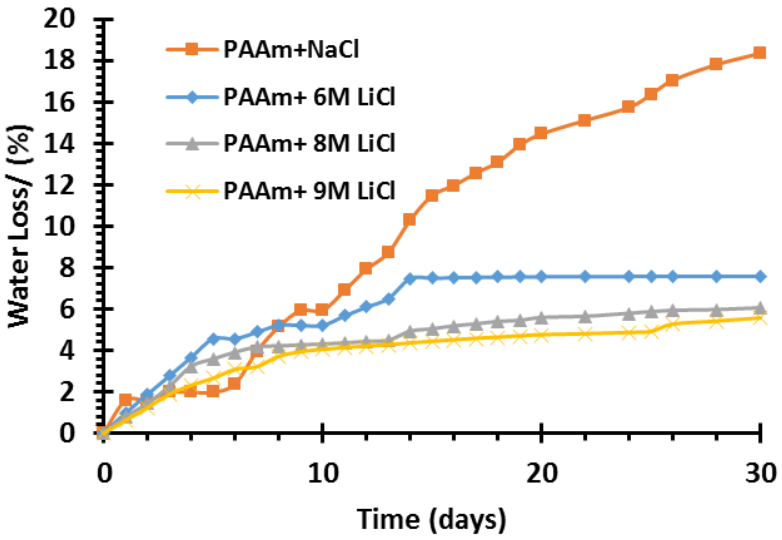

Figure 4.2 A typical diagram between water loss percentages versus time for PAAm-salt hydrogels samples. This experiment was repeated three times from three different samples.

4.2 Mechanical Characteristics

Tensile testing was carried out on dog bone shaped samples, as describes in the experimental section (Chapter 2). The selected samples were characterised for their ability to exhibit distinct mechanical properties in previous works. [18], [273] Stress-strain measurements were recorded while hydrogels were extended to failure (Figure 4.3). PAAm hydrogels containing NaCl were seen to outperform those containing LiCl, with failure point occurring at higher stresses and strains.

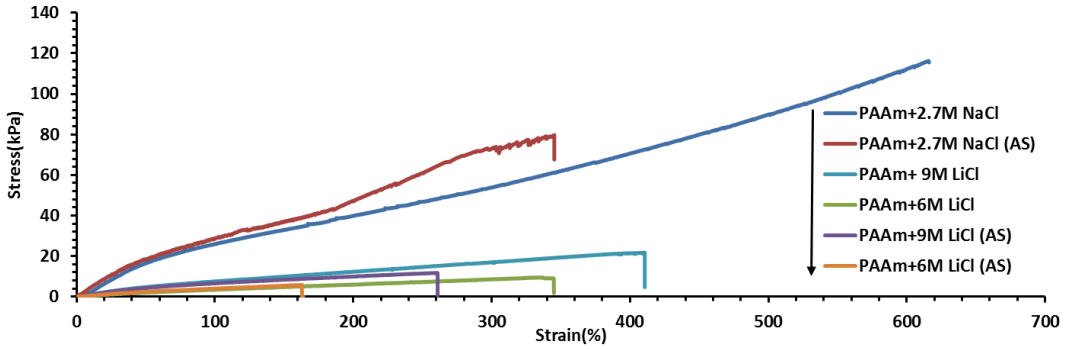

Figure 4.3 Stress-strain curves for ionic PAAm hydrogels with NaCl and LiCl before and after soaking (AS) in specified salt solutions. This experiment was repeated three times from three different samples.

Values for modulus, strength, and failure point were calculated (Table 4.1). PAAm-NaCl hydrogels exhibited higher ductility than their LiCl counterparts (600 % extension at failure, compared to 200-400 %). Ultimate strength measurements were also an order of magnitude higher. On the other hand, samples containing 9 M LiCl displayed marginally better mechanical properties compared to samples containing 6 M LiCl. This trend was observed previously by Bai *et al.* [273] in their study which compared PAAm hydrogels with varying concentrations of LiCl. Decreases in sample strengths from before to after soaking can be accounted for by their increased water contents.

The water content of the PAAm hydrogel with 9M LiCl measured as the following:

Wt of AAm =16 g/100 ml water, therefore, wt of AAm= 8 g/50 ml water.

To measure the required Wt of LiCl required to prepare 9 M LiCl in 50 ml water:

Mole= Volume (L)*Concentration (M), Mole=0.05 L* 9 M= 0.45 mole of LiCl,

Wt of required LiCl= mole* Mwt of LiCl, Wt of LiCl= 0.45*42.4=19.08 g of LiCl.

Wt of MBAAm in 100 ml water is 0.1 g, therefore, Wt of MBAAm in 50 ml water is 0.05 g.

Wt of α-ketoglutaric acid in 100 ml water is 0.014 g, therefore, Wt of α-ketoglutaric acid in 50 ml water is 0.007 g.

Water percentage of the prepared hydrogel after adding all he required chemical components in 50 ml water is measured as the following: *100= 64.82%=65%

The water content of the hydrogel after soaking it in 9M LiCl solution can measured as described in the following equation = **$((W_{swollen} - W_{dry})/ W_{Swollen})*100$= ((33.4 g-4.3 g)/33.4 g) Water percentage = 84%.**

The volume of soaked hydrogels has increased and this also was obvious from the increase of the water content of the soaked hydrogels samples on table 4.1 in page. Furthermore, all the changed dimensions of the soaked hydrogels has been also accounted in the stress/ strain calculations.

Table 4.1 Tensile test values for PAAm hydrogels with NaCl and LiCl before and after soaking in specified salts.

Parameters	PAAm+6 M LiCl		PAAm+2.7 M NaCl		PAAm+9 M LiCl	
	Before soaking	After Soaking	Before soaking	After Soaking	Before soaking	After Soaking
Water content (%)	69±2	87±2	66±1	78±2	65±2	84±1
Tensile Modulus (kPa)	4.6±0.1	5±1	42±3	45±1	13±2	9±1
Tensile strength (kPa)	9.5±0.1	5±1	116±7	84±4	22±1	11±1
Extension of Failure (%)	343±1	150±13	622±6	344±8	411±18	290±29
Work of extension (kJ m^{-3})	17±1	4±1	420±77	152±9	50±4	19.4±0.3

Cyclic compression testing was carried out on PAAm hydrogel samples containing 2.7 M NaCl and 9 M LiCl (Figure 4.4). Six compression cycles from 0% to 80% strain were run on cylindrical gels as described in chapter two.

It is noted that, although PAAm-NaCl hydrogels displayed higher first-cycle stress at 80% strain when compared with PAAm-LiCl (550 kPa and 225 kPa, respectively), they showed rapid degradation over six cycles, whereas PAAm-LiCl showed zero hysteresis over all six strain cycles. The reason behind this significant difference on the hysteresis over all six cycles was the difference in the water retention capacity of the PAAm+2.7 M NaCl and PAAm+9 M LiCl hydrogels after applying compression stress over several cycles.

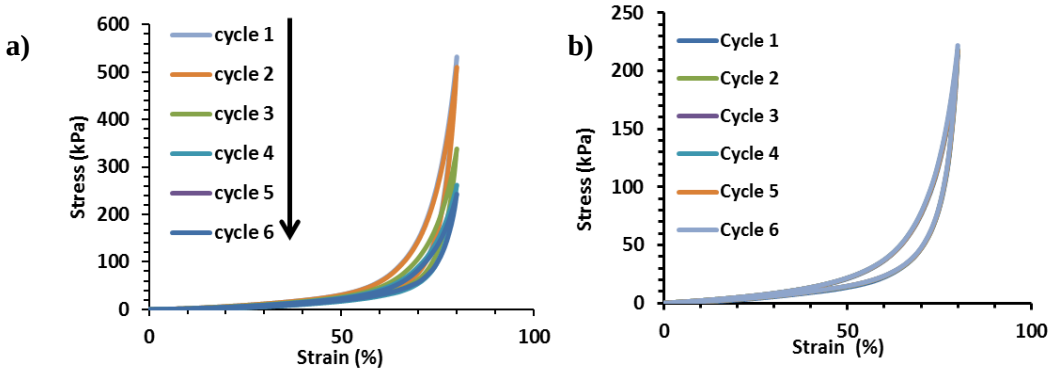

Figure 4.4 Cyclic compression testing for PAAm hydrogels containing a) 2.7 M NaCl and b) 9 M LiCl from 0-80 % strain. This experiment was repeated three times from three different samples.

4.3 Electrical Characteristics

For these PAAm hydrogels to be useful for applications in soft robotics and other device design, they must be adequately electrically conductive. Traditionally, electrical characteristics of materials are elucidated through surface techniques such as 4-point-probe measurements. In this study; conductive pathways are present due to the inclusion of ionic charge carriers, as such, resistance (or impedance) is predicted to be frequency-dependent, resulting in the need for an alternative experimental technique. Therefore, the electrical impedance was recorded for frequencies between 1 Hz and 100 kHz using a custom-designed setup, as described in previous studies. [173]

Various types of salts were added during the preparation of the PAAm hydrogels such as $CaCl_2$, NaCl, LiCl and CsCl. Their concentrations were varied to investigate their mechanical and electrical properties, as well as the water loss percentages. It was obvious from previous studies that at any given concentration of the pure salt aqueous solution, the conductivity values change in the following order $Li^+ < Na^+ < Cs^+$. [330] This was also concluded from our prepared hydrogel conductivities. This is because Cs^+ ions have greater mobility through the polymer matrix due to it being less a polarising cation because of the shielding effect of three additional electron shells compared with Na^+ and four additional electron shells compared to Li^+ ions, which would interact more with the polymer chains. This explains why the ionic hydrogel with CaCl displayed higher conductivity than ionic hydrogel with LiCl.

The conductivity was measured for each PAAm gel type (Table 4.2). The data for samples measured prior to soaking shows that the 2.7 M NaCl-containing gels demonstrate an ionic conductivity which is the same as those which contain 9 M LiCl, within experimental error (112±17 $mS.cm^{-1}$ versus 114±17 $mS.cm^{-1}$,

respectively). However, after their soaking treatments, water content was increased and PAAm-NaCl samples out-performed PAAm-LiCl by more than 50 $mS.cm^{-1}$. This is attributed to the increased mobility of sodium ions across the polymer matrix due to the shielding effect of an additional electron shell compared to that of Li^{+} ions, which is more likely to interact with the polymer chains. [273]

Table 4.2 Electrical conductivity and water contents values for PAAm+2.7 M NaCl, PAAm+6 M LiCl and PAAm+ 9 M LiCl hydrogels at frequency range (1-10) kHz. This experiment was repeated three times from three different samples.

Hydrogel	PAAm+2.7 M NaCl		PAAm+6 M LiCl		PAAm+9 M LiCl	
	Before soaking	**After Soaking**	**Before soaking**	**After Soaking**	**Before soaking**	**After Soaking**
Conductivity ($mS.cm^{-1}$) at frequency range (1-10) kHz	112±17	204 ± 17	99±7	129±15	114±17	133±6
Water content %	66	78	69	87	65	84

4.4 Rheology

In preparation for 3D extrusion printing of the PAAm hydrogels, it was necessary to determine the flow properties of the material. For direct writing applications, the ink is required to be shear thinning; i.e. the rest viscosity is higher than during the writing process, such that ink is only extruded when desired. Furthermore, once extruded, the ink is required to maintain its structure rather than wetting to ensure a well-defined pattern.

In order to determine a suitable temperature for extrusion, the flow properties of the various PAAm-salt hydrogels were measured rheometrically at a nominated constant shear rate (100 s^{-1}) while varying the temperature from -6 to 16 °C as shown in (Figure 4.5a). Each sample exhibited increasing viscosity with decreasing temperature, as was expected. It was further noted that AAm-salt samples recorded viscosities which were at least twice that of as-prepared AAm. This can be attributed to the lower water content in the presence of salt. Since AAm-LiCl (9 M) sample showed the highest viscosity, the effect of LiCl concentration on the flow properties were studied (Figure 4.5b). A two-fold increase in viscosity was observed when the concentration of LiCl was increased from 6 M to 9 M. As such, for optimum extrusion

printing, salt concentrations of AAm were maximised to sufficiently thicken the ink. To establish the rate at which the extruded materials formed a hydrogel, once patterned, the dynamic modulus was monitored as a function of UV-irradiation time using a quartz bottom plate accessory on the rheometer (Table 4.3). PAAm-LiCl was shown to cure in 5 minutes, compared to PAAm-NaCl, which took 15 minutes. However, PAAm-NaCl formed a much firmer gel once the photo-curing process was completed. This is because LiCl has a hygroscopic nature, which makes water molecules surround Li^+ particles, leaving few available free water molecules in the polymer for curing. On the other hand, the PAAm-NaCl hydrogel has higher water content, providing more free water molecules to convert it to gel.

In attempts to optimise the mechanical and the electrical properties for the hydrogel, different concentrations of LiCl were added to the PAAm hydrogel. The required time to initiate photo-curing for PAAm-LiCl hydrogel was reduced with increasing salt-content due to the higher salt content decreasing the water content allowing less free water molecules, in the gelation of the polymer. Therefore, PAAm with 9 M LiCl displayed the lowest gelation time with 3 minutes when compared to other LiCl concentrations. This study shows that PAAm+9 M LiCl hydrogel exhibited the best mechanical, electrical and lowest gelation time.

Table 4.3 Maximum complex viscosity (MCV) and gelation times (GT) for different hydrogels at 20 and -6 °C. This experiment repeated three times from three different samples.

Hydrogel	GT at 20 °C (min)	MCV at 20 °C (Pa.s)	GT at -6 °C (min)	MCV at -6 °C (Pa.s)
AAm	20	387±2	37	410±2
AAm+2.7 M NaCl	15	2250±2	20	2650±10
AAm+6 M LiCl	5	730±40	8	810±27

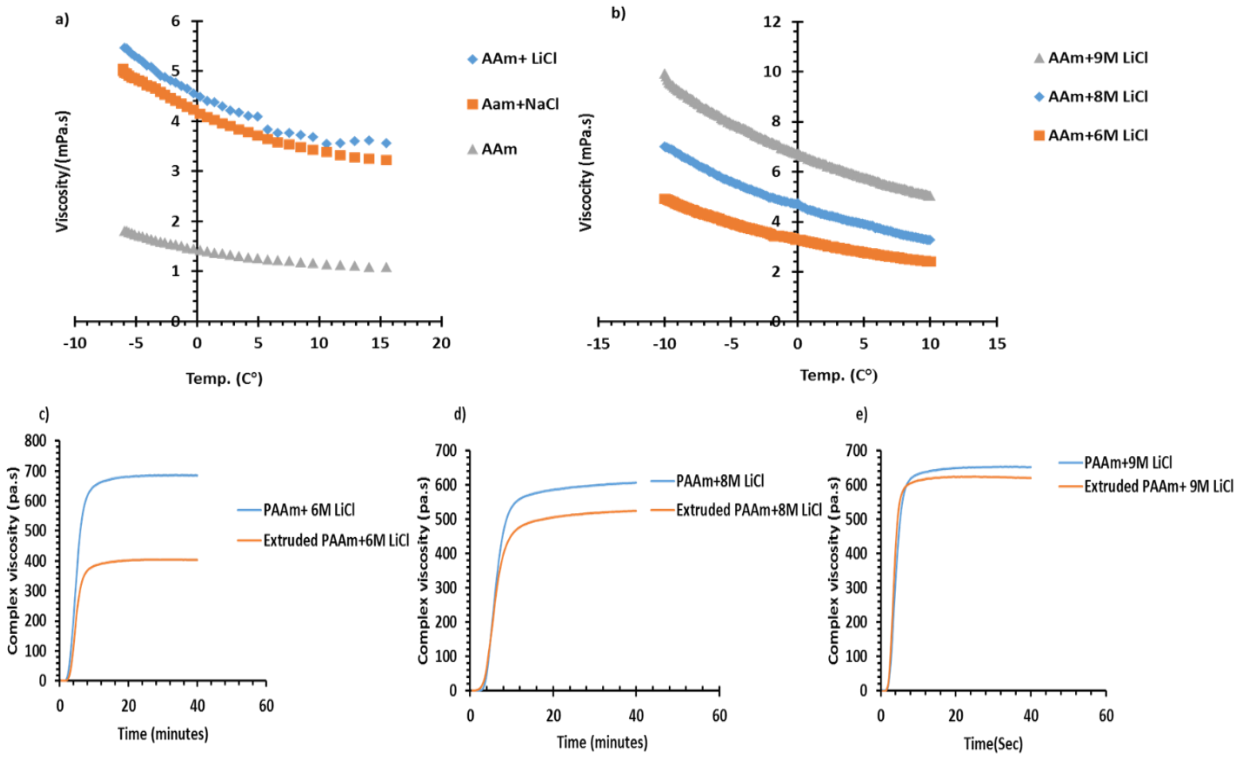

Figure 4.5 A typical diagram demonstrates a) the effect of changing temperature on the viscosity of each AAm, AAm+LiCl and AAm+NaCl ink solutions b) the effect of changing temperature on the viscosity of AAm+6 M LiCl, AAm+8 M LiCl and AAm+9 M LiCl ink solutions c) complex viscosities versus time of gelation for PAAm+6 M LiCl d) PAAm+8 M LiCl e) PAAm+9 M LiCl before and after extruding the AAm ink solutions with LiCl. This experiment was repeated three times from three different samples.

It's clear from these results that the difference in the MCV values between extruded and casted hydrogel and the lower value of MCV in the extruded hydrogel is most likely due to a decreased level of interaction between adjacent filament lines during the printing process, along with less inter-layer connectivity associated with curing layers individually. (Further explination has been added at Appendix 3, p248 for clarification).

4.5 3D printing ionic PAAm

PAAm patterns were printed with a direct-writing extrusion printing technique using optimised AAm-LiCl (9 M LiCl) inks. Sample containers were covered in aluminum foil during the printing process to prevent premature curing from the UV light source and to maintain a cold temperature (-6 °C) for the duration of

the print job. Glass substrates were pre-treated with paraffin oil (Diggers) to provide a hydrophobic surface which lessened line wetting and therefore increased feature definition (Figure 4.6).

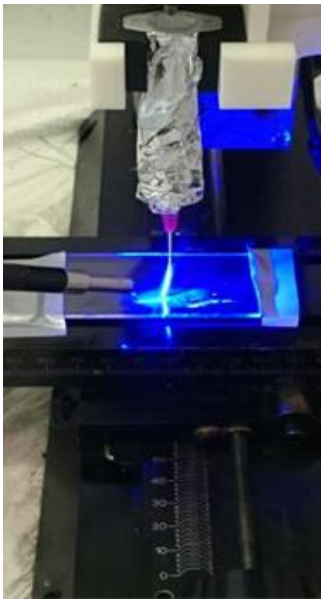

Figure 4.6 An image showing focusing the UV light on the extruded precursor ink solution during printing.

The electrical conductivity of the printed pattern of PAAm+9 M LiCl (Figure 4.7) was 117±13 $mS.cm^{-1}$ before and 146 ±4 $mS.cm^{-1}$ after soaking in 9 M LiCl. This is within experimental error of unprinted, cast samples (Table 4.2), indicating that the printing process was not detrimental to the conductivity.

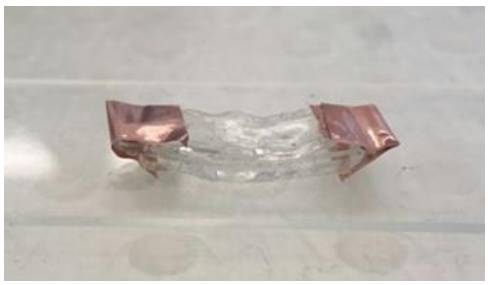

Figure 4.7 3D printed PAAm+9 M LiCl hydrogel device with copper tape electrodes

Mechanical tensile testing of dog-bone shaped hydrogels (Figure 4.8) revealed a decrease of Young's modulus and tensile strength when compared to their casted counterparts (Table 4.4). This is most likely due to a decreased level of interaction between adjacent filament lines during the printing process, along with less inter-layer connectivity associated with curing layers individually. However, both the printed and casted gels could be stretched up to 4 times their own length.

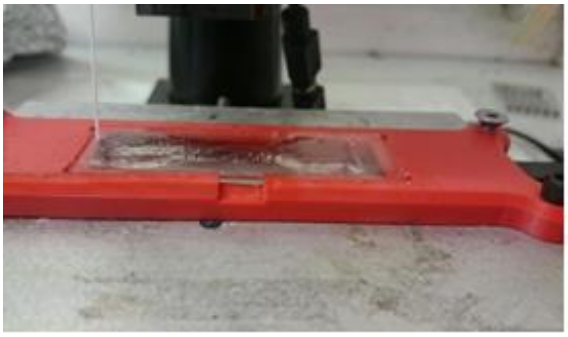

Figure 4.8 3D printed PAAm+9 M LiCl hydrogel in a bone shape design

Table 4.4 Mechanical parameters values for the fabricated PAAm+9 M LiCl after the tensile test analysis. This experiment was repeated three times from three different samples.

Hydrogel	Young's modulus (kPa)	Tensile strength (kPa)	Extension to failure (%)
Casted PAAm+9 M LiCl	13±2	22±1	411±18
3D printed PAAm+9 M LiCl	7±0.5	13±3	435±5

Moreover, the rheological investigations for the fabricated PAAm-9M LiCl hydrogel revealed the lowest difference in the complex viscosities between the extruded and the moulded gel (Figure 4.5 C, D and E). This means PAAm containing 9 M LiCl would be more reliable for extrusion for its lower complex viscosity difference from the casted gel of the same material.

4.6 Conclusions

The preparation, optimisation and characterisation of 3D printed ionic PAAm hydrogels were investigated. In terms of water-loss, it was found that LiCl-containing PAAm hydrogels remained stable over 30 days, whereas the NaCl-containing gels continued to dry out over time. The mechanical analysis of hydrogel samples showed that a trade-off of increased stability with LiCl came at the expense of lower tensile strength and ionic conductivity when compared to those containing NaCl. Optimised PAAm-LiCl hydrogel samples that were soaked in 9 M LiCl to attain 84% water content yielded a conductivity of 133±6 $mS.cm^{-1}$ with the maximum tensile extension of 290±29%. Furthermore, the mechanical and electrical properties of the printed PAAm containing 9 M LiCl hydrogel displayed very close parameter's values to that casted one. Numerous potential applications for these conducting, flexible materials lie in soft robotics and medical bionics.

Chapter 5

Wearable remote soft sensor device development from ionic PAAm hydrogel

5.0 Introduction

This chapter examines the operation of a soft sensor device (SSD) and innovations with its use. The mechanical and the electrical performance were examined after applying multiple cycles of compression stress before and after one year of the initial examination. Furthermore, the device was connected to an Arduino device to supply a power current from either a Li-battery or solar cell power bank and to send a Bluetooth signal to a mobile phone containing a specific application called UOW data sender. This application then sends two types of information to the database including coordination and text message help. The information, in turn, should be sent to another mobile phone (relative to the SSD holder or service center). Ionic skin is the utilisation of the flexibility, strength and biocompatibility of hydrogel materials in combination with the electrical conduction of ionic conductors. The ability of ionic skin to interface with electronic devices to make new types of transparent, elastic sensors and devices enables new opportunities both scientifically and commercially. In an effort to contribute to the state-of-the-art in this field, a wearable SSD was developed consisting of two lithium chloride conducting PAAm soft electrodes separated by a perforated elastomeric very high bonded (VHB) tape as shown in figure 5.1 a and b

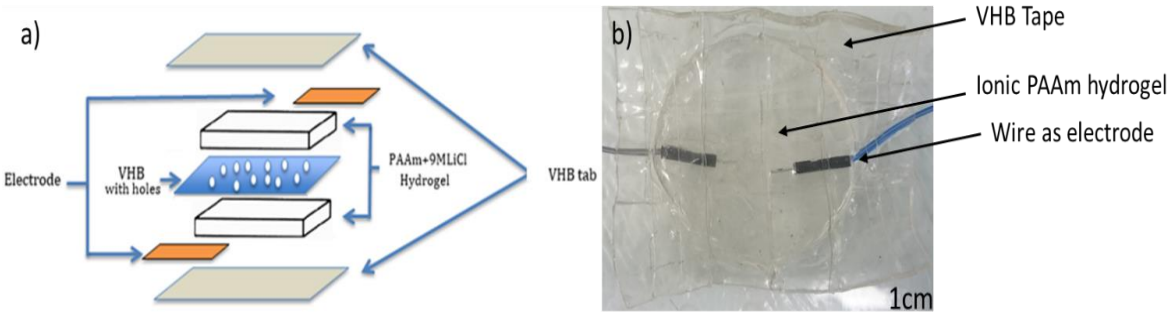

Figure 5.1 a) A typical figure of PAAm+9 M LiCl hydrogel sensor device components with b) a typical photo for the soft sensor device.

The novel perforation of the elastomeric material separating the electrodes enabled the creation of a sensor with an imbued threshold of operation. The device allowed for the detection of mechanical stress *via* a change in resistance within the electrodes, which enabled the device to operate at a much higher range of stress than was used in previous sensors by *Sun et. al.* [188] who relied on transmitting capacitance signal as a result of compression and strain actions. However, this attempt failed to be employed in our experiment application after the discovery that the ionic sensory sheet was unable to fulfil the project purpose. This was due to its inability to transmit sufficient DC current from the compression action on the soft sensory

sheet to the Arduino device (further explanation has been added for clarification in Appendix 3 point no.2, p249). This inspired the development of a (switch on/off) soft sensory sheet by adopting *Weigel et. al.* [331] sensory sheet. The SSD was shown to be durable, with mechanical recovery over fifty cycles of compressive stress for over one year. This SSD was linked with an Arduino device to send a signal to a mobile phone, creating a custom built a remote sensor. This work has the potential to enable better data collection for enhanced logistical decision making and emergency response *via* applications such as elastic sensors for remote areas.

5.1 Characterising the mechanical properties of the SSD

The mechanical properties of an SSD having dimensions of 50 mm diameter and 5 mm height were characterised *via* compression testing with the results shown in figure 5.2

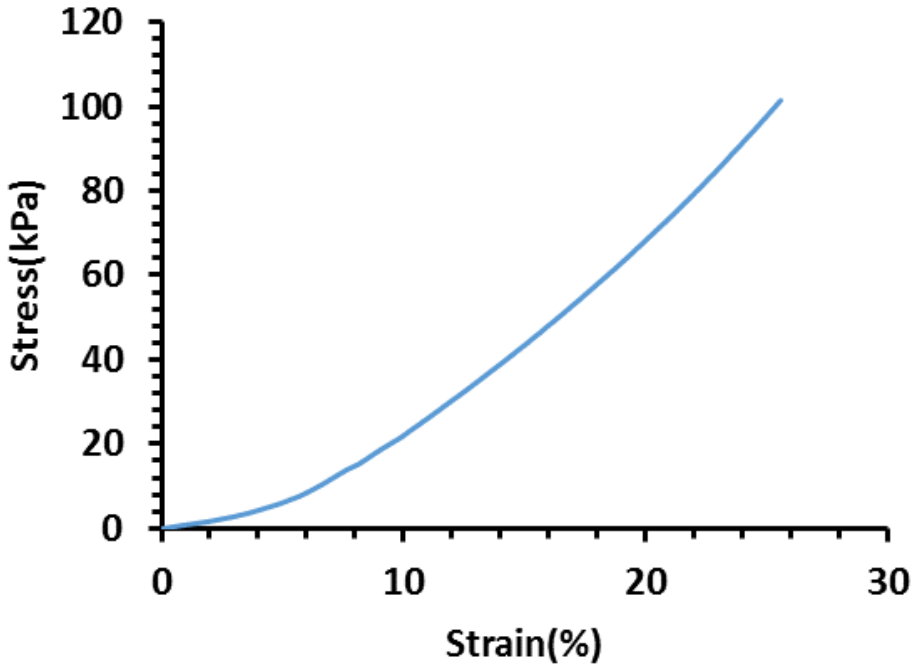

Figure 5.2 Compressive stress versus strain for the SSD. This experiment was repeated three times.

Table 5.1 shows the compression test analysis parameters for the SSD. This experiment was repeated three times.

Compression secant Modulus at (10-15%) strain (kPa)	Maximum Compression stress (kPa)	Maximum compressive strain (%)	Work of compression (J/m^3)
426±22	101.7±0.1	24±1	10.4±0.4

From figure 5.2 and table 5.1, it can be seen that the SSD was unbreakable even after applying over 100 kPa of compressive stress. Moreover, it is obvious that the error ranges of these data in table 5.1 were based on calculating the standard deviation of replicating the experimental assessment three times on the SSD. These results indicated that the device could be easily used as a pressure sensor for a durable SSD such as a touch screen or, as in our case, a flexible, robust, soft button for emergency response.

5.2 Electrical characterisations for the SSD:

The electrical properties of the SSD were examined *via* measuring the current and resistance of the device during compression testing with approximately 13 kPa of compression stress for five cycles (loading/unloading). These were performed to determine the minimum stress required to achieve a DC current. The correlation between applied stress and current creation of the device was measured and analyzed to understand and utilise the output signals for the Arduino device for the creation of a remote, soft, durable, reliable, cheap and novel pressure sensor.

5.2.1 DC current measurements

Figures 5.3 and 5.4 illustrate the correlation between current and applied stress from applying more than 13 kPa of cyclic compression stress on the SSD. The minimum stresses required for activation and maintaining of the output signal were examined to determine the effective thresholds for a clear output signal from the SSD.

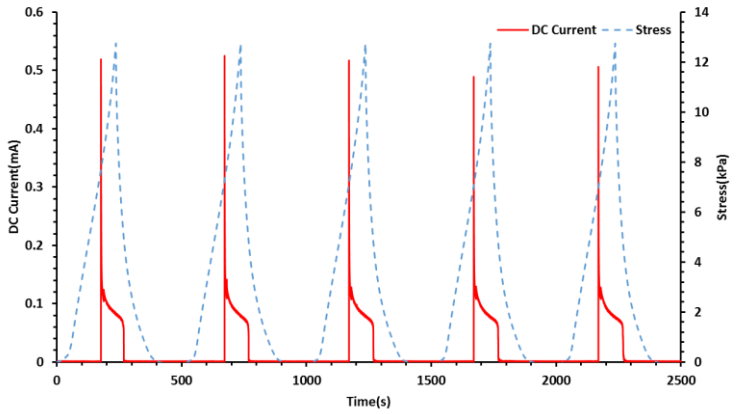

Figure 5.3 Stress/DC current vs time during applying compressive stress on the hydrogel sensor device for loading/unloading five cycles after applying 3V as a DC source. This experiment was repeated three times.

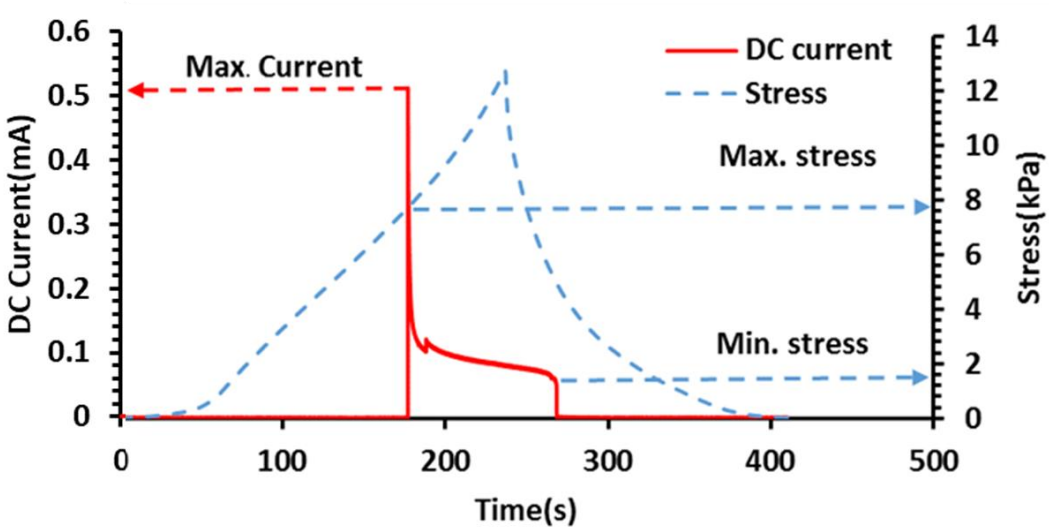

Figure 5.4 Shows DC current values for the SSD under one cycle compressive stress as a function of time. This experiment was repeated three times.

Figure 5.3 reveals stress/current vs time after applying five cycles loading/unloading compressive stress on the SSD. This figure also displays stress and current parameter values required for switching on/off the SSD as described in table 5.2. Figure 5.4 shows the DC current signal under one cycle compressive stress as a function of time. These two figures display an approximate maximum and minimum stress required for switching on/off the fabricated SSD.

These figures show that spiked signals were created after each compression cycle on the SSD due to compression of the SSD device resulting in the discharge of most of the charge after physical contact between the two conducting hydrogels through the perforated VHB layer. The continuous contact of the hydrogels leads to discharge of all the ions and this leads to the gradual weakening of the current signal. Therefore, lower stress is required for turning off the current activation as shown in figures 5.3 and 5.4.

Table 5.2 shows the maximum DC current and time on/off parameters when applying approximately 13 kPa of compression stress on the soft sensor device (SSD). This experiment repeated three times.

Compressive stress of current activation (kPa)	**Maximum created current (μA)**	**Min. stress for continuous activation (kPa)**	**Time on (ms)**	**Time off (ms)**
7.4±0.2	508±14	1.58±0.05	21±7	112±13

It is clear from figures 5.3 and 5.4 that the maximum stress to create a clear DC current signal was 7.4±0.2 kPa. While the minimum stress required to maintain a signal was approximately 1.58±0.05 kPa as shown in table 5.2. Furthermore, figure 5.3 shows that the stresses for activation and maintaining a signal are consistent over repeated uses, demonstrating the creation of a new, novel on/off SSD. The error ranges of the data shown in table 5.2 were based on calculating the standard deviation of replicating the experimental assessment three times on the SSD.

5.2.2 Resistance examination

The resistance of the SSD was also examined under 13 kPa of compression stress for five cycles (loading/unloading), with the results illustrated in figure 5.5.

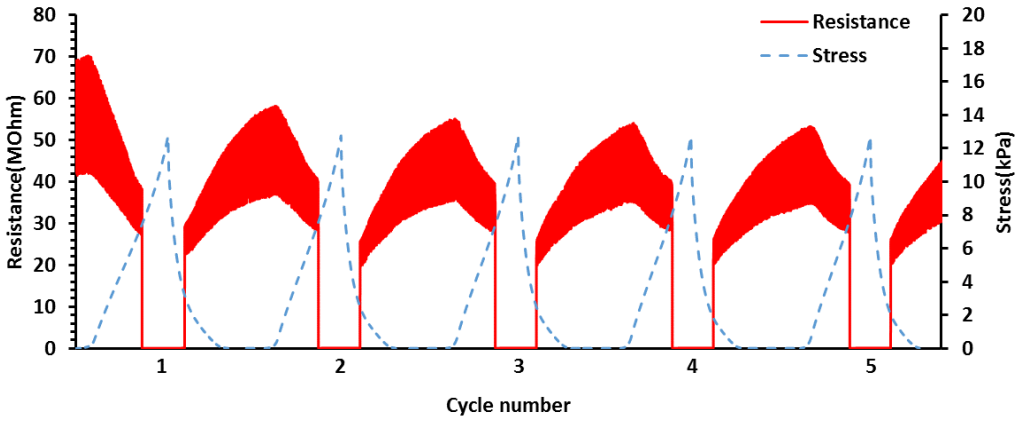

Figure 5.5 Shows stress/resistance vs time after applying compressive stress on the hydrogel sensor device for loading/unloading five cycles of the hydrogel sensor device. This experiment was repeated three times.

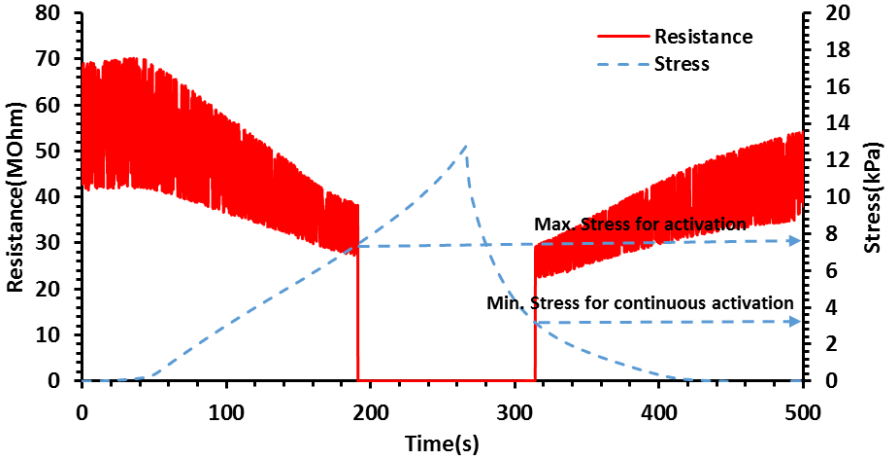

Figure 5.6 Shows stress/resistance vs time after applying compressive stress on the hydrogel sensor device for loading/unloading first cycle of the hydrogel sensor device. This experiment was repeated three times.

Figures 5.5 and 5.6 display that the maximum stress to create a signal was approximately 7.5±0.1 kPa. These results correlated with those found in section 5.2.1. Moreover, the minimum stress to maintain the signal was around 2.3±0.3 kPa. These values were found to be consistent over five (loading/unloading) compression cycles. The difference between the minimum stresses needed to maintain the signal when measuring the resistance compared to the current (2.3±0.3 kPa and 1.58±0.05 kPa, respectively) may have been a result of capacitance developing within the device. This suggests that resistance measurements

should be used for a more accurate output signal. The error ranges of these data were based on calculating the standard deviation of replicating the experimental assessment three times on the SSD.

Table 5.3 shows resistance and time parameters values after applying a compression test on the soft sensor device (SSD). This experiment repeated three times.

Compressive stress activation (kPa)	Minimum activated stress (kPa)	Minimum resistance (kOhm)	Steady resistance (kOhm)	Time on (ms)	Time off (ms)
7.5±0.1	2.3±0.3	21±11	40±20	128 ±30	148±77

The minimum resistance signal generated as a result of the minimum activated stress was 21±11 kOhm as shown in table 5.3. This value was difficult to display in figure 5.6 due to the high resistance scale values in (MOhm) before reaching the activation threshold when compared to the lower resistance values in (kOhm) created after activating the required signal for operating the SSD.

In addition, table 5.2 and figure 5.4 as well as table 5.3 and figure 5.6, show that the change in the minimum activated stress measured for both resistance and current varies slightly. The values of the minimum stress required for activating current and resistance signals were 1.58±0.05 kPa and 2.3±0.3 kPa, respectively. Furthermore, the possibility of SSD movement during the 5 continuous loading/unloading cycles may have affected measurement precision. Another reason for expecting some experimental error arises from repeating the experiments at different times as all these experiments used the same sample which might have a slight impact on its mechanical behaviour.

5.3 Durability characterisation:

The SSD was kept for one year with its mechanical, electrical and sensitivity properties analyzed and compared to its ‘as prepared’ state to determine its potential for applications requiring longer periods of functioning.

5.3.1 Mechanical testing

The mechanical durability of the SSD was characterised after applying and comparing fifty cycles of 14 kPa of compression stress for an ‘as prepared’ SSD and an SSD after one-year storage at room temperature and pressure. The results are displayed in figure 5.7.

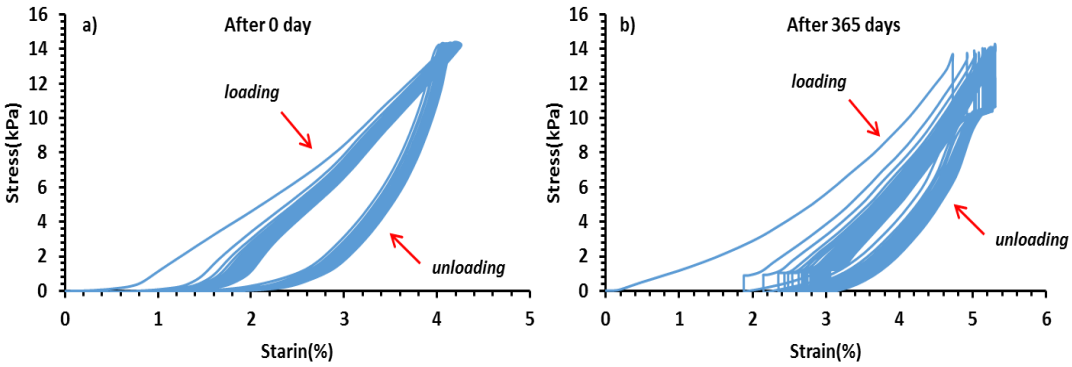

Figure 5.7 Shows stress-strain curves for loading/unloading fifty cycles of the hydrogel sensor device a) after 0 day and b) after 365 days. This experiment was repeated three times.

It was noticeable (Figure 5.7a) that the SSD exhibited high recoverability with a slight shifting in the strain during the fifty cycles of 14 kPa compressive stress, giving a hysteresis 565±36 mJ. m^{-3}. This was due to sliding or moving of the VHB tape from the hydrogel as a result of the interface bonding between the hydrogel and the VHB tape being weak as the PAAm-LiCl hydrogel is hydrophilic, while the VHB elastomers are hydrophobic. However, it was noticeable that the recoverability was also slightly decreased after one year due to the creeping of the hydrogel sensor. [332] The device displayed lower hysteresis at 107±26 mJ. m^{-3} due to the effect of time increasing the roughness of the elastomeric tape. [333] This demonstrated the effect of time on the SSD mechanical properties and could be considered a disadvantage when compared to using conductive additive-filled nanocomposites. [334]

5.3.2 Electrical properties

The phenomena of decreased mechanical durability due to the VHB tape delamination did not appear to significantly affect the electrical stability; whereby the device displayed a consistent average resistance

output of 435 ± 2 kOhm over fifty cycles, as shown in figure 5.8.

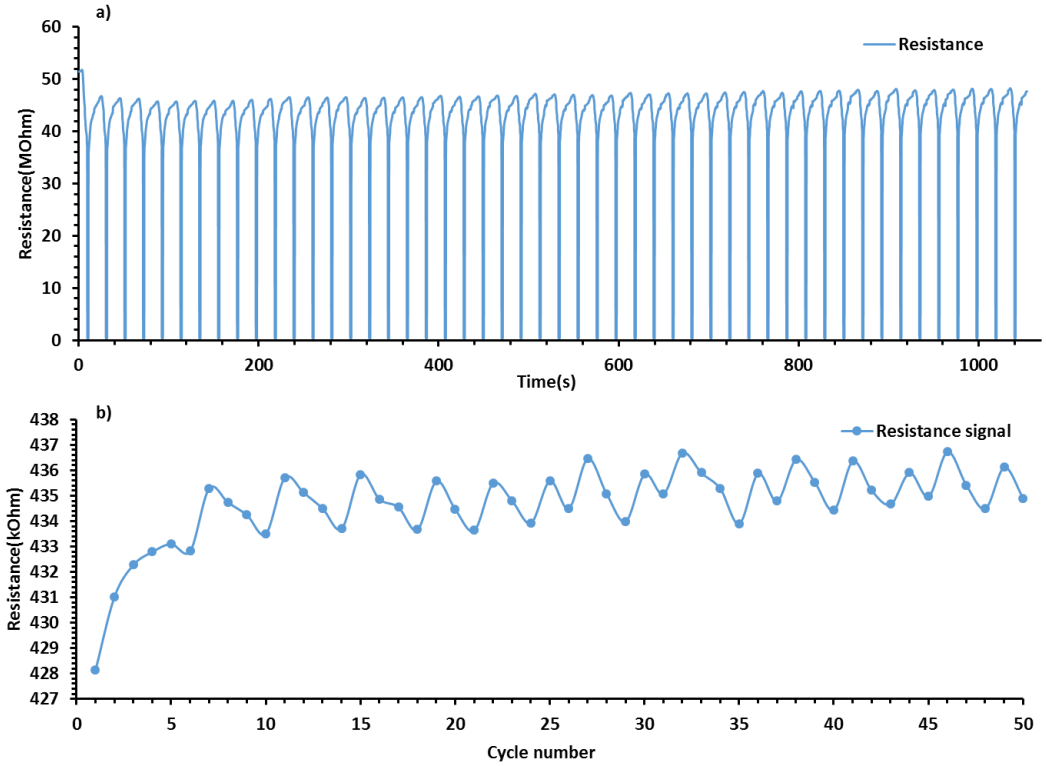

Figure 5.8 a) Shows the resistance stability after loading/unloading fifty cycles compression stress of 14 kPa and b) the loading resistance trend versus the compressive cycle number.

The resistance values shown in figure 5.8b were taken directly from the multimeter device, with the fluctuation in resistance signals due to the impact of applying constant pressure on the hydrogel structure impacting the ion and chemical polymer chain networks. Another adverse consequence of applying multiple cycles of pressure on the SSD to obtain precise electrical readout was the possibility of spatial displacement of the SSD due to the adhesion of the covering VHB layers of the SSD to the steel plate of the mechanical analyser instrument.

In addition, it is clear from figure 5.8b that the resistance signals for the first five cycles increased by approximately five kOhm due to the interface issue between the hydrogel and the elastomer tape. However, the resistance trend stabilized, fluctuating between 433-436 kOhm. The slight increase was determined to give 2±1 kOhm from the fifth loading cycle to the fiftieth cycle. This slight increase could be attributed to the impact of both the interface hydrophobicity difference and the hydrogel creeping after applying fifty compressive cycles continuously.

5.3.3 Device Sensitivity

The electrical sensitivity was also characterised after applying fifty cycles of 14 kPa compression stress on the SSD to determine if the device could also function as a more precise pressure sensor for more complex applications. The examination performed before and after keeping the SSD for one year displayed a consistent sensitivity of 5800±500 Ohm/Pa for the instant test and sensitivity of 1000±100 Ohm/Pa after one year, as shown in figure 4.9 a and b.

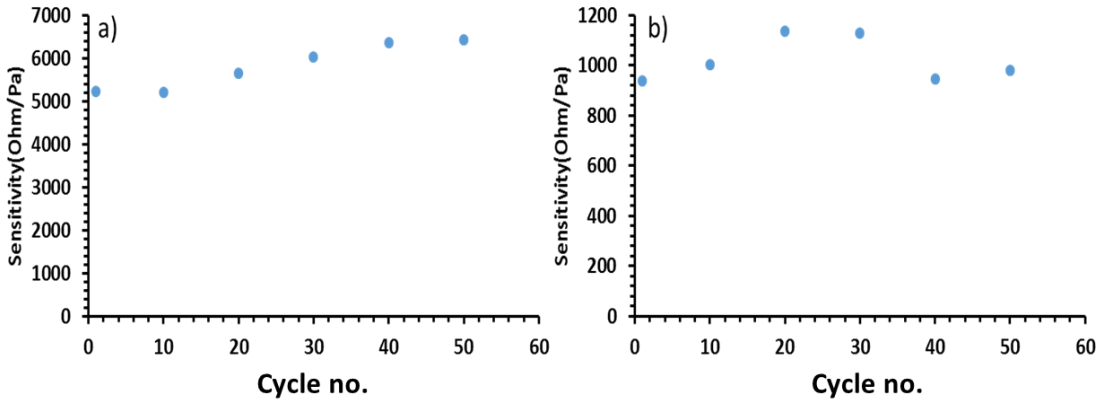

Figure 5.9 The electrical sensitivity of SSD after applying a 14 kPa compressive stress on SSD a) instant test b) after one year.

The significant decrease in the sensitivity was attributed to creeping both of the conducting hydrogel and the elastomeric VHB tape which were affected by two factors; time and the temperature. [335] However, the sensitivity trends reveal the existence of the electrical response at the SSD even after one year of storage at RT.

5.4 SSD application as a remote transferring signal:

The prepared SSD was connected to an Arduino device to be used as a pressure sensor, as shown in figure 5.10.

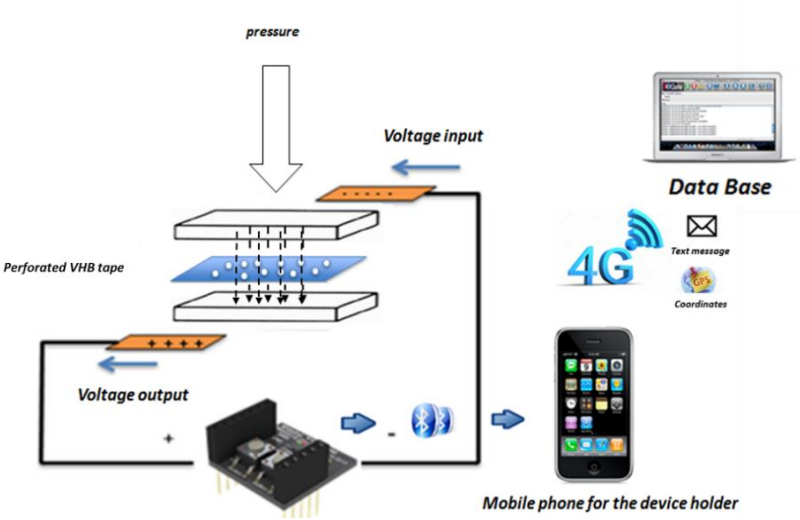

Figure 5.10 A schematic figure of the mechanism of transferring an electrical signal from PAAm+9M LiCl hydrogel sensor device to the Arduino (Bluetooth sensor device) that send a Bluetooth signal to the mobile phone (iPhone). This figure was generated by the candidate.

Figure 5.10 illustrates that when applying pressure above a specific threshold (7.5±0.1 kPa) on the SSD, an electrical circuit is created, whereby the ions within the hydrogel electrodes are able to travel through the perforated VHB. This detection of an applied pressure was then sent to a remote Arduino Bluetooth device. The reaction time between the application of the pressure and the Arduino device recording a change was 0.8±0.2 seconds while the time taken to detect the removal of the pressure was 2.4±0.5 seconds. The Bluetooth device internally translated the received electrical signal to a mobile phone using a customised application named the UOW_data-sender. This transmitted signal from the SSD can then be combined with GPS data, creating a novel type of soft, cheap, durable, remote pressure sensor. This work created new opportunities for logistics analysis, material analysis or, as has been explored in our research, emergency response applications.

5.4.1 Signal sender, location and data receiver

The Bluetooth chip was coded *via* associated virtual port drivers, which were designed to identify active (On) and inactive (Off) SSD activity *via* the application and removal of pressure, respectively. The data was then sent with a customizable message to a phone.

The phone received the Bluetooth signal from the SSD *via* a specific UOW-coded application named the "UOW_Data-sender". Xcode was used to create this software and was written in objective c (c sharp) and

was designed to perform two functions; to receive the Bluetooth signal of the SSD sensor with location coordinates using the phone GPS manager, and turning/ sending the received signal with the GPS data to a database centre.

Once the database centre received the code linked to the SSD, a socket stream was opened which accessed the device on the specified IP (UOW internet provider IP) through the specified port (6798 has been chosen as a temperate port for this project). When the socket established a connection to the computer, it was first required to pass through the router as the IP is the router IP and not the computer's IP. The net settings were altered through the router using the routers default LAN IP (Uni-default router IP) as a gateway; this required administrative access to the router, which the port was mapped to so that any incoming traffic on the routers IP on port 6798 would be redirected to the specified device, in this case a computer on the specified port 6798. Although it did not have to be a different port which may be used, it was required to be send by LAN IP, so the device requires a static IP which is set in networking --> adapter settings --> IP4.

The server-side software (computer program) could now establish a socket with the phone's side application. This was established through the use of the Winsock libraries and the phones ns socket libraries. Although these libraries are designed for different programming languages, c++ and c# respectively, and run on two completely different operating systems, they are ultimately similar and function without issue. After the socket was established, the server-side program sets its side of the socket into listening mode, and the phone sends the message (Help, assistance, etc) *via* the newly established socket. The server-side program receives the message and echoes it back to the phones at the same time. The server-side socket must have a character buffer (an array of char variables of definitive length, in this case, it was 100) if the received message is larger than the character buffer the program will crash due to it making an attempt to access data that is not within the buffers set limits and it will access another program's memory which is not allowed. The message was then written to a text file, where this text file was placed within a server shared file so it can be accessed over the internet. Team viewer was used to control the server-side computer for demonstration as a remote administration tool (rat).

The data receiver (UOW_Data-Receiver application) was also written in Xcode in c#. The application sent a set of characters, including the phone IP to the server (of the database centre), as the server can only send back the signal to the same LAN IP that it has received and recorded. When the data receiver application was connected to the server, it established a socket connection *via* the phones IP address. However the

phone IP is dynamic as well, so the WAN IP address also changes as the phone connects to a network. Thus, a 'family/relative' phone could be added to the server, connecting through 4G internet. After that, the server reads the data file and finds the last entry data received from the SSD (every time pressure on the SSD occurred) and sends it back as a data echo to the UOW_Data-Receiver(s).

Finally, the data on the receiver phone displays a text message, e.g. "Help", with GPS coordinates. The location code uses location core services lib, this is an automatic referencing c#, returning a location manager that contains the locations object.

The major idea from characterising the SSD was to develop it as a wearable device for its skin convenience and durable mechanical characteristics. The SSD will be connected to the Arduino device which has the ability to transmit the signal coded using a Bluetooth device to the mobile phone (iPhone) with a specific app. The signal would transmit again providing a text message with the location coordinates for the SSD by using the 4G network technology to send it to the database computer. The database computer then will record and turn the original SSD message with the coordinators to a relatives' phone, tablet or computer.

In conclusion, the SSD device was prepared from PAAm containing LiCl hydrogel and VHB tape and customized to emit an electrical signal after exceeding a pressure/stress threshold. This could help many people by sending an SOS signal to their relatives or a service center in an emergency, as shown in figure 5.11.

Figure 5.11 a schematic figure describes how the wearable soft sensor device works. This illustration was made by the candidate.

Figure 5.10 displays the SSD attached to the back of a hand connecting to an Arduino device. This device is then placed in a fabricated box bonded to a rubber wrist band. In an emergency the pressure on that SSD will create a current, resulting in a signal to the Arduino device. The Arduino device will send a Bluetooth signal to the mobile phone having the customized application. The mobile phone would send a signal through 4G internet service to the computer database providing a text message and coordinates for the soft sensor device location to relatives or emergency response.

Additionally, it is possible to change the Li battery with a solar cell power bank to allow for longer and more remote applications, as shown in figure 5.12.

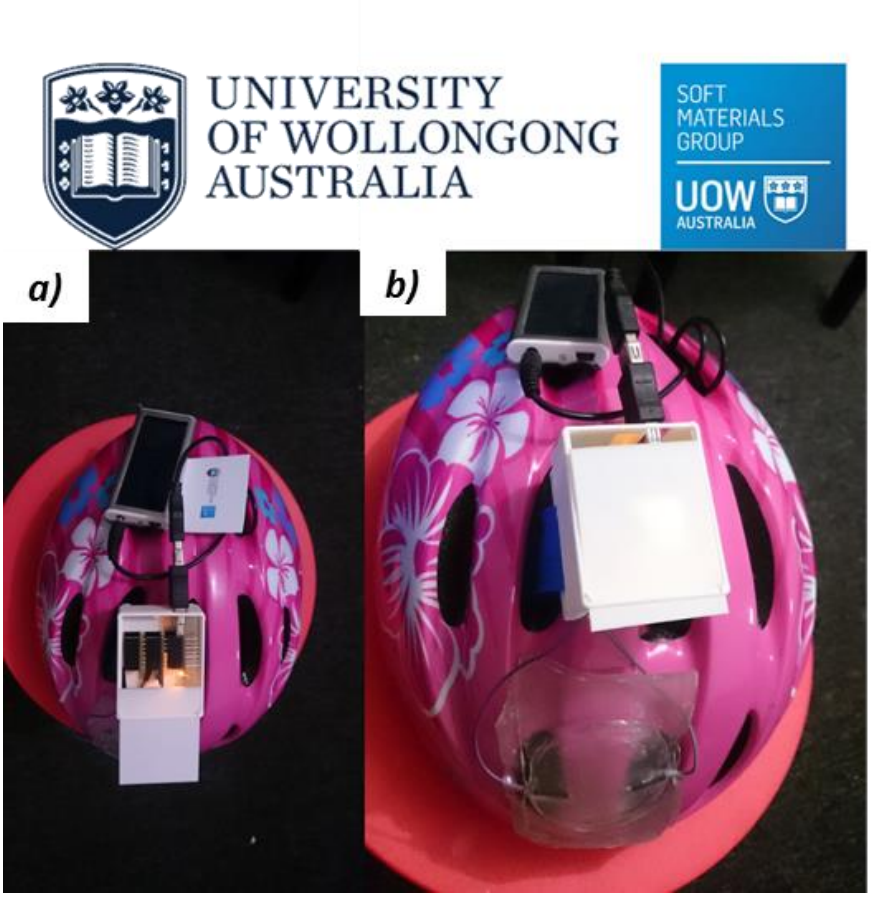

Figure 5.12 a) Shows Images of the Arduino device inside a fabricated box, connected to the solar cell power bank and bonded on a bicycle helmet. b) The Arduino device inside a 3D fabricated box connected to the SSD.

5.5 Conclusions

In summary, a wearable SSD has been fabricated successfully using elastic conductive hydrogel with VHB tape. The mechanical and the electrical durability of the SSD have been characterised over fifty cycles even after one year of storing the device. The SSD was demonstrated as a pressure sensor to detect static and dynamic pressure to be used as a resistive sensor that offers a higher range of stress than was used in previous sensors. Based on that, this SSD was combined with an Arduino device to send a signal to a mobile phone, creating a custom-built remote sensor. This application was achieved allowing the SSD to send an electrical signal giving consistent sensitivity of 5800±500 Ohm/Pa. Two types of power sources were used; a Li-battery and a solar cell power bank to provide DC current to the SSD. This type of project has the potential to enable better data collection for enhancing the emergency response via applications such as this wearable, durable, flexible sensor device.

Chapter 6

Handheld printing of soft, stretchable conductive component for a strain gauge device

6.0 Introduction

This chapter describes fabricating a durable soft strain gauge device, named here as HEH, composed of a printed soft, stretchable conductive hydrogel. The device was produced by extruding an ionic AAm ink solution over a VHB tape substrate which was cured using UV light to initiate the photopolymerisation reaction. The mechanical and the electrical performance before and after one year of the initial assessment were carried out after applying multiple cycles of the tensile test. Furthermore, the resistance sensitivity for the HEH over a finger bending was examined and compared after one year of the initial characterisation.

Highly flexible soft electronics have attained increasing attention in recent years due to its promise in several applications. [32], [94], [108], [188], [222], [336-352] 3D Printing of soft stretchable and conductive materials with intrinsically elastic components could establish a new generation of wearable electronics. However, many obstacles must be overcome to develop this technology for commercialisation such as complicated experimental techniques, expensive cost and durability issues. [222], [353-355] This project aimed to fabricate a soft elastic strain gauge device using a facile method to fabricate durable, soft, low-cost devices for wearable electronics. In particular, a handheld printing technique was utilised to extrude non-precious materials PAAm containing lithium chloride. These inks were used to print simple geometries shapes; sinewave tracks and/or straight lines, onto elastic very high bonding (VHB) tape and UV cured to form a hydrogel-elastomer hybrid (HEH) device. The mechanical and the electrical properties of the HEH devices were examined before and after one year of storage in a plastic Petri-dish at RT.

6.1 Hydrogel sensor device fabrication

An AAm ink solution containing 4 M LiCl hydrogel was prepared as shown previously in section 2.2.2 and was extruded onto a VHB substrate of 60 mm in a straight line and zigzag shape patterns. A UV light source polymerised the AAm ink into PAAm. Additionally, an alternative printing method was also explored using a handheld extrusion device at a specific flow rate to make the HEH device as described previously in chapter two and figure 2.9.

Several challenges arose from complications created at the interface between the hydrogel and the elastomers as a result of the high permeability of elastomers to oxygen that yielded oxygen inhibited polymerisation of the PAAm. This was due to the hampering of free-radical polymerisation on the surface of the hydrogel polymers preventing covalent cross-linking. [356] Furthermore, the hydrophobic nature of the elastomer surfaces adversely affected the hydrogel –elastomers bonding. [357] The free radical

inhibition was addressed by removing the oxygen *via* vacuuming the AAm precursor ink solution in a desiccator for 20 minutes before the curing process. Hydrogel-elastomer bonding was formed by focusing ultraviolet irradiation to intiate a photo-polarisation reaction between the two layers. The resultant hydrogel–elastomer hybrid formed extremely robust interfaces due to the covalently anchored polymer network onto the elastomer. [358] The hybrids were able to be highly stretched without interfacial failure by creating an interpenetrating covalent network, as shown in figure 6.1.

In general, interpenetrating covalent networks produce tough and stretchy hydrogels *via* dissipation of mechanical energy during deformation. [79], [151], [359] Using this premise, our hydrogel-elastomer model was produced with physical crosslinks enabling the hydrogel to keep its pre-designed form during assembly. [79], [119], [151], [360]

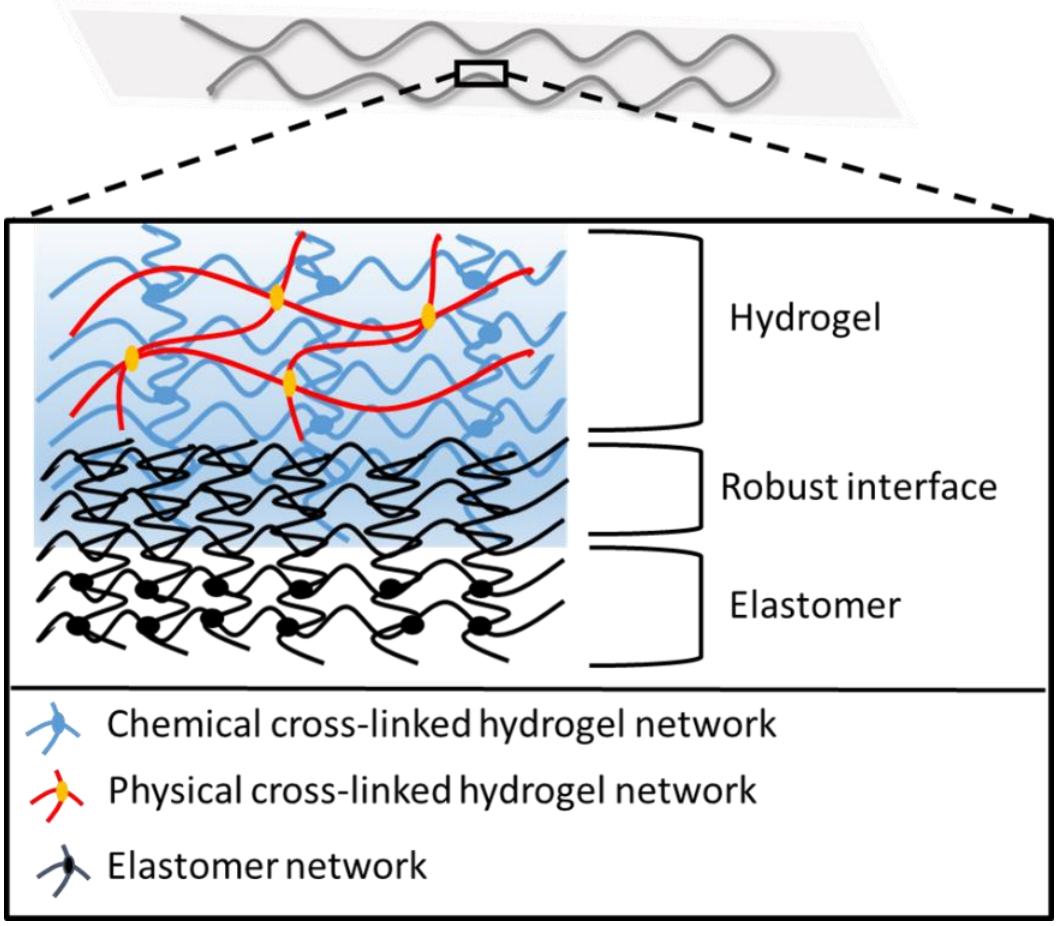

Figure 6.1 illustrates the hydrogel-elastomeric interface networks in the HEH. This illustration was modified and reconstructed after adopted from reference. [357]

The cross-sectional profiles for the straight line printed hydrogel was investigated by studying the geometry

of the fabricated design using 3D optical profilometer as shown in figure 6.2.

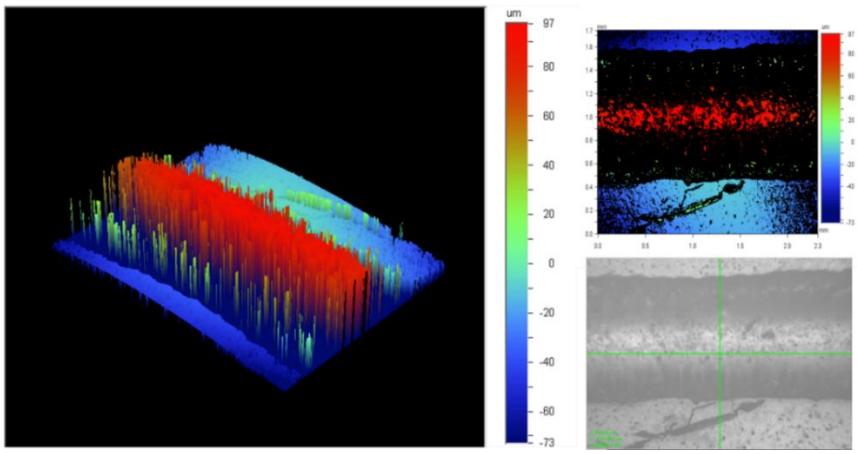

Figure 6.2 Optical profilometry images and the cross-sectional profiles of the gel line with one hydrogel layer of HEH. The black colour represents the interface layer of the hydrogel with the VHB tape layer which is called the robust interface as shown in appendix 3, p251.

Figure 6.2 shows that the printed hydrogel line over the elastic substrate displayed a half semi-oval form with an average width 1.17±0.04 mm and average height 91±6 µm. This demonstrated that the steady shape for the hydrogel filament gesture confirms the ink remains stable with time after being cured. Upon curing, monolithic, highly extensible, conformal HEH is produced. (Further explanation has been added for clarification on Appendix 3 point no. 3, p251.

6.2 Strain gauge characterisations:

6.2.1 Mechanical characterisation

Tensile test analysis was performed on the HEH until failure at 5 mm/min. Figure 6.3 and table 6.1 revealed that the HEH has the ability to exhibit large extensibility, up to six times its original length elongation at a break and a tensile strength of 222±13 kPa.

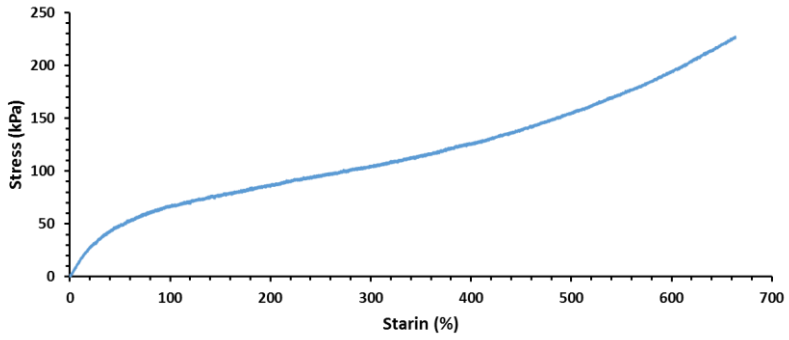

Figure 6.3 Tensile test diagram showing the stress versus strain for the HEH. This experiment repeated was three times from three different samples.

Table 6.1 Tensile test analysis parameters for HEH until failure. This experiment was repeated three times from three different samples.

Parameters	Values
Tensile Modulus (kPa) to 25% strain	121±5
Tensile strength (kPa)	222±13
Extension of Failure (%)	650±30

6.2.2 Electrical characterisation

The electrical properties were investigated by characterising the resistance of the printed hydrogel on a VHB elastomeric tape during tensile testing until failure. The change in the resistance of the HEH device was described as a ratio between R_o and R, where R_o was the initial resistance and R the change in resistance. Similarly, the change in the length of the HEH device was described as a ratio between L_o and L, where L_o was the initial length and L the change in length. These assumptions predict that the ratio of a resistance of the stretched HEH over the initial, unstretched resistance was given by increasing the R/R_o ratio by 0.8 over the strain ratio when the printed HEH was stretched by 350% strain. As shown in figure 6.4.

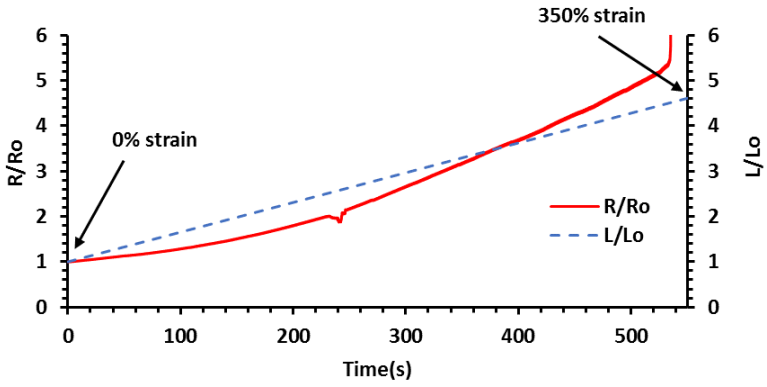

Figure 6.4 the normalised resistance and the stretch of HEH is measured as a function of time stating between (0-350%) strain states applied on the HEH. This experiment was repeated three times from three different samples.

6.2.3 Mechanical durability

The mechanical hysteresis for the HEH was assessed before and after one year of storing at 21 °C to investigate the mechanical durability. The HEH devices were stretched ten times to 215% strain with results shown in figure 6.5.

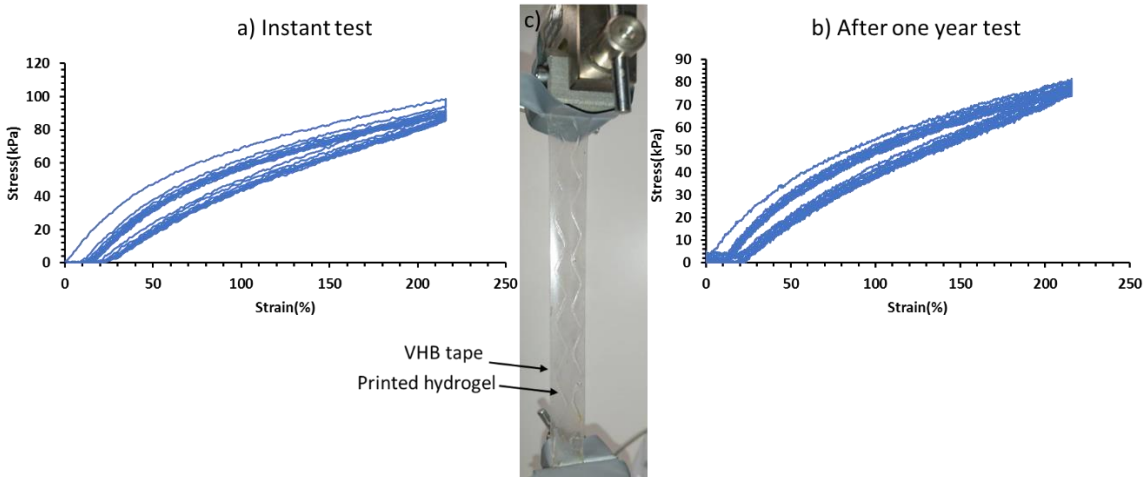

Figure 6.5 Stress as a function of strain after applying ten tensile cycles at (215% strain) on the HEH during a) instant test and b) after one year test with c) a typical photo of the HEH during a tensile test. This experiment was repeated three times from three different samples.

Figure 6.5 showed that the HEH displayed near identical mechanical behaviour after one year of storage. The HEH device was stored in the lab inside a closed glass Petri dish. The temperature of the lab was 21 °C and the measured humidity was between 45-55% during the year. It was shown that the HEH devices were able to be stretched to 215% repeatedly with no issue both initially and after one year of storage. However, although the strain was unaffected by time, the mechanical stress of extension to 215% strain decreased slightly from 98 kPa to 85 kPa for the as-prepared compared to the one year stored HEH devices, respectively. This could be a result of the creeping effect on the hydrogel and acrylate elastomeric tape. Creeping effect on the hydrogel is defined as the effect of the hydrogel degradation over time that will impact on the mechanical behaviour of the hydrogel during storage. [361-362] Furthermore, the mechanical hysteresis of the 10th cycle also displayed a decrease of about 0.05 kJ/m^3. These outcomes showed that although the HEH devices did experience a slight decrease in mechanical properties after one year of degradation, these effects were minimal. Therefore, this illustrates the reliable mechanical durability of the HEH device.

6.2.4 Electrical durability

The electrical properties of the prepared HEH sample were examined for five cycles of tensile testing at 215% strain before and after one year; results are shown in figure 6.6.

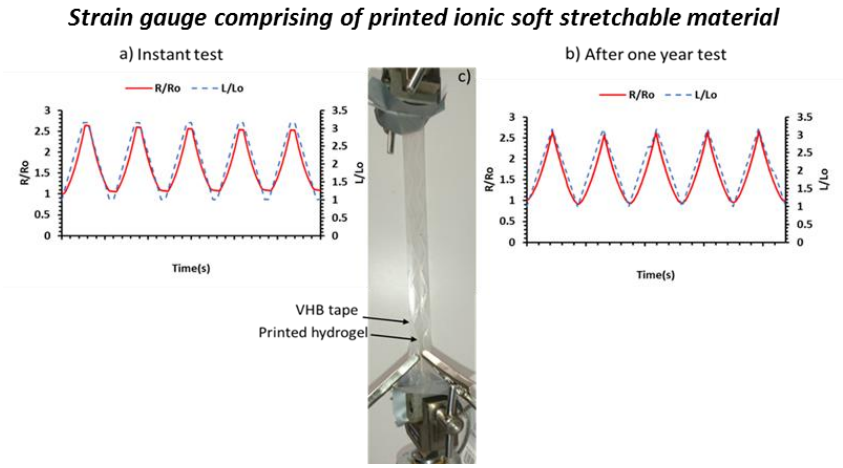

Figure 6.6 the normalised resistance of the printed gel-elastomer hybrid consisting of PAAm with 4 M LiCl during five cycles of stretching at 215% strain using mechanical analyser a) before and b) after storing the HEH for one year with c) a typical photo of HEH under tensile test. This experiment was repeated three times from three different samples.

It can be seen from figure 6.6 that the relationship between the normalized resistance (R/R_o) and the strain (L/L_o) at 215% are incredibly consistent, recording an average normalized resistance and average extension change ratios of 2.4 and 3.1, respectively. Furthermore, these values are near identical after one year of storing, recording 2.6 and 3.1 for both resistance and strain change ratio, respectively. Moreover, it is clear that the L/Lo values in figures 6.4 and 6.6 both started from 1. However, the L/L_o values were different in these two figures because the HEH stretched to different levels. For example, the HEH stretched to 350% strain in Fig. 6.4 but, the same device stretched up to 215% strain in Fig. 6.6. On the other hand R/R_o, also started from 1 in both figures but their values were different when they stretched because they were stretched to different levels of strains as shown in the illustrated figures 6.4 and 6.6, respectively.

The Gauge factor for the HEH was determined and compared to the as-prepared device and after one year of examination giving a sensitivity of 0.7±0.1 and 0.74±0.01, respectively.

The electric responses of the HEH were investigated after fixing it to a finger to examine the resistance sensitivity during bending of a finger, as shown in figure 6.7 and 6.8. This experiment was performed before and after one year of storing.

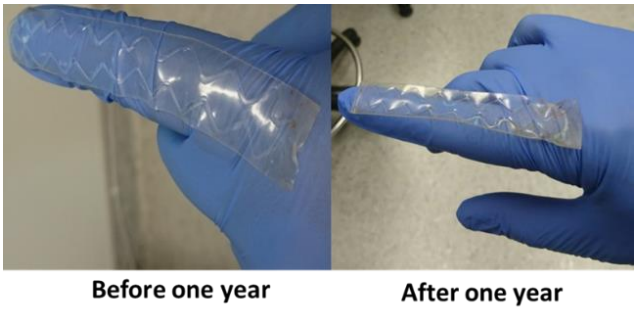

Figure 6.7 Photos of printed HEH before and after one year bonded on a finger.

It is evident from figure 6.7 that the HEH has no major change in shape. The water percentage for the salt containing PAAm within the HEH was also determined to be 79% (w/w). This percentage decreased by 2% (w/w) after one year of storage. This low water loss percentage value was attributed to the addition of hydroscopic LiCl salt to the printed hydrogel within the HEH. This agent has the ability to substitute the water loss by withdrawing the moisture from the environment and therefore extending the lifetime of the sample. [273] The length difference between being fully bent and fully straightened action of the finger was 20 mm. As the HEH length is 60 mm, this means that the HEH will extend to 30% strain when the finger is in a fully bending position as shown in figure 6.8.

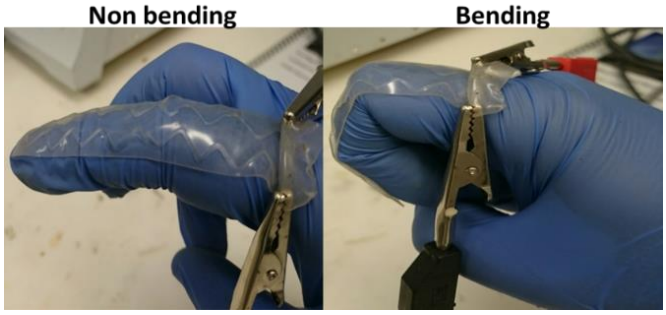

Figure 6.8 Bending and non-bending action finger with the HEH gauge.

The piezoresistance terminology has been used extensively in several recent studies with the elastomeric conductive sensors, to describe the change in the electrical resistivity when mechanical strain is applied. [363-366].The piezoresistance displayed a stable resistance response after stretching the HEH for multiple cycles during bending a finger. The normalized resistance was determined by recording 1.35±0.02 Ohms, as shown in figure 6.9.

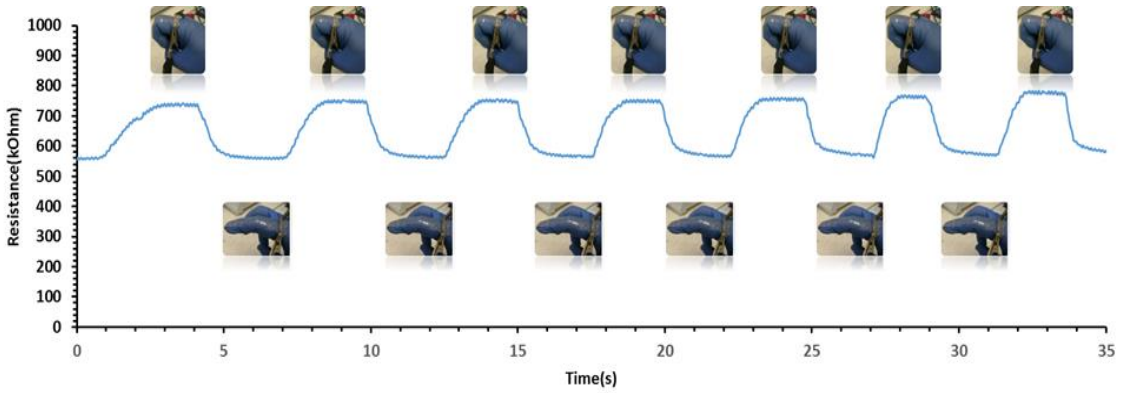

Figure 6.9 Resistance responses of a bonded HEH on a finger during bending and non-bended action. This experiment was repeated three times from three different samples.

Furthermore, the durable performance of the HEH was assessed after one year. The stable R/R_o data was clear and consistent after 1000 cycles of stretching during finger bending, giving a change ratio of 1.3±0.1. It was observed that the R/R_o difference for both periods, before and after one year of storing, was only 0.05, as shown in figure 6.10

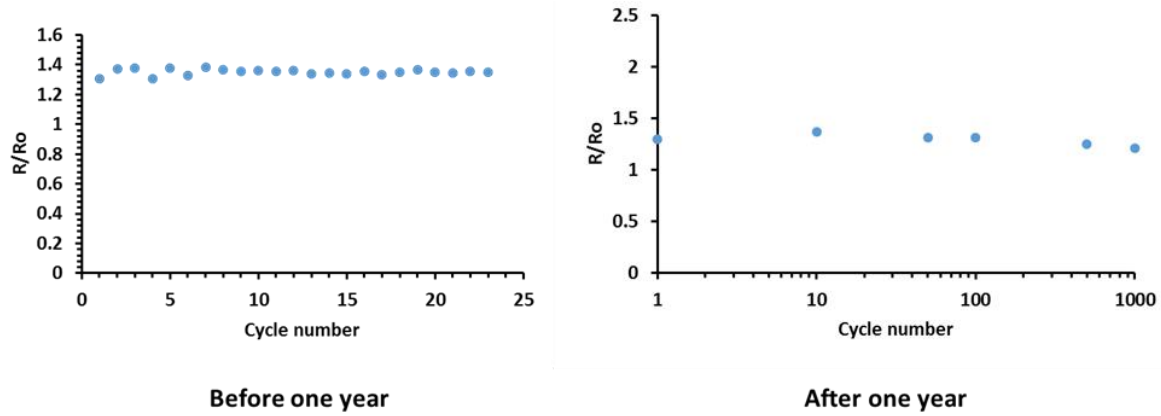

Figure 6.10 Shows R/R_o effect under multiple cycles of bending/non-bending finger positions at the time of start of the experiment and after one year of storing the HEH in a plastic Petri-dish at RT. This experiment was repeated three times from three different samples.

These results illustrated that this decrease does not have any major effect on the piezoresistance activity for the HEH even after one year of degradation. Further, no delamination or fracture was observed during these experiments.

6.3 Conclusions

In summary, an affordable, soft, stretchable, conductive and durable HEH resistance sensing device was fabricated. This device was achieved *via* 3D printing of a soft ionic hydrogel having a robust interface with an elastomeric matrix using a simple interpenetration polymerisation method. Furthermore, the non-static instruments allow for the sensor geometry and properties to be independently tuned by controlling the print path and filament cross-section. This approach opens new avenues for developing soft functional devices that can be used in wearable electronics, human/machine interfaces and soft robotics using a facile technique and non-static instruments.

Chapter 7

Preparation, characterisation and application of cellulose sponge-PAAm material as a strain sensing element

7.0 Introduction

This work demonstrated a new type of non-toxic, cheap and high performing strain gauge that has the potential to open new avenues in multiple fields including soft robotics, physical monitoring and material analysis. This experimental chapter adapted a commercial kitchen cellulose sponge to fabricate strain sensing material. The mechanical and the electrical properties were characterised to examine the material reliability to be utilised as a strain gauge.

7.1 Mechanical analysis:

Different samples of 'as bought' cellulose sponge, dried cellulose sponge, wet cellulose sponge, PAAm, cellulose sponge-PAAm hybrid, PAAm with 6 M LiCl and cellulose sponge+PAAm containing 6 M LiCl were analysed using mechanical testing. The mechanical properties of these samples were analysed using compression and tensile testing to determine the optimum mechanical properties for the development of a strain-gauge device.

7.1.1 Compression test analysis

A compression test analysis was conducted on the samples at 21-23 °C, with the data compared and displayed in table 7.1:

Table 7.1 Compression test analysis parameters for cellulose sponge, wet sponge, dried sponge, PAAm hydrogel, sponge-PAAm hybrid, PAAm containing 6 M LiCl and sponge+PAAm containing 6 M LiCl samples with their water content and surface area. This experiment was repeated three times from three different samples. (Further explanation has been added for clarification on Appendix 3, point no. 4, p252).

Parameters	Sponge	Wet sponge	Dried sponge	PAAm	PAAm+sponge	PAAm+6 M LiCl	Sponge+PAAm_6M LiCl
Water content (%)	12.6±0.4	71±1	0	86	60.16±0.02	76	53.8±0.2
Surface area (cm^2)	9.12	8.64	8.16	---	10.56	---	9.12
Compression secant modulus to 2% strain (kPa)	136±23	84±7	361±38	18±4	34±7	10±1	94±9
Compression stress at failure (kPa)	105±2	84±10	344±4	2241±1	315±46	709±102	304±14
Failure strain (%)	76.921±0.003	83.337±0.002	85±1	89±1	70±8	81±1	56±1
Work of Compression ($kJ\ m^{-3}$)	12±1	9.9±0.3	280±20	25±17	41±37	16±12	3±2

Table 7.1 illustrates the effect of water on the mechanical properties of the cellulose sponges, whereby an increase in water content resulted in a decrease in mechanical properties. This effect was explained to be a result of the added water interacting with the hydroxyl groups of the cellulose within the sponges. The water allows the cellulose molecules to rearrange themselves to minimize energy, therefore under applied stress the wet sponges' cellulose rearranges and displays reduced compressive mechanical properties. This explains the difference between an as bought sponge and "dried sponges" mechanical properties due to the as bought sponge absorbing moisture from the air, as depicted in figure 7.1. [367-368] However, for this work, a water content was required to allow for ionic conduction, so the dried sponge samples were not explored further.

It was shown that the addition of a PAAm network within the cellulose sponges resulted in a strengthening

of the samples when compared to cellulose sponge samples of similar water content, from 84±10 kPa to 315±46 kPa for a wet sponge compared to a sponge-PAAm hybrid (Table 7.1). This was thought to be a result of the PAAm network creating an IPN within the sponges, resulting in synergistic strengthening *via* dissipation of mechanical stress throughout the sample. [369-370]

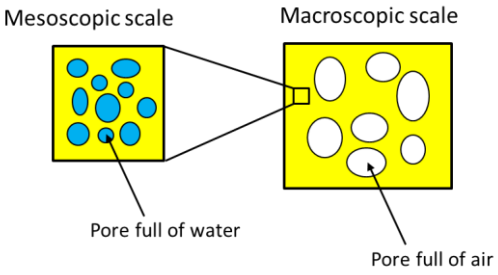

Figure 7.1 Two-scale porosity model for cellulose sponge. This figure was reconstructed after adaption from. [369]

7.1.2 Tensile test analysis

A tensile test analysis was also investigated for the dry sponge, as the bought sponge, wet sponge, PAAm, cellulose sponge-PAAm gel hybrid, PAAm with 6 M LiCl and cellulose sponge- PAAm containing 6 M LiCl gel at 21-23 ◦C as shown in table 7.2.

Table 7.2 Tensile test analysis parameters for cellulose sponge, wet sponge, dried sponge PAAm hydrogel, sponge-PAAm hybrid, PAAm containing 6 M LiCl and sponge-PAAm containing 6 M LiCl samples with their water content and surface area. This experiment repeated three times from three different samples.

Parameters	Sponge	Wet sponge	Dried sponge	PAAm	PAAm+sponge	PAAm+LiCl	Sponge+PAAm+6 M LiCl
Water content (%)	20±1	77±1	0	86	72.6±0.1	76	64.2±0.2
Surface area (cm^2)	21	21	21	---	19	---	21
Tensile Modulus (kPa) to 3 % strain	105±7	63±12	2926±112*	4±2	113±11	6.1±0.4	137±14
Tensile strength (kPa)	174±8	145±2	56±6	8±1	63±10	12±1	40±2
Extension of Failure (%)	54±1	64±6	26±3	127±16	61±2	240±68	53±3
Work of extension ($kJ\ m^{-3}$)	39±2	39±4	11±1	6±1	31±5	19±8	12±1

(*)Tensile modulus of dried sponge only was calculated at 0.3 % strain due to its high slope when compared to other materials.

The tensile test analysis illustrated that there was no significant impact from adding PAAm hydrogel with

LiCl to the cellulose sponge extension to failure, as displayed in table 7.2. However, the sponge hybridisation with PAAm and LiCl hydrogel increased its tensile modulus from 105±7 kPa and 113±11 kPa to 137±14 kPa when compared to the sponge alone and sponge hybridised with PAAm hydrogel, respectively. This addition of LiCl salt to the PAAm hydrogel increased the tensile modulus when added to the hybrid samples, and resulted in an increment of the tensile robustness. This suggests that the ionic LiCl reacted with the cellulose network making it resist deformation under higher loads compared to the other sponge samples as shown in table 7.2. This effect could be explored in future research as an alternative means of tailoring the mechanical properties of the system by altering the LiCl content. There is a noticeable decrease of both tensile strength and work of extension values of the fabricated cellulose sponge with PAAm+LiCl hydrogel from 145±2 kPa and 39±4 kJ m^{-3} to 40±2 kPa and 12±1 kJ m^{-3}, respectively. This could be a result of the capability of the cellulose sponge structure to stretch and then dissipate the energy over the entire structure in a homogenous manner, more so than the cellulose sponge with PAAm+LiCl hydrogel structure. This effect also can be studied in the future as an alternative means of tailoring the mechanical properties of the system after adding different types of hydrogel to the cellulose sponge.

7.2 Water content study

The water content of each sample was determined by cutting different sizes of prepared sponge's samples to explain the capacity of these samples to absorb water when their surface areas were increased.which will influence on both the mechanical and electrical properties; results are shown in figure 7.2.

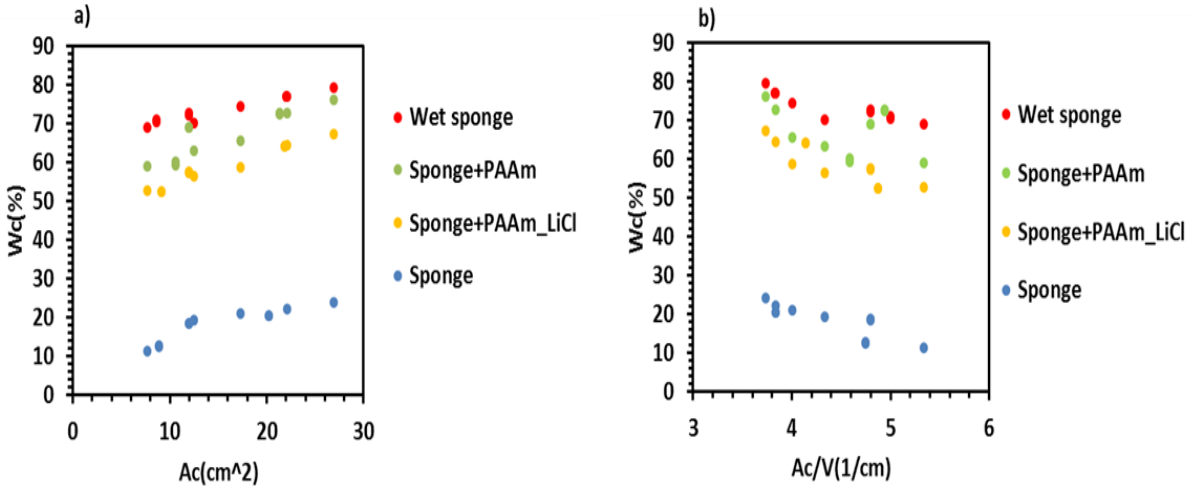

Figure 7.2 Plots of water content as a function of a) surface area (Ac), b) surface area to volume ratio (Ac/V) of the wet, cellulose sponge, PAAm with cellulose sponge and PAAm+6 M LiCl with a cellulose sponge. This experiment was repeated three times from three different samples. Uncertainty values associated with data in these graphs are shown in table 7.2.

The water content percentages of the various sponges were evaluated using equation 7.1. All the weights were recorded using a digital lab balance.

$$\text{Water content } \% = \frac{\text{Mass of wet sponge} - \text{Mass of dry sponge}}{\text{Mass of wet sponge}} \times 100, \quad \textbf{.....(Eq.7.1)}$$

Furthermore, the water content percentages in the PAAm hydrogels were evaluated using equation 7.2.

$$\text{Water content } \% = \frac{\text{Mass of water in gram}}{\text{Total Mass of hydrogel composites}} \times 100, \quad \textbf{.....(Eq.7.2)}$$

However, the water content percentages of sponge with PAAm or PAAm+LiCl hydrogels composite samples were evaluated using equation 7.3.

$$\text{Water content } \% = \frac{\text{Mass of gelled sponge} - \text{Mass of dry sponge}}{\text{Mass of gelled sponge}} \times \frac{\text{Mass of water in gram in the hydrogel}}{\text{Total Mass of hydrogel composites}} \text{x } 100$$

,.....(Eq.7.3)

It can be seen from figure 7.2a that the water content in the sponge increased with increasing the surface area. Moreover, the water content was determined as a function of surface area to volume ratio to investigate the capability of the water molecules to occupy the sponge holes as shown in figure 7.2b. It was found that the water content fluctuation with decreasing surface area to volume ratio in all sponges. However, all samples revealed clear trends whereby the water content increased with the decreasing surface area to volume ratio.

Therefore, this demonstrated the idea that the water content magnitude would be affected by the total volume and surface area of the sponge samples resulting from occupying the water molecules inside the sponge holes which would reflect directly on the mechanical and the electrical behaviours.

7.3 Optical Microscopy Imaging

To confirm the effectiveness of hybridising PAAm containing 6 M LiCl within the cellulose sponge, photos were taken using optical microscopy before and after hybridisation with the PAAm containing 6 M LiCl hydrogel, as shown in figure 7.3.

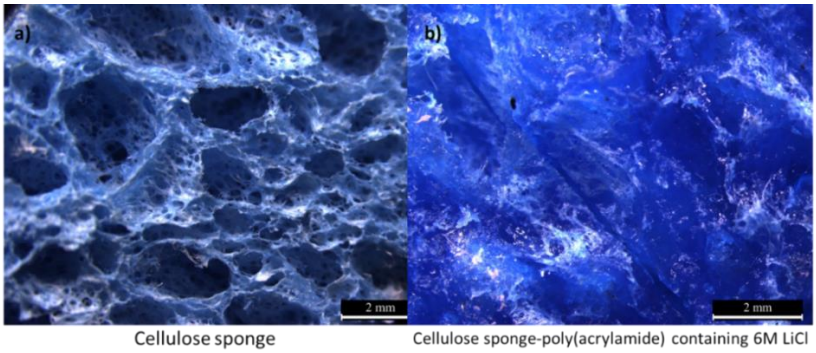

Figure 7.3 Typical images for a) cellulose sponge and b) cellulose sponge-PAAm containing 6 M LiCl hydrogel samples.

It is evident from the difference between figures 7.3a and 7.3b that the PAAm hydrogel displayed homogeneous dispersion over the entire structure of the cellulose sponge. These results correlated with the assumption from sections 7.1.1 and 7.1.2 that the hydrogel created an IPN within the sponges to strengthen the mechanical properties of the cellulose sponge as outlined in figure 7.4.

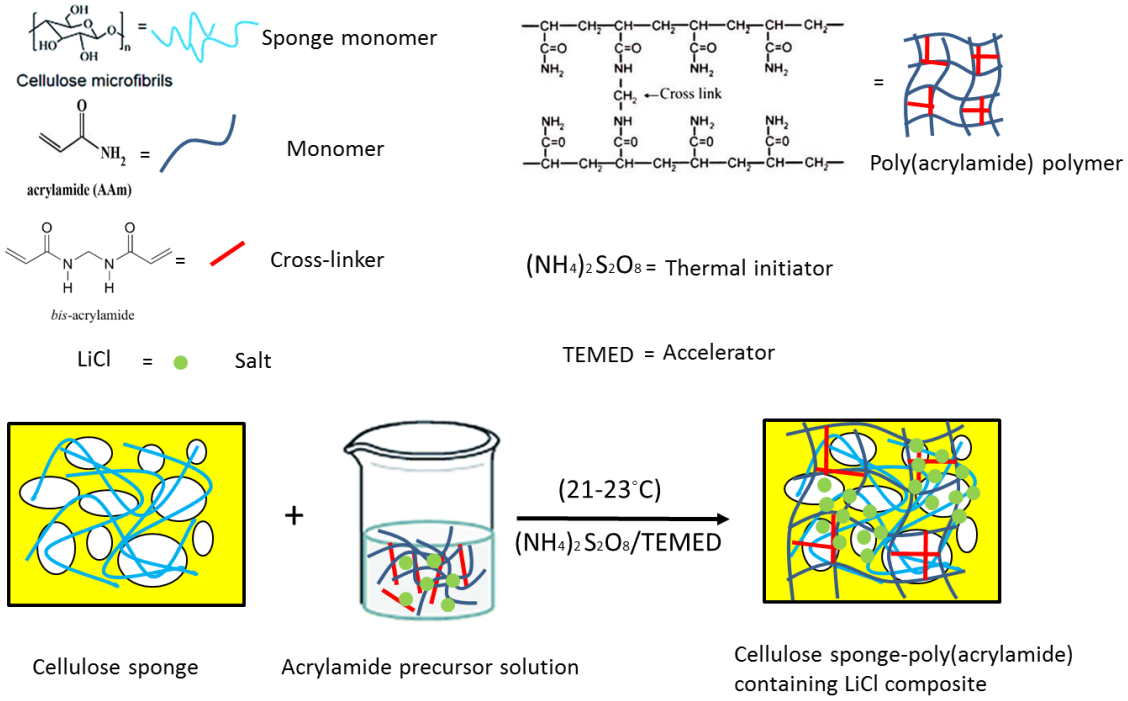

Figure 7.4 A schematic figure for cellulose sponge-PAAm containing 6 M LiCl hydrogel hybridisation process. This illustration was produced by the candidate.

7.4 Electrical properties study

The electrical properties were characterised for the prepared samples of 1 cm height × 1 cm width × 2.5 cm length. Results are displayed in figure 7.5 and table 7.3, respectively.

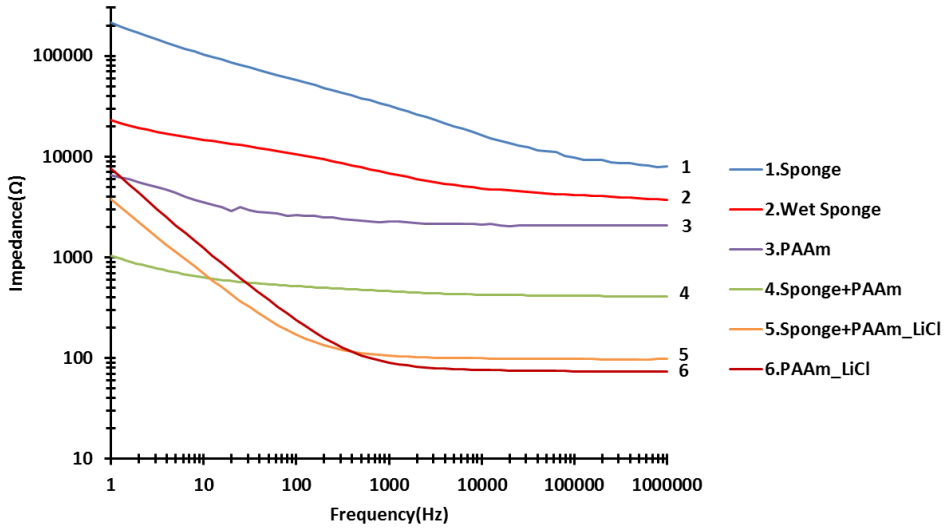

Figure 7.5 Bode plot is showing impedance vs frequency of dried and wet sponge, PAAm, PAAm+6 M LiCl, PAAm+sponge and sponge+PAAm_6 M LiCl.

Table 7.3 Impedance values at a frequency range from 25 kHz-1 MHz with its water content for the sponge, wet sponge, dried sponge, AAm monomer with a sponge, PAAm hydrogel, cellulose sponge- PAAm, cellulose sponge-PAAm containing 6 M LiCl. This experiment was repeated three times from three different samples.

Hydrogel	Sponge	Wet sponge	Dried sponge	AAm+sponge	PAAm	PAAm+sponge	PAAm_LiCl	Sponge+PAAm_6 M LiCl
Impedance at frequency range 25 kHz-1 MHz (Ohm)	9819±64	4320±141	$>10^6$	8010±212	2078±32	411±2	75±1	99±1
Water content %	19±2	72.9±0.2	0	72.4±0.3	86	69.1±0.2	76	57.3±.4
Surface area (cm^2)	12	12	12	12	12	12	12	12

It is clear from table 7.3 that the cellulose sponge+PAAm with 6 M LiCl had the lowest impedance reading of the cellulose sponge containing samples at 99±1 Ohm. Furthermore, the cross-linked PAAm hydrogel within the cellulose sponge displayed superior conductivity when compared to the uncross-linked AAm within a sponge. This difference is thought to be a result of the addition of the initiator APS to the hydrogel. Moreover, the inclusion of LiCl had the greatest effect on lowering the resistance. The added LiCl ions resulted in a rapid decrease in resistance within the materials as the ionic charge carriers increased the ionic conduction within the materials. Correspondingly, this means that the conductivity will be increased because of the reversible relationship between the electrical resistance and electrical conductivity according to equation 1.5. [171]

Where ρ is the electrical resistivity and R is the electrical resistance of a uniform specimen of the material (Figure. 1.17) and *l* is the length of the piece of material while A is the cross-sectional area of the sample. Additionally, the water content among cellulose sponge-hydrogel and cellulose sponge samples was observed to have a direct impact on the electrical impedance, as shown in table 7.4. The increase in the water content within the sponge decreased the electrical impedance according to the following materials series:

Wet sponge > as bought sponge > dried sponge

This was attributed to the ability of the water molecules to fill the sponge holes and facilitated the ionic

conduction within the materials.

The addition of 6 M LiCl to the cellulose sponge-PAAm demonstrates a new type of material with an electrical impedance of 99±1 Ohm.

Furthermore, the use of LiCl salt was chosen for its hygroscopic moiety, which helped absorb moisture or water molecules from the surrounding environment and hence prolongs the hydrogel and the device durability. [273]

7.5 Strain sensing gauge from cellulose sponge-PAAm containing LiCl hydrogel composites:

A strain gauge was fabricated using cellulose sponges with PAAm. The mechanical and electrical properties were investigated using mechanical testing and impedance analysis, respectively. This study was performed to determine the mechanical parameters in which the design could function and the device sensitivity as a strain gauge. The device was prepared as shown in figure 7.6.

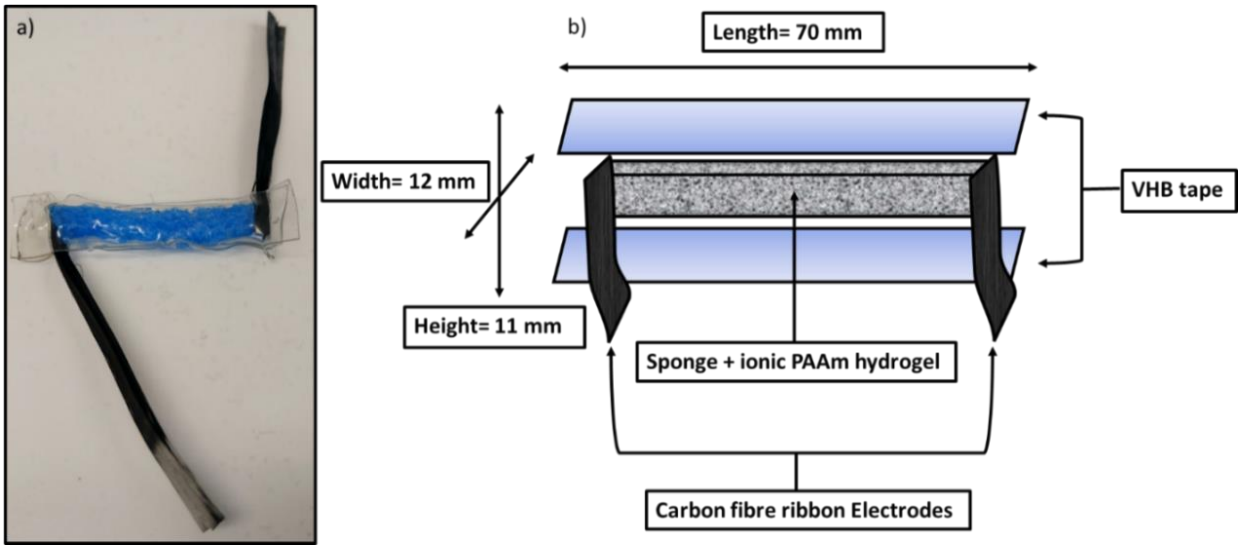

Figure 7.6 a) A photo of a soft strain gauge device made from cellulose sponge and PAAm with LiCl hydrogel. b) The typical figure describes the soft strain gauge device components. This figure was produced by the candidate

As shown in figure 7.6 a sponge-hydrogel composite was attached between two carbon fiber electrodes and sealed by two layers of VHB tape. The tape was chosen to cover the device for three primary reasons; firstly, the tape has a pronounced elasticity that conserves the mechanical integrity of the device. Secondly, the tape has no conductivity and can be used as a dielectric material for its ability to isolate the conductive

elements. Finally, covering the device with VHB tape will help preserve the water content in the sponge-hydrogel composite.

7.5.1 Strain sensing gauge mechanical characterisation

The mechanical properties of the samples were determined using tensile test analysis. The device described in figure 7.6 and all of their components were testing using ten cycles of tensile stress to 15% strain. This was performed to identify the effect of each added component towards the mechanical properties of the device. The results are shown in figure 7.7.

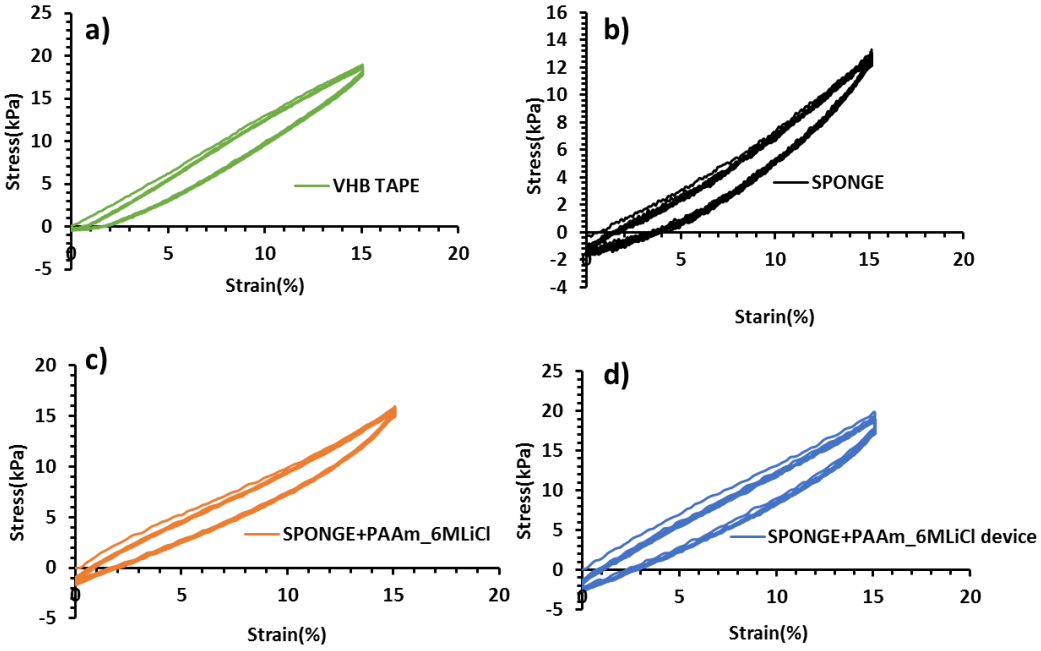

Figure 7.7 Ten cycles tensile stress under 15% strain plot for each a) VHB tape b) cellulose sponge c) sponge with PAAm+6 M LiCl and d) a sponge-PAAm with 6 M LiCl sealed within two layers of VHB tapes.

The fabricated sponge-hydrogel device composed of two layers of VHB tape, cellulose sponge, and PAAm with LiCl hydrogel. Figure 7.7a displayed the mechanical behaviour of stretching the VHB tape to 15% strain for ten cycles. Figures 7.7b and 7.7c display the mechanical impact of hybridising the cellulose sponge with the PAAm hydrogel resulting in a recovery strain decreased from 4.5% to 2% after multiple cycles of stretching. This was also reported after crosslinking the cellulose sponge with 3-mercaptopropionic acid. [369] The third cycle of each composite was chosen to be analysed and compared because of the concentration stress or 'stress raisers effect' that is inherent in the first two cycles. This can

be caused by many reasons such as geometric discontinuities; cracks, holes, sharp corners and changes in the cross-sectional area, which cause the material to display a local increase in the intensity of a stress field as shown in figure 7.8. [370]

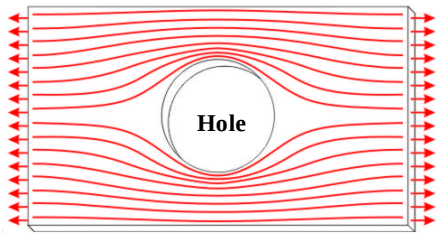

Figure 7.8. A typical illustration showing the internal force lines are denser near the hole. This figure was adapted from. [369]

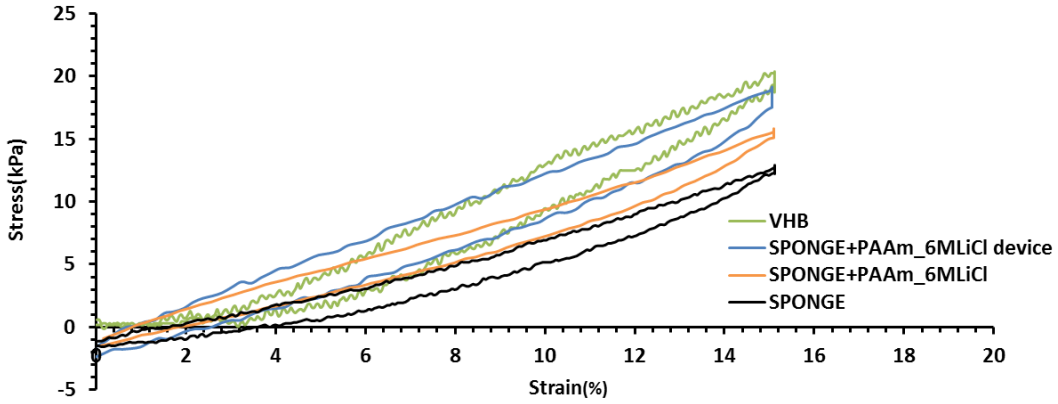

Figure 7.9 Third cycle tensile stress under 15% strain plot for each sponge, two layers of VHB tape and sponge with PAAm +6 M LiCl before and after covering it with two layers of VHB tape and making it as a strain gauge device.

Figure 7.9 showed that the cellulose sponge and cellulose sponge with PAAm do not recover to their original length due to the stretching effect after the third cycle. This could be a result of breaking some of the hydrogen bonds that link the cellulose chains [369], [371-372] Furthermore, the cellulose sponge alone displayed the lowest tensile stress with the lowest tensile modulus at 15% strain when compared to sponge with PAAm before and after sealing it with VHB tapes giving 14±3 kPa with 147±3 kPa, 15.9±0.1 with 184±17 kPa and 19±1 kPa with 246±10 kPa, respectively (Table 7.4). Alternatively, the double layers of the elastomeric VHB tape presented the highest stress at a break between all the components including the

device itself but with the lowest tensile modulus at 15% strain from all other components including the device itself reporting 20.5±0.1 kPa and 112±3 kPa, respectively. It is evident from figure 7.9 and table 7.4 that the mechanical parameters values revealed an essential impact of both hybridising PAAm with LiCl hydrogel to the cellulose sponge and sealing the hybridised structure with two layers of VHB tape on improving the mechanical robustness of the produced device. Furthermore the hysteresis value of the combined hybrid device consisting of (sponge, hydrogel and VHB faucet) displayed better mechanical properties when compared to the hysteresis values of the individual components composing this hybrid device. Generally, all the parts revealed a hysteresis magnitude resulted from a loading and unloading difference for each cycle which represents the dissipated energy within the material. Therefore, the excellent mechanical robustness and the hysteresis in the sponge-hydrogel device was due to the combination of the component mechanical robustness (Table 7.4).

Table 7.4 Third cycle tensile test analysis parameters for two layer of VHB tape, Sponge with PAAm and 6 M LiCl before and after covering it by two layers of VHB tape. This experiment was repeated three times from three different samples.

Parameters	VHB Tape	Sponge	Sponge+PAAm_6 M LiCl	Sponge+PAAm_6 M LiCl Device
Tensile Modulus (kPa) at 15% strain	112±3	147±4	184±17	246±10
Tensile strength (kPa)	20.5±0.1	14±3	15.9±0.1	19±1
Extension of Failure (%)	15.09±0.01	15.2±0.1	15.07±0.02	15.07±0.01
Hysteresis value ($kJ.m^{-3}$)	0.9±0.4	0.2±0.1	0.8±0.3	1.01±0.03

7.5.2 Strain sensing gauge electrical characterisation

The resistance and the impedance data collected using a Keithley Digital Multimeter device after applying constant DC voltage and Gamry Potentiostat Galvanostat device at frequency 25 kHz as shown in figure 7.10.

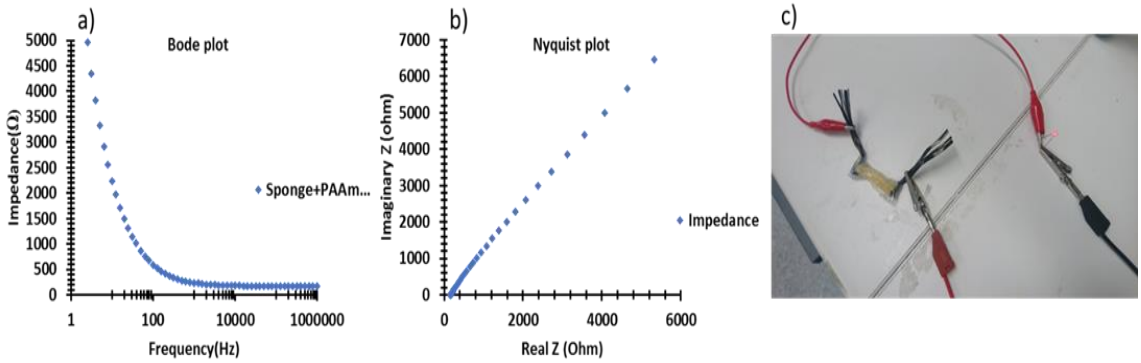

Figure 7.10 a) Bode plot b) Nyquist plot and c) A typical photo shows the sponge-ionic hydrogel hybrid conductivity after connection with 5 V power supply and led light. This experiment was repeated three times from three different samples.

It was noted that there was a big difference between the impedance and the resistance readings; this could be attributed to the capacitance created from a DC voltage during resistance measurements collected from the multimeter device while the impedance was determined using AC at frequency 25 kHz as shown in table 7.5.

Table 7.5 Impedance and resistance for the Sponge+PAAm_6 M LiCl device. This experiment was repeated three times from three different samples.

Material	Impedance (Ohm) at a 25 kHz frequency	Resistance (kOhm)
Sponge+PAAm_6 M LiCl device	167±1	464±2

Furthermore, it can be seen from table 7.5 that the impedance value for the sponge-hydrogel device was 167±1 Ohm, which is more than the impedance value of the cellulose sponge-PAAm with 6 M LiCl sample at 99±1 Ohm. This is a result of the surface area and volume of the device being higher than the sponge-hydrogel sample from previous sections.

To determine the device's operational threshold, the sponge-hydrogel hybrid device was extended to breaking with the overlaid electrical and mechanical results shown in figure 7.11.

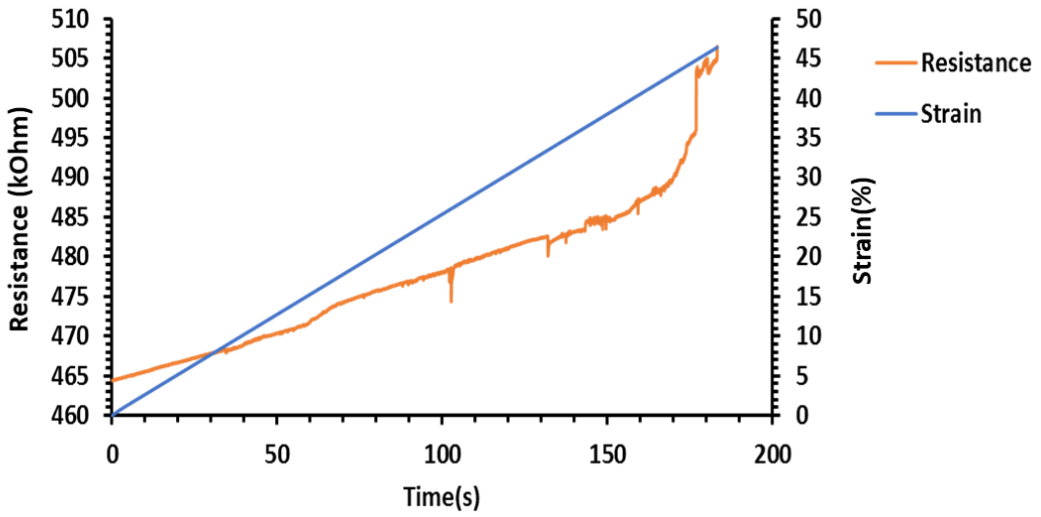

Figure 7.11 Resistance change under the effect of tensile strain until failure for the cellulose sponge-PAAm with 6 M LiCl hybrid device.

The device reported an ascending increase in the resistance with gauge stretching until approximately 40% strain. The resistance was shown to increase rapidly when pulled more than 40% strain. The device resistance stopped responding after stretching beyond 45% strain. As a result of these responses, the devices operational limit was set to 15% strain.

To characterise the device sensitivity or "gauge factor", the resistance of the fabricated device was measured simultaneously while stretching to 15% strain over six cycles. A Keithley Digital Multimeter was used to determine the resistance at 2 W during pulling of the sponge-gel device as described in the experimental section 2.5.3. Results are shown in figure 7.12.

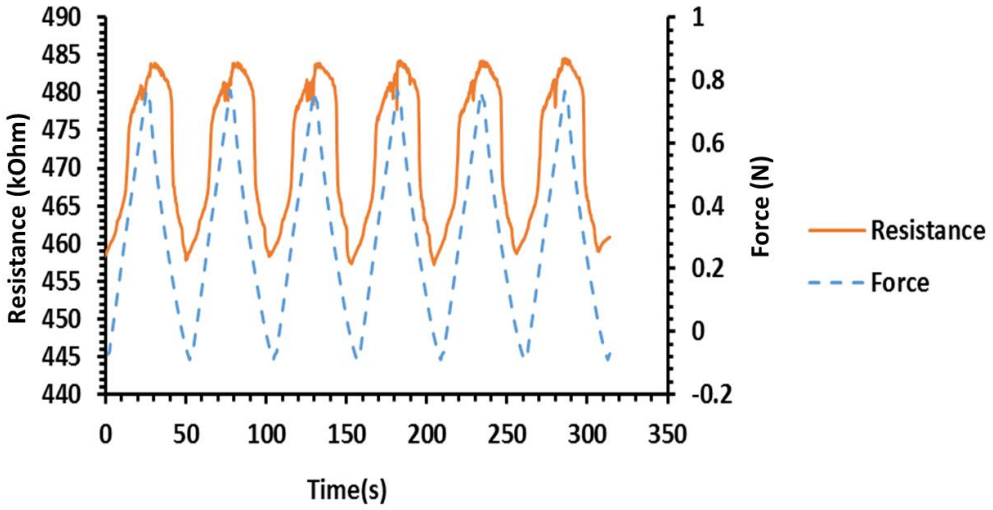

Figure 7.12 Resistance vs tensile force for cellulose sponge with PAAm with 6 M LiCl after stretching six cycles of 15 % strain. This experiment was repeated three times from three different samples.

Figure 7.12 demonstrated the consistent resistance change for six cycles of the sponge-hydrogel device during extension. The results indicated a maximum resistance of approximately 484 kOhm and a baseline of approximately 457 kOhm. Moreover, the maximum force to reach 15% strain was approximately 0.75 N.

Furthermore, an essential parameter of the strain gauge is its sensitivity to strain, described numerically as the gauge factor (GF). The gauge factor was defined as the ratio of fractional change in electrical resistance to the fractional change in length (strain) which is expressed in equation 1.7. [195, 373]

Where ΔR is the resistance change between the status of the deformed and undeformed sponge-hydrogel device, R is the resistance magnitude for the undeformed device. ΔL is the change in the deformation length change in mm and L is the undeformed length of the device and sometimes ($\frac{\Delta L}{L}$) called by strain (ε) as shown in figure 1.19.

Stretching the device to 15% strain resulted in a significant increase in the resistance readings to an average of 24.9±0.6 kOhm, giving a consistent gauge factor of 0.38±0.04 over eighteen cycles as shown in figure 7.13.

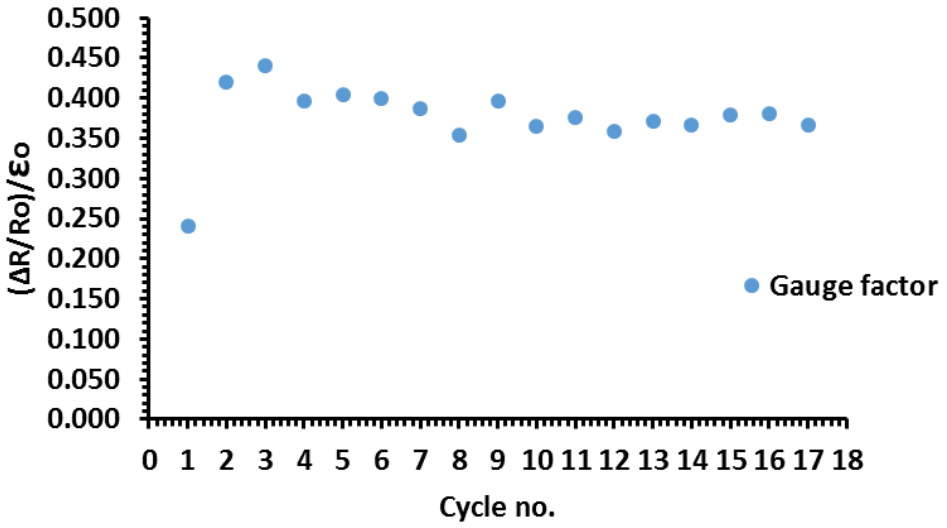

Figure 7.13 Gauge factor as a function of cycle number for sponge soaked with ionic PAAm hydrogel. This experiment was repeated three times from three different samples.

It is also clear from figure 7.13 that cycles 2 to 18 displayed a stable gauge factor trend. However, the first cycle presented a low GF value of 0.24, which could be due to the device establishing contact between the different layers.

7.6 Conclusions

This work demonstrated a new form of cheap, durable, non-toxic strain gauge from the hybridisation of cellulose kitchen sponge with PAAm containing 6 M LiCl hydrogel. The mechanical recovery was investigated for all the sponge device components using tensile testing to determine the mechanical parameters in which the design could function as a recoverable mechanical behaviour. The whole sponge-hydrogel device exhibited the highest tensile strength, tensile modulus as well as hysteresis compared to cellulose sponge with or without PAAm containing LiCl as it adopted the best mechanical properties from each of its constituents.

The electrical impedance was also performed to understand the electrical behaviour for all of the sponge's components. The cross-linked PAAm hydrogel within the cellulose sponge displayed superior conductivity when compared to the uncross-linked AAm within a sponge, sponge with water or sponge alone. This was clear when the sponge/hydrogel hybrid reported the lowest impedance value at a frequency range from 25 kHz-1 MHz at 99±1 Ohm. Furthermore, it was observed that the increase of the water content within the sponge decreased the electrical impedance due to the ability of the water molecules to fill the sponge holes

and facilitated the ionic conduction within the materials. The sponge-hydrogel sample was extended to breaking with the overlaid electrical and mechanical responses to determine the devices operational threshold. Based on these responses, the devices operational limit was set to 15% strain. The device exhibited a significant increase in the resistance readings to an average of 24.9±0.6 kOhm, giving a consistent gauge factor of 0.38±0.04 over eighteen cycles. This work opens new possibilities to advance the state of the art for multiple fields such as medical diagnosis, materials development and soft sensing applications.

Chapter 8

Designed conducting polymer composites that facilitate long-lived, light-driven oxygen and hydrogen evolution from water in a photoelectrochemical concentration cell (PECC)

This chapter has been adapted from the manuscript " Designed Conducting Polymer Composites That Facilitate Long-Lived, Light-Driven Oxygen and Hydrogen Evolution from Water in a Photo electrochemical Concentration Cell (PECC)" which is published in the journal of composites science as part of the Special Issue Recent Advances in Conductive Polymer Composites and I was listed as a second author for this manuscript as shown in the following link: https://www.mdpi.com/2504-477X/3/4/108/htm

The participants' names of this manuscript, were:

Mohammed Alsultan, Khalid Zainulabdeen, Pawel Wagner, Gerhard F. Swiegers and Holly Warren.

(Published December 2019.

8.0 Introduction

This chapter describes the development of a novel, mechanically durable, highly electrically conductive, and flexible PAAm containing a CsCl hydrogel and its application as a separator for two water splitting half cells (cathode and anode). The cells split water upon exposure to an electrical current with the hydrogel as shown in figure 8.1. The feasibility of (and properties of) a chemical rather than an electrical potential to drive water splitting needs to be studied to investigate the fundamental reliability of light-driven water-splitting in a photoelectrochemical concentration cell when employing electrodes that operate efficiently at moderate pH, even with low levels of light illumination and eventually, to evaluate the designed conducting hydrogel for this application.

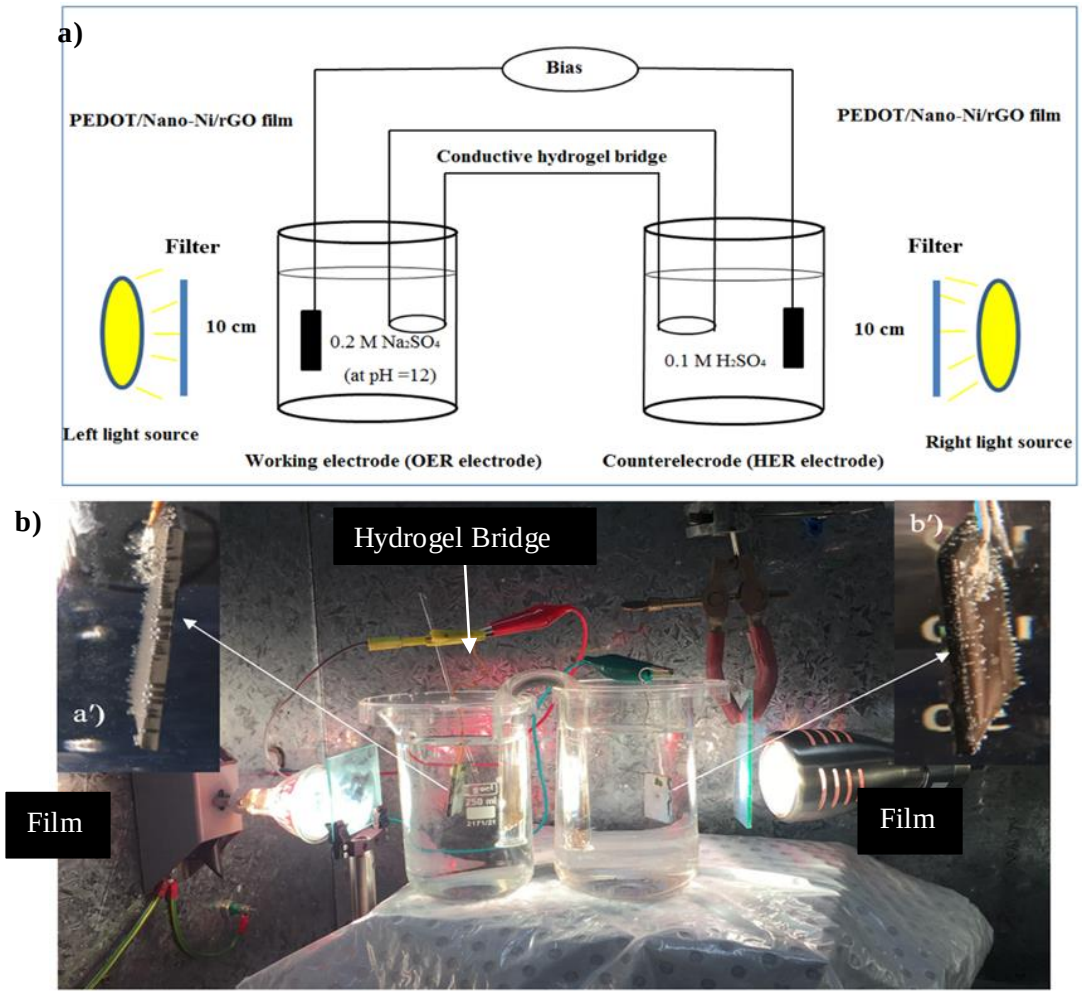

Figure 8.1 (a) Schematic illustration of a photo electrochemical cell (PEC) utilising PEDOT/nano-Ni/rGO films for water-splitting with no voltage bias applied. In the left half-cell, a light-assisted anode for oxygen evolution reaction (OER) catalysis is combined, on the right, with a light-assisted cathode half-cell for hydrogen evolution reaction (HER) catalysis. A hydrogel bridge is provided between the two half-cells. (b) Photograph of the PEC cell setup used.

8.1 Electrical and mechanical properties of conductive PAAm hydrogel- CsCl

The hydrogel separator was found to have high conductivity (up to 310±31 $mS.cm^{-1}$; Figure 8.2). The conductivity was higher than previously reported for PAAm hydrogels, which was 100 $mS.cm^{-1}$. [110] The significant value of this conductivity was probably related to the presence of Cs^+ and Cl^- ions in the gel. Cs^+ ions have greater mobility through the polymer matrix due to it being less a polarising cation because of the shielding effect of the two additional electron shells compared with

Li^+ ions, which would interact more with the polymer chains.

Moreover, the water content (%) in the hydrogel increased from 65% to 95% when the hydrogel was immersed in both electrolytes providing more carriers of water molecules to enhance the hydrogel conductivity as shown in table 8.1. The pH was measured before gelating the hydrogel which to displayed a slight increase over fourteen hours of PEC operation (Table 8.1).

The mechanical properties of hydrogel bridge PAAm-CsCl hydrogel were examined before use in water splitting systems to assess its mechanical durability. [374-376]

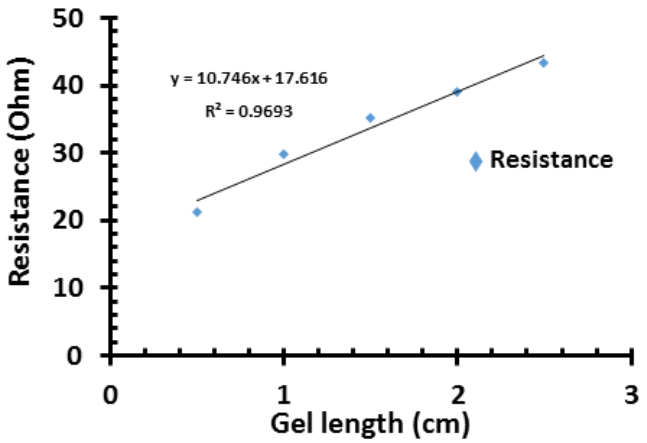

Figure 8.2 Resistance as a function of length of the hydrogel separator used in this study.

Table 8.1 Conductivity, pH and water content of hydrogel bridge (PAAm+CsCl). This experiment was repeated three times.

Parameter	Gel before experiment	Gel after experiment
Conductivity ($mS.cm^{-1}$)	265±21	310±31
Water Content (%)	65	95
pH	2.5	3.1

Figure 8.3 and figure 8.4 show the tensile and compression test analyses, respectively. The hydrogel displayed a tensile strength of 26±7 kPa with an ability to stretch to approximately three times its original length, providing reliable applicability as a stretchable conductive gel bridge. The hydrogel exhibited a tensile modulus of 18±3 kPa with a significant ability to stretch of 298±19% (Table 8.2).

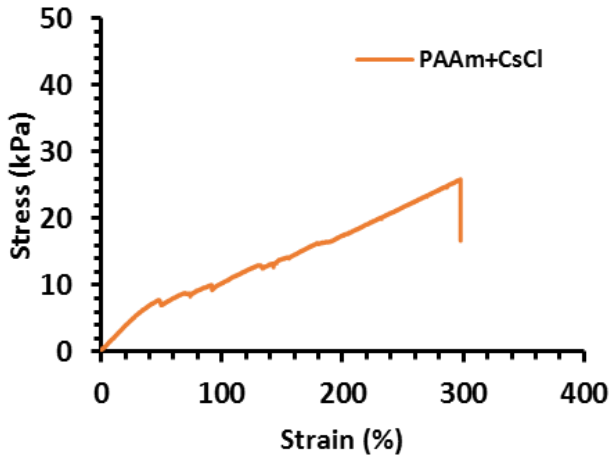

Figure 8.3 Stress-strain curves for the ionic PAAm+CsCl hydrogel used in this study after applying tensile stress.

Table 8.2 Tensile test parameters for PAAm+CsCl hydrogel used in this study. This experiment was repeated three times.

Parameters	Values
Tensile Modulus (kPa)	18±3
Tensile strength (kPa)	26±7
Extension to Failure (%)	298±19

Furthermore, the compression test analysis was examined on the prepared hydrogel to assess its mechanical properties after applying compression action on it. Figure 8.3 displays the mechanical parameters of the hydrogel, such as compression secant modulus, ultimate compression stress and strain to the failure. Examining these mechanical properties was necessary to understand the mechanical durability of the gel. As can be seen in table 8.3 and figure 8.4, the data for compression

modulus, ultimate compression and strain to failure (%) revealed that the hydrogel had reliable mechanical properties after applying more than 800 kPa compression stress.

Table 8.3 Compression test parameters for PAAm+CsCl hydrogel. This experiment was repeated three times.

Parameters	Values
Compression Modulus at (20-30) % (kPa)	24±2
Ultimate compression (kPa)	824±31
Strain to failure (%)	91±8

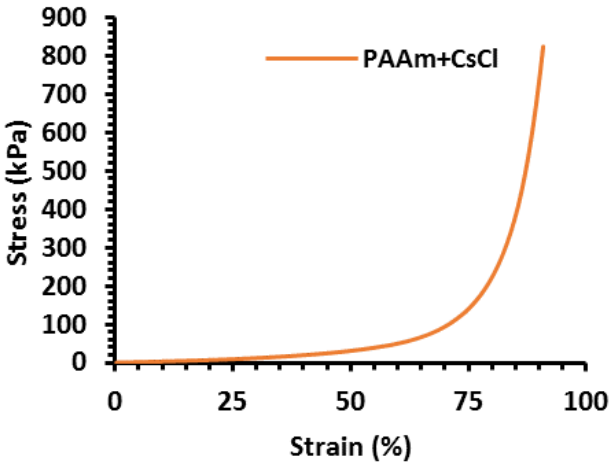

Figure 8.4 Stress versus strain after applying compression test on PAAm+CsCl hydrogel. This experiment was repeated three times.

Finally, the hydrogel sample was stored at room temperature (21°C) and relative humidity (RH) of 50% to test the water retention capacity of the hydrogel for fifteen days. Hydrogel samples exhibited gradual shrinking, as shown in figure 8.5. The water loss of the hydrogel was approximately steady at 11% after storing it for fifteen days. The main reason for the slow water loss during this period is that the hydrogen was embedded with CsCl salt that is considered to be a hygroscopic agent. It absorbs moisture from the air to balance the water content and substitute the water loss in the hydrogel. Based on that, the hydrogel substrate remained rich in water, enhancing its mechanical and electrical durability when compared to other gels. [108], [174], [274].

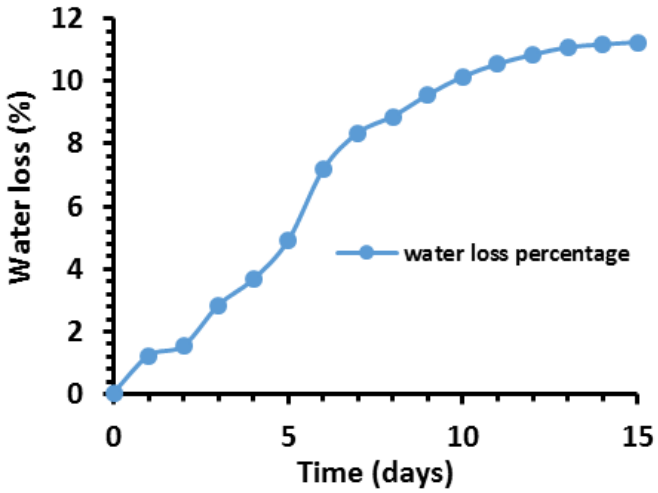

Figure 8.5 A typical plot between water loss percentage and time in days for the PAAm-CsCl hydrogel.

Since the left half-cell represents PEDOT/Nano-Ni/rGO containing 125 mg of nano-Ni and 6 mg of rGO. While the right half-cell represents PEDOT/Nano-Ni/rGO containing 125 mg of nano-Ni and 5.4 mg of rGO applied. Additionally, the hydrogel participated in both mechanism by playing a crucial role as ion-exchange membranes facilitating water-splitting performance.

8.2 Conclusions

Two thin film electrodes of PEDOT containing nano-Ni and rGO have been applied in a PEC as working and counter electrode. The electrode for OER catalysis was immersed in aqueous alkaline 0.2 M Na_2SO_4 adjusted to pH 12. The counter electrode for HER catalysis was immersed in 0.1 M H_2SO_4. The half-cell electrolytes were connected *via* a novel, durable, conductive hydrogel bridge. The hydrogel exhibited excellent charge transfer mobility between the two half-cell electrolytes for periods of fourteen hours of testing. To the best of our knowledge, no other separator has been demonstrated to be capable of facilitating fourteen hours of continuous operation. The cell exhibits higher current at 1.5 V than at 1.23 V. However, the current at 1.23 V was sustained and relatively constant over fourteen hours of PEC operation; it declined only 11.8% from its stabilised current. In contrast, the current at 1.5 V degraded to 59% of its stabilised current after fourteen hours of operation. The electrochemical properties of hydrogel were investigated before and after the operation.

This study demonstrated that ionic PAAm hydrogels could be an effective salt bridge device for

water splitting application for periods of at least fourteen hours of operation. The electrical and mechanical features have been investigated.

This research contributes to the development of conducting, flexible and durable hydrogel materials for water-splitting application.

Chapter 9

Development of reinforced polyacrylamide electrodes with customizable mechanical properties

9.0 Introduction

PDMS sponge material has an extensive reputation by recent researches. However, several technical procedures has displayed complicated methods in attempts to produce conducting-strechable device composing of this material (PDMS). A calcium chloride hard template has been used for its hygroscopic properties, to fabricate a porous PDMS sponge. The preparation technique of the PDMS was developed by removing the hard template in six hours after soaking in milli-Q water. The mechanical charaterisation were carried out by applying tensile test analysis on the washed PDMS sponges to assess its mechanical properties. The maximum tensile stress of that PDMS sponge was 106±22 kPa. Furthermore, ionic PAAm/PDMS was fabricated after embedding PAAm containing 6 M LiCl hydrogel sealed by VHB tape within the PDMS template. The mechanical and electrical properties were investigated on the resulting electrode. This work reveals new horizons for researchers to make developments in customizing the mechanical properties of PDMS sponges using porosity diameter studies of the PDMS sponge for manufacturing stretchable non-toxic electronics.

A Variety of PDMS sponge substrates were produced using different sacrificial templates of different pore sizes. The sponges were developed using templates of $CaCl_2$, NaCl, LiCl, brown sugar and white sugar. White and brown sugar were used because of their ability to produce a porous PDMS structure after dissolving them in water. Furthermore, previous studies have utilised these materials to fabricate porous conductor devices using brown [323] or white sugars [324] to synthesis porous templates saturated with carbon fibers. Moreover, different PDMS/filler sponge templates were produced by mixing NaCl, LiCl and $CaCl_2$ as well as white and brown sugars, with uncured PDMS material. Porous PDMS templates were produced after curing then washing in water to remove the salts or the sugars fillers. The effect that these different sacrificial templates had on the mechanical properties were analysed *via* tensile test analysis. Furthermore, robust ionic PAAm/PDMS electrodes were fabricated by embedding polyacrylamide (PAAm) containing 6 M LiCl hydrogel within the PDMS template. The mechanical and electrical properties were investigated for the produced electrodes.

9.1 Mechanical Properties

The mechanical properties of the produced PDMS sponge samples were performed after applying a tensile test using a universal mechanical testing device as described in section 2.5.1. Optical microscopy was also utilised to determine the average pore diameter of the internal sponge structure of the PDMS to find out the

correlation between the pore diameter and the mechanical behaviour. The results are shown in table 9.1.

Table 9.1 Mechanical parameters and pore diameters of PDMS sponges with different fillers (salts and sugars). The values determined using tensile test analysis and optical microscopy. All experiments were performed at RT. This experiment was repeated three times using three different samples.

Sample	Maximum tensile stress (kPa)	Maximum tensile strain (%)	Young's modulus (kPa)	Work of extension (kJ m^{-3})	Pore diameter (µm)
$CaCl_2$	106±22	43±6	221±44	23±7	404±140
NaCl	221±46	67±8	252±34	69±17	379±100
LiCl	313±60	75±8	325±84	105±17	208±52
Brown sugar	83±20	41±4	162±49	16±4	603±193
White sugar	139±25	50±6	196±38	32±9	452±100

From table 9.1 it can be seen that the mechanical parameters for these PDMS sponges correlated strongly with the pore size of the templates. This is demonstrated by the Young's modulus correlating reversibly with increasing pore diameter whereby the PDMS produced using LiCl displayed the highest Young's modulus at 325±84 kPa, with the lowest pore diameter at 208±52 µm. The PDMS/LiCl sponges also displayed a maximum tensile strain and work of extension at 75±8% and 105±17 kJ/m^3, respectively. Furthermore, the PDMS/brown sugar sponge template exhibited the lowest Young's modulus at 162±49 kPa, with the highest pore diameter at 603±193 µm and lowest tensile strain and work of extension at 41±4 % and 16±4 kJ.m^{-3}, respectively. These data illustrates that producing denser and smaller pore sizes of the constructed PDMS sponges' results in increased mechanical performance. This means using removable smaller grains size fillers in preparation of PDMS sponge would help to improve the mechanical features as displayed with PDMS/LiCl sponge. On the other hand, constructing PDMS sponges using removable larger filler grains which were filled with air will affect the mechanical characteristics adversely. Furthermore, this investigation leads to the possibility of customising the mechanical performance of the PDMS sponges using the grain diameter study using equation 9.1 as shown in figure 9.1 a.

$$\text{Young's Modulus (kPa)} = -0.4253 \times \text{Pore Size (µm)} + 405.21, \quad \textbf{(Eq.9.1)}$$

This equation is derived from a linear regression plot as displayed in figure 9.2b between Young's Modulus in kPa and pore diameters in µm of the PDMS sponge.

Therefore, PDMS/LiCl has an optimum mechanical property among the other sponge templates. However, PDMS/$CaCl_2$ sponge was nominated to construct the PDMS/PAAm electrodes as it had the highest efficiency of filler removal, and it displayed significant mechanical behaviour (Figure 9.1 b) as illustrated by preliminary work from our group as described previously in table 9.1.

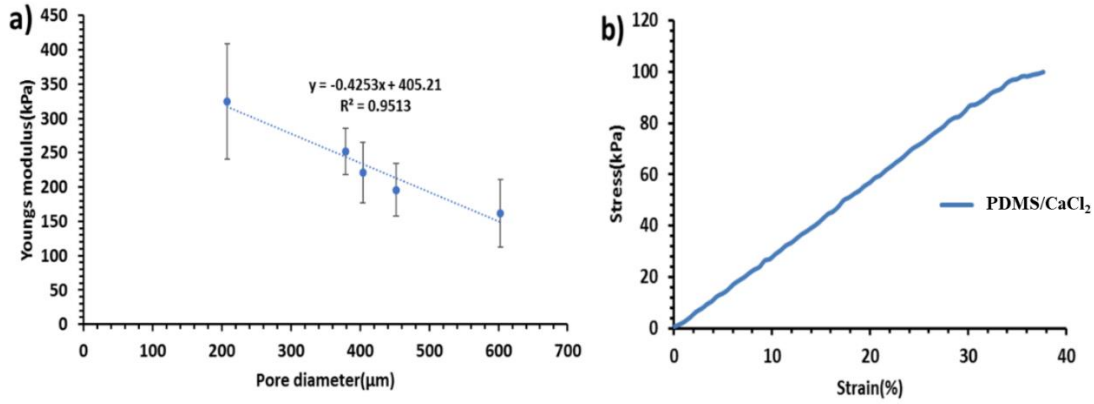

Figure 9.1 a) Linear regression equation between Young's modulus versus pore diameters of PDMS sponges with different fillers (salts and sugars) and b) Stress versus strain plot for describing the tensile strength of PDMS/$CaCl_2$ sponge. These experiments were repeated six times.

9.2 Fabrication of PDMS Sponge electrode

PDMS sponges have gathered extensive reputation within the scientific community for their use in elastic electrodes such as a backbone/substrate for conductive materials. These stretchable conductors could find a broad range of applications to be utilised in different approaches, such as wearable electronics. A plethora of studies have been recruited to the construction of a conductive PDMS sponge by including silver, [377] gold [325-326] or carbon nanotubes. [378] However, these achievements typically used materials with high cost, toxic components or complicated manufacturing methods. Therefore, the potential in developing of these devices requires a simple, cheap method for the fabrication of a highly conductive, durable, stretchable conductor by combining PDMS sponge with non-toxic ionic PAAm as shown in figure 9.2. The mechanical and electrical properties were assessed and outlined in table 9.2.

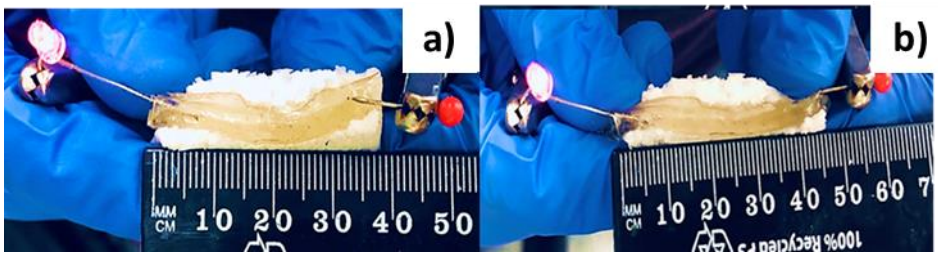

Figure 9.2 a) Fabricated PDMS sponge electrodes with embedded polyacrylamide un-stretched and b) stretched.

Table 9.2 Mechanical and electrical parameter values of PDMS sponge with ionic PAAm hydrogel conductor. Experiments carried out at RT. This experiment was repeated three times using three different samples.

Sample	Maximum Tensile stress (kPa)	Maximum Tensile Strain (%)	Young's modulus (kPa)	Work of extension ($J\ m^{-3}$)	Conductivity ($mS.cm^{-1}$)
PDMS/PAAm	39±3	46±3	117±22	10±1	35±1

None of the previous studies has attempted to combine ionically conductive stretchable hydrogel with a PDMS sponge structure. This was due to the challenges corresponding to the hydrophobicity difference between each material. Therefore, this study was aimed at fabricating an ionically conductive stretchable PDMS sponge electrode, which can be applied for the development of wearable and implantable sensing and conducting devices. The PDMS/PAAm electrode was produced by embedding PAAm containing 6 M LiCl hydrogel within the PDMS sponge structure using a specific technique. PAAm was chosen for its distinct mechanical and electrical properties, possessing high conductivity (Table 9.2) and significant stretchability (Figure 9.2 a and b) as described also in chapter one and chapter four previously (a limitation of all metals with PDMS). Furthermore, this material is relatively low cost, [379] non-toxic and biocompatible which makes it reliable for developing implantable devices [380-381].

The PAAm was synthesised with 6 M lithium chloride as described in section 2.3.3. Two VHB tape layers were used to seal the hydrogel before being cast within the PDMS. The VHB tape was utilised to prevent any water contact from the PDMS as it adversely impacted the PDMS curing and also to avoid any

dehydration of the hydrogel during and after the casting process as shown in figure 9.2. The resulting PDMS/PAAm electrode displayed an excellent stretchability with an optimum strain at 46±3% for the PDMS/PAAm as shown in table 9.2 and figure 9.2. Furthermore, it was noticeable that its stretchability was higher than the unmodified PDMS sponge's template (Table 9.2 and table 9.3), suggesting the ionic PAAm inclusion does not affect the elasticity of the PDMS sponges. The mechanical properties revealed a significant performance, reporting maximum tensile stress of 39±3 kPa. However, Young's modulus and work of extension parameters values were lower than that of PDMS sponge alone. This could be attributed to the reduction of the water content of the hydrogel during the PDMS polymerisation that leads to lowering of mechanical characteristics.

The mechanical properties of both PDMS/PAAm+LiCl structure and cellulose sponge/PAAm+LiCl structure as described in chapter 7 were compared while applying a tensile test to distinguish the best mechanical robustness between these electrodes. The impact of hybridising or embedding both cellulose sponges and PDMS sponges on the mechanical behaviour of PAAm+LiCl hydrogel is shown in table 9.3.

Table 9.3 The mechanical parameters of each PAAm+LiCl, Cellulose sponge/PAAm+LiCl and PDMS/PAAm+LiCl after applying the tensile test. This experiment repeated three times.

Sample	Maximum Tensile stress (kPa)	Maximum Tensile Strain (%)	Young's modulus (kPa)	Work of extension ($J\ m^{-3}$)
PAAm+LiCl	12±1	240±68	6.1±0.4	19±8
Cellulose sponge/PAAm+LiCl	40±2	53±3	137±15	12±1
PDMS/PAAm+LiCl	39±3	46±3	120±23	10±1

It is evident from table 9.3 that hybridising cellulose sponge and PDMS sponge with PAAm+LiCl hydrogel increases the tensile stress from 12±1 kPa to 40±2 kPa and 39±3 kPa, and Young's modulus from 6.1±0.4 kPa to 137±15 kPa and 120±23 kPa, respectively. This mechanical enhancement is attributed to the addition of the physical crosslinking between the ionic PAAm hydrogel with both cellulose and the PDMS sponges

to produce stronger structures. Moreover, it is noticeable that cellulose sponge/PAAm+LiCl and PDMS/PAAm+LiCl structures displayed approximate tensile stress values at 40±2 kPa and 39±3 kPa, respectively. However, Young's modulus displayed a slight increment into the benefit of a cellulose sponge/PAAm+LiCl structure, revealing an approximate difference of 17 kPa. This difference likely arises from the variation in engineering processes of both structures, such as hybridisation and embedding methods of the ionic hydrogel within hydrophobic materials such as cellulose and PDMS sponges. However, these procedures succeeded in producing more robust structures that reflect the positive impact of fabricating devices using affordable, non-toxic materials such as cellulose and PDMS sponges with soft, stretchable material such as PAAm containing LiCl hydrogel.

Finally, the conductivity of the PAAm containing 6 M LiCl /PDMS revealed remarkable value, to fabricate a stretchable electrode giving a conductivity of 35±1 $mS.cm^{-1}$. Furthermore, this study demonstrated the direct correlation between the electrode length and the electrode impedance value as shown in figure 9.3. Therefore; this study investigated the fabrication of a novel, non-toxic hydrogel/PDMS combination that would introduce the sophistication of a mechanically customizable PDMS electrode for wearable and implantable conducting and sensing applications.

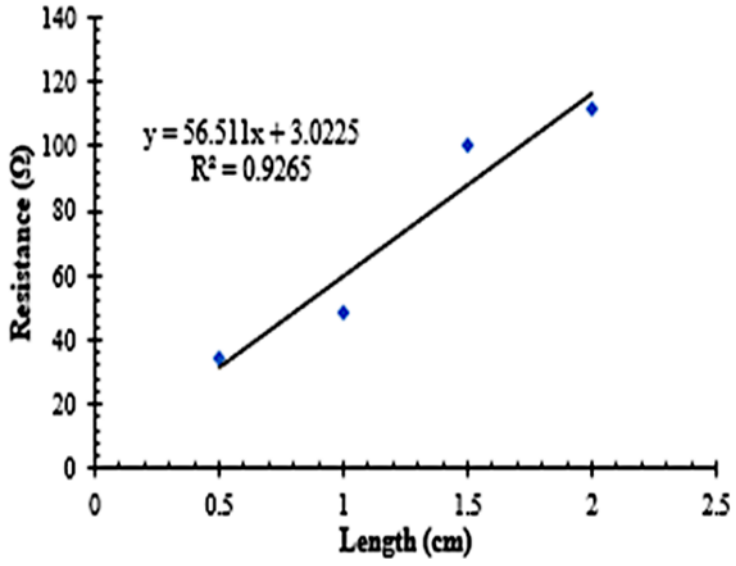

Figure 9.3 Linear regression relationship between impedance values and PAAm/PDMS sponge electrode lengths.

9.7 Conclusions

This study revealed new horizons for researchers to make developments in customising the mechanical performance of PDMS sponge to produce stretchable non-toxic electronics using a novel, cheap, facile, green technology.

PDMS sponges were utilised for fabricating stretchable conducting electrodes after embedding PAAm containing 6 M LiCl hydrogel. Different salts were mixed with the PDMS before curing to produce a porous PDMS template after removing the hard fillers by dissolving the template in Milli-Q water for twelve hours. The mechanical properties of these sponges were determined by applying tensile test analysis on the washed PDMS sponges to assess its mechanical reliability. The mechanical properties revealed that Young's modulus correlated reversibly with increasing the pore size, as shown with the PDMS sponges produced using LiCl displaying the highest Young's modulus at 325±84 kPa, with the lowest pore size at 208±52 µm. These data illustrate the direct correlation of smaller pore size with increased mechanical performance. The PDMS/$CaCl_2$ sponge was chosen for fabricating a stretchable electrode as it had the highest efficiency of filler removal, as illustrated previously, and still possessed respectable mechanical properties for the potential use in wearable or implantable electronic application.

Furthermore, PDMS sponges embedded with PAAm containing 6 M LiCl hydrogel sealed with VHB tape were produced to develop stretchable, conductive and non-toxic electrodes. The mechanical and the electrical properties were investigated for the PDMS/PAAm electrode, which revealed a maximum tensile strain of 46±3% and conductivity of 35±1 $mS.cm^{-1}$. From this it can be seen that the PAAm/PDMS electrodes displayed excellent stretchability and conductivity, demonstrating the ability of these sponges in acting as reinforcing substrates for stretchable electrodes which can also have their mechanical properties customised for specific tasks by altering the pore dimensions of the PDMS substrates. This project illustrated a novel combination of biocompatible PDMS/PAAm sponge structure electrode. Therefore, this work could aid in the development of wearable, implantable, conducting and sensing applications.

Chapter 10

Conclusions and Future Direction

10.1 General conclusions

The overall aim in this thesis was to synthesise, characterise and examine the suitability of using PAAm containing either LiCl or CsCl salts in soft conducting sensing devices, i.e. a wearable soft compressive sensor device, soft strain gauges and a conducting soft bridge. The 3D printing technique was also utilised due to the potential for producing predictable conducting and sensing devices composed entirely of 3D printed soft, stretchable, and conducting hydrogels.

Furthermore, several materials were synthesised either from chemical cross-linking of PAAm with GG, by physical cross-linking, by hybridising PAAm containing 6 M LiCl with cellulose sponge or embedding it within PDMS sponge, to maximise their potential to function in the flexible sensing and the conducting applications. Therefore, the mechanical, electrical stability performances were investigated for all the fabricated devices.

Chapter three describes ionic-covalent entanglement hydrogels consisting of ionically cross-linked GG and $CaCl_2$ with covalently cross-linked PAAm and MBAAm. Previous studies detailed the mechanical properties including toughness, [382] degradation [383] and recovery of the ICE hydrogels [128]. However, there were no further attempts to optimise the mechanical properties of this hydrogel without changing the hydrogel components. Other studies have attempted to improve the electrical behaviour of this hydrogel by adding carbon nanofibers and PEDOT:PSS materials. [384] This paper showed that the addition could adversely impact the mechanical properties of this hydrogel. Therefore, we focused on optimising the mechanical properties of the prepared hydrogel by altering the ionic and the covalent polymers ratio. We found that cross-linked gels prepared with 0.1 M $CaCl_2$ and 1.11% (w/v) GG with PAAm consisting of 4.44% (w/v) AAm with 3% (w/v) MBAAm displayed optimum mechanical characteristics giving 216±12 kPa (compressive stress to failure) and 264±5 kPa (shear modulus). The electrical properties were also determined for the hydrogel ratio that gave optimal mechanical properties for utilisation in the conducting and sensing applications. The electrical conductivity and the water content for the optimised ICE gel exhibited a significant increase from 3.3±0.5 $mS.cm^{-1}$ to 127±15 $mS.cm^{-1}$ and from 78 to 85, respectively, after immersing it in 2.7 M NaCl. Based on these mechanical and electrical properties, this material is considered to be promising for producing robust, conducting, deformable and swelling electronics.

In addition, in the aim of potentially producing soft, conducting, stretchable electronics using different techniques such as 3D printing technology, we successfully demonstrated in chapter four that the PAAm

containing 9 M LiCl hydrogels could be processed using 3D printing. Previous research demonstrated that physically entangled, photopolymerised PAAm could be patterned using a direct-writing technique to prepare hydrogel scaffolds for 3T3 fibroblasts [105]. Related studies focused on the preparation of ionic PAAm using either NaCl or LiCl as the ionic pathway [108, 109]. This chapter also described the electrical and mechanical characteristics of 3D printed PAAm hydrogel materials when compared to the cast gels. The rheological properties of the prepared PAAm containing salt materials were also studied, i.e. starting materials, inks, cast, and printed structures, to determine their potential for 3D fabrication of soft electronic devices or soft sensory gauges using both direct-ink writing and hand-held printing techniques. The rheological analysis showed that controlled UV-crosslinking while cooling to -6 °C, enabled 3D printing of the PAAm without the need for any additional rheological modifiers as used previously by Lewis *et al.* [196] The 3D printed PAAm with 9 M LiCl hydrogel materials exhibited conductivity values of 117±13 $mS.cm^{-1}$ and could be stretched up to four times their length. This excellent conductivity of the 3D printed hydrogel considered the highest of any other hydrogel constructed via the same technique which can be stretched to this amount based on our literature search to the best of our knowledge. Accordingly, the excellent performance of PAAm containing 9 M LiCl hydrogel as reported in chapter five, inspired its utilisation in the development of a durable, flexible, and soft wearable sensor device (SSD) which had the ability to send an SOS signal remotely even after one year of keeping the device at room temperature. This SSD consisted of two lithium chloride conducting PAAm electrodes separated by a perforated elastomeric VHB tape. The novel perforation of the elastomeric material separating the electrodes enabled the creation of a sensor with an imbued threshold of operation. The device enabled the detection of mechanical stress *via* a change in resistance within the electrodes. This enabled the device to operate at a much higher range of stress than was used in previous sensors relying on capacitance change. [188]

The mechanical investigations revealed the SSD was very strong and did not break even after applying over 100 kPa of compressive stress. These results indicate that the device could easily be used as a pressure sensor for an active SSD. The mechanical stability of the SSD was characterised by comparing performance over fifty cycles of 14 kPa of compression stress for an as prepared SSD and an SSD after one-year storage at RT. The SSD exhibited high recoverability with a slight shifting in the strain during the fifty cycles of 14 kPa compressive stress.

The electrical properties of the SSD were examined by measuring the current and resistance of the device during compression testing for five cycles (loading/unloading). These were performed to determine the

minimum stress required to complete a DC current circuit. The correlation between applied stress and the current creation of the device was measured and analyzed to understand the required electrical output signals for operating the Arduino device to send a Bluetooth signal to the mobile phone.

The hydrogel device displayed a consistent average resistance output of 435±2 kOhm over fifty cycles of 14 kPa compressive stress. The electrical sensitivity was also determined after applying the same compressive cycles on the SSD to determine if the device could also function as a more precise pressure sensor for more complex applications. The examination performed initially and after keeping the SSD for one year displayed a consistent sensitivity of 5800±500 Ohm/Pa for the initial test and sensitivity of 1000±100 Ohm/Pa after one year. The significant decrease in the sensitivity is attributed to creeping both of the conducting hydrogel and the elastomeric VHB tape, which were affected by two factors: time and the temperature. However, the sensitivity trends confirmed the existence of the electrical response at the SSD even after one year of storing it at RT. The SSD was then operated after placing it on different positions such as bikes helmet, hand palm after combining it with an Arduino device to send a signal to a mobile phone, creating a custom-built a remote sensor.

It was observed that when pressure was applied above a specific threshold 7.5±0.1 kPa on the SSD an electrical circuit was created, in which the ions within the hydrogel electrodes were able to travel through the perforated VHB. This detection of an applied pressure was sent to the Arduino device to transmit the coded signal, using Bluetooth, to a mobile phone (I-phone). The mobile phone has a specific application named UOW_data-sender. The signal was forwarded to the database computer, using the 4G network, providing a text message with the GPS data giving the location coordinates for the SSD. The database computer then recorded and sent the original SSD message with the coordinates to a relative's phone, tablet or computer. The reaction time between the application of the pressure and the Arduino device recording a change was 0.8±0.2 seconds while the time taken to detect the removal of the pressure was 2.4±0.5 seconds. This study culminated in an investigation into assessing a soft pressure sensor device able to create a signal after one year of storage.

Chapter six investigated the implementation of an easier, cheaper, non-stationary facility to extrude PAAm containing LiCl using a handheld technique on an acrylated VHB tape substrate to fabricate a durable, soft, strain gauge device, which was named HEH. The device produced a robust interface between the printed hydrogel and an elastomeric matrix using a simple interpenetration polymerisation method without adding any rheological modifiers [111] [357] or performing oxygen plasma treatments [111] to alter the substrate

hydrophobicity surface. The mechanical and the electrical properties of the HEH devices were examined before and after one year of storage in a plastic Petri-dish at RT.

The HEH exhibited almost no deterioration in mechanical behavior even after one year of storage. It was shown that the HEH devices were able to be stretched to 215 % repeatedly with no issues both initially and after one year of storage. This value of stretching is higher than the previously reported study when a fabricated soft gauge device stretched up to 150 % using more complicated printing facilities. [111] Despite the low gauge factor values when compared to a conventional semiconductor [385] and metallic strain gauge, [386] our gauge factor for the HEH was determined for the as-prepared device and compared with that after one year giving a sensitivity of 0.7±0.1 and 0.74±0.01, respectively, which does not exist for the other strain gauges.

Furthermore, the sensing investigations revealed stable R/R_o data after 1000 cycles of stretching during finger bending, with a change ratio of 1.3±0.1. It was observed that the R/R_o difference for both periods, initially and after one year of storing, was only 0.05. For more investigation, the water percentage for the salt containing PAAm within the HEH was determined to be 79% (w/w). This percentage decreased by 2% (w/w) after one year of storage. This low water loss percentage value was attributed to the addition of hydroscopic LiCl salt to the printed hydrogel within the HEH. This agent has the ability to substitute the water loss by withdrawing the moisture from the environment and therefore extending the lifetime of the fabricated device. [273]

This project revealled the stability performance of a soft sensory device from measuring the electrical and mechanical properties before and after storing the device for one year.

Chapter seven was carried out to overcome some other challenges in fabricating wearable sensors such as extensibility, high cost, and poor durability, which limited their application in wearable sensors. [382] Therefore, this chapter investigated the possibility of fabricating a strain gauge device by employing an affordable, non-expensive material such as cellulose kitchen sponge (4$AU) [387] after hybridising it with PAAm [378] containing salt hydrogel material.

The mechanical recovery was investigated for all the sponge device components using tensile testing to determine the mechanical parameters within which the design could function with recoverable mechanical behavior. The whole sponge-hydrogel device comprised of cellulose sponge, PAAm containing 6 M LiCl and two layers of VHB tapes covering the entire components and exhibited the highest tensile strength (19±1) kPa, tensile modulus (131±2) kPa as well as hysteresis (1.1±0.03) $kJ.m^{-3}$ when they were stretched

up to 15% compared to cellulose sponge with or without (PAAm containing LiCl) as it adopted the best mechanical properties from each of its constituents.

The electrical impedance was also determined to understand the electrical behaviour for all the sponge's components. The cross-linked PAAm hydrogel within the cellulose sponge displayed superior conductivity when compared to the uncross-linked AAm within a sponge, wet sponge or sponge alone. This was clear when the sponge/hydrogel hybrids exhibited the lowest impedance value at a frequency range from 25 kHz - 1 MHz at 99±1 Ohm. Furthermore, it was also observed that increasing the sponge water content decreased the electrical impedance due to the ability of the water molecules to fill the sponge holes and facilitate ionic conduction within the materials.

The sponge-hydrogel sample was extended to a breaking point, with the overlaid electrical and mechanical responses, to determine the device's operational threshold. The operational limit set at 15% strain. The device exhibited a significant increase in the resistance readings to an average of 24.9±0.6 kOhm, giving a consistent gauge factor of 0.38±0.04 over eighteen cycles. A recent study attempted to increase the sensory gauge factor up to 9.4 by hybridising reduced graphene oxide and a carbon nanotube with a cellulose sponge and PDMS. [388] However, this study needs a more complicated processes and higher cost requirements for fabricating these strain gauges. [389]

Last but not least, a conductive and durable non-precious soft bridge was fabricated for the oxygen and hydrogen evolution reaction using bifunctional composite PEDOT/nano-Ni/rGO films, (Chapter eight). Previously, using Nafion as a source of cations, and exchange membranes as a source of anions have been used as separators [390-394] However, there were problems of using them as separators. Firstly, they have a narrow range of pH applications, either 1-7 or 7-14. Secondly, maintaining pH in both basic and acidic media is difficult due to the neutralisation processes as a result of OH^- and H^+ consumption in both anolyte and catholyte, respectively during the electrocatalytic process. Due to its properties, PAAm containing CsCl hydrogel was prepared and used to fabricate a soft ionic conductive bridge material. The influence of hydrogel water content on its mechanical and electrical properties was examined. The water content (%) in the hydrogel was increased from 65% to 95% when the hydrogel was immersed in both electrolytes providing more carriers of water molecules to enhance the hydrogel conductivity from 265±21 $mS.cm^{-1}$ to 310±31 $mS.cm^{-1}$, and the hydrogel could be stretched up to three times its length.

Based on these distinct features, the hydrogel was then fabricated as a soft salt bridge and was assessed in the oxygen and hydrogen evolution reaction. The application succeeded in working for fourteen hours

which is the highest operation time until now using soft material applied for the same purpose to the best of our literature knowledge.

Finally, PDMS sponges were utilised for fabricating stretchable conducting electrodes after embedding PAAm containing 6 M LiCl hydrogel. Different salts were mixed with the PDMS before curing to produce a porous PDMS template after removing the hard fillers by dissolving the template in milli-Q water for twelve hours to assess the fillers removal efficiency by the effect of the hydrophilicity. The mechanical properties were carried out by applying tensile test analysis on the washed PDMS sponges to assess its mechanical reliability. The mechanical properties displayed that Young's modulus correlated reversibly with increasing the pore diameter displaying the highest Young's modulus at 325±84 kPa, respectively, with the lowest pore diameter at 208±52 µm. This was clear for the PDMS/LiCl sponge which also displayed a maximum tensile strain and work of extension at 325±84 % and 105±17 $kJ.m^{-3}$, respectively. However, PDMS/brown sugar sponge template exhibited the lowest Young's modulus at 162±49 kPa, with the highest pore size at 603±193 µm and lowest tensile strain and work of extension at 41±4 % and 16±4 $kJ.m^{-3}$, respectively. These data illustrated the direct correlation of producing denser and smaller pore size of the constructed PDMS sponge from smaller filler grains with the mechanical behaviour. Therefore, PDMS/LiCl sponge was observed to display an optimum mechanical property among the other sponge templates. However, PDMS/$CaCl_2$ sponge was nominated as it had the highest efficiency of filler removal, as illustrated previously in chapter 9, and still possessed respectable mechanical properties for the potential use in wearable or implantable electronic application.

Furthermore, PDMS embedded with PAAm containing 6 M LiCl hydrogel sealed with VHB tape separately was fabricated for an attempt to innovate stretchable, conductive and nontoxic electrodes. The mechanical and the electrical properties were investigated which revealed maximum tensile strain 46±3 % and a conductivity 35±1 $mS.cm^{-1}$, respectively. This demonstrates that a PDMS sponge can be utilised to enhance and customise the mechanical properties of PAAm electrodes. Therefore, this study investigates the construction of a novel, non-toxic hydrogel/PDMS combination that could aid in the development of wearable, implantable, conducting and sensing applications.

In summary, PAAm hydrogels containing various salts were successfully synthesised, characterised and utilised for the fabrication and development of various novel devices using different techniques such as 3D printing with the potential of applying these devices in both wearable or implantable sensing and conducting applications.

10.2 Future directions

Projects arising from this thesis culminated in the development of a novel soft, conducting, pressure and strain sensor devices. However, sustainability, biodegradability, biocompatibility, durability and low cytotoxicity are all challenges concomitant with synthesizing and fabricating new soft materials and devices, which require further study to contribute significantly to a plethora of applications such as in the entertainment and biomedical fields. For example, synthesising and characterising functional flexible, conducting, more durable hydrogels for wearable and sensing applications is an essential direction. These durable hydrogels should possess the ability to resist and adapt to the high-temperature environment by either swapping the water solvent with others that should be characterised by its reliable conductivity and higher boiling point taking in account maintaining reliable mechanical properties. Furthermore, it is importantant to develop the conductivity of the soft materials to make it close to the electrical properties of metals such as copper and gold. This enhancement will evolve several wearable devices specially if this material can be 3D printed, for example to design and fabricate a hearing aid as a soft stretchable device. Therefore, it is also crucial to develop 3D printing techniques to be able to offer the non-stationary field with fine control of printing materials able to mimic chosen properties of human skin in an appropriate manner over all the body parts. This sophistication will provide the facile use of this technology with an accuracy performance which can be implemented in wider functions of soft conducting and sensing applications. On the other hand, among various flexible energy storage devices, flexible batteries are considered as the most promising candidates to power the future flexible/wearable electronics due to their relatively high energy density and long cycle life. Therefore, it is possible to utilise stretchable hydrogels such as PAAm containing LiCl or CsCl hydrogels that can be functionalised as a wearable battery or solar battery devices. This is especially important when these materials (characterised by their significant conductivity and stretchability) can be easily 3D printed. However, more effort is needed to overcome challenges in the commercialization of current 1D batteries and prospective opportunities in the field for approaching reliable mechanical robustness and stable electrochemical performance under a physical strain. On the other hand, it is possible to functionalize cellulose sponge within 3D or even 4D printing technology for its non-toxicity, affordability and low cost. Additionally, further predictable future studies can be initiated in this field such as printing a stretchable soft hearing aid device from using conductive hydrogels to replace the sold plastic materials that are being used in the current markets. Another study can be applied

on fabricating a bullet shield connected to soft sensor device functioning similar to that fabricated in chapter 5. This application will enhance the communication technology in the military field. Finally, there is a possibility of 3D printing of the entire component of the PDMS sponge electrode. This promising technology could enable the development of implanting non-toxic, deformable electronics. These suggestions could open the horizons of developing the materials and the technology of the industry of wearable soft sensor devices.

List of references

(1) Li, Y.; Huang, G.; Zhang, X.; Li, B.; Chen, Y.; Lu, T.; Lu, T. J.; Xu, F. Magnetic Hydrogels and Their Potential Biomedical Applications. *Adv. Funct. Mater.* **2013**, *23* (6), 660–672.

(2) Newell, J. *Essentials of Modern Materials Science and Engineering / James Newell.*; Hoboken, N.J. : Wiley, c2009., **2009**.

(3) Maimain, T. © 1960 Nature Publishing Group. *Nature* **1960**, *187* (4736), 493–494.

(4) Nierzwicki, W.; Prins, W. Hydrogels of Crosslinked Poly(1-glyceryl Methacrylate) and Poly(2-hydroxypropyl Methacrylamide). *J. Appl. Polym. Sci.* **1975**, *19* (7), 1885–1892.

(5) Hoffman, A. S., Hydrogels for biomedical applications. *Advanced Drug Delivery Reviews* **2012,** *64*, 18-23.

(6) Swarbrick, J. Encyclopedia of Pharmaceutical Technology. Boca Raton: CRC Press, **2007**. https://doi.org/10.1201/b19309.

(7) Nguyen, K. T.; West, J. L. Photopolymerizable Hydrogels for Tissue Engineering Applications. *Biomaterials* **2002**, *23* (22), 4307–4314.

(8) Peppas, N. A.; Bures, P.; Leobandung, W.; Ichikawa, H., Hydrogels in pharmaceutical formulations. *European Journal of Pharmaceutics and Biopharmaceutics* **2000,** *50* (1), 27-46.

(9) Sawhney, A. S.; Pathak, C. P.; van Rensburg, J. J.; Dunn, R. C.; Hubbell, J. A., Optimization of photopolymerized bioerodible hydrogel properties for adhesion prevention. *Journal of Biomedical Materials Research* **1994,** *28* (7), 831-838.

(10) Miyata, T.; Uragami, T.; Nakamae, K. Biomolecule-Sensitive Hydrogels. *Adv. Drug Deliv. Rev.* **2002**, *54* (1), 79–98.

(11) Chang, C.; Duan, B.; Cai, J.; Zhang, L. Superabsorbent Hydrogels Based on Cellulose for Smart Swelling and Controllable Delivery. *Eur. Polym. J.* **2010**, *46* (1), 92–100.

(12) Teßmar, J.; Brandl, F.; Göpferich, A. Hydrogels for Tissue Engineering. *Fundam. Tissue Eng. Regen. Med.* **2009**, *101* (7), 495–517.

(13) Calvert, P. Hydrogels for Soft Machines. *Adv. Mater.* **2009**, *21* (7), 743–756.

(14) Discher, D. E.; Mooney, D. J.; Zandstra, P. W. Growth Factors, Matrices, and ForcesCombine and Control Stem Cells. *Science (80).* **2009**, *324* (5935), 1673–1677.

(15) Mark, J. E.; Allcock, H. R.; West, R. *Inorganic Polymers, Second Edition*; 2005.

(16) McCormick, C. L.; Lowe, A. B. Aqueous RAFT Polymerization: Recent Developments in Synthesis of Functional Water-Soluble (Co)Polymers with Controlled Structures. *Acc. Chem. Res.* **2004**.

(17) Frey, H. *Handbook of Industrial Water Soluble Polymers. Edited by Peter Williams.*; Oxford ; Ames, Iowa : Blackwell Pub., **2007**., 2008; Vol. 9.

(18) Rosiak, J. M.; Janik, I.; Kadlubowski, S.; Kozicki, M.; Kujawa, P.; Stasica, P.; Ulanski, P. Radiation Formation of Hydrogels for Biomedical Application. *Iaea-Tecdoc-1324* **2002**.

(19) Spizzirri, U. G.; Iemma, F.; Puoci, F.; Cirillo, G.; Curcio, M.; Parisi, O. I.; Picci, N. Synthesis of Antioxidant Polymers by Grafting of Gallic Acid and Catechin on Gelatin. *Biomacromolecules* **2009**, *10* (7), 1923–1930.

(20) Carretti, E.; Dei, L.; Weiss, R. G. Soft Matter and Art Conservation. Rheoreversible Gels and Beyond. *Soft Matter* **2005**, *1* (1), 17–22.

(21) Muller, G., Polymères hydrosolubles d'origine naturelle et synthétique Relation structure/propriétés en solution. *Rev. Inst. Fr. Pét.* **1990,** *45* (6), 703-717.

(22) Ullah, F.; Othman, M. B. H.; Javed, F.; Ahmad, Z.; Akil, H. M., Classification, processing and application of hydrogels: A review. *Materials Science and Engineering: C* **2015,** *57*, 414-433.

(23) Baughman, D. R.; Liu, Y. A. Development of Expert Networks: A Hybrid System of Expert Systems and Neural Networks. In *Neural Networks in Bioprocessing and Chemical Engineering*; Baughman, D. R., Liu, Y. A. B. T.-N. N. in B. and C. E., Eds.; Academic Press: Boston, 2014; pp 365–433.

(24) Xu, J.; Liu, X.; Ren, X.; Gao, G. The Role of Chemical and Physical Crosslinking in Different Deformation Stages of Hybrid Hydrogels. *Eur. Polym. J.* **2018**, *100* (January), 86–95.

(25) Mohd, K.; Zakaria, S.; Shaiful, M.; Gan, S.; Hua, C.; Nabihah, S.; Jaafar, S.; Adli, U. International Journal of Biological Macromolecules Chemically Crosslinked Hydrogel and Its Driving Force towards Superabsorbent Behaviour. *Int. J. Biol. Macromol.* **2018**, *118*, 1422–1430.

(26) http://large.stanford.edu/courses/2012/ph241/weil1/

(27) Kashyap, N.; Kumar, N.; Kumar, M. N. V. R. Hydrogels for Pharmaceutical and Biomedical Applications. *Crit. Rev. Ther. Drug Carrier Syst.* **2005**, *22* (2), 107–150.

(28) Schacht, E. H. Polymer Chemistry and Hydrogel Systems. *J. Phys. Conf. Ser.* **2004**, *3*, 22–28.

(29) Zohuriaan, M. J.; Kabiri, K. Superabsorbent Polymer Materials: A Review. *Iran. Polym. J.* **2008**, *17* (6), 451–477.

(30) Dadhaniya, P. V.; Patel, M. P.; Patel, R. G. Swelling and Dye Adsorption Study of Novel Superswelling [Acrylamide/N-Vinylpyrrolidone/3(2-Hydroxyethyl Carbamoyl) Acrylic Acid] Hydrogels. *Polym. Bull.* **2006**, *57* (1), 21–31.

(31) Ramazani-Harandi, M. J.; Zohuriaan-Mehr, M. J.; Yousefi, A. A.; Ershad-Langroudi, A.; Kabiri, K. Rheological Determination of the Swollen Gel Strength of Superabsorbent Polymer Hydrogels. *Polym. Test.* **2006**, *25* (4), 470–474.

(32) Akhtar, M. F.; Hanif, M.; Ranjha, N. M. Methods of Synthesis of Hydrogels … A Review. *Saudi Pharm. J.* **2016**, *24* (5), 554–559.

(33) Paradossi, G.; Finelli, I.; Cerroni, B.; Chiessi, E. Adding Chemical Cross-Links to a Physical Hydrogel. *Molecules* **2009**, *14* (9), 3662–3675.

(34) Peppas, N. A.; Huang, Y.; Torres-Lugo, M.; Ward J. H. and Zhang, J. Phyiochemical Foundations and Structural Design of Hydrogels in Medicine and Biology. *Annu. Rev. Biomed* **2000**, No. 02, 9–29.

(35) https://www.thermofisher.com/au/en/home/life-science/protein-biology/protein-biology-learning-center/protein-biology-resource-library/pierce-protein-methods/crosslinking-applications.html.

(36) Drury, J. L.; Mooney, D. J. Hydrogels for Tissue Engineering: Scaffold Design Variables and Applications. *Biomaterials* **2003**, *24* (24), 4337–4351.

(37) Nair, L. S.; Laurencin, C. T. Biodegradable Polymers as Biomaterials. *Prog. Polym. Sci.* **2007**, *32* (8–9), 762–798.

(38) Morfin, I.; Hazot, P.; Guillot, F.; Soler, C.; Korwin-Zmijowska, C.; Tahiri, K.; Chevalier, X.; Corvol, M.; Domard, A. Percolating Hydrogels for Tissue Engineering. *Eur. Cells Mater.* **2002**, *4* (SUPPL. 1), 55–56.

(39) George, J.; Onodera, J.; Miyata, T. Biodegradable Honeycomb Collagen Scaffold for Dermal Tissue Engineering. J. Biomed. Mater. Res. - Part A 2008, 87 (4), 1103–1111.

(40) Bahram, M.; Mohseni, N.; Moghtader, M.. An Introduction to Hydrogels and Some Recent Applications; 2016; 8-38. https://doi.org/10.5772/64301.

(41) Zheng, H., Du, Y., Yu, J., Huang, R. and Zhang, L. Preparation and characterization of chitosan/poly(vinyl alcohol) blend fibers. *J. Appl. Polym. Sci.* **2001**, 80: 2558-2565. doi:10.1002/app.1365.

(42) Wang, L.; Shan, G.; Pan, P. A Strong and Tough Interpenetrating Network Hydrogel with Ultrahigh Compression Resistance. *Soft Matter* **2014**, *10* (21), 3850–3856.

(43) Hüther, A.; Schäfer, B.; Xu, X.; Maurer, G. Phase Equilibria of Hydrogel Systems. *Phys. Chem. Chem. Phys.* **2002**, *4* (6), 835–844.

(44) Kim, S. J.; Shin, S. R.; Spinks, G. M.; Kim, I. Y.; Kim, S. I. Synthesis and Characteristics of a Semi-Interpenetrating Polymer Network Based on Chitosan/Polyaniline under Different PH Conditions. *J. Appl. Polym. Sci.* **2005**, *96* (3), 867–873.

(45) Hu, X.; Feng, L.; Xie, A.; Wei, W.; Wang, S.; Zhang, J.; Dong, W. Synthesis and Characterization of a Novel Hydrogel: Salecan/Polyacrylamide Semi-IPN Hydrogel with a Desirable Pore Structure. *J. Mater. Chem. B* **2014**, *2* (23), 3646–3658.

(46) Osada, B. Y.; Gong, J. Soft and Wet Materials : *Polymer Gels*. **1998**, No. 11, 827–837.

(47) Rackus, D. G.; Shamsi, M. H.; Wheeler, A. R. Electrochemistry, Biosensors and Microfluidics: A Convergence of Fields. *Chem. Soc. Rev.* **2015**, *44* (15), 5320–5340.

(48) Siriwatwechakul, W.; Teraphongphom, N.; Ngaotheppitak, V.; Kunataned, S., Thermo-sensitive hydrogel: Control of hydrophilic-hydrophobic transition. *International Journal of Chemical and Molecular Engineering* **2008**; Vol. 1, p 165-170.

(49) Kayo, U.; Yoshihito, O., Self-Sustained Nonlinear Oscillation of Hydrogen Ions in the Polyelectrolyte Gels. *Chemistry Letters* **1987,** *16* (9), 1795-1798.

(50) 6891-44-7, [2-(methacryloyloxy)ethyl]trimethylammonium methyl sulphate, CAS No 6891-44-7 [2-(methacryloyloxy)ethyl]trimethylammonium methyl sulphate id (chemnet.com).

(51) Khorram, M.; Vasheghani-farahani, E.; Ebrahimi, N. G. Fast Responsive Thermosensitive Hydrogels as Drug Delivery Systems. *Iran. Polym. J.* **2002**, *12* (4), 315–322.

(52) Biswal, A.; Panda, S.; Rao, Pv.; Roy, H.; Parida, K.; Dash, J. Composite Alginate Hydrogel Microparticulate Delivery System of Zidovudine Hydrochloride Based on Counter Ion Induced Aggregation. *Int. J. Appl. Basic Med. Res.* **2014**, *4* (3), 31.

(53) Sampathkumar, L., Christopher Selvin, P., Selvasekarapandian, S. *et al.* Synthesis and characterization of biopolymer electrolyte based on tamarind seed polysaccharide, lithium

perchlorate and ethylene carbonate for electrochemical applications. *Ionics* **2019**, 25**,** 1067–1082. https://doi.org/10.1007/s11581-019-02857-1.

(54) Ohmine, I.; Tanaka, T. Salt Effects on the Phase Transition of Ionic Gels. *J. Chem. Phys.* **1982**, *77* (11), 5725–5729.

(55) Kudo, S.; Konno, M.; Saito, S. Swelling Equilibria of Cationic Polyelectrolyte Gels in Aqueous Solutions of Various Electrolytes. *Polymer* **1993**, *34* (11), 2370–2373.

(56) Khokhlov, A. R.; Kramarenko, E. Y. Polyelectrolyte/Ionomer Behavior in Polymer Gel Collapse. *Macromol. Theory Simulations* **1994**, *3* (1), 45–59.

(57) Philippova, O. E.; Pieper, T. G.; Sitnikova, N. L.; Starodoubtsev, S. G.; Khokhlov, A. R.; Kilian, H. G. *Conformational Transitions in Polyelectrolyte Networks in Binary Solvents: Microheterogeneities in the Collapsed State*; **1995**; Vol. 28.

(58) Starodoubtsev, S. G.; Khokhlov, A. R.; Sokolov, E. L.; Chu, B. Evidence for Polyelectrolyte/Ionomer Behavior in the Collapse of Polycationic Gels. *Macromolecules* **1995**, *28* (11), 3930–3936.

(59) Smirnov, V. A.; Philippova, O. E.; Sukhadolski, G. A.; Khokhlov, A. R. Multiplets in Polymer Gels. Rare Earth Metal Ions Luminescence Study. *Macromolecules* **1998**, *31* (4), 1162–1167.

(60) Nishiyama, Yuji & Satoh, Mitsuru. Solvent- and counterion-specific swelling behavior of poly(acrylic acid) gels. *Journal of Polymer Science Part B: Polymer Physics* **2000**. 38. 2791 - 2800. 10.1002/1099-0488(20001101)38:21<2791::AID-POLB80>3.0.CO;2-1.

(61) Gasek, N.; Weiss, D. J.. Effect of Temperature on Gelation and Cross-linking of Gelatin Methacryloyl for Biomedical Applications. *Physics of Fluids* **2020**, *32* (3), 033102.

(62) Holland, S., Tuck, C. & Foster, T. Fluid Gels: a New Feedstock for High Viscosity Jetting. *Food Biophysics* **2018**. 13**,** 175–185. https://doi.org/10.1007/s11483-018-9523-x.

(63) Lee, S. J.; Park, K. Synthesis and Characterization of Sol-Gel Phase-Reversible Hydrogels Sensitive to Glucose. *J. Mol. Recognit.* **1996**, *9* (5–6), 549–557.

(64) Lander, P. E. Valkanas. United States Patent 5,137,563 (19). **1992**, No. 19.

(65) Furukawa, H.; Horie, K.; Nozaki, R.; Okada, M. Swelling-Induced Modulation of Static and Dynamic Fluctuations in Polyacrylamide Gels Observed by Scanning Microscopic Light Scattering. *Phys. Rev. E - Stat. Physics, Plasmas, Fluids, Relat. Interdiscip. Top.* **2003**, *68* (3), 14.

(66) Hsu, T. P.; Ma, D. S.; Cohen, C. Effects of Inhomogeneities in Polyacrylamide Gels on Thermodynamic and Transport Properties. *Polymer (Guildf)*. **1983**, *24* (10), 1273–1278.

(67) Al-Rashid, M.; Khan, W.; Vemulapalli, K. Principles of Fracture Fixation in Orthopaedic Trauma Surgery. *J. Perioper. Pract.* **2010**, *20* (3), 113–117.

(68) Chen, Q.; Chen, H.; Zhu, L.; Zheng, J. Fundamentals of Double Network Hydrogels. *J. Mater. Chem. B* **2015**, *3* (18), 3654–3676.

(69) Yannas, I. V.; Huang, C. Viscoelastic Distinction between Helical and Coiled Macromolecules. *Macromolecules* **1972**, *5* (1), 99–100.

(70) Tanaka, Y.; Fukao, K.; Miyamoto, Y. Fracture Energy of Gels. *Eur. Phys. J. E* **2000**, *3* (4), 395–401.

(71) Zarzycki, J. Critical Stress Intensity Factors of Wet Gels. *J. Non. Cryst. Solids* **1988**, *100* (1–3), 359–363.

(72) Gong, J. P.; Katsuyama, Y.; Kurokawa, T.; Osada, Y. Double-Network Hydrogels with Extremely High Mechanical Strength. *Adv. Mater.* **2003**, *15* (14), 1155–1158.

(73) Zhou, H.; Shen, C.; Lu, Y.; Wang, J.; Qing, X.; Dai, T. Mechanically Strong Conducting Hydrogels with Special Double-Network Structure. *Synth. Met.* **2010**, *160* (7–8), 791–796.

(74) Gu, Z.; Huang, K.; Luo, Y.; Zhang, L.; Kuang, T.; Chen, Z.; Liao, G.. Double Network Hydrogel for Tissue Engineering. *WIREs Nanomedicine and Nanobiotechnology* **2018**, *10* (6), e1520.

(75) Choudhary, S.; White, J. C.; Stoppel, W. L.; Roberts, S. C.; Bhatia, S. R. Gelation Behavior of Polysaccharide-Based Interpenetrating Polymer Network (IPN) Hydrogels. *Rheol. Acta* **2011**, *50* (1), 39–52.

(76) Şolpan, D.; Torun, M. Synthesis and Characterization of Sodium Alginate/Acrylamide Semi-Interpenetrating Polymer Networks. *J. Appl. Polym. Sci.* **2006**, *100* (1), 335–342.

(77) Gong, J. P. Why Are Double Network Hydrogels so Tough? *Soft Matter*. 2010, pp 2583–2590.

(78) Dai, T.; Qing, X.; Lu, Y.; Xia, Y. Conducting Hydrogels with Enhanced Mechanical Strength. *Polymer (Guildf)*. **2009**, *50* (22), 5236–5241.

(79) Tirumala, V. R.; Tominaga, T.; Lee, S.; Butler, P. D.; Lin, E. K.; Gong, J. P.; Wu, W. L. Molecular Model for Toughening in Double-Network Hydrogels. *J. Phys. Chem. B* **2008**, *112* (27), 8024–8031.

(80) Brown, H. R. A Model of the Fracture of Double Network Gels. *Macromolecules* **2007**, *40* (10), 3815–3818.

(81) Gong, J. P.; Yu, Q. M.; Tanaka, Y.; Furukawa, H.; Kurokawa, T. Direct Observation of Damage Zone around Crack Tips in Double-Network Gels. *Macromolecules* **2009**, *42* (12), 3852–3855.

(82) Webber, R. E.; Creton, C.; Brown, H. R.; Gong, J. P. Large Strain Hysteresis and Mullins Effect of Tough Double-Network Hydrogels. *Macromolecules* **2007**, *40* (8), 2919–2927.

(83) Rathna, G. V. N. Gelatin Hydrogels: Enhanced Biocompatibility, Drug Release and Cell Viability. *J. Mater. Sci. Mater. Med.* **2008**, *19* (6), 2351–2358.

(84) Wamala, I.; Horvath, M. A.; Pigula, F. A.; Bautista-Salinas, D.; Roche, E. T.; Payne, C. J.; Thalhofer, T.; Saeed, M.; Vasilyev, N. V.; Walsh, C. J.; et al. An Implantable Extracardiac Soft Robotic Device for the Failing Heart: Mechanical Coupling and Synchronization. *Soft Robot.* **2017**, *4* (3), 241–250.

(85) Mazzolai, B.; Margheri, L.; Cianchetti, M.; Dario, P.; Laschi, C. Soft-Robotic Arm Inspired by the Octopus: II. From Artificial Requirements to Innovative Technological Solutions. *Bioinspir. Biomim.* **2012**, *7* (2), 25005.

(86) Pfeifer, R.; Lungarella, M.; Iida, F. The Challenges Ahead for Bio-Inspired "Soft" Robotics. *Commun. ACM* **2012**, *55* (11), 76–87.

(87) Albu-Schaffer, A.; Eiberger, O.; Grebenstein, M.; Haddadin, S.; Ott, C.; Wimbock, T.; Wolf, S.; Hirzinger, G. Soft Robotics. *IEEE Robot. Autom. Mag.* **2008**, *15* (3), 20–30.

(88) Krebs, H.I., Volpe, B.T., Aisen, M.L. & Hogan, N. Increasing Productivity and Quality of Care : Robot-Aided. *J. Rehabil. Res. Dev.* **2000**, No. December, 639–652.

(89) Laschi, C.; Cianchetti, M. Soft Robotics: New Perspectives for Robot Bodyware and Control. *Front. Bioeng. Biotechnol.* **2014**, *2* (January), 1–5.

(90) Landers, R.; Hübner, U.; Schmelzeisen, R.; Mülhaupt, R. Rapid Prototyping of Scaffolds Derived from Thermoreversible Hydrogels and Tailored for Applications in Tissue Engineering. *Biomaterials* **2002**, *23* (23), 4437–4447.

(91) Majidi, C.; Kramer, R.; Wood, R. J. A Non-Differential Elastomer Curvature Sensor for Softer-than-Skin Electronics. *Smart Mater. Struct.* **2011**, *20* (10), 105017.

(92) Dhert, W. J. A.; Alblas, J.; Hennink, W. E.; de Wijn, J. R.; Fedorovich, N. E.; Verbout, A. J. Hydrogels as Extracellular Matrices for Skeletal Tissue Engineering: State-of-the-Art and Novel Application in Organ Printing. *Tissue Eng.* **2007**, *13* (8), 1905–1925.

(93) Kim, D. H.; Rogers, J. A. Stretchable Electronics: Materials Strategies and Devices. *Adv. Mater.* **2008**, *20* (24), 4887–4892..

(94) Rogers, J. A.; Someya, T.; Huang, Y.; Sorensen, A. E.; Lian, J.; Greer, J. R.; Valdevit, L.; Carter, W. B.; Ge, Q.; Jackson, J. A.; et al. Materials and Mechanics for Stretchable Electronics. *Science (80-.).* **2010**, *327* (5973), 1603–1607.

(95) Sekitani, T.; Noguchi, Y.; Hata, K.; Fukushima, T.; Aida, T.; Someya, T. A Rubberlike Stretchable Active Matrix Using Elastic Conductors. *Science (80-.).* **2008**, *321* (5895), 1468 LP-1472.

(96) Dae-Hyeong Kim, 1* Nanshu Lu, 1* Rui Ma, 2* Yun-Soung Kim, 1 Rak-Hwan Kim, 1; Shuodao Wang, 3 Jian Wu, 3 Sang Min Won, 1 Hu Tao, 4 Ahmad Islam, 1 Ki Jun Yu, 1; Tae-il Kim, 1 Raeed Chowdhury, 2 Ming Ying, 1 Lizhi Xu, 1 Ming Li, 3, 6 Hyun-Joong Chung, 1; Hohyun Keum, 1 Martin McCormick, 2 Ping Liu, 5 Yong-Wei Zhang, 5 Fiorenzo G. Omenetto, 4; Yonggang Huang, 3 Todd Coleman, 2 John a. Rogers1. RESEARCH ARTICLES Epidermal Electronics. *Science (80-.).* **2011**, *333* (September), 838–844.

(97) Mannoor, M. S.; Tao, H.; Clayton, J. D.; Sengupta, A.; Kaplan, D. L.; Naik, R. R.; Verma, N.; Omenetto, F. G.; Mcalpine, M. C. Graphene-Based Wireless Bacteria Detection on Tooth Enamel. *Nat. Commun.* **2012**, *3*, 763–768.

(98) Kim, Y.S.; Kim, R.H.; Li, M.; Islam, A.; Ma, R.; Xu, L.; Wu, J.; Ying, M.; Kim, D.H.; Rogers, J. A.; et al. *Epidermal Electronics*; **2011**; 12; 333(6044), 838-843. https://doi.org/10.1126/science.1206157.

(99) Omenetto, F. G.; Whalen, M. J.; Tien, L. W.; Hu, X.; Tang-Schomer, M. D.; Kaplan, D. L.; Hronik-Tupaj, M. Film-Based Implants for Supporting Neuron-Electrode Integrated Interfaces for The Brain. *Adv. Funct. Mater.* **2013**, *24* (13), 1938–1948.

(100) Viventi, J.; Kim, D.; Vigeland, L.; Frechette, E. S.; Blanco, J. A.; Kim, Y.; Avrin, A. E.; Tiruvadi, V. R.; Hwang, S.; Vanleer, A. C.; et al. T e c h n Ic a l r e p o r t s Electrode Array for Mapping Brain Activity in Vivo. *Nat. Neurosci.* **2011**, *14* (12), 1599–1605.

(101) Ruskin, J.; D'Angelo, R.; Liu, Z.; de Graff, B.; Li, Y.; Kim, Y.-S.; Omenetto, F. G.; Lee, S. P.; Zhang, Y.; Ghaffari, R.; et al. Electronic Sensor and Actuator Webs for Large-Area Complex Geometry Cardiac Mapping and Therapy. *Proc. Natl. Acad. Sci.* **2012**, *109* (49), 19910–19915.

(102) Kim, J.-G.; Kim, Y.; Uher, C.; Yoo, S. J.; Yeom, B.; Di Prima, M.; Kotov, N. A.; Su, X.; Zhu, J. Stretchable Nanoparticle Conductors with Self-Organized Conductive Pathways. *Nature* **2013**, *500* (7460), 59–63.

(103) Lacour, S. P.; Benmerah, S.; Tarte, E.; Fitzgerald, J.; Serra, J.; Mcmahon, S.; Fawcett, J.; Graudejus, O.; Yu, Z.; Morrison, B.. Flexible and Stretchable Micro-electrodes for in Vitro and in Vivo Neural Interfaces. *Medical & Biological Engineering & Computing* **2010**, *48* (10), 945–954.

(104) Polikov, V. S.; Tresco, P. A.; Reichert, W. M. Response of Brain Tissue to Chronically Implanted Neural Electrodes. *J. Neurosci. Methods* **2005**, *148* (1), 1–18.

(105) Green, R. A.; Hassarati, R. T.; Goding, J. A.; Baek, S.; Lovell, N. H.; Martens, P. J.; Poole-Warren, L. A. Conductive Hydrogels: Mechanically Robust Hybrids for Use as Biomaterials. *Macromol. Biosci.* **2012**, *12* (4), 494–501.

(106) Mawad, D.; Stewart, E.; Officer, D. L.; Romeo, T.; Wagner, P.; Wagner, K.; Wallace, G. G. A Single Component Conducting Polymer Hydrogel as a Scaffold for Tissue Engineering. *Adv. Funct. Mater.* **2012**, *22* (13), 2692–2699.

(107) Sasaki, M.; Karikkineth, B. C.; Nagamine, K.; Kaji, H.; Torimitsu, K.; Nishizawa, M. Highly Conductive Stretchable and Biocompatible Electrode-Hydrogel Hybrids for Advanced Tissue Engineering. *Adv. Healthc. Mater.* **2014**, *3* (11), 1919–1927.

(108) Sun, J.-Y.; Foo, C. C.; Keplinger, C.; Suo, Z.; Whitesides, G. M.; Rothemund, P. Stretchable, Transparent, Ionic Conductors. *Science (80-.).* **2013**, *341* (6149), 984–987.

(109) Bai, Y.; Chen, B.; Zhou, J.; Suo, Z.; Chiang Foo, C.; Jiang, Y.; Wang, H.; Xiang, F.; Zhou, Y. Cyclic Performance of Viscoelastic Dielectric Elastomers with Solid Hydrogel Electrodes. *Appl. Phys. Lett.* **2014**, *104* (6), 062902.

(110) Chen B, Lu JJ, Yang CH, Yang JH, Zhou J, Chen YM, Suo Z. Highly stretchable and transparent ionogels as nonvolatile conductors for dielectric elastomer transducers. *ACS Appl Mater Interfaces*. **2014** May 28;6(10):7840-5. doi: 10.1021/am501130t. Epub 2014 May 2. PMID: 24758275.

(111) Bakarich, S. E.; in het Panhuis, M.; Tian, K.; Spinks, G. M.; Yang, C.; Vlassak, J. J.; Gately, R. D.; Bae, J.; Suo, Z. 3D Printing of Transparent and Conductive Heterogeneous Hydrogel-Elastomer Systems. *Adv. Mater.* **2017**, *29* (10), 1604827.

(112) Roylance, D. Stress-Strain Curves. **2001**, 1–15. https://resources.saylor.org/wwwresources/archived/site/wpcontent/uploads/2012/09/ME1022.2.4.pdf

(113) Naficy, S.; Brown, H. R.; Razal, J. M.; Spinks, G. M.; Whitten, P. G. Progress toward Robust Polymer Hydrogels. *Aust. J. Chem.* **2011**, *64* (8), 1007–1025.

(114) Okumura, Y.; Ito, K., The Polyrotaxane Gel: A Topological Gel by Figure-of-Eight Cross-links. *Advanced Materials* **2001,** *13* (7), 485-487.

(115) Haraguchi, K.; Takehisa, T., Nanocomposite Hydrogels: A Unique Organic–Inorganic Network Structure with Extraordinary Mechanical, Optical, and Swelling/De-swelling Properties. *Advanced Materials* **2002,** *14* (16), 1120-1124.

(116) Huang, T.; Zhu, L. P.; Brown, H. R.; Xu, H. G.; Wang, H. L.; Jiao, K. X. A Novel Hydrogel with High Mechanical Strength: A Macromolecular Microsphere Composite Hydrogel. *Adv. Mater.* **2007**, *19* (12), 1622–1626.

(117) Dubois, P.; Liao, Q.; Hedrick, J. L.; Hawker, C. J.; Malkoch, M.; Gupta, N.; Mason, A. F.; Vestberg, R.; Frank, C. W.; Mespouille, L.; et al. Synthesis of Well-Defined Hydrogel Networks Using Click Chemistry. *Chem. Commun.* **2006**, No. 26, 2774.

(118) Sasaki, N.; Matsunaga, T.; Shibayama, M.; Suzuki, S.; Yamamoto, Y.; Yoshida, R.; Ito, C.; Sakai, T.; Chung, U. Design and Fabrication of a High-Strength Hydrogel with Ideally Homogeneous Network Structure from Tetrahedron-like Macromonomers. *Macromolecules* **2008**, *41* (14), 5379–5384.

(119) Sun, J.; Zhao, X.; Illeperuma, W. R. K.; Chaudhuri, O.; Oh, K. H.; Mooney, D. J.; Vlassak, J. J.; Suo, Z. Highly Stretchable and Tough Hydrogels. *Nature* **2012**, *489* (7414), 133–136.

(120) Passaglia, E.; Bertoldo, M.; Coiai, S.; Augier, S.; Savi, S.; Ciardelli, F. Thermal & Mechanical Properties of Electrospun PMMA, PVC, Nylon. *Polym. Adv. Technol.* **2008**, *19* (April), 560–568.

(121) Naficy, S.; Kawakami, S.; Sadegholvaad, S.; Wakisaka, M.; Spinks, G. M. Mechanical Properties of Interpenetrating Polymer Network Hydrogels Based on Hybrid Ionically and Covalently Crosslinked Networks. *J. Appl. Polym. Sci.* **2013**, *130* (4), 2504–2513.

(122) Engberg, K.; Waters, D. J.; Jackson, A. J.; Toney, M. F.; Frank, C. W.; Parke-Houben, R.; Ta, C. N. Structure and Mechanism of Strength Enhancement in Interpenetrating Polymer Network Hydrogels. *Macromolecules* **2011**, *44* (14), 5776–5787.

(123) Tanaka, Y.; Kuwabara, R.; Na, Y. H.; Kurokawa, T.; Gong, J. P.; Osada, Y. Determination of Fracture Energy of High Strength Double Network Hydrogels. *J. Phys. Chem. B* **2005**, *109* (23), 11559–11562.

(124) Gong, J. P.; Osada, Y.; Tanaka, Y.; Furukawa, H.; Nakajima, T.; Kurokawa, T. True Chemical Structure of Double Network Hydrogels. *Macromolecules* **2009**, *42* (6), 2184–2189.

(125) Shin, M. S.; Kim, S. J.; Park, S. J.; Lee, Y. H.; Kim, S. I. Synthesis and Characteristics of the Interpenetrating Polymer Network Hydrogel Composed of Chitosan and Polyallylamine. *J. Appl. Polym. Sci.* **2002**, *86* (2), 498–503.

(126) Ju, H. K.; Kim, S. Y.; Lee, Y. M. pH/temperature-Responsive Behaviors of Semi-IPN and Comb-Type Graft Hydrogels Composed of Alginate and poly(N-Isopropylacrylamide). *Polymer (Guildf).* **2001**, *42* (16), 6851–6857.

(127) Sun, J.; Xiao, W.; Tang, Y.; Li, K.; Fan, H. Biomimetic Interpenetrating Polymer Network Hydrogels Based on Methacrylated Alginate and Collagen for 3D Pre-Osteoblast Spreading and Osteogenic Differentiation. *Soft Matter* **2012**, *8* (8), 2398–2404.

(128) Bakarich, SE, Pidcock, GC, Balding, P, Stevens, L, Calvert, P, & In Het Panhuis, M 2012, 'Recovery from an applied strain in interpenetrating polymer network hydrogels with ionic and covalent cross-links', *Soft Matter*, vol. 8, no. 39, pp. 9985–9988.

(129) Tanaka, Y.; Kawauchi, Y.; Kurokawa, T.; Furukawa, H.; Okajima, T.; Gong, J. P. Localized Yielding Around Crack Tips of Double-Network Gels. *Macromol. Rapid Commun.* **2008**, *29* (18), 1514–1520.

(130) Lake, G. J.; Thomas, A. G.; Tabor, D., The strength of highly elastic materials. *Proceedings of the Royal Society of London. Series A. Mathematical and Physical Sciences* **1967,** *300* (1460), 108-119.

(131) Nasrullah, S.; Synthesis and inter-network interaction in double network (DN) hydrogels, Doctor of Philosophy thesis, School of Mechanical, Material & Mechatronic Engineering, University of Wollongong, **2010**. https://ro.uow.edu.au/theses/3259

(132) Ferris, C. J.; Gilmore, K. J.; Wallace, G. G.; Panhuis, M. in het. Modified Gellan Gum Hydrogels for Tissue Engineering Applications. *Soft Matter* **2013**, *9* (14), 3705–3711.

(133) Takeno, H.; Kimura, Y.; Nakamura, W. Mechanical, Swelling, and Structural Properties of Mechanically Tough Clay-Sodium Polyacrylate Blend Hydrogels. *Gels* . 2017.

(134) Cipriano, B. H.; Banik, S. J.; Sharma, R.; Rumore, D.; Hwang, W.; Briber, R. M.; Raghavan, S. R. Superabsorbent Hydrogels That Are Robust and Highly Stretchable. *Macromolecules* **2014**, *47* (13), 4445–4452.

(135) Zohuriaan-Mehr, M. J.; Omidian, H.; Doroudiani, S.; Kabiri, K. Advances in Non-Hygienic Applications of Superabsorbent Hydrogel Materials. *J. Mater. Sci.* **2010**, *45* (21), 5711–5735.

(136) Finch, C. A., Superabsorbent polymers—science and technology. Acs symposium series no. 573. Edited by F. L. Buchholz and N. A. Peppas. American chemical society, Washington DC, 1994. pp. ix + 148. ISBN 0-8412-3039-0. *Polymer International* **1996,** *39* (1), 78-78. doi:10.1002/pi.1996.210390115.

(137) Lee, W.-F.; Wu, R.-J. Superabsorbent Polymeric Materials. I. Swelling Behaviors of Crosslinked Poly(Sodium Acrylate-Co-Hydroxyethyl Methacrylate) in Aqueous Salt Solution. *J. Appl. Polym. Sci.* **1996**, *62* (7), 1099–1114.

(138) Ping Gong, J.; Tanaka, Y., Osada, Yoshihito. Polymer Gels, *Journal of Macromolecular Science, Part C* **2004,** *44* (1), 87-112.

(139) Laftah, W.; Hashim, S.; Akos, N. A Review, Polymer-Plastics Technology and Engineering *Polymer Hydrogels: A Review*; **2011**, 50 (14), 1475-1486. DOI: 10.1080/03602559.2011.593082.

(140) Peak, C. W.; Wilker, J. J.; Schmidt, G. A Review on Tough and Sticky Hydrogels. *Colloid Polym. Sci.* **2013**, *291* (9), 2031–2047.

(141) Zhao, X. Multi-Scale Multi-Mechanism Design of Tough Hydrogels: Building Dissipation into Stretchy Networks. *Soft Matter* **2014**, *10* (5), 672–687.

(142) Haraguchi, K.; Farnworth, R.; Ohbayashi, A.; Takehisa, T. Compositional Effects on Mechanical Properties of Nanocomposite Hydrogels Composed of Poly(N,N-Dimethylacrylamide) and Clay. *Macromolecules* **2003**, *36* (15), 5732–5741.

(143) Haraguchi, K.; Li, H. J. Mechanical Properties and Structure of Polymer-Clay Nanocomposite Gels with High Clay Content. *Macromolecules* **2006**.

(144) Yang, W.; Furukawa, H.; Gong, J. P. Highly Extensible Double-Network Gels with Self-Assembling Anisotropic Structure. *Adv. Mater.* **2008**, *20* (23), 4499–4503.

(145) Xiao, L.; Liu, C.; Zhu, J.; Pochan, D. J.; Jia, X. Hybrid, Elastomeric Hydrogels Crosslinked by Multifunctional Block Copolymer Micelles. *Soft Matter* **2010**, *6* (21), 5293–5297.

(146) Lin, W. C.; Fan, W.; Marcellan, A.; Hourdet, D.; Creton, C. Large Strain and Fracture Properties of Poly(Dimethylacrylamide)/Silica Hybrid Hydrogels. *Macromolecules* **2010**, *43* (5), 2554–2563.

(147) Hao, J.; Weiss, R. A. Viscoelastic and Mechanical Behavior of Hydrophobically Modified Hydrogels. *Macromolecules* **2011**, *44* (23), 9390–9398.

(148) Hu, Y.; Du, Z.; Deng, X.; Wang, T.; Yang, Z.; Zhou, W.; Wang, C. Dual Physically Cross-Linked Hydrogels with High Stretchability, Toughness, and Good Self-Recoverability. *Macromolecules* **2016**, *49* (15), 5660–5668.

(149) Tuncaboylu, D. C.; Sahin, M.; Argun, A.; Oppermann, W.; Okay, O. Dynamics and Large Strain Behavior of Self-Healing Hydrogels with and without Surfactants. *Macromolecules* **2012**, *45* (4), 1991–2000.

(150) Tew, G. N.; Griffin, D. M.; Lackey, M. A.; Cui, J.; Madkour, A. E.; Saffer, E. M.; Bhatia, S. R.; Crosby, A. J. Synthetically Simple, Highly Resilient Hydrogels. *Biomacromolecules* **2012**, *13* (3), 584–588.

(151) Li, X.; Yang, Q.; Zhao, Y.; Long, S.; Zheng, J. Dual Physically Crosslinked Double Network Hydrogels with High Toughness and Self-Healing Properties. *Soft Matter* **2017**, *13* (5), 911–920.

(152) Valavala, Pavan Kumar, "Multiscale constitutive modeling of polymer materials", Dissertation, Michigan Technological University, **2008**. https://digitalcommons.mtu.edu/etds/417

(153) Mitchell, G., *Rheology : Theory, Properties and Practical Applications;* **2014**, Nova, Physics and Astronomy, Physics Research and Technology. ISBN: 978-1-62618-963-8.

(154) Hamad, B. A.; He, M.; Xu, M.; Liu, W.; Mpelwa, M.; Tang, S.; Jin, L.; Song, J.. A Novel Amphoteric Polymer as a Rheology Enhancer and Fluid-loss Control Agent for Water-based Drilling Muds at Elevated Temperatures. *ACS Omega* **2020**, *5* (15), 8483–8495.

(155) Steffe, J.F. Rheological Methods in Food Process Engineering, second edition (second printing). *Freeman Press*, , East Lansing, MI, USA; **1996**.

(156) Rheology (hyperleap.com).

(157) https://cohlife.org/wp-content/uploads/Rheology-Wikipedia.pdf.

(158) Roussel, N.; Bessaies-Bey, H.; Kawashima, S.; Marchon, D.; Vasilic, K.; Wolfs, R.. Recent Advances on Yield Stress and Elasticity of Fresh Cement-based Materials. *Cement and Concrete Research* **2019**, *124*, 105798."

(159) Hsu, C. H.; Hu, S. Y.; Kung, K. Y.; Kuo, C. C.; Chang, C. C.. A Study on the Flow Patterns of a Second Grade Viscoe-lastic Fluid Past a Cavity in a Horizontal Channel. *Journal of Mechanics* **2013**, *29* (2), 207–215.

(160) Bondi, A. Chapter 1 - Viscosity and Molecular Structure. In *Rheology*; EIRICH, F. R. B. T.-R., Ed.; Academic Press, **1967**; pp 1–83.

(161) Fox, R. W.; McDonald, A. T.; Pritchard, P. J. *Introduction to Fluid Mechanics / Robert W. Fox, Philip J. Pritchard, Alan T. McDonald.*; Hoboken, N.J. : John Wiley, c**2009**, 2009.

(162) http://URN.fi/URN:NBN:fi:tty-201605093945.

(163) Manandhar, P.; Calvert, P. D.; Buck, J. R. Elastomeric Ionic Hydrogel Sensor for Large Strains. *IEEE Sens. J.* **2012**, *12* (6), 2052–2061.

(164) Bauer, S.; Bauer-Gogonea, S.; Graz, I.; Kaltenbrunner, M.; Keplinger, C.; Schwodiauer, R. 25th Anniversary Article: A Soft Future: From Robots and Sensor Skin to Energy Harvesters. *Adv. Mater.* **2014**, *26* (1), 149–161.

(165) Zhang, X.; Pint, C. L.; Lee, M. H.; Schubert, B. E.; Jamshidi, A.; Takei, K.; Ko, H.; Gillies, A.; Bardhan, R.; Urban, J. J.; et al. Optically- and Thermally-Responsive Programmable Materials Based on Carbon Nanotube-Hydrogel Polymer Composites. *Nano Lett.* **2011**, *11* (8), 3239–3244.

(166) Wang, E.; Desai, M. S.; Lee, S. W. Light-Controlled Graphene-Elastin Composite Hydrogel Actuators. *Nano Lett.* **2013**, *13* (6), 2826–2830.

(167) Green, R. A.; Lovell, N. H.; Wallace, G. G.; Poole-Warren, L. A. Conducting Polymers for Neural Interfaces: Challenges in Developing an Effective Long-Term Implant. *Biomaterials* **2008**, *29* (24–25), 3393–3399.

(168) Warren, H., Soft conducting hydrogel materials, Doctor of Philosophy thesis, School of Chemistry, University of Wollongong, **2014**. https://ro.uow.edu.au/theses/4281.

(169) Pissis, P.; Kyritsis, A.; Shilov, V. V. Molecular Mobility and Protonic Conductivity in Polymers: Hydrogels and Ionomers. *Solid State Ionics* **1999**, *125* (1), 203–212.

(170) Aouada, F. A.; Guilherme, M. R.; Campese, G. M.; Girotto, E. M.; Rubira, A. F.; Muniz, E. C. Electrochemical and Mechanical Properties of Hydrogels Based on Conductive Poly(3,4-Ethylene Dioxythiophene)/Poly(Styrenesulfonate) and PAAm. *Polym. Test.* **2006**, *25* (2), 158–165.

(171) Dai, T.; Qing, X.; Zhou, H.; Shen, C.; Wang, J.; Lu, Y. Mechanically Strong Conducting Hydrogels with Special Double-Network Structure. *Synth. Met.* **2010**, *160* (7–8), 791–796.

(172) Kishi, R.; Hiroki, K.; Tominaga, T.; Sano, K. I.; Okuzaki, H.; Martinez, J. G.; Otero, T. F.; Osada, Y. Electro-Conductive Double-Network Hydrogels. *J. Polym. Sci. Part B Polym. Phys.* **2012**, *50* (11), 790–796.

(173) Warren, H.; Gately, R. D.; O'Brien, P.; Gorkin, R.; In Het Panhuis, M. Electrical Conductivity, Impedance, and Percolation Behavior of Carbon Nanofiber and Carbon Nanotube Containing Gellan Gum Hydrogels. *J. Polym. Sci. Part B Polym. Phys.* **2014**, *52* (13), 864–871.

(174) Ahmed, E. M. Hydrogel : Preparation , Characterization , and Applications : A Review. *J. Adv. Res.* **2015**, *6* (2), 105–121.

(175) Koivisto, J. T.; Joki, T.; Parraga, J. E.; Paakkönen, R.; Yla-Outinen, L.; Salonen, L.; Jönkkari, I.; Peltola, M.; Ihalainen, T. O.; Narkilahti, S.; et al. Bioamine-Crosslinked Gellan Gum

Hydrogel for Neural Tissue Engineering. *Biomedical Materials (Bristol)*. **2017**, *12*(2), [025014]. https://doi.org/10.1088/1748-605X/aa62b0.

(176) N. Chirani, L.H. Yahia, L. Gritsch, F.L. Motta, S. Chirani, S. Fare. History and Applications of Hydrogels. *J. Biomed. Sci.* **2017**, *04* (02), 100013.

(177) Ulery, B. D.; Nair, L. S.; Laurencin, C. T. Biomedical Applications of Biodegradable Polymers. *Journal of Polymer Science, Part B: Polymer Physics*. **2011**, 49: 832-864. doi:10.1002/polb.22259.

(178) Kaklamani G, Kazaryan D, Bowen J, Iacovella F, Anastasiadis SH, Deligeorgis G. On the electrical conductivity of alginate hydrogels. *Regen Biomater*. **2018**; 5 (5): 293-301. doi:10.1093/rb/rby019.

(179) Mawad, D.; Lauto, A.; Wallace, G. G., Conductive Polymer Hydrogels. In *Polymeric Hydrogels as Smart Biomaterials*, Kalia, S., Ed. Springer International Publishing: Cham, **2016**; 19-44.

(180) Pissis, P; Kyritsis, A. Electrical Conductivity Studies in Hydrogels, *Solid State Ionics*; **1997**; 97 (1-4): 105-113. https://doi.org/10.1016/S0167-2738(97)00074-X.

(181) Konsta, A. A.; Daoukaki, D.; Pissis, P.; Vartzeli, K. Hydration and Conductivity Studies of Polymer-Water Interactions in Polyacrylamide Hydrogels. *Solid State Ionics;* **1999**, 125 (1–4), 235-241. https://doi.org/10.1016/S0167-2738(99)00180-0.

(182) Wu, Y.; Joseph, S.; Aluru, N. R. Effect of Cross-Linking on the Diffusion of Water, Ions, and Small Molecules in Hydrogels. *J. Phys. Chem. B* **2009**, *113* (11), 3512–3520. https://doi.org/10.1021/jp808145x..

(183) Raj Singh, T. R.; Woolfson, A. D.; Donnelly, R. F. Investigation of Solute Permeation across Hydrogels Composed of Poly(methyl Vinyl Ether- *Co* -Maleic Acid) and Poly(ethylene Glycol). *J. Pharm. Pharmacol.* **2010**, 62 (7): 829-837. https://doi.org/10.1211/jpp.62.07.0003.

(184) Hamilton, C. J.; Murphy, S. M.; Atherton, N. D.; Tighe, B. J., Synthetic hydrogels: 4. The permeability of poly(2-hydroxyethyl methacrylate) to cations—an overview of solute—water interactions and transport processes. *Polymer* **1988,** *29* (10), 1879-1886. https://doi.org/10.1016/0032-3861(88)90406-5.

(185) Peppas, N. A.; Wright, S. L. Drug Diffusion and Binding in Ionizable Interpenetrating Networks from Poly(vinyl Alcohol) and Poly(acrylic Acid). *Eur. J. Pharm. Biopharm.* **1998**, 46 (1): 15-29. https://doi.org/10.1016/S0939-6411(97)00113-6.

(186) Å. Sandvand, E. Halvorsen and K. E. Aasmundtveit, "Finite element modelling of influence of bonding material distribution in precision piezoresistive MEMS pressure-sensors," *Proceedings of the 5th Electronics System-integration Technology Conference (ESTC)*, Helsinki, **2014**, pp. 1-4, doi: 10.1109/ESTC.2014.6962829.

(187) Å. Sandvand, E. Halvorsen, K.E. Aasmundtveit and H. Jakobsen, "Influence of sensor-package hermeticity-level on long-term drift for a piezoresistive MEMS pressure-sensor", Microelectronics Packaging Conference (EMPC), Friedrichshafen, Germany, 14-16 September **2015.**

(188) Sun, J. Y.; Keplinger, C.; Whitesides, G. M.; Suo, Z. Ionic Skin. *Adv. Mater.* **2014**, 26: 7608-7614. https://doi.org/10.1002/adma.201403441.

(189) https://rvi.biz/rfduino-prototyping-shield-accessory-board-rfd22125/15754789254684872500.

(190) Hossain, A.; Mian, A. Four-Terminal Square Piezoresistive Sensors for MEMS Pressure Sensing. *J. Sensors* **2017**. https://doi.org/10.1155/2017/6954875.

(191) Stovall, J. R., Capacitance strain gauge. US2576489A, United States Patent and Trademark Office, Application filed by Tinius olsen testing machine Co., 20 January **1950**. Google Patents, patents.google.com/patent/US2576489A/en.#patentCitationspatent/US5971829A/en?oq=5971829.

(192) Harish, D.; Schultz, J., Capacitive strain gauge system and method. US20090158856A1, United States Patent and Trademark Office, Application filed by Ypoint Capital Inc., 25 July. Google Patents, patents, patents.google.com/patent/US20090158856A1/en?q=CAPACITIVE&q=STRAIN+GAUGE&before=priority:20071231&after=priority:20070101&oq=CAPACITIVE+STRAIN+GAUGE+2007#patentCitations.

(193) C. Pidcock, G.; in het Panhuis, M. Extrusion Printing of Flexible Electrically Conducting Carbon Nanotube Networks. Adv. *Funct. Mater*. **2012**; 22: 4790-4800. https://doi.org/10.1002/adfm.201200724.

(194) Yamada, T.; Hayamizu, Y.; Yamamoto, Y.; Yomogida, Y.; Izadi-Najafabadi, A.; Futaba, D. N.; Hata, K. A Stretchable Carbon Nanotube Strain Sensor for Human-Motion Detection. *Nat. Nanotechnol*. **2011;** 6 (5): 296-301. https://doi.org/10.1038/nnano.2011.36.

(195) https://docplayer.net/31289318-Strain-gauge-measurement-a-tutorial.html.

(196) Barry, R. A.; Shepherd, R. F.; Hanson, J. N.; Nuzzo, R. G.; Wiltzius, P.; Lewis, J. A. Direct-Write Assembly of 3D Hydrogel Scaffolds for Guided Cell Growth. *Adv. Mater*. **2009**, *21* (23), 2407–2410. https://doi.org/10.1002/adma.200803702.

(197) Lin, S.; Cao, C.; Wang, Q.; Gonzalez, M.; Dolbow, J. E.; Zhao, X. Design of Stiff, Tough and Stretchy Hydrogel Composites via Nanoscale Hybrid Crosslinking and Macroscale Fiber Reinforcement. *Soft Matter*. **2014**; 10 (38): 7519-7527. https://doi.org/10.1039/c4sm01039f.

(198) Calvert, P. Inkjet Printing for Materials and Devices. *Chemistry of Materials*. **2001**. https://doi.org/10.1021/cm0101632.

(199) Van Osch, T. H. J.; Perelaer, J.; De Laat, A. W. M.; Schubert, U. S. Inkjet Printing of Narrow Conductive Tracks on Untreated Polymeric Substrates. *Adv. Mater*. **2008**. https://doi.org/10.1002/adma.200701876.

(200) Teng, W. D.; Edirisinghe, M. J.; Evans, J. R. G. Optimization of Dispersion and Viscosity of a Ceramic Jet Printing Ink. *J. Am. Ceram. Soc*. **2005**. https://doi.org/10.1111/j.1151-2916.1997.tb02855.x.

(201) Ellis, J.; Mavromatos, N. E.; Nanopoulos, D. V.; Sakharov, A. S. Cosmology: Synchrotron Radiation and Quantum Gravity. *Nature* **2004**, *428* (6981), 2481.

(202) Bakarich, S. E.; Panhuis, M. in Het; Beirne, S.; Wallace, G. G.; Spinks, G. M. Extrusion Printing of Ionic–covalent Entanglement Hydrogels with High Toughness. *J. Mater. Chem. B* **2013**, *1* (38), 4939.

(203) https://3dprinting.com/what-is-3d-printing/.

(204) Ferris, C. J.; Gilmore, K. G.; Wallace, G. G.; In Het Panhuis, M. Biofabrication: An Overview of the Approaches Used for Printing of Living Cells. *Appl. Microbiol. Biotechnol*. **2013**, *97* (10), 4243–4258.

(205) Huey, D. J.; Hu, J. C.; Athanasiou, K. A. Unlike Bone, Cartilage Regeneration Remains Elusive. *Science*. **2012**, pp 917–921.

(206) Murphy, S. V.; Skardal, A.; Atala, A. Evaluation of Hydrogels for Bio-Printing Applications. *J. Biomed. Mater. Res. - Part A* **2013**, *101 A* (1), 272–284.

(207) Billiet, T.; Vandenhaute, M.; Schelfhout, J.; Van Vlierberghe, S.; Dubruel, P. A Review of Trends and Limitations in Hydrogel-Rapid Prototyping for Tissue Engineering. *Biomaterials* **2012**, *33* (26), 6020–6041.

(208) Melchels, F. P. W.; Domingos, M. A. N.; Klein, T. J.; Malda, J.; Bartolo, P. J.; Hutmacher, D. W. Additive Manufacturing of Tissues and Organs. *Prog. Polym. Sci.* **2012**, *37* (8), 1079–1104.

(209) SHAINBERG, I.; LEVY, G. J., Organic polymers and soil sealing in cultivated soils. *Soil Science* **1994,** *158* (4), 267-273.

(210) Rong, Q.; Lei, W.; Liu, M. Conductive Hydrogels as Smart Materials for Flexible Electronic Devices. *Chem. - A Eur. J.* **2018**, *24* (64), 16930–16943.

(211) Moroni, L.; Burdick, J. A.; Highley, C. B.; Lee, S. J.; Morimoto, Y.; Takeuchi, S.; Yoo, J. J.; Boland, T.; Burdick, J. A.; De Maria, C.; et al. Proposal to Assess Printability of Bioinks for Extrusion-Based Bioprinting and Evaluation of Rheological Properties Governing Bioprintability. *Biofabrication* **2016**.

(212) Zhao, Y.; Huang, X. Mechanisms and Materials of Flexible and Stretchable Skin Sensors. *Micromachines* **2017**, *8* (3).

(213) Chen, Q. L.; Liu, Z.; Shum, H. C. Three-Dimensional Printing-Based Electro-Millifluidic Devices for Fabricating Multi-Compartment Particles. *Biomicrofluidics* **2014**, *8* (6).

(214) Gul, J. Z.; Sajid, M.; Rehman, M. M.; Siddiqui, G. U.; Shah, I.; Kim, K. H.; Lee, J. W.; Choi, K. H. 3D Printing for Soft Robotics–a Review. *Sci. Technol. Adv. Mater.* **2018**, *19* (1), 243–262.

(215) Gowers, S. A. N.; Curto, V. F.; Seneci, C. A.; Wang, C.; Anastasova, S.; Vadgama, P.; Yang, G. Z.; Boutelle, M. G. 3D Printed Microfluidic Device with Integrated Biosensors for Online Analysis of Subcutaneous Human Microdialysate. *Anal. Chem.* **2015**, *87* (15), 7763–7770.

(216) Sun, S.; Yang, M.; Kostov, Y.; Rasooly, A. ELISA-LOC: Lab-on-a-Chip for Enzyme-Linked Immunodetection. *Lab Chip* **2010**, *10* (16), 2093–2100.

(217) Kong, Y. L.; Tamargo, I. A.; Kim, H.; Johnson, B. N.; Gupta, M. K.; Koh, T. W.; Chin, H. A.; Steingart, D. A.; Rand, B. P.; McAlpine, M. C. 3D Printed Quantum Dot Light-Emitting Diodes. *Nano Lett.* **2014**, *14* (12), 7017–7023.

(218) Lewis, J. A.; Ahn, B. Y. Three-Dimensional Printed Electronics. *Nature* **2015**, *518* (7537), 42–43.

(219) Johnson, B. N.; Lancaster, K. Z.; Zhen, G.; He, J.; Gupta, M. K.; Kong, Y. L.; Engel, E. A.; Krick, K. D.; Ju, A.; Meng, F.; et al. 3D Printed Anatomical Nerve Regeneration Pathways. *Adv. Funct. Mater.* **2015**, *25* (39), 6205–6217.

(220) Mannoor, M. S.; Jiang, Z.; James, T.; Kong, Y. L.; Malatesta, K. A.; Soboyejo, W. O.; Verma, N.; Gracias, D. H.; McAlpine, M. C. 3D Printed Bionic Ears. *Nano Lett.* **2013**, *13* (6), 2634–2639.

(221) Kolesky, D. B.; Truby, R. L.; Gladman, A. S.; Busbee, T. A.; Homan, K. A.; Lewis, J. A. 3D Bioprinting of Vascularized, Heterogeneous Cell-Laden Tissue Constructs. *Adv. Mater.* **2014**, *26* (19), 3124–3130.

(222) Muth, J. T.; Vogt, D. M.; Truby, R. L.; Mengüç, Y.; Kolesky, D. B.; Wood, R. J.; Lewis, J. A. Embedded 3D Printing of Strain Sensors within Highly Stretchable Elastomers. *Adv. Mater.* **2014**, *26* (36), 6307–6312.

(223) Farahani, R. D.; Dalir, H.; Le Borgne, V.; Gautier, L. A.; El Khakani, M. A.; Lévesque, M.; Therriault, D. Direct-Write Fabrication of Freestanding Nanocomposite Strain Sensors. *Nanotechnology* **2012**, *23* (8).

(224) Guo, S.; Yang, X.; Heuzey, M.-C.; Therriault, D. 3D Printing of a Multifunctional Nanocomposite Helical Liquid Sensor. *Nanoscale* **2015**, *7* (15), 6451–6456.

(225) Robinson, S. S.; O'Brien, K. W.; Zhao, H.; Peele, B. N.; Larson, C. M.; Mac Murray, B. C.; Van Meerbeek, I. M.; Dunham, S. N.; Shepherd, R. F. Integrated Soft Sensors and Elastomeric Actuators for Tactile Machines with Kinesthetic Sense. *Extrem. Mech. Lett.* **2015**, *5*, 47–53.

(226) Bakarich, S. E.; Balding, P.; Gorkin, R.; Spinks, G. M.; In Het Panhuis, M. Printed Ionic-Covalent Entanglement Hydrogels from Carrageenan and an Epoxy Amine. *RSC Adv.* **2014**, *4* (72), 38088–38092.

(227) Evans, R. P.; Nelson, C. L.; Bowen, W. R.; Kleve, M. G.; Hickmon, S. G. Visualization of Bacterial Glycocalyx with a Scanning Electron Microscope. *Clin. Orthop. Relat. Res.* **1998**, No. 347, 243–249.

(228) Fialho, A. M.; Moreira, L. M.; Granja, A. T.; Popescu, A. O.; Hoffmann, K.; Sá-Correia, I. Occurrence, Production, and Applications of Gellan: Current State and Perspectives. *Appl. Microbiol. Biotechnol.* **2008**, *79* (6), 889–900.

(229) Kedzierewicz, F.; Lombry, C.; Rios, R.; Hoffman, M.; Maincent, P. Effect of the Formulation on the In-Vitro Release of Propranolol from Gellan Beads. *Int. J. Pharm.* **1999**, *178* (1), 129–136.

(230) Sultana, Y.; Aqil, M.; Ali, A. Ion-Activated, Gelrite®-Based in Situ Ophthalmic Gels of Pefloxacin Mesylate: Comparison with Conventional Eye Drops. *Drug Deliv. J. Deliv. Target. Ther. Agents* **2006**, *13* (3), 215–219.

(231) Ciardelli, G.; Chiono, V.; Vozzi, G.; Pracella, M.; Ahluwalia, A.; Barbani, N.; Cristallini, C.; Giusti, P. Blends of Poly-(ε-Caprolactone) and Polysaccharides in Tissue Engineering Applications. *Biomacromolecules* **2005**, *6* (4), 1961–1976.

(232) Smith, A. M.; Shelton, R. M.; Perrie, Y.; Harris, J. J. An Initial Evaluation of Gellan Gum as a Material for Tissue Engineering Applications. *J. Biomater. Appl.* **2007**, *22* (3), 241–254.

(233) Nakano, M.; Niimi, Y.; Kobayashi, D.; Watanabe, A. Adventitious Shoot Regeneration and Micropropagation of Hybrid Tuberous Begonia (Begonia x Tuberhybrida Voss). *Sci. Hortic. (Amsterdam).* **1999**, *79* (3–4), 245–251.

(234) Klimaszewska, K. Plantlet Development from Immature Zygotic Embryos of Hybrid Larch through Somatic Embryogenesis. *Plant Sci.* **1989**, *63* (1), 95–103.

(235) Rule, P. L.; Alexander, A. D. Gellan Gum as a Substitute for Agar in Leptospiral Media. *J. Clin. Microbiol.* **1986**, *23* (3), 500–504.

(236) O'Neill, M. A.; Selvendran, R. R.; Morris, V. J., Structure of the acidic extracellular gelling polysaccharide produced by Pseudomonas elodea. *Carbohydrate Research* **1983,** *124* (1), 123-133.

(237) Biskup, J.; Preuß, M. Information Control by Policy-Based Relational Weakening Templates. *Lect. Notes Comput. Sci. (including Subser. Lect. Notes Artif. Intell. Lect. Notes Bioinformatics)* **2016**, *9879 LNCS*, 361–381.

(238) Kuo, M. S.; Mort, A. J.; Dell, A. Identification and Location of L-Glycerate, an Unusual Acyl Substituent in Gellan Gum. *Carbohydr. Res.* **1986**, *156* (C), 173–187.

(239) Bakarich, S. E.; Marc In Het Panhuis, A. *Soft and Tough Gellan Gum-Polyacrylamide Double Network Hydrogels With Multi-Walled Carbon Nanotubes*; Bachelor of Nanotechnology with Honours thesis from The University of Wollongong **2011**.

(240) Cole, K. D. Reversible Gels for Electrophoresis and Isolation of DNA. *Biotechniques* **1999**, *26* (4), 748–756.

(241) Chandrasekaran, R.; Puigjaner, L. C.; Joyce, K. L.; Arnott, S. Cation Interactions in Gellan: An x-Ray Study of the Potassium Salt. *Carbohydr. Res.* **1988**, *181* (C), 23–40.

(242) Nazir, A.; Asghar, A.; Aslam Maan, A. Food Gels: Gelling Process and New Applications; *Adv. Food Rheol. Appl.* **2016**, 52, 335–353. doi: 10.1016/b978-0-08-100431-9.00013-9.

(243) Smith, A. M.; Shelton, R. M.; Perrie, Y.; Harris, J. J. An Initial Evaluation of Gellan Gum as a Material for Tissue Engineering Applications. *J. Biomater. Appl.* **2007**, *22* (3), 241–254.

(244) Ferris, C. J.; In Het Panhuis, M. Conducting Bio-Materials Based on Gellan Gum Hydrogels. *Soft Matter* **2009**, *5* (18), 3430–3437.

(245) Pines, E.; Prins, W. Structure-Property Relations of Thermoreversible Macromolecular Hydrogels. *Macromolecules* **1973**, *6* (6), 888–895.

(246) Zhao, X.; Huebsch, N.; Mooney, D. J.; Suo, Z. Stress-Relaxation Behavior in Gels with Ionic and Covalent Crosslinks. *J. Appl. Phys.* **2010**, 107 (6): 63509. doi: 10.1063/1.3343265.

(247) Gregoriou, V. G. Fourier Transform Infrared Spectroscopy of Polymers. In *Applied Polymer Science: 21st Century*; Springer Berlin Heidelberg: Berlin, Heidelberg, **2007**; pp 709–757.

(248) Higgins, S. J.; Hames, B. D., *RNA Processing: A Practical Approach*. IRL Press at Oxford University Press: **1994**.

(249) Stephen Horvath, Z.; Corthals, G.; W. Wrigley, C.; Margolis, J. Multifunctional Apparatus for Electrokinetic Processing of Proteins; *ELECTROPHORESIS*, **1994**, 15: 968-971. doi:10.1002/elps.11501501141.

(250) Zheng H., Ma J., Zhu C., Zhang Z., Liu L., Sun Y., Tang X. Synthesis of anion polyacrylamide under UV initiation and its application in removing dioctyl phthalate from water through flocculation process; *Separation and Purification Technology*, **2014**, 123, 35-44.

(251) Gerhardt, W. W.; Noga, D. E.; Hardcastle, K. I.; García, A. J.; Collard, D. M.; Weck, M. Functional Lactide Monomers: Methodology and Polymerization. *Biomacromolecules* **2006**, *7* (6), 1735–1742.

(252) HONGHUI ZHU, D. W. S. H. Z. and; STANLEY, S. J. Improving removal of turbidity causing materials by using polymers as a filter aid. *Water Res.* **1996**, *30* (1), 103–114.

(253) Caulfield, M. J.; Hao, X.; Qiao, G. G.; Solomon, D. H. Degradation on Polyacrylamides. Part I. Linear Polyacrylamide. *Polymer (Guildf).* **2003**, *44* (5), 1331–1337.

(254) Seybold, C. A. Polyacrylamide Review: Soil Conditioning and Environmental Fate. *Commun. Soil Sci. Plant Anal.* **1994**, *25* (11–12), 2171–2185.

(255) Riley, D. Copy 79. *Manager* **2010**, *56* (6), 1926–1932.

(256) https://polymerdatabase.com/polymer%20classes/Polyacrylamide%20type.html.

(257) Azzam, R. A. I. Agricultural Polymers Polyacrylamide Preparation, Application and Prospects in Soil Conditioning. *Commun. Soil Sci. Plant Anal.* **1980**, *11* (8), 767–834.

(258) Raymond, S.; Weintraub, L. Acrylamide Gel as a Supporting Medium for Zone Electrophoresis. *Science (80-).* **1959**, *130* (3377), 711.

(259) Peter Chabrecek, R; Dieter Lohmann, M.,. 'PROCESS FOR COATING A MATERIAL SURFACE', filed by Novartis AG, Basel (CH), US6,465,056 B1, United States Patent and Trademark Office, 10 April **2000**.

(260) Bamford C.H., Al-Lamee K.G. Studies in polymer surface modification and grafting for biomedical uses: 2. Application to arterial blood filters and oxygenators. Polymer. **1996**;3 7:4885–4889. doi: 10.1016/0032-3861(96)00538-1

(261) Hartmann, H.; Denzinger, W.; Kroener, M.; Nilz, C. filed by BASF SE, US5578678A, United States Patent and Trademark Office, 26 November **1996**.

(262) Marshall, T.; Williams, K. M. The Simplified Technique of High Resolution Two-Dimensional Polyacrylamide Gel Electrophoresis: Biomedical Applications in Health and Disease. *Electrophoresis* **1991**, *12* (7-8), 461–471.

(263) Caulfield, M. J.; Qiao, G. G.; Solomon, D. H. Some Aspects of the Properties and Degradation of Polyacrylamides. *Chem. Rev.* **2002**, *102* (9), 3067–3083.

(264) Assi, A.; Khazeem, R.; Salem, A.; Ali, A. Studying the Effects of Different Polymers on Rheological Properties of Water Base Muds. *Eng. J.* **2018**, *24*, 12-25.

(265) http://www.chm.bris.ac.uk/motm/acrylamide/ACRYLAMIDE%20MOTM%20draft.doc

(266) Mun, G. A.; Nurkeeva, Z. S.; Dergunov, S. A.; Nam, I. K.; Maimakov, T. P.; Shaikhutdinov, E. M.; Lee, S. C.; Park, K. Studies on Graft Copolymerization of 2-Hydroxyethyl Acrylate onto Chitosan. *React. Funct. Polym.* **2008**, *68* (1), 389–395.

(267) Okada, M.; Masunaga, H.; Furukawa, H. Concentric Pattern Formation during Phase Separation Induced by a Cross-Linking Reaction. *Macromolecules* **2000**, *33* (20), 7238–7240.

(268) Rusu, D.; Ciolacu, D.; Simionescu, B., Cellulose-based hydrogels in tissue engineering applications. *Cellulose Chemistry and Technology* **2019,** *53*, 907-923.

(269) Holliman, P. J.; Clark, J. A.; Williamson, J. C.; Jones, D. L. Model and Field Studies of the Degradation of Cross-Linked Polyacrylamide Gels Used during the Revegetation of Slate Waste. *Sci. Total Environ.* **2005**, *336* (1–3), 13–24.

(270) Singh, B.; Chauhan, G. S.; Kumar, S.; Chauhan, N. Synthesis, Characterization and Swelling Responses of PH Sensitive Psyllium and Polyacrylamide Based Hydrogels for the Use in Drug Delivery (I). *Carbohydr. Polym.* **2007**, *67* (2), 190–200.

(271) Soppimath, K. S.; Kulkarni, A. R.; Aminabhavi, T. M. Chemically Modified Polyacrylamide-g-Guar Gum-Based Crosslinked Anionic Microgels as PH-Sensitive Drug Delivery Systems: Preparation and Characterization. *J. Control. Release* **2001**, *75* (3), 331–345.

(272) Cohen, Y.; Ramon, O.; Kopelman, I. J.; Mizrahi, S. Characterization of Inhomogeneous Polyacrylamide Hydrogels. *J. Polym. Sci. Part B Polym. Phys.* **1992**, *30* (9), 1055–1067.

(273) Bai, Y.; Chen, B.; Xiang, F.; Zhou, J.; Wang, H.; Suo, Z. Transparent Hydrogel with Enhanced Water Retention Capacity by Introducing Highly Hydratable Salt. *Appl. Phys. Lett.* **2014**, *105* (15).

(274) Stples, R. H.; Robinson, R. A.; Stples, R. H.; Robinson, R. A. Ionic Hydration and Activity in Electrolyte Solutions. *J. Am. Chem. Soc.* **1948**, *70* (5), 1870–1878.

(275) Rodbbush, W. H. The Freezing Points of Concentrated Solutions and the Free Energy of Solution of Salts. *J. Am. Chem. Soc.* **1918**, *40* (8), 1204–1213.

(276) Glueckauf, E. The Influence of Ionic Hydration on Activity Coefficients in Concentrated Electrolyte Solutions. **1955**, 1235–1244.

(277) Du, Y.; Cheng, H.; Li, Y.; Wang, B.; Mao, Z.; Xu, H.; Zhang, L.; Zhong, Y.; Yan, X.; Sui, X. Temperature-Responsive Cellulose Sponge with Switchable Pore Size: Application as a Water Flow Manipulator. *Mater. Lett.* **2018**, *210*, 337–340.

(278) Sun, M. H.; Huang, S. Z.; Chen, L. H.; Li, Y.; Yang, X. Y.; Yuan, Z. Y.; Su, B. L. Applications of Hierarchically Structured Porous Materials from Energy Storage and Conversion, Catalysis, Photocatalysis, Adsorption, Separation, and Sensing to Biomedicine. *Chem. Soc. Rev.* **2016**, *45* (12), 3479–3563.

(279) Slater, A. G.; Cooper, A. I. Function-Led Design of New Porous Materials. *Science (80-.).* **2015**, *348* (6238), aaa8075.

(280) Chen, H.; Ruckenstein, E. Nanomembrane Containing a Nanopore in an Electrolyte Solution: A Molecular Dynamics Approach. *J. Phys. Chem. Lett.* **2014**, *5* (17), 2979–2982.

(281) Klemm, D.; Kramer, F.; Moritz, S.; Lindström, T.; Ankerfors, M.; Gray, D.; Dorris, A. Nanocelluloses: A New Family of Nature-Based Materials. *Angew. Chemie - Int. Ed.* **2011**, *50* (24), 5438–5466.

(282) Missoum, K.; Belgacem, M. N.; Bras, J. Nanofibrillated Cellulose Surface Modification: A Review. *Materials (Basel).* **2013**, *6* (5), 1745–1766.

(283) Zhou, C.; Wu, Q.; Yue, Y.; Zhang, Q. Application of Rod-Shaped Cellulose Nanocrystals in Polyacrylamide Hydrogels. *J. Colloid Interface Sci.* **2011**, *353* (1), 116–123.

(284) Wang, B.; Sain, M.; Oksman, K. Study of Structural Morphology of Hemp Fiber from the Micro to the Nanoscale. *Appl. Compos. Mater.* **2007**, *14* (2), 89–103.

(285) Nguyen, S. T.; Feng, J.; Le, N. T.; Le, A. T. T.; Hoang, N.; Tan, V. B. C.; Duong, H. M. Cellulose Aerogel from Paper Waste for Crude Oil Spill Cleaning. *Ind. Eng. Chem. Res.* **2013**, *52* (51), 18386–18391.

(286) Capodicasa, S.; Fedi, S.; Porcelli, A. M.; Zannoni, D. The Microbial Community Dwelling on a Biodeteriorated 16th Century Painting. *Int. Biodeterior. Biodegrad.* **2010**, *64* (8), 727–733.

(287) Hwang, T. I.; Maharjan, B.; Tiwari, A. P.; Lee, S.; Joshi, M. K.; Park, C. H.; Kim, C. S. Facile Fabrication of Spongy Nanofibrous Scaffold for Tissue Engineering Applications. *Mater. Lett.* **2018**, *219*, 119–122.

(288) Joshi, M. K.; Tiwari, A. P.; Pant, H. R.; Shrestha, B. K.; Kim, H. J.; Park, C. H.; Kim, C. S. In Situ Generation of Cellulose Nanocrystals in Polycaprolactone Nanofibers: Effects on Crystallinity, Mechanical Strength, Biocompatibility, and Biomimetic Mineralization. *ACS Appl. Mater. Interfaces* **2015**, *7* (35), 19672–19683.

(289) Spagnol, C.; Rodrigues, F. H. A.; Neto, A. G. V. C.; Pereira, A. G. B.; Fajardo, A. R.; Radovanovic, E.; Rubira, A. F.; Muniz, E. C. Nanocomposites Based on Poly(Acrylamide-Co-Acrylate) and Cellulose Nanowhiskers. *Eur. Polym. J.* **2012**, *48* (3), 454–463.

(290) Qian, C.; Zhang, T.; Gravesande, J.; Baysah, C.; Song, X.; Xing, J. Injectable and Self-Healing Polysaccharide-Based Hydrogel for PH-Responsive Drug Release. *Int. J. Biol. Macromol.* **2019**, *123*, 140–148.

(291) Yao, Y.; Chi, X.; Zhou, Y.; Huang, F. A Bola-Type Supra-Amphiphile Constructed from a Water-Soluble Pillar[5]Arene and a Rod-Coil Molecule for Dual Fluorescent Sensing. *Chem. Sci.* **2014**, 5, 2778-2782. https://doi.org/10.1039/C4SC00585F.

(292) Parlato, M.; Reichert, S.; Barney, N.; Murphy, W. L. Poly(Ethylene Glycol) Hydrogels with Adaptable Mechanical and Degradation Properties for Use in Biomedical Applications. *Macromol. Biosci.* **2014**, *14* (5), 687–698.

(293) Liu, H.; Liu, J.; Qi, C.; Fang, Y.; Zhang, L.; Zhuo, R.; Jiang, X. Thermosensitive Injectable In-Situ Forming Carboxymethyl Chitin Hydrogel for Three-Dimensional Cell Culture. *Acta Biomater.* **2016**, *35*, 228–237.

(294) Du, Z.; Li, N.; Hua, Y.; Shi, Y.; Bao, C.; Zhang, H.; Yang, Y.; Lin, Q.; Zhu, L. Physiological PH-Dependent Gelation for 3D Printing Based on the Phase Separation of Gelatin and Oxidized Dextran. *Chem. Commun.* **2017**, *53* (97), 13023–13026.

(295) Wan, Y.; Liu, L.; Yuan, S.; Sun, J.; Li, Z. PH-Responsive Peptide Supramolecular Hydrogels with Antibacterial Activity. *Langmuir* **2017**, *33* (13), 3234–3240.

(296) Xia, Y.; Whitesides, G. M. Soft Lithography. *Annu. Rev. Mater. Sci.* **1998**, *28* (1), 153–184.

(297) Subramaniam, A.; Sethuraman, S. Biomedical Applications of Nondegradable Polymers. *Nat. Synth. Biomed. Polym.* **2014**, 301–308.

(298) Wong, I.; Ho, C. M. Surface Molecular Property Modifications for Poly(Dimethylsiloxane) (PDMS) Based Microfluidic Devices. *Microfluid. Nanofluidics* **2009**, *7* (3), 291–306.

(299) Wu, M. H. Simple Poly(Dimethylsiloxane) Surface Modification to Control Cell Adhesion. *Surf. Interface Anal.* **2009**, *41* (1), 11–16.

(300) Pinto, S.; Alves, P.; Matos, C. M.; Santos, A. C.; Rodrigues, L. R.; Teixeira, J. A.; Gil, M. H. Poly(Dimethyl Siloxane) Surface Modification by Low Pressure Plasma to Improve Its Characteristics towards Biomedical Applications. *Colloids Surfaces B Biointerfaces* **2010**, *81* (1), 20–26.

(301) Seethapathy, S.; Górecki, T. Applications of Polydimethylsiloxane in Analytical Chemistry: A Review. *Anal. Chim. Acta* **2012**, *750*, 48–62.

(302) https://www.elveflow.com/microfluidic-tutorials/microfluidic-reviews-and-tutorials/the-poly-di-methyl-siloxane-pdms-and-microfluidics/

(303) Mark, J.; Allcock, H.; West, R., Inorganic Polymers Prentice Hall. *New Jersey, USA* **1992**.

(304) Kim, N. H.; Yoon, S.; Jung, K. I.; Lee, D. G.; Bang, J.; Jung, H. W. Crosslinking Behaviors and Mechanical Properties of Curable PDMS and PEG Films with Various Contents of Glycidyl Methacrylate. *J. Appl. Polym. Sci.* **2018**, 2019.

(305) Hanson, D. E. An Explicit Polymer and Node Network Model to Compute Micromechanical Properties of Silica-Filled Polydimethylsiloxane. *Polymer (Guildf).* **2004**, *45* (3), 1055–1062.

(306) https://consumer.dow.com/en-us/document viewer.html?docType=SDS&contentType=SDS&materialNumber=1023993&selectedCountry=Australia&selectedLanguage=EN&recordNumber=27175193.

(307) Gaydon, a. G.; Moore, N. P. W.; Simonson, J. R. Chemical and Spectroscopic Studies of Blue Flames in the Auto-Ignition of Methane. *Proc. R. Soc. A Math. Phys. Eng. Sci.* **1955**, *230* (1180), 1–19.

(308) Zhu, Y.-C.; Zhang, X.-H.; Qiao, J.; Wei, G.-S. *A Study on Radiation Crosslinking of Polydimethylsiloxane (PDMS) Rubber Latex*; **2004**; Vol. 22.

(309) CHARLESBY, A. Effect of Molecular Weight on the Cross-Linking of Siloxanes by High-Energy Radiation. *Nature* **1954**, *173*, 679.

(310) https://www.diva-portal.org/smash/get/diva2:121034/FULLTEXT01.pdf

(311) Lee, J. N.; Park, C.; Whitesides, G. M. Solvent Compatibility of Poly(Dimethylsiloxane)-Based Microfluidic Devices. *Anal. Chem.* **2003**, *75* (23), 6544–6554.

(312) Bourgoin, J. P.; Vuillaume, D.; Goffman, M. F.; Filoramo, A. Molecular Electronics. Nanosci. *Nanotechnologies Nanophysics* **2007**, 43 (2003), 447–501.

(313) Khang, D.-Y.; Jiang, H.; Huang, Y.; Rogers, J. A. A Stretchable Form of Single-Crystal. *Science (80-.).* **2006**, *311* (January), 208–212.

(314) Park, J.; Wang, S.; Li, M.; Ahn, C.; Hyun, J. K.; Kim, D. S.; Kim, D. K.; Rogers, J. A.; Huang, Y.; Jeon, S. Three-Dimensional Nanonetworks for Giant Stretchability in Dielectrics and Conductors. *Nat. Commun.* **2012**, *3* (May), 916–918.

(315) Duan, S.; Yang, K.; Wang, Z.; Chen, M.; Zhang, L.; Zhang, H.; Li, C. Fabrication of Highly Stretchable Conductors Based on 3D Printed Porous Poly(Dimethylsiloxane) and Conductive Carbon Nanotubes/Graphene Network. *ACS Appl. Mater. Interfaces* **2016**, *8* (3), 2187–2192.

(316) Chen, M.; Zhang, L.; Duan, S.; Jing, S.; Jiang, H.; Li, C. Highly Stretchable Conductors Integrated with a Conductive Carbon Nanotube/Graphene Network and 3D Porous Poly (Dimethylsiloxane). *Adv. Funct. Mater.* **2014**, *24* (47), 7548–7556.

(317) Choi, S. J.; Kwon, T. H.; Im, H.; Moon, D. Il; Baek, D. J.; Seol, M. L.; Duarte, J. P.; Choi, Y. K. A Polydimethylsiloxane (PDMS) Sponge for the Selective Absorption of Oil from Water. *ACS Appl. Mater. Interfaces* **2011**, *3* (12), 4552–4556.

(318) Long, R. Q.; Yang, R. T. Carbon Nanotubes as Superior Sorbent for Dioxin Removal [1]. *J. Am. Chem. Soc.* **2001**, *123* (9), 2058–2059.

(319) Yu, C.; Yu, C.; Cui, L.; Song, Z.; Zhao, X.; Ma, Y.; Jiang, L. Facile Preparation of the Porous PDMS Oil-Absorbent for Oil/Water Separation. *Adv. Mater. Interfaces* **2017**, 4, 1600862.

(320) Ren, X.; Lu, H.; Zhou, J. G.; Chong, P. L. G.; Yuan, W.; Noh, M. Porous Polydimethylsiloxane as a Gas-Liquid Interface for Microfluidic Applications. *J. Microelectromechanical Syst.* **2017**, *26* (1), 120–126.

(321) Zhang, A.; Chen, M.; Du, C.; Guo, H.; Bai, H.; Li, L. Poly(Dimethylsiloxane) Oil Absorbent with a Three-Dimensionally Interconnected Porous Structure and Swellable Skeleton. *ACS Appl. Mater. Interfaces* **2013**, *5* (20), 10201–10206.

(322) Zhao, X.; Li, L.; Li, B.; Zhang, J.; Wang, A. Durable Superhydrophobic/Superoleophilic PDMS Sponges and Their Applications in Selective Oil Absorption and in Plugging Oil Leakages. *J. Mater. Chem. A* **2014**, *2* (43), 18281–18287.

(323) Wu, S.; Zhang, J.; Ladani, R. B.; Ravindran, A. R.; Mouritz, A. P.; Kinloch, A. J.; Wang, C. H. Novel Electrically Conductive Porous PDMS/Carbon Nanofiber Composites for Deformable Strain Sensors and Conductors. *ACS Appl. Mater. Interfaces* **2017**, *9* (16), 14207–14215.

(324) Tran, D. N. H.; Kabiri, S.; Sim, T. R.; Losic, D. Selective Adsorption of Oil-Water Mixtures Using Polydimethylsiloxane (PDMS)-Graphene Sponges. *Environ. Sci. Water Res. Technol.* **2015**, *1* (3), 298–305.

(325) Patel, J. N.; Kaminska, B.; Gray, B. L.; Gates, B. D. A Sacrificial SU-8 Mask for Direct Metallization on PDMS. *J. Micromechanics Microengineering* **2009**, *19* (11), 115014. https://doi.org/10.1088/0960-1317/19/11/115014.

(326) Gupta, R. Fabrication of Stretchable Compliant Electrodes on PDMS with Au Nanoparticles. *Bull. Mater. Sci.* **2018**, *41* (5), 114.

(327) Liu, J.; Mahony, J. B.; Selvaganapathy, P. R. Low-Cost and Versatile Integration of Microwire Electrodes and Optical Waveguides into Silicone Elastomeric Devices Using Modi Fi Ed Xurographic Methods. *Nat. Publ. Gr.* **2017**, No. 3**,** 17040, 1–7.

(328) Chen, C. J.; Lai, C. C.; Tseng, M. C.; Liu, Y. C.; Liu, Y. H.; Chiou, L. W.; Tsai, F. J. A Novel Titanium Dioxide-Polydimethylsiloxane Plate for Phosphopeptide Enrichment and Mass Spectrometry Analysis. *Anal. Chim. Acta* **2014**, *812*, 105–113.

(329) Xiao, Y.; Friis, E. A.; Gehrke, S. H.; Detamore, M. S. Mechanical Testing of Hydrogels in Cartilage Tissue Engineering: Beyond the Compressive Modulus. *Tissue Eng. Part B Rev.* **2013**, *19* (5), 403–412.

(330) Szymczak-1975-Electrical-conductivity-of-aqueous-.pdf.

(331) Weigel, M.; Lu, T.; Bailly, G.; Oulasvirta, A.; Majidi, C.; Steimle, J. ISkin: Flexible, Stretchable and Visually Customizable On-Body Touch Sensors for Mobile Computing. *Proc. 33rd Annu. ACM Conf. Hum. Factors Comput. Syst. - CHI '15* **2015**, 2991–3000.

(332) Xu, Y.; Guan, J. Biomaterial Property-Controlled Stem Cell Fates for Cardiac Regeneration. *Bioact. Mater.* **2016**, *1* (1), 18–28.

(333) McKeen, L. W. 7 - Polyolefins and Acrylics. In *The Effect of Creep and Other Time Related Factors on Plastics and Elastomers (Third Edition)*; McKeen, L. W., Ed.; Plastics Design Library; William Andrew Publishing: Boston, **2015**; pp 321–353.

(334) Park, J.; Choi, S.; Janardhan, A. H.; Lee, S. Y.; Raut, S.; Soares, J.; Shin, K.; Yang, S.; Lee, C.; Kang, K. W.; et al. Electromechanical Cardioplasty Using a Wrapped Elasto-Conductive Epicardial Mesh. *Sci. Transl. Med.* **2016**, *8* (344), 1–12.

(335) Nohava, J.; Swain, M.; Eberwein, P. Micromechanical Properties of Polyacrylamide Hydrogels Measured by Spherical Nanoindentation. *Key Eng. Mater.* **2014**, *606* (January), 121–124.

(336) Yannas, I. V.; Burke, J. F.; Orgill, D. P.; Skrabut, E. M. Wound Tissue Can Utilize a Polymeric Template to Synthesize a Functional Extension of Skin. *Science (80-.).* **1982**, *215* (4529), 174–176.

(337) Peppas, N. A.; Hilt, J. Z.; Khademhosseini, A.; Langer, R. Hydrogels in Biology and Medicine: From Molecular Principles to Bionanotechnology. *Adv. Mater.* **2006**, *18* (11), 1345–1360.

(338) Jeong, J.-W.; McCall, J. G.; Shin, G.; Zhang, Y.; Al-Hasani, R.; Kim, M.; Li, S.; Sim, J. Y.; Jang, K.-I.; Shi, Y.; et al. Wireless Optofluidic Systems for Programmable In Vivo Pharmacology and Optogenetics. *Cell* **2015**, *162* (3), 662–674.

(339) Park, S. Il; Brenner, D. S.; Shin, G.; Morgan, C. D.; Copits, B. A.; Chung, H. U.; Pullen, M. Y.; Noh, K. N.; Davidson, S.; Oh, S. J.; et al. Soft, Stretchable, Fully Implantable Miniaturized Optoelectronic Systems for Wireless Optogenetics. *Nat. Biotechnol.* **2015**, *33*, 1280.

(340) Whitesides, G. M. The Origins and the Future of Microfluidics George M. Whitesides1 The. *Nature* **2006**, *442*, 368–373.

(341) Brakke, K.; Keller, N. P.; Casavant, B. P.; Montanez-Sauri, S. I.; Bischel, L. L.; Hedman, C. J.; Bushman, W.; Theberge, A. B.; Beebe, D. J.; Berthier, J.; et al. Suspended Microfluidics. *Proc. Natl. Acad. Sci.* **2013**, *110* (25), 10111–10116.

(342) Dong, L.; Agarwal, A. K.; Beebe, D. J.; Jiang, H. Adaptive Liquid Microlenses Activated by Stimuli-Responsive Hydrogels. *Nature* **2006**, *442* (7102), 551–554.

(343) Choi, M.; Choi, J. W.; Kim, S.; Nizamoglu, S.; Hahn, S. K.; Yun, S. H. Light-Guiding Hydrogels for Cell-Based Sensing and Optogenetic Synthesis in Vivo. *Nat. Photonics* **2013**, *7* (12), 987–994.

(344) Choi, M.; Humar, M.; Kim, S.; Yun, S. H. Step-Index Optical Fiber Made of Biocompatible Hydrogels. *Adv. Mater.* **2015**, *27* (27), 4081–4086.

(345) Kim, D.-H.; Ahn, J.-H.; Choi, W. M.; Kim, H.-S.; Kim, T.-H.; Song, J.; Huang, Y. Y.; Liu, Z.; Lu, C.; Rogers, J. A. Stretchable and Foldable Silicon Integrated Circuits. *Science (80-.).* **2008**, *320* (5875), 507 LP-511.

(346) Xu, S.; Zhang, Y.; Jia, L.; Mathewson, K. E.; Jang, K.-I.; Kim, J.; Fu, H.; Huang, X.; Chava, P.; Wang, R.; et al. Soft Microfluidic Assemblies of Sensors, Circuits, and Radios for the Skin. *Science* **2014**, *344* (6179), 70–74.

(347) Mammerickx, J.; Fox, P. J.; Alexander, R. T.; Pockalny, R.; Gente, P.; Shah, A.; Cochran, J. R. Re s Ear Ch | r e p o r t S. **2015**, *350* (6258).

(348) Shepherd, R. F.; Ilievski, F.; Choi, W.; Morin, S. A.; Stokes, A. A.; Mazzeo, A. D.; Chen, X.; Wang, M.; Whitesides, G. M. Multigait Soft Robot. *Proc. Natl. Acad. Sci.* **2011**.

(349) Morin, S. A.; Shepherd, R. F.; Kwok, S. W.; Stokes, A. A.; Nemiroski, A.; Whitesides, G. M. Camouflage and Display for Soft Machines. *Science (80-.).* **2012**, *337* (6096), 828 LP-832.

(350) Yang, C. H.; Chen, B.; Lu, J. J.; Yang, J. H.; Zhou, J.; Chen, Y. M.; Suo, Z. Ionic Cable. *Extrem. Mech. Lett.* **2015**, *3*, 59–65.

(351) Lin, S.; Yuk, H.; Zhang, T.; Parada, G. A.; Koo, H.; Yu, C.; Zhao, X. Stretchable Hydrogel Electronics and Devices. *Adv. Mater.* **2016**, *28* (22), 4497–4505.

(352) Casares, L.; Vincent, R.; Zalvidea, D.; Campillo, N.; Navajas, D.; Arroyo, M.; Trepat, X. Hydraulic Fracture during Epithelial Stretching. *Nat. Mater.* **2015**, *14* (3), 343–351.

(353) Tian, K.; Bae, J.; Bakarich, S. E.; Yang, C.; Gately, R. D.; Spinks, G. M.; in het Panhuis, M.; Suo, Z.; Vlassak, J. J. 3D Printing of Transparent and Conductive Heterogeneous Hydrogel–Elastomer Systems. *Adv. Mater.* **2017**, *29* (10), 1–8.

(354) Odent, J.; Wallin, T. J.; Pan, W.; Kruemplestaedter, K.; Shepherd, R. F.; Giannelis, E. P. Highly Elastic, Transparent, and Conductive 3D-Printed Ionic Composite Hydrogels. *Adv. Funct. Mater.* **2017**, *27* (33), 1–10.

(355) Wang, J.; Cai, G.; Li, S.; Gao, D.; Xiong, J.; Lee, P. S. Printable Superelastic Conductors with Extreme Stretchability and Robust Cycling Endurance Enabled by Liquid-Metal Particles. *Adv. Mater.* **2018**, *30* (16), 24–26.

(356) Dendukuri, D.; Panda, P.; Kim, J. M.; Hatton, T. A.; Doyle, P. S.; Haghgooie, R. Modeling of Oxygen-Inhibited Free Radical Photopolymerization in a PDMS Microfluidic Device Modeling of Oxygen-Inhibited Free Radical Photopolymerization in a PDMS Microfluidic Device. *Macromolecules* **2008**, *41*, 8547–8556.

(357) Zhou, J.; Ellis, A. V.; Voelcker, N. H. Recent Developments in PDMS Surface Modification for Microfluidic Devices. *Electrophoresis* **2010**, *31* (1), 2–16.

(358) Yuk, H.; Zhang, T.; Parada, G. A.; Liu, X.; Zhao, X. Skin-Inspired Hydrogel-Elastomer Hybrids with Robust Interfaces and Functional Microstructures. *Nat. Commun.* **2016**, *7* (May), 1–11.

(359) Zhao, X. Multi-Scale Multi-Mechanism Design of Tough Hydrogels: Building Dissipation into Stretchy Networks. *Soft Matter* **2014**, *10* (5), 672–687.

(360) Hong, S.; Sycks, D.; Chan, H. F. ai; Lin, S.; Lopez, G. P.; Guilak, F.; Leong, K. W.; Zhao, X. 3D Printing: 3D Printing of Highly Stretchable and Tough Hydrogels into Complex, Cellularized Structures. *Adv. Mater.* **2015**, *27* (27), 4034.

(361) Kocen, R.; Gasik, M.; Gantar, A.; Novak, S. Viscoelastic Behaviour of Hydrogel-Based Composites for Tissue Engineering under Mechanical Load. *Biomed. Mater.* **2017**, *12* (2), 025004.

(362) Ahearne, M.; Yang, Y.; El Haj, A. J.; Then, K. Y.; Liu, K. K. Characterizing the Viscoelastic Properties of Thin Hydrogel-Based Constructs for Tissue Engineering Applications. *J. R. Soc. Interface* **2005**, *2* (5), 455–463.

(363) Orthner, M. P.; Buetefisch, S.; Magda, J.; Rieth, L. W.; Solzbacher, F.. Development, Fabrication, and Characterization of Hydrogel Based Piezoresistive Pressure Sensors with Perforated Diaphragms. *Sensors and Actuators A: Physical* **2010**, *161* (1-2), 29–38.

(364) Erfkamp, J.; Guenther, M.; Gerlach, G.. Piezoresistive Hydrogel-based Sensors for the Detection of Ammonia. *Sensors* **2019**, *19* (4), 971.

(365) Trinh, Q.-T.; Guenther, M.; Sorber, J.; Gerlach, G.. Hydrogel-based Piezoresistive Ph Sensors: Modeling, Simulation and Experimental Verification; 2006; p.

(366) Khalili, N.; Naguib, H. E.; Kwon, R. H.. A Constriction Resistance Model of Conjugated Polymer Based Piezoresistive Sensors for Electronic Skin Applications. *Soft Matter* **2016**, *12* (18), 4180–4189.

(367) Rey, J.; Vandamme, M., On the Shrinkage and Stiffening of a Cellulose Sponge Upon Drying. *Journal of Applied Mechanics* **2013,** *80* (2), 020908-020908-6.

(368) Wu, Z.; Li, Y.; Zhang, L.; Zhong, Y.; Xu, H.; Mao, Z.; Wang, B.; Sui, X. Thiol-Ene Click Reaction on Cellulose Sponge and Its Application for Oil/Water Separation. *RSC Adv.* **2017**, *7* (33), 20147–20151.

(369) Bathias, C.; Pineau, A., Fatigue of materials and structures ; application to design and damage / *edited by Claude Bathias, André Pineau*. London : ISTE ; Hoboken, NJ : Wiley, **2011**.

(370) Huang, H.; Chen, P.; Zhang, X.; Lu, Y.; Zhan, W. Edge-to-Edge Assembled Graphene Oxide Aerogels with Outstanding Mechanical Performance and Superhigh Chemical Activity. *Small* **2013**, *9* (8), 1397–1404.

(371) Yang, X.; Cranston, E. D. Chemically Cross-Linked Cellulose Nanocrystal Aerogels with Shape Recovery and Superabsorbent Properties. *Chem. Mater.* **2014**, *26* (20), 6016–6025.

(372) Pickford, M. *Strain Gauge Technology*; Elsevier Applied Science: London; New York, **2003**; Vol. 9.

(373) http://elektron.pol.lublin.pl/elekp/ap_notes/NI_AN078_Strain_Gauge_Meas.pdf

(374) Bhadani, R.; Mitra Uttam, K. Synthesis and Studies on Water Swelling Behaviour of Polyacrylamide Hydrogels. *Macromolecular Symposia* **2016**, *369* (1), 30-34.

(375) Gupta, N. V.; Shivakumar, H. G. Investigation of Swelling Behavior and Mechanical Properties of a pH-Sensitive Superporous Hydrogel Composite. *Iran. J. Pharm. Res. : IJPR* **2012**, *11* (2), 481-493.

(376) Ullah, F.; Othman, M. B. H.; Javed, F.; Ahmad, Z.; Akil, H. M. Classification, processing and application of hydrogels: A review. *Materials Science and Engineering: C* **2015**, *57*, 414-433

(377) Zhu, C. H.; Li, L. M.; Wang, J. H.; Wu, Y. P.; Liu, Y. Three-Dimensional Highly Conductive Silver Nanowires Sponges Based on Cotton-Templated Porous Structures for Stretchable Conductors. *RSC Adv.* **2017**, *7* (1), 51–57.

(378) Song, Y.; Chen, H.; Su, Z.; Chen, X.; Miao, L.; Zhang, J.; Cheng, X.; Zhang, H. Highly Compressible Integrated Supercapacitor–Piezoresistance-Sensor System with CNT–PDMS Sponge for Health Monitoring. *Small* **2017**, *13* (39), 1–10.

(379) Wang, D.; Shi, J.; Carlson, S. R.; Cregan, P. B.; Ward, R. W.; Diers, B. W. A Low-Cost, High-Throughput Polyacrylamide Gel Electrophoresis System for Genotyping with Microsatellite DNA Markers. *Crop Sci.* **2003**, *43*, 1828–1832.

(380) Sun, J.-Y.; Johnson, C.; Mooney, D. J.; Mehta, M.; Darnell, M. C.; Suo, Z.; Arany, P. R. Performance and Biocompatibility of Extremely Tough Alginate/Polyacrylamide Hydrogels. *Biomaterials* **2013**, *34* (33), 8042–8048.

(381) Lin, S.; Lu, T. K.; Tang, T.-C.; Yuk, H.; Zhao, X.; Tham, E.; Liu, X. Stretchable Living Materials and Devices with Hydrogel–elastomer Hybrids Hosting Programmed Cells. *Proc. Natl. Acad. Sci.* **2017**, *114* (9), 2200–2205.

(382) Stevens, L.; Calvert, P.; Wallace, G. G.; Panhuis, M. in Het. Ionic-Covalent Entanglement Hydrogels from Gellan Gum, Carrageenan and an Epoxy-Amine. *Soft Matter* **2013**, 9, 3009.

(383) De Silva, D. A.; Martens, P. J.; Gilmore, K. J.; Panhuis, M. In Het. Degradation Behavior of Ionic-Covalent Entanglement Hydrogels. *J. Appl. Polym. Sci.* **2014**, *132* (1), 1–10.

(384) Warren, H.; In Het Panhuis, M. Highly Conducting Composite Hydrogels from Gellan Gum, PEDOT:PSS and Carbon Nanofibres. *Synth. Met.* **2015**, *206*, 61–65.

(385) Kim, H. J.; Sim, K.; Thukral, A.; Yu, C. Rubbery Electronics and Sensors from Intrinsically Stretchable Elastomeric Composites of Semiconductors and Conductors. *Sci. Adv.* **2017**, *3* (9), 1–9.

(386) Andersen, N. Y. Force and Strain Sensing Techniques. In *Instrumentation Systems*; Durbin, E. J. B. T.-I. S. (Second E., Ed.; Pergamon, **2014**; p 1–IIA7:33.

(387) https://www.aldi.com.au/en/special-buys/special-buys-sat-16-march/saturday-detail-wk11/ps/p/cellulose-shaped-sponge-4pk/.

(388) Li, X.; Zhang, R.; Yu, W.; Wang, K.; Wei, J.; Wu, D.; Cao, A.; Li, Z.; Cheng, Y.; Zheng, Q.; et al. Stretchable and Highly Sensitive Graphene-on-Polymer Strain Sensors. *Sci. Rep.* **2012**, *2*, 1–6.

(389) Wu, S.; Peng, S.; Wang, C. H. Sensors and Actuators A : Physical Stretchable Strain Sensors Based on PDMS Composites with Cellulose Sponges Containing One- and Two-Dimensional Nanocarbons. *Sensors Actuators A. Phys.* **2018**, *279*, 90–100.

(390) Berger, A.; Segalman, R. A.; Newman, J. Material Requirements for Membrane Separators in a Water-Splitting Photoelectrochemical Cell. *Energy Environ. Sci.* **2014**, *7* (4), 1468–1476.

(391) Walczak, K.; Chen, Y.; Karp, C.; Beeman, J. W.; Shaner, M.; Spurgeon, J.; Sharp, I. D.; Amashukeli, X.; West, W.; Jin, J.; et al. Modeling, Simulation, and Fabrication of a Fully Integrated, Acidstable, Scalable Solar-Driven Water-Splitting System. *ChemSusChem* **2015**, *8* (3), 544–551.

(392) Lei, B.; Li, G. R.; Chen, P.; Gao, X. P. A Solar Rechargeable Battery Based on Hydrogen Storage Mechanism in Dual-Phase Electrolyte. *Nano Energy* **2017**, *38* (May), 257–262.

(393) Hernández-Pagán, E. A.; Vargas-Barbosa, N. M.; Wang, T.; Zhao, Y.; Smotkin, E. S.; Mallouk, T. E. Resistance and Polarization Losses in Aqueous Buffer-Membrane Electrolytes for Water-Splitting Photoelectrochemical Cells. *Energy Environ. Sci.* **2012**, *5* (6), 7582–7589.

(394) Nomura, M.; Okuda, H.; Kasahara, S.; Nakao, S. I. Optimization of the Process Parameters of an Electrochemical Cell in the IS Process. *Chem. Eng. Sci.* **2005**, *60* (24), 7160–7167.

(395) Menezes, P. W.; Indra, A.; Levy, O.; Kailasam, K.; Gutkin, V.; Pfrommer, J.; Driess, M. Using nickel manganese oxide catalysts for efficient water oxidation. *Chem.Commun.* **2015**, *51* (24), 5005-5008.

(396) Gong, M.; Zhou, W.; Tsai, M.-C.; Zhou, J.; Guan, M.; Lin, M.-C.; Zhang, B.; Hu, Y.; Wang, D.-Y.; Yang, J.; Pennycook, S. J.; Hwang, B.-J.; Dai, H. Nanoscale nickel oxide/nickel heterostructures for active hydrogen evolution electrocatalysis. *Nature Communications* **2014**, *5*, 4695.

(397) Gennero de Chialvo, M. R.; Chialvo, A. C. Oxygen evolution reaction on thick hydrous nickel oxide electrodes. *Electrochimica Acta* **1988**, *33* (6), 825-830.

Appendix

Appendix 1/ Compressive and rheological optimisation analysis for different ratios of ICE hydrogel

- **Compressive strain stress test figures:**

a. Studying changing the ratio of MBAAm/AAm on ICE network hydrogels

1- 0.5 % (w/v) MBAAm:

AVG work of compression	2.17E+01
AVG compression tan modulus	4.82E+01
AVG stress	9.83E+01
AVG strain	5.16E+01
AVG STDEV stress	9.186557
AVG STDEV strain	7.28538
AVG STDEV work of compression	0.294595
AVG STDEV compression modulus	0.147897

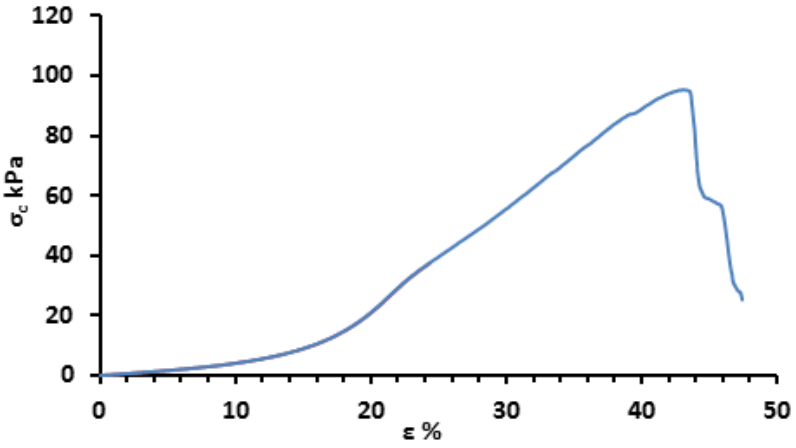

Figure (a1.1) Typical compressive stress versus strain plots of ICE network hydrogels with concentration 0.5 % (w/v) MBAAm.

2- 0.75 % (w/v) MBAAm:

AVG work of compression	1.10E+01
AVG compression tan modulus	5.26E+01
AVG stress	7.83E+01
AVG strain	3.90E+01
AVG STDEV stress	10.52171
AVG STDEV strain	7.28487
AVG STDEV work of compression	0.21421
AVG STDEV compression modulus	0.160602

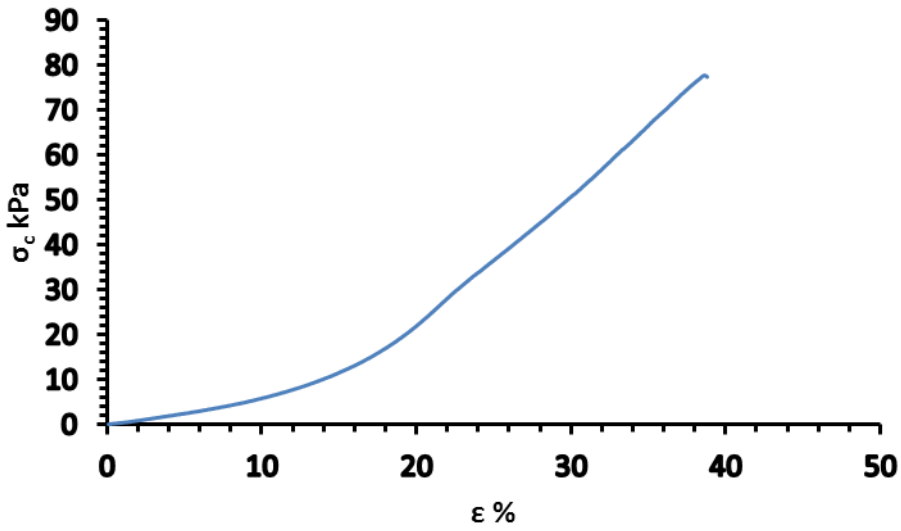

Figure (a1.2) Typical compressive stress versus strain plots of ICE network hydrogels with concentration 0.75 % (w/v) MBAAm.

3- 1 % (w/v) MBAAm:

AVG work of compression	9.29E+00	
AVG compression tan modulus	4.51E+01	
AVG stress	7.96E+01	
AVG strain	4.84E+01	
AVG STDEV stress	7.476639	
AVG STDEV strain	7.211159	
AVG STDEV work of compression		0.171103
AVG STDEV compression modulus		0.191801

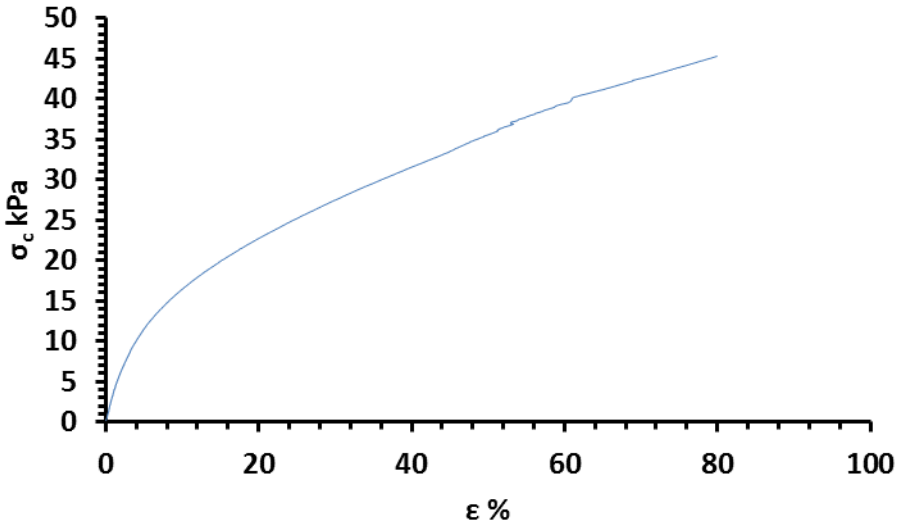

Figure (a1.3) Typical compressive stress versus strain plots of ICE network hydrogels with concentration 1 % (w/v) MBAAm.

4- 2 % (w/v) MBAAm:

AVG work of compression	27.50E+00
AVG compression tan modulus	2.69E+01
AVG stress	1.47E+02
AVG strain	4.83E+01
AVG STDEV stress	11.61607
AVG STDEV strain	6.586697
AVG STDEV work of compression	0.268468
AVG STDEV compression modulus	0.10314

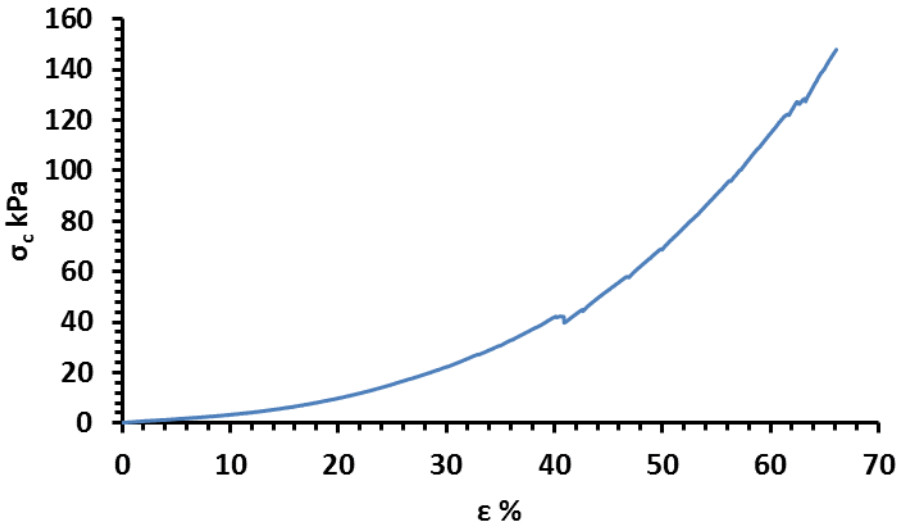

Figure (a1.4) Typical compressive stress versus strain plots of ICE network hydrogels with concentration 2 % (w/v) MBAAm.

5- 2.66 % (w/v) MBAAm:

AVG work of compression	3.30E+01
AVG compression tan modulus	3.79E+01
AVG stress	1.80E+02
AVG strain	5.90E+01
AVG STDEV stress	9.730262
AVG STDEV strain	7.286014
AVG STDEV work of compression	0.439559
AVG STDEV compression modulus	0.351043

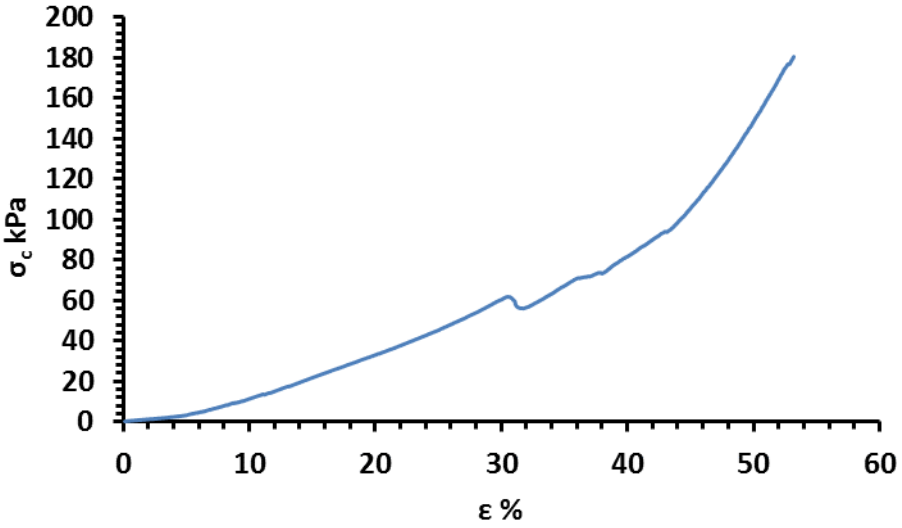

Figure (a1.5) Typical compressive stress versus strain plots of ICE network hydrogels with concentration 2.66 % (w/v) MBAAm.

6- 3 % (w/v) MBAAm:

AVG work of compression	4.68E+01
AVG compression tan Modulus	1.41E+02
AVG stress	2.16E+02
AVG strain	5.52E+01
AVG STDEV stress	12.42473
AVG STDEV strain	7.205444
AVG STDEV work of compression	0.531481
AVG STDEV compression modulus	0.10083

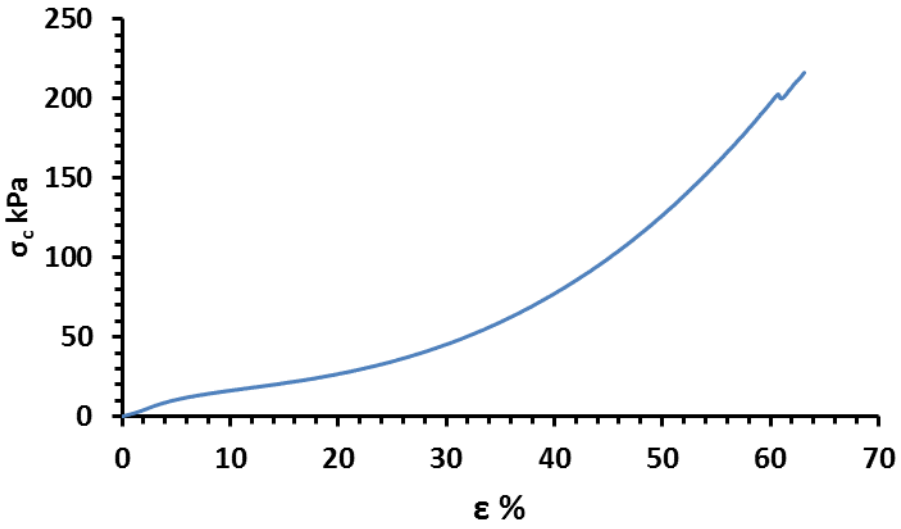

Figure (a1.6) Typical compressive stress versus strain plots of ICE network hydrogels with concentration 3 % (w/v) MBAAm.

7- 3.108 % (w/v) MBAAm:

AVG work of compression	3.38E+01
AVG compression tan Modulus	2.56E+01
AVG stress	1.61E+02
AVG strain	6.28E+01
AVG STDEV stress	8.92535
AVG STDEV strain	7.286039
AVG STDEV work of compression	0.436206
AVG STDEV compression modulus	0.164587

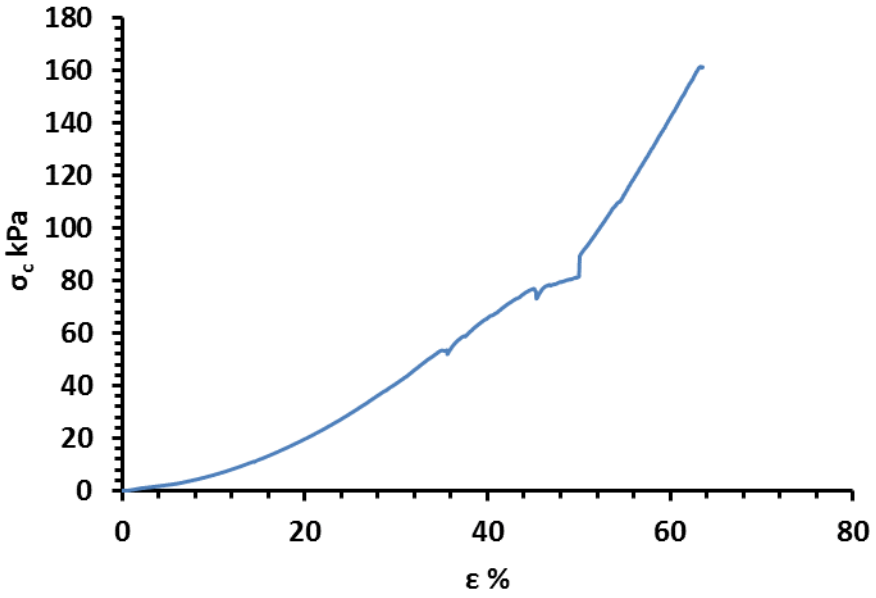

Figure (a1.7) Typical compressive stress versus strain plots of ICE network hydrogels with concentration 3.108 % (w/v) MBAAm.

8- 4 % (w/v) MBAAm:

AVG work of compression	6.99E+00
AVG compression tan Modulus	3.06E+01
AVG stress	6.16E+01
AVG strain	3.51E+01
AVG STDEV stress	11.75465
AVG STDEV strain	6.613889
AVG STDEV work of compression	0.164272
AVG STDEV compression modulus	0.224048

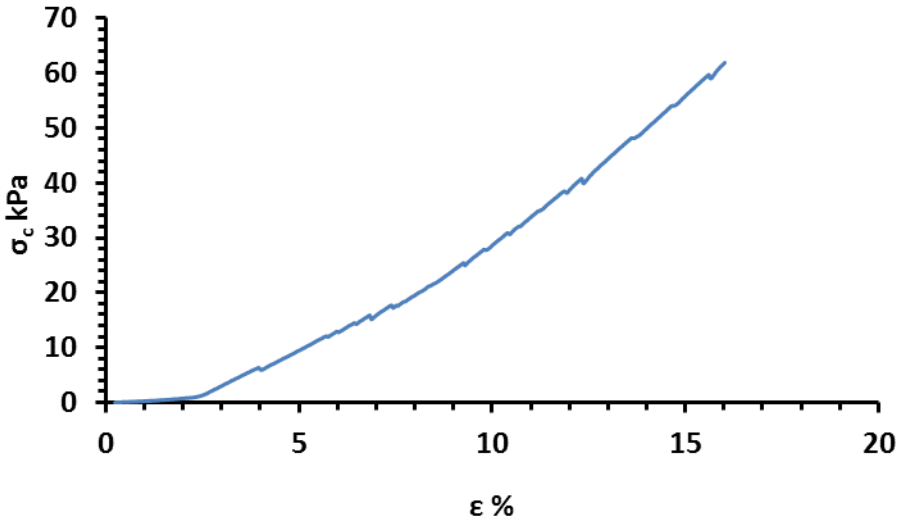

Figure (a1.8) Typical compressive stress versus strain plots of ICE network hydrogels with concentration 4 % (w/v) MBAAm.

9- 5 % (w/v) MBAAm:

AVG work of compression	4.03E+00
AVG compression tan modulus	1.62E+01
AVG stress	5.13E+01
AVG strain	2.05E+01
AVG STDEV stress	7.656113832
AVG STDEV strain	5.827421743
AVG STDEV work of compression	0.138429022
AVG STDEV compression modulus	0.266135578

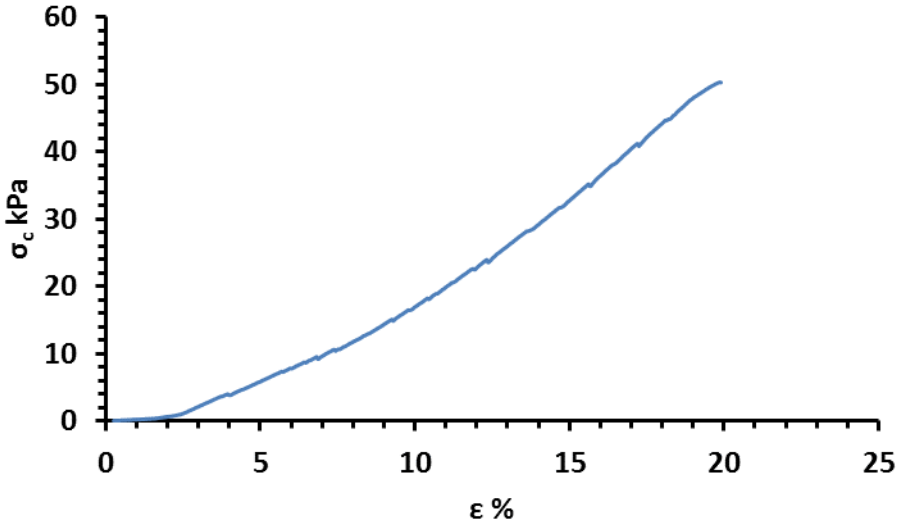

Figure (a1.9) Typical compressive stress versus strain plots of ICE network hydrogels with concentration 5 % (w/v) MBAAm.

b. Studying changing the ratio of Ca^{+2}/ GG on ICE network hydrogels:

1. 0 M $CaCl_2$:

AVG work of compression	9.63E-01
AVG compression tan Modulus	4.04E+01
AVG stress	1.08E+01
AVG strain	2.73E+01
AVG STDEV stress	2.926238
AVG STDEV strain	7.879389
AVG STDEV work of compression	0.062818
AVG STDEV compression modulus	0.058753

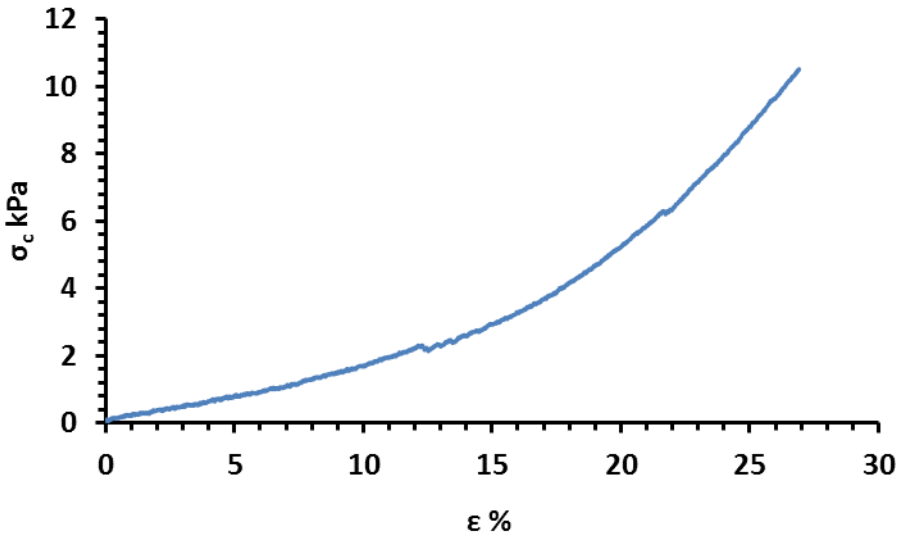

Figure (a1.10) Typical compressive stress versus strain plots of ICE network hydrogels with concentration 0 M $CaCl_2$.

2- 0.01 M $CaCl_2$:

AVG work of compression	2.10E+00
AVG compression tan Modulus	2.83E+01
AVG stress	1.92E+01
AVG strain	4.00E+01
AVG STDEV stress	2.256306
AVG STDEV strain	8.091299
AVG STDEV work of compression	0.07734
AVG STDEV compression modulus	0.072253

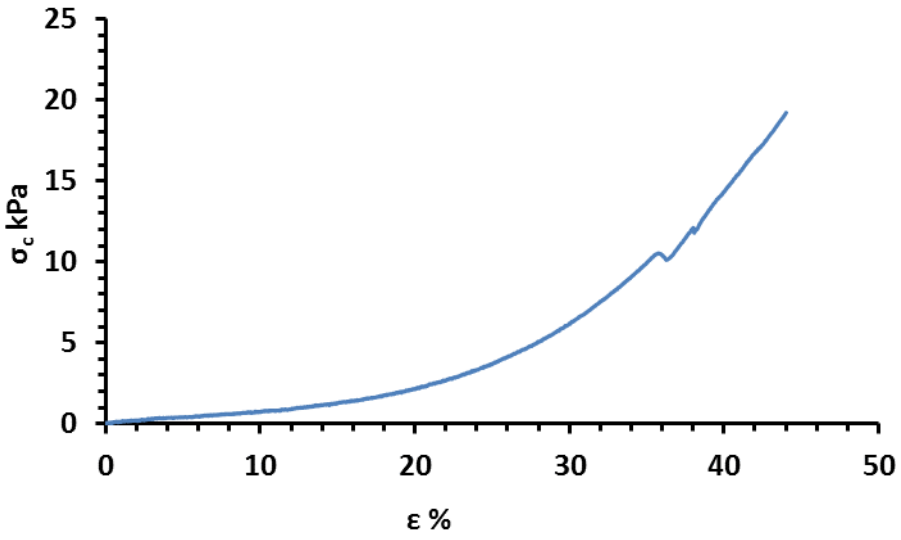

Figure (a1.11) Typical compressive stress versus strain plots of ICE network hydrogels with concentration 0.01 M $CaCl_2$.

3- 0.05 M $CaCl_2$:

AVG work of compression	2.87E+01
AVG compression tan Modulus	8.08E+01
AVG stress	1.16E+02
AVG strain	5.53E+01
AVG STDEV stress	11.63999
AVG STDEV strain	7.202756
AVG STDEV work of compression	0.312574
AVG STDEV compression modulus	0.055208

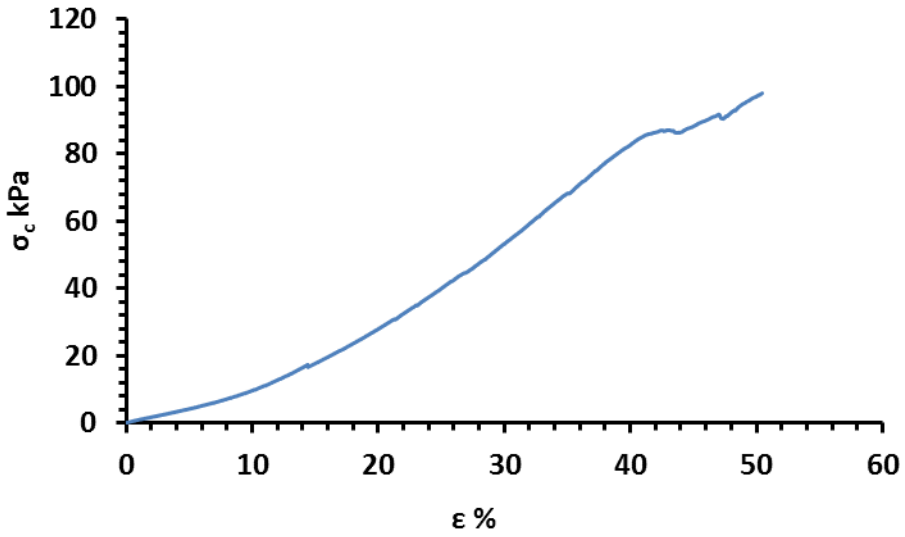

Figure (a1.12) Typical compressive stress versus strain plots of ICE network hydrogels with concentration 0.05 M $CaCl_2$.

4- 0.075 M $CaCl_2$:

AVG work of compression	3.86E+01
AVG compression tan Modulus	5.80E+01
AVG stress	9.97E+01
AVG strain	5.67E+01
AVG STDEV stress	8.640209
AVG STDEV strain	7.203665
AVG STDEV work of compression	3.86E+01
AVG STDEV compression modulus	8.367694
AVG work of compression	0.062489

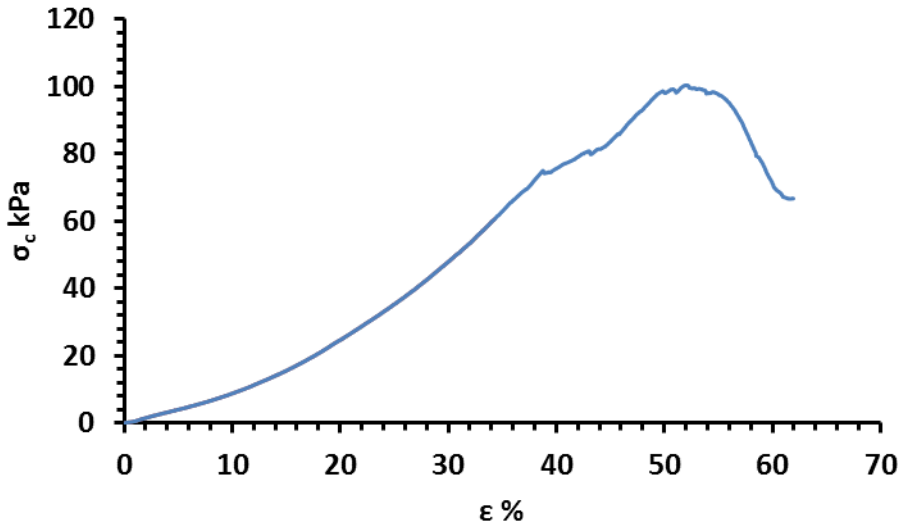

Figure (a1.13) Typical compressive stress versus strain plots of ICE network hydrogels with concentration 0.075 M $CaCl_2$.

5- 0.1 M $CaCl_2$:

AVG work of compression	4.68E+01
AVG compression tan Modulus	1.41E+02
AVG stress	2.16E+02
AVG strain	5.52E+01
AVG STDEV stress	12.42473
AVG STDEV strain	7.205444
AVG STDEV work of compression	0.531481
AVG STDEV compression modulus	0.10083

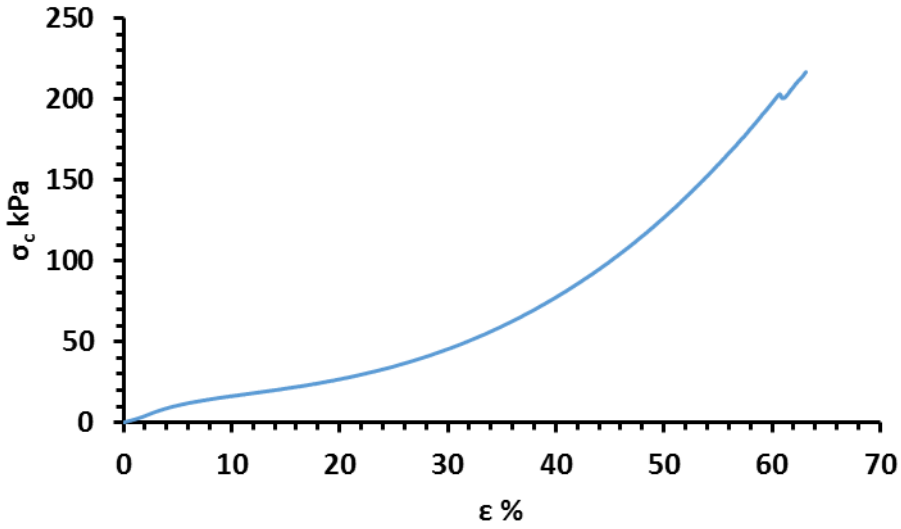

Figure (a1.14) Typical compressive stress versus strain plots of ICE network hydrogels with concentration 0.1 M $CaCl_2$.

6- 0.25 M $CaCl_2$:

AVG work of compression	3.51E+01
AVG compression tan Modulus	5.65E+01
AVG stress	8.61E+01
AVG strain	5.15E+01
AVG STDEV stress	9.929403
AVG STDEV strain	7.204635
AVG STDEV work of compression	3.5867
AVG STDEV compression modulus	0.085565

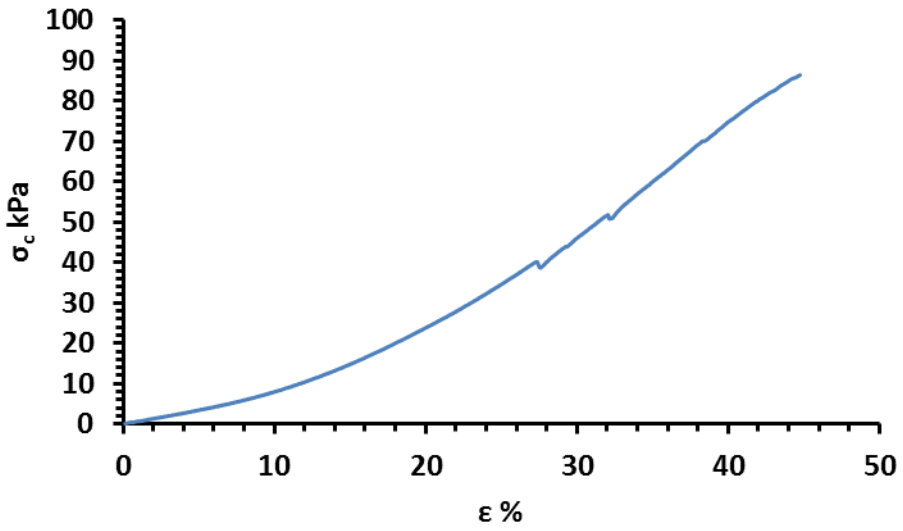

Figure (a1.15) Typical compressive stress versus strain plots of ICE network hydrogels with concentration 0.25 M $CaCl_2$.

7- 0.5 M $CaCl_2$:

AVG work of compression	7.31E+00
AVG compression tan Modulus	2.79E+01
AVG stress	5.26E+01
AVG strain	4.26E+01
AVG STDEV stress	6.154976
AVG STDEV strain	7.205483
AVG STDEV work of compression	0.135254
AVG STDEV compression modulus	0.402609

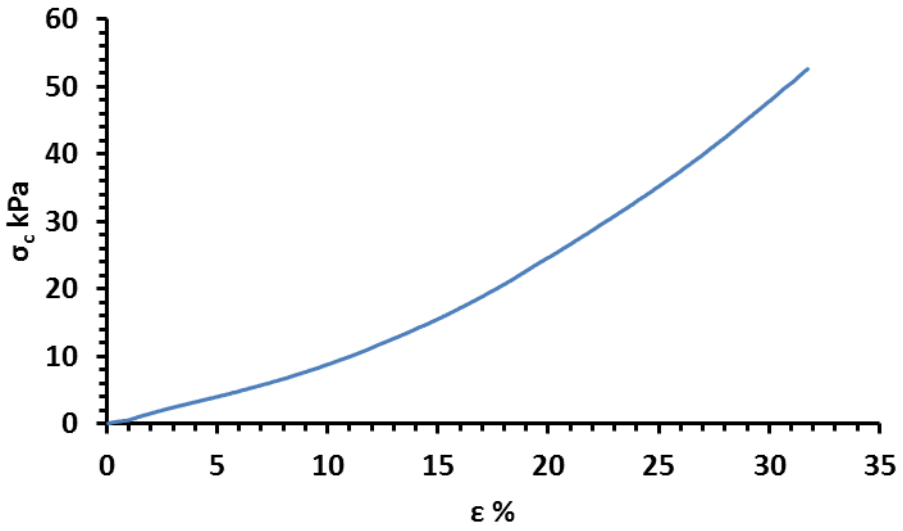

Figure (a1.16) Typical compressive stress versus strain plots of ICE network hydrogels with concentration 0.5 M $CaCl_2$.

8- 0.7 M $CaCl_2$:

AVG work of compression	5.60E+01
AVG compression tan Modulus	6.87E+00
AVG stress	5.11E+01
AVG strain	3.06E+01
AVG STDEV stress	13.29197
AVG STDEV strain	7.284484
AVG STDEV work of compression	0.146713
AVG STDEV compression modulus	0.096353

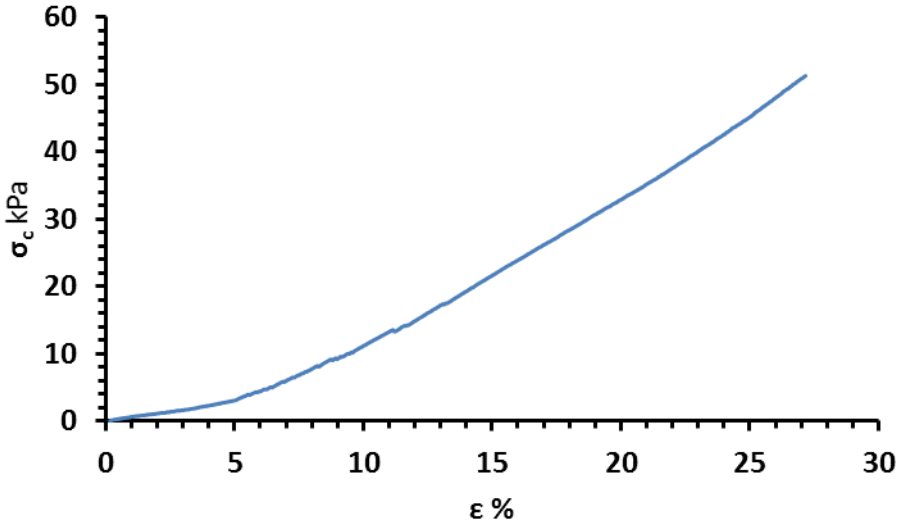

Figure (a1.17) Typical compressive stress versus strain plots of ICE network hydrogels with concentration 0.7 M $CaCl_2$

9. 1 M CaCl2:

AVG work of compression	8.45E+00
AVG compression tan Modulus	8.74E+01
AVG stress	4.67E+01
AVG strain	3.44E+01
AVG STDEV stress	13.303
AVG STDEV strain	7.206274
AVG STDEV work of compression	0.140799
AVG STDEV compression modulus	0.114988

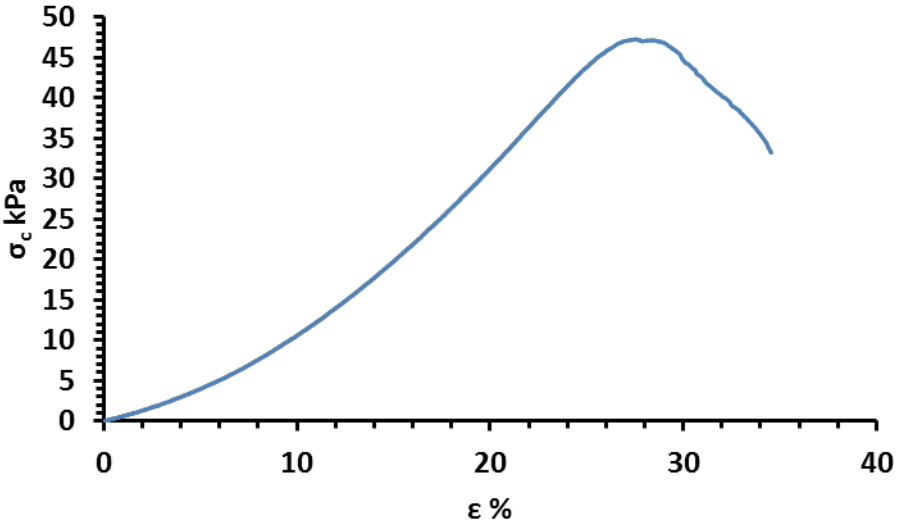

Figure (a1.18) Typical compressive stress versus strain plots of ICE network hydrogels with concentration 1 M $CaCl_2$

c. Studying the effect of changing the ratio of AAm/ GG on ICE network hydrogels:

1- 3.774 GG+1.776 AAm:

AVG work of compression	6.05E+00
AVG compression tan Modulus	1.89E+01
AVG stress	5.61E+01
AVG strain	3.58E+01
AVG STDEV stress	6.942643
AVG STDEV strain	7.206105
AVG STDEV work of compression	0.118725
AVG STDEV compression modulus	0.175424

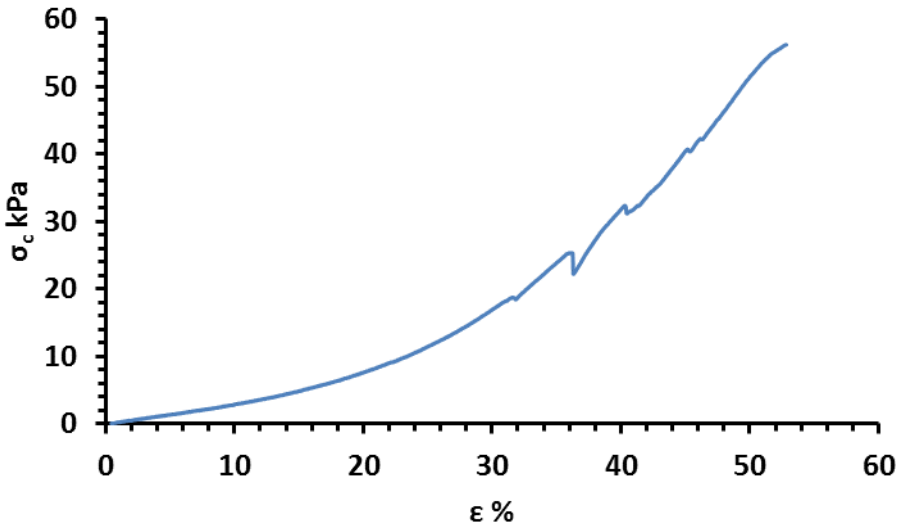

Figure (a1.19) Compressive mechanical stress at failure of different ratios from GG and AAm ICE network hydrogels.

2- 3.4 GG+ 2.15 AAm:

AVG work of compression	1.07E+01
AVG compression tan Modulus	2.90E+01
AVG stress	8.24E+01
AVG strain	3.53E+01
AVG STDEV stress	6.510988
AVG STDEV strain	10.78112
AVG STDEV work of compression	0.450561
AVG STDEV compression modulus	0.179898

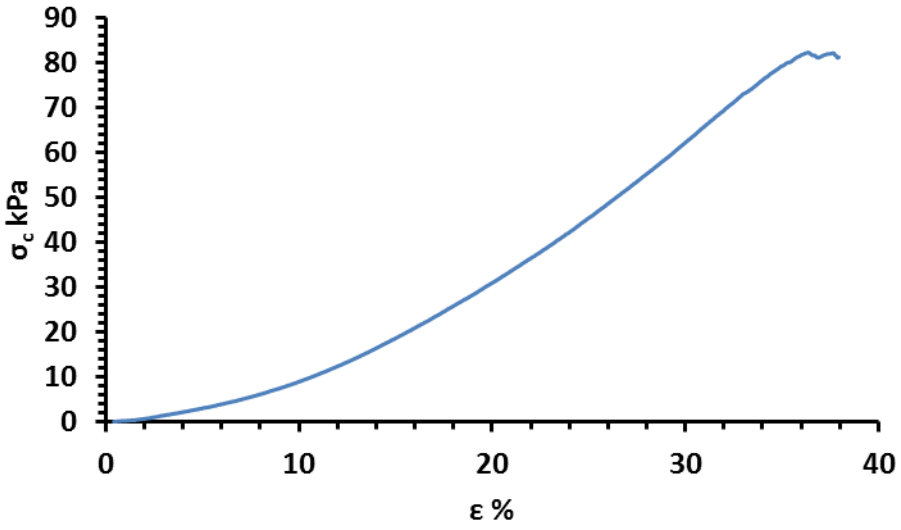

Figure (a1.20) Compressive mechanical stress at failure of different ratios from GG and AAm ICE network hydrogels.

3- 1.998 GG+3.552 AAm:

AVG work of compression	1.81E+01
AVG compression tan Modulus	9.75E+01
AVG stress	1.86E+02
AVG strain	5.15E+01
AVG STDEV stress	11.33701
AVG STDEV strain	7.285247
AVG STDEV work of compression	0.263185
AVG STDEV compression modulus	0.110271

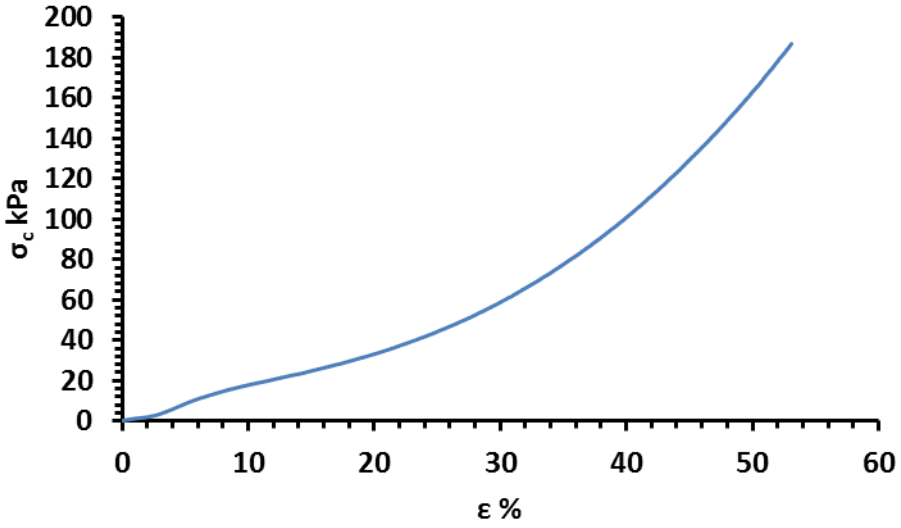

Figure (a1.21) Compressive mechanical stress at failure of different ratios from GG and AAm ICE network hydrogels.

4- 1.11 GG+4.44 AAm:

AVG work of compression	4.68E+01
AVG compression tan Modulus	1.41E+02
AVG stress	2.16E+02
AVG strain	5.52E+01
AVG STDEV stress	12.42473
AVG STDEV strain	7.205444
AVG STDEV work of compression	0.531481
AVG STDEV compression modulus	0.10083

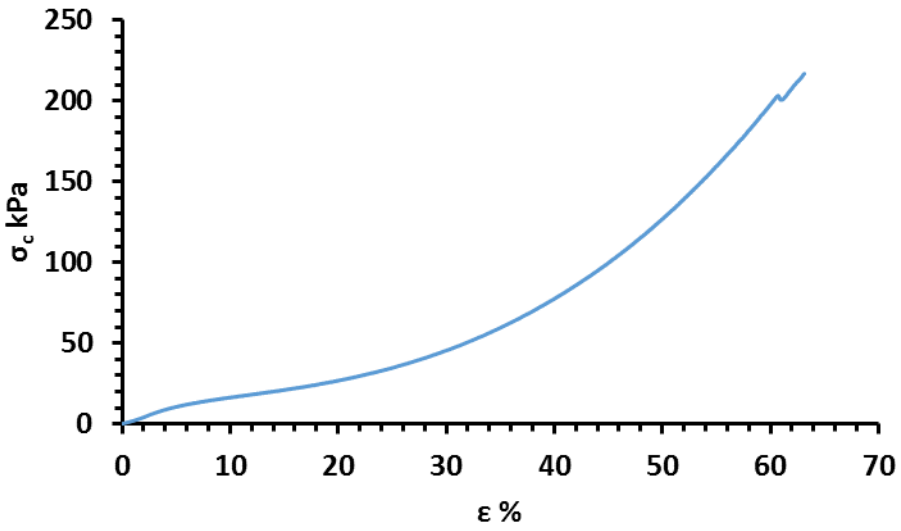

Figure (a1.22) Compressive mechanical stress at failure of different ratios from GG and AAm ICE network hydrogels.

5- 0.88 GG+ 4.66 AAm:

AVG work of compression	2.30E+01
AVG compression tan Modulus	9.35E+00
AVG stress	1.61E+02
AVG strain	9.84E+01
AVG STDEV stress	0.403814
AVG STDEV strain	7.285294
AVG STDEV work of compression	0.657784
AVG STDEV compression modulus	0.299219

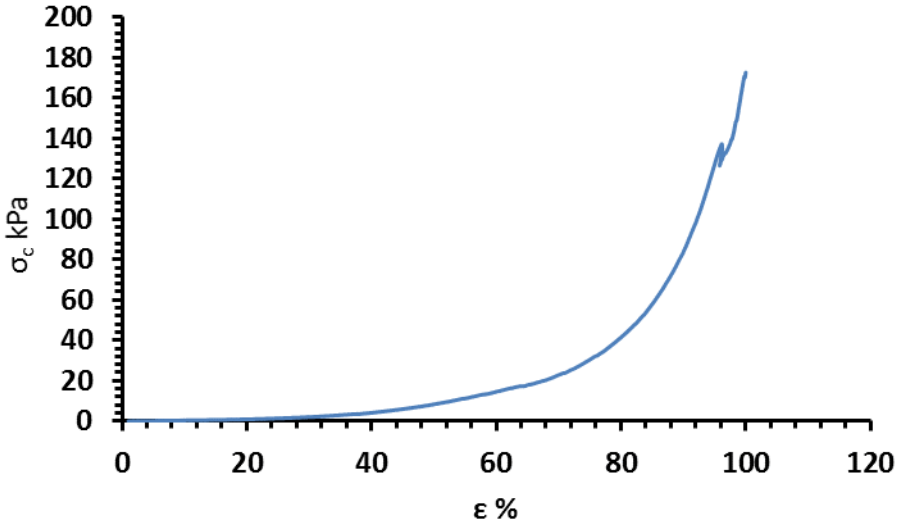

Figure (a1.23) Compressive mechanical stress at failure of different ratios from GG and AAm ICE network hydrogels.

6- 0.66 GG+ 4.89 AAm:

AVG work of compression	1.05E+01
AVG compression tan modulus	1.85E+01
AVG stress	9.59E+01
AVG strain	4.46E+01
AVG STDEV stress	6.955433568
AVG STDEV strain	7.206127455
AVG STDEV work of compression	0.268635197
AVG STDEV compression modulus	8.337898403

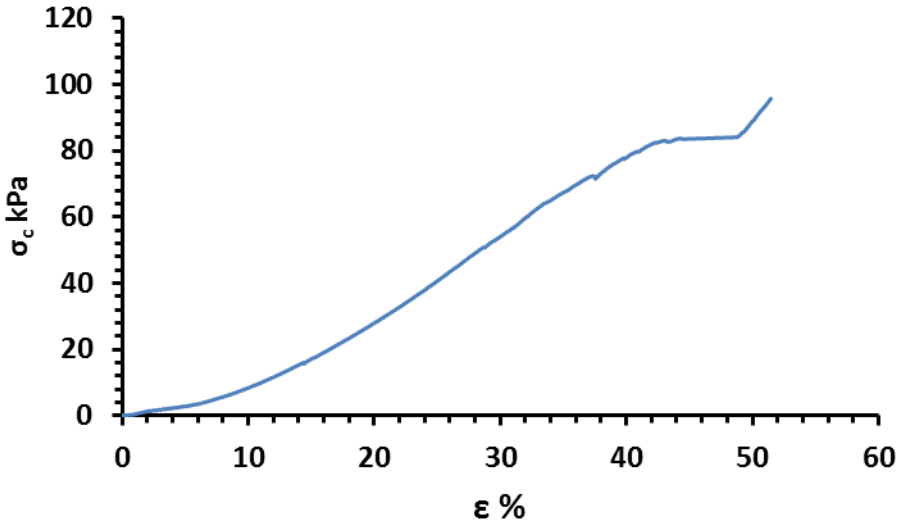

Figure (a1.24) Compressive mechanical stress at failure of different ratios from GG and AAm ICE network hydrogels.

7- 0.44 GG+ 5.11 AAm:

AVG work of compression	1.45E+01
AVG compression tan modulus	4.97E+01
AVG stress	8.38E+01
AVG strain	4.38E+01
AVG STDEV stress	10.69532612
AVG STDEV strain	7.996293074
AVG STDEV work of compression	0.442588287
AVG STDEV compression modulus	0.202527327

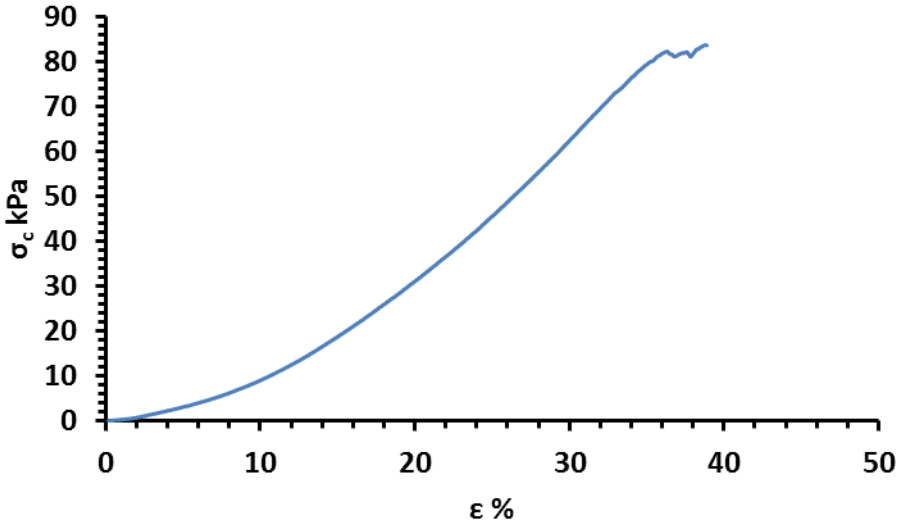

Figure (a1.25) Compressive mechanical stress at failure of different ratios from GG and AAm ICE network hydrogels.

8- 0.33 GG+ 5.22 AAm:

AVG work of compression	1.79E+01
AVG compression tan modulus	2.28E+01
AVG stress	7.37E+01
AVG strain	5.04E+01
AVG STDEV stress	5.862989299
AVG STDEV strain	9.555670316
AVG STDEV work of compression	0.117451392
AVG STDEV compression modulus	0.869610277

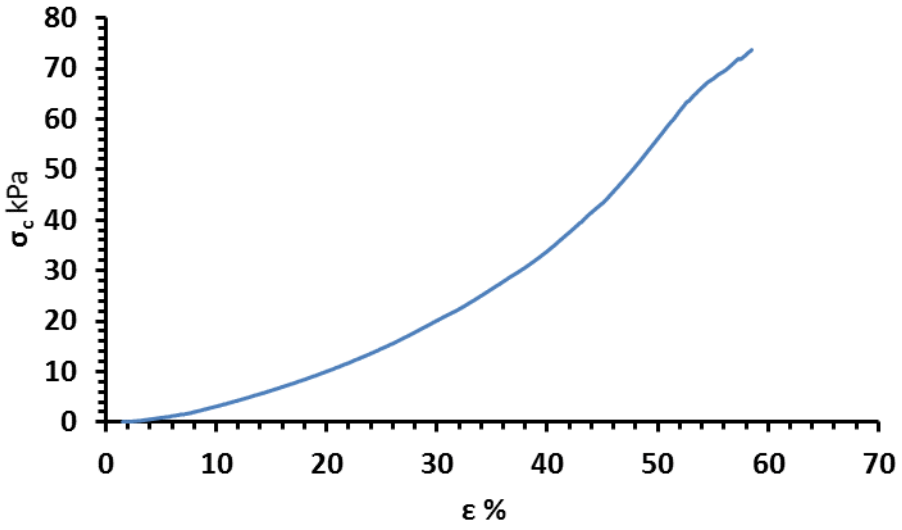

Figure (a1.26) Compressive mechanical stress at failure of different ratios from GG and AAm ICE network hydrogels.

Oscillatory Rheological test figures:

a. Studying changing the ratio of MBAAm/AAm on ICE network hydrogel:

1- 0.5 % (w/v) MBAAm:

Average LVE= 36827.27 Pa

STDEV= 16854.81 Pa

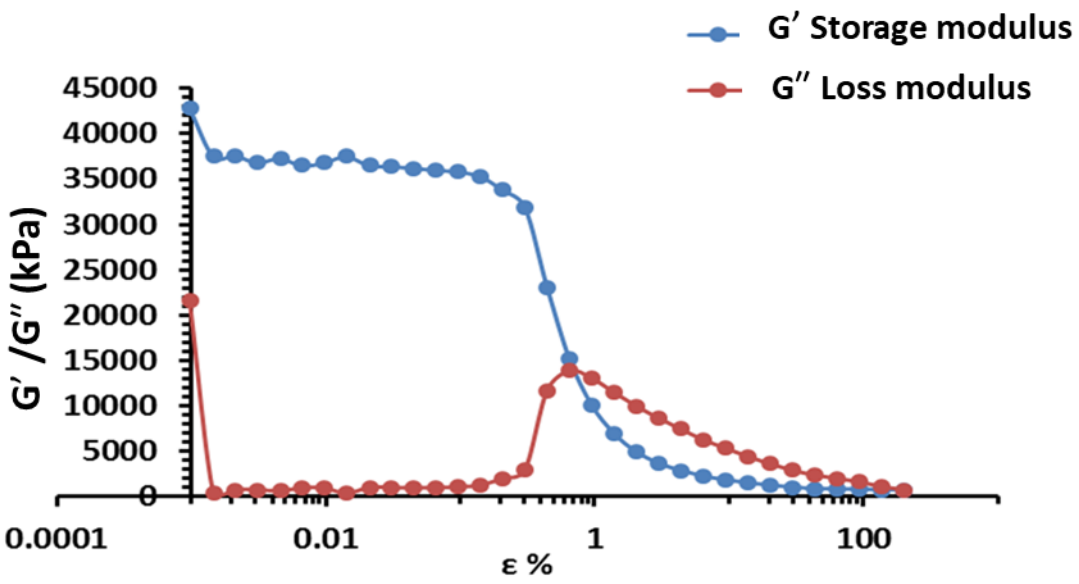

Figure (a1.27) Strain Vs Storage modulus / Loss Modulus of 0.5 % (w/v) MBAAm.

2- 0.75 % (w/v) MBAAm:

Average LVE = 32650 Pa

STDEV= 108.7114613 Pa

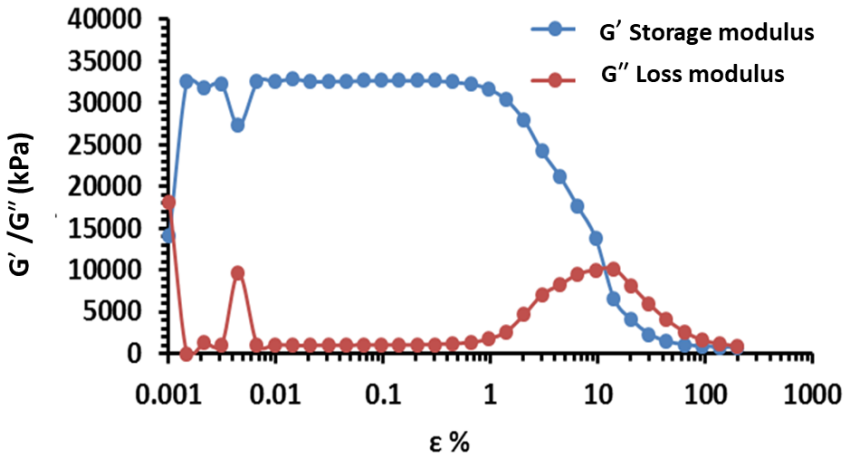

Figure (a1.28) Strain Vs Storage modulus / Loss Modulus of 0.75 % (w/v) MBAAm.

3- 1 % (w/v) MBAAm:

Average LVE = 35144.44444 Pa

STDEV= 328.2952601 Pa

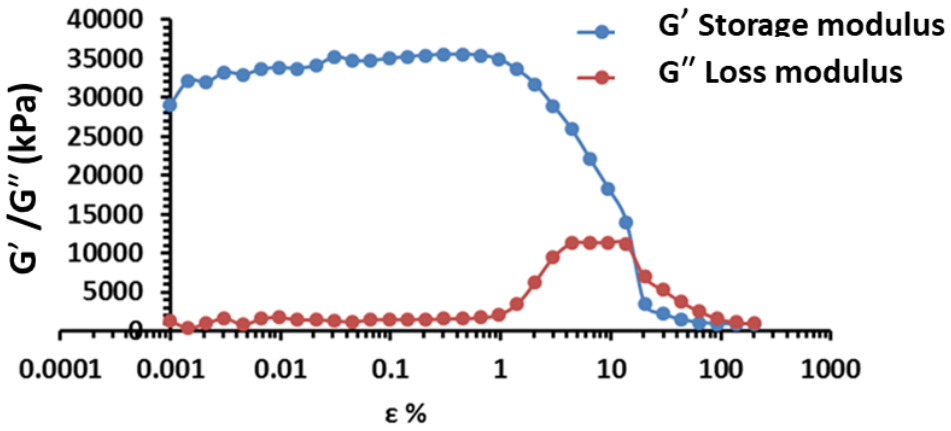

Figure (a1.29) Strain Vs Storage modulus / Loss Modulus of 1 % (w/v) MBAAm.

4- 2 % (w/v) MBAAm:

Average LVE = 3.15E+04 Pa

STDEV= 90.45340337 Pa

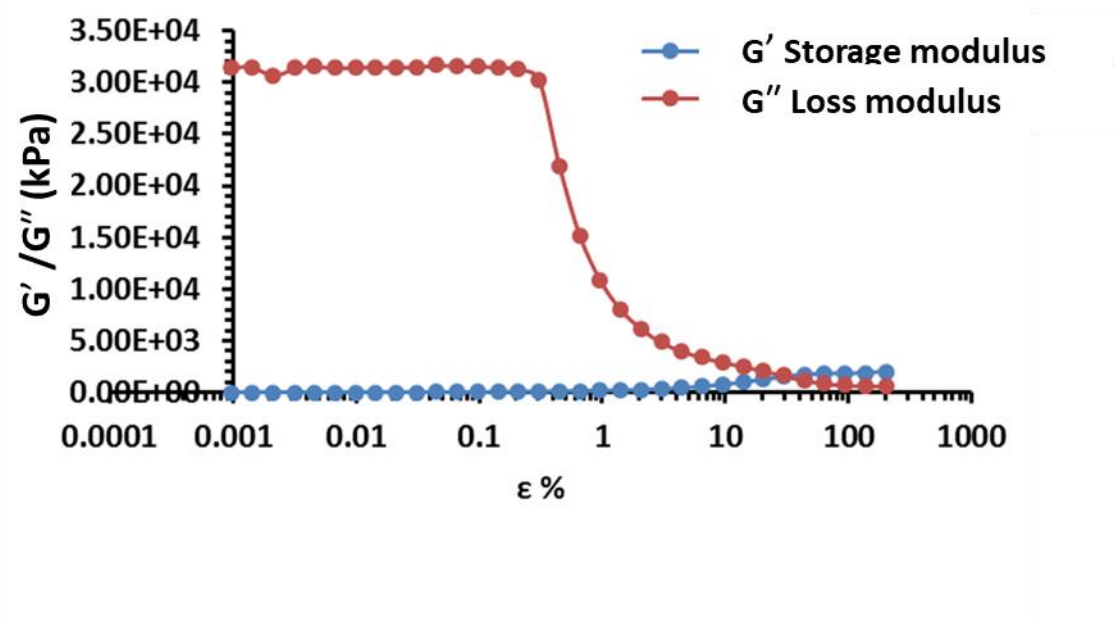

Figure (a1.30) Strain Vs Storage modulus / Loss Modulus of 2 % (w/v) MBAAm.

5- 2.664 % (w/v) MBAAm:

Average LVE = 45400 Pa

STDEV = 209.7617696 Pa

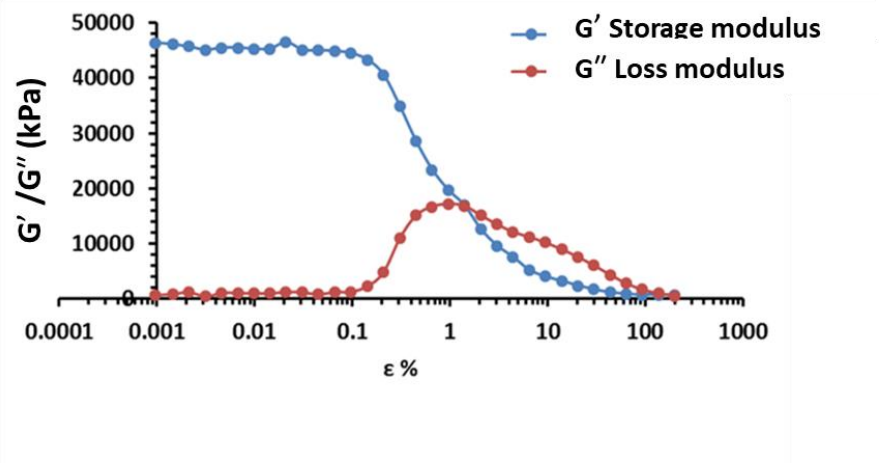

Figure (a1.31) Strain Vs Storage modulus / Loss Modulus of 2.664 % (w/v) MBAAm.

6- 3 % (w/v) MBAAm:

Average LVE = 68700 Pa

STDEV = 582.046199 Pa

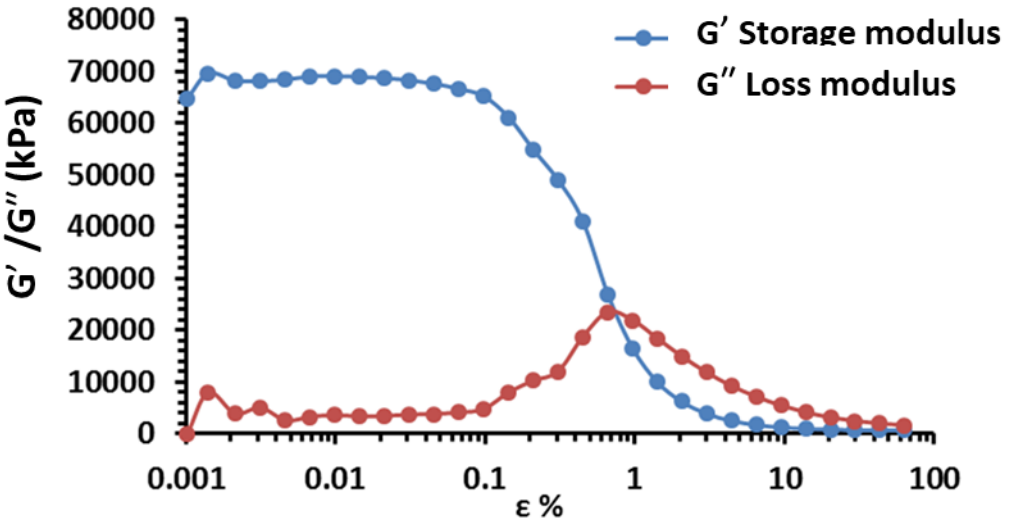

Figure (a1.32) Strain Vs Storage modulus / Loss Modulus of 3 % (w/v) MBAAm.

7- 3.108 % (w/v) MBAAm:

Average LVE = 44820 Pa

STDEV = 414.9479705 Pa

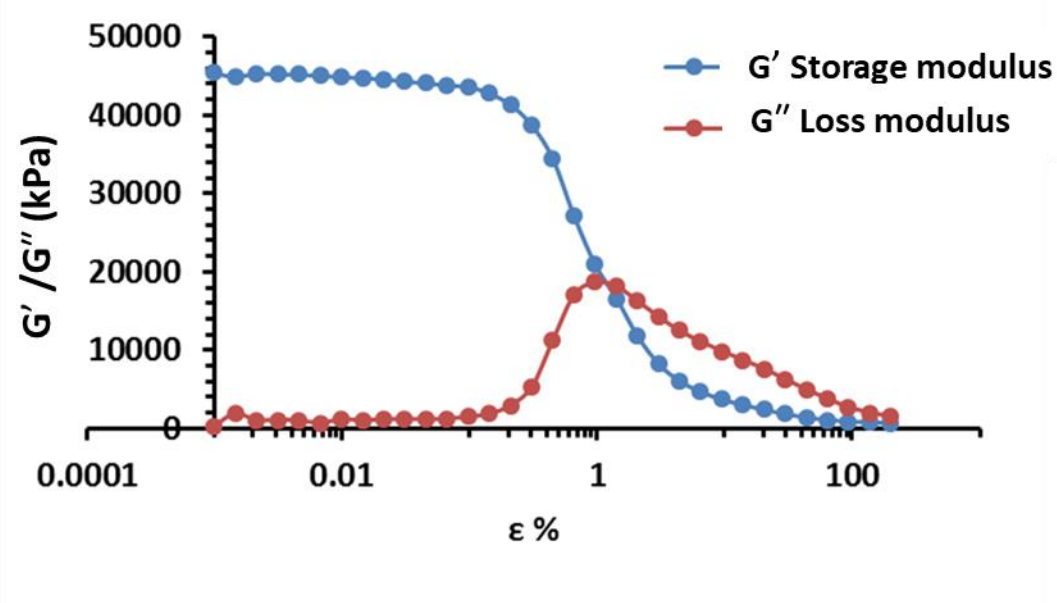

Figure (a1.33) Strain Vs Storage modulus / Loss Modulus of 3.108 % (w/v) MBAAm.

8- 4 % (w/v) MBAAm:

Average LVE = 23073.33333 Pa

STDEV = 166.7618776 Pa

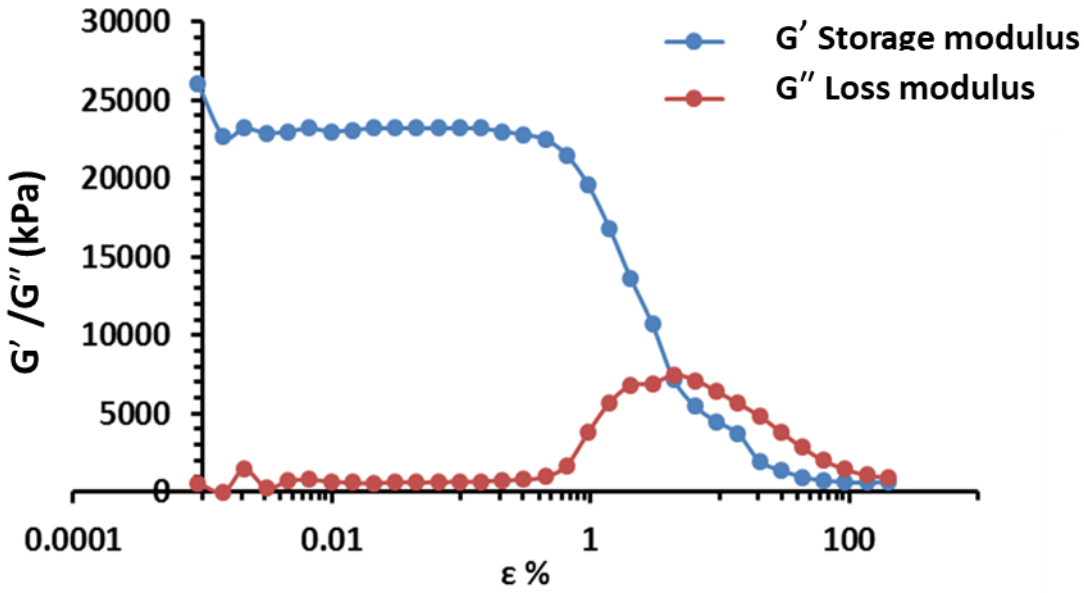

Figure (a1.34) Strain Vs Storage modulus / Loss Modulus of 4 % (w/v) MBAAm.

9- 5 % (w/v) MBAAm:

Average LVE = 18021.42857 Pa

STDEV = 157.7659973 Pa

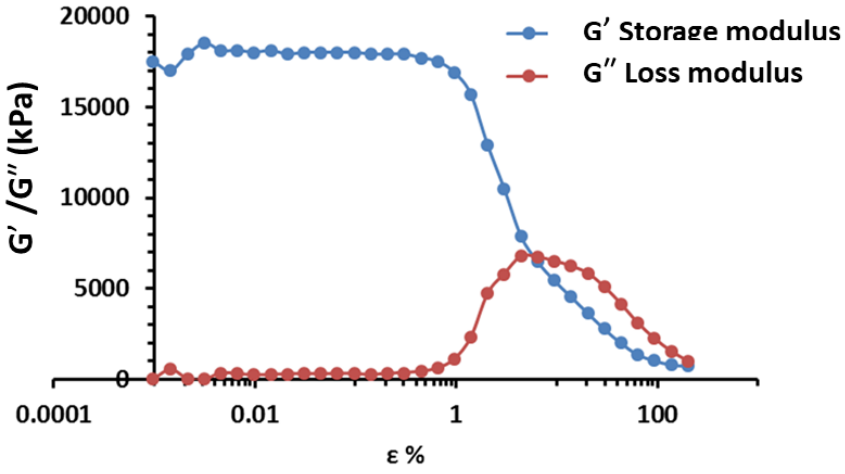

Figure (a1.35) Strain Vs Storage modulus / Loss Modulus of 5 % (w/v) MBAAm.

b. Studying the changing ratio of (Ca^{+2}/ GG) on ICE network hydrogels:

1. 0 M $CaCl_2$:

Average LVE =	1921.25	Pa
STDEV =	9.91031209	Pa

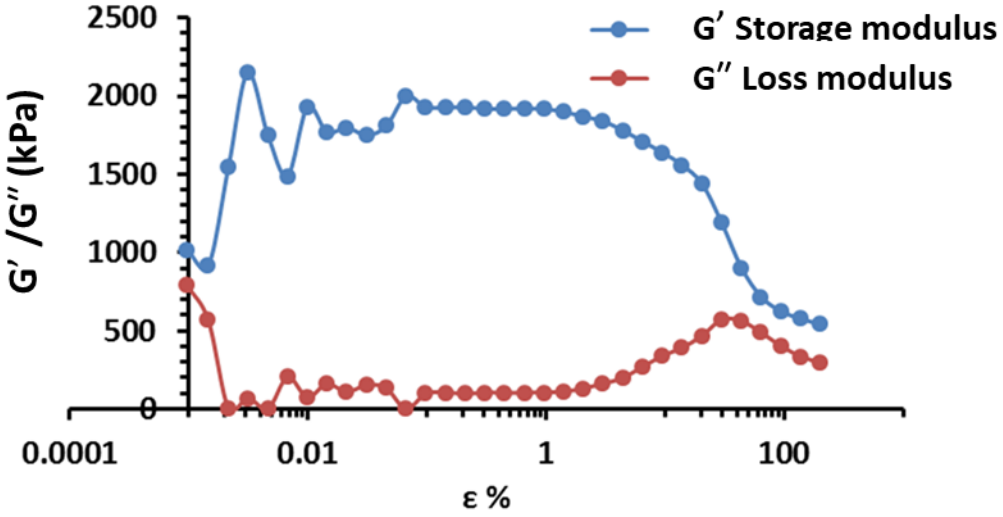

Figure (a1.36) Strain Vs Storage modulus / Loss Modulus of 0 M $CaCl_2$.

2. 0.01 M $CaCl_2$:

Average LVE =	12152.94118	Pa
STDEV =	150.4893977	Pa

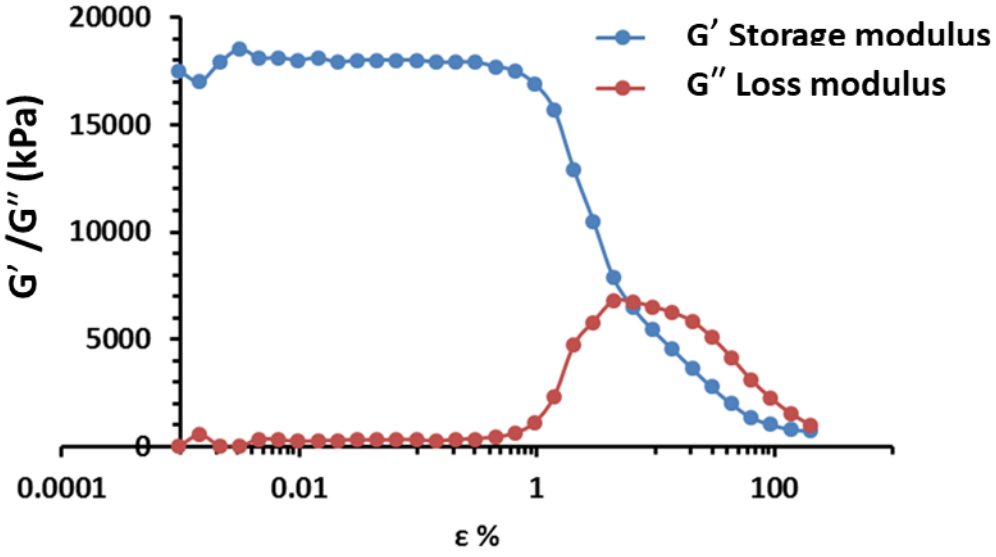

Figure (a1.37) Strain Vs Storage modulus / Loss Modulus of 0.01 M $CaCl_2$.

3. 0.05 M $CaCl_2$:

Average LVE = 22141.66667 Pa

STDEV = 350.2746175 Pa

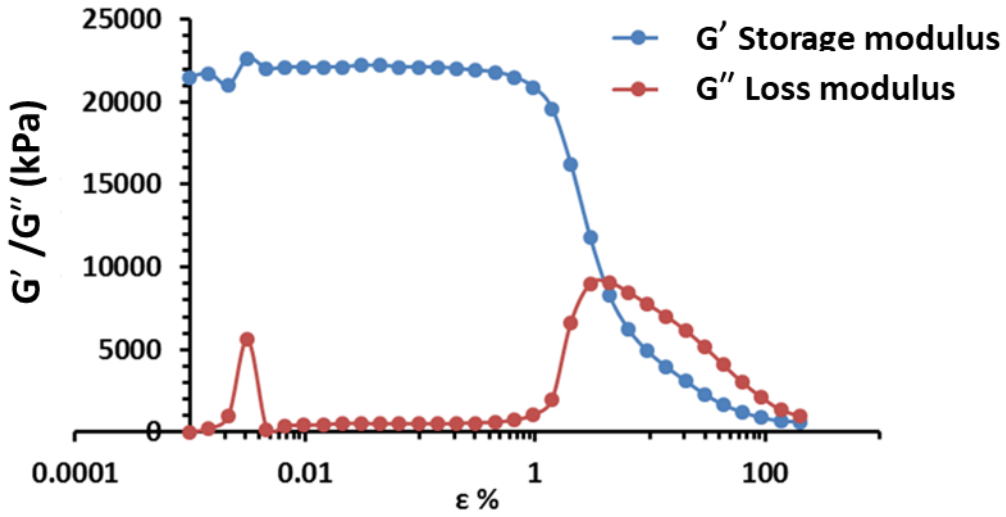

Figure (a1.38) Strain Vs Storage modulus / Loss Modulus of 0.05 M $CaCl_2$.

4. 0.075 M $CaCl_2$:

Average LVE = 130444.4444 Pa

STDEV = 726.4831573 Pa

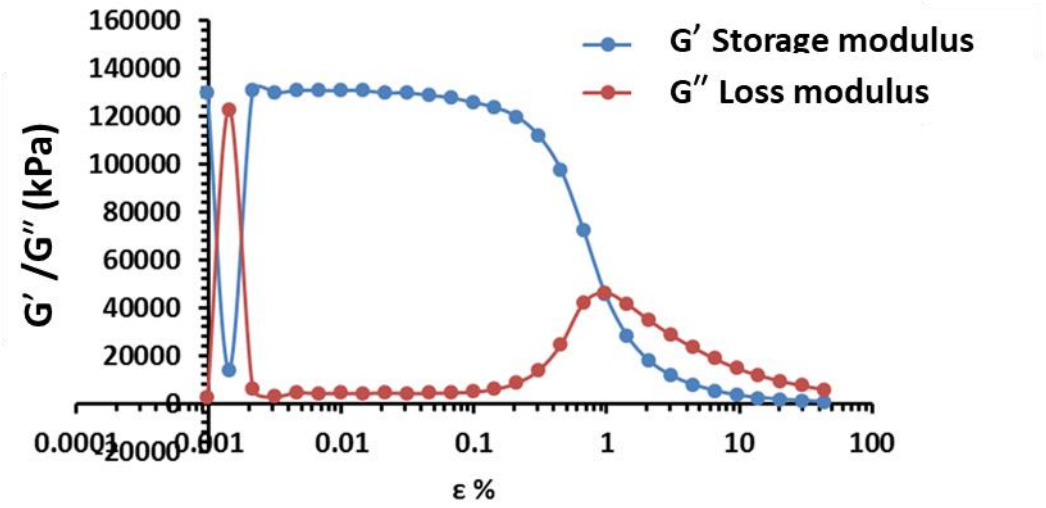

Figure (a1.39) Strain Vs Storage modulus / Loss Modulus of 0.075 M $CaCl_2$.

5. 0.1 M $CaCl_2$:

Average LVE = 264333.3333 Pa

STDEV = 2943.920289 Pa

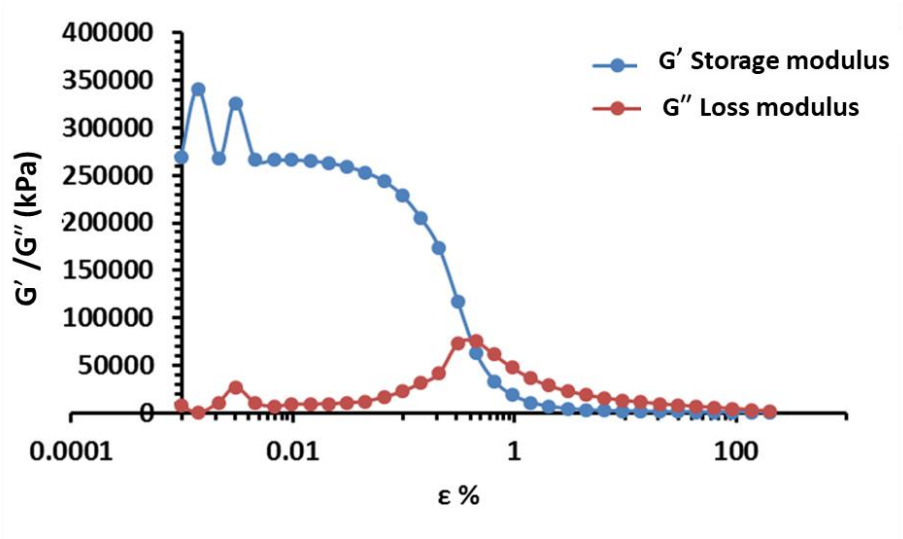

Figure (a1.40) Strain Vs Storage modulus / Loss Modulus of 0.1 M $CaCl_2$.

6. 0.25 M $CaCl_2$:

Average LVE = 121000 Pa

STDEV = 2549.509757 Pa

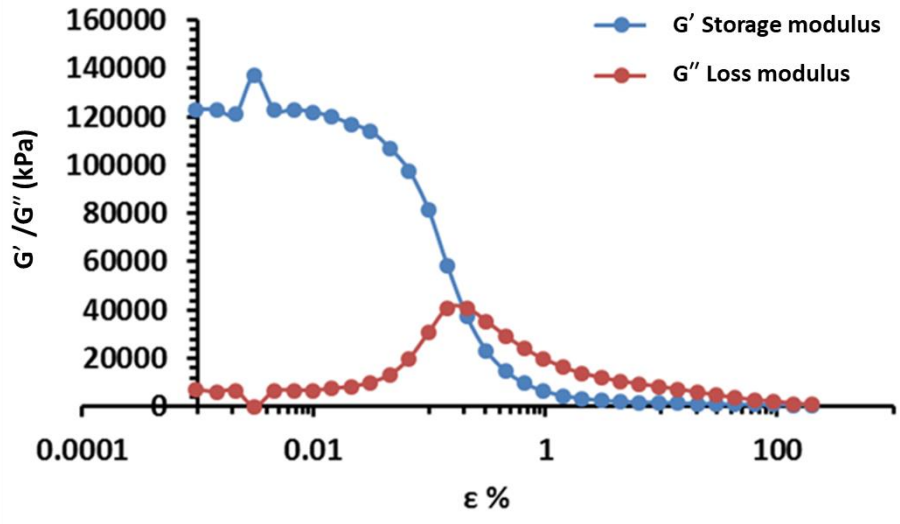

Figure (a1.41) Strain Vs Storage modulus / Loss Modulus of 0.25 M $CaCl_2$.

7. 0.5 M $CaCl_2$:

Average LVE = 86175 Pa

STDEV = 2596.326076 Pa

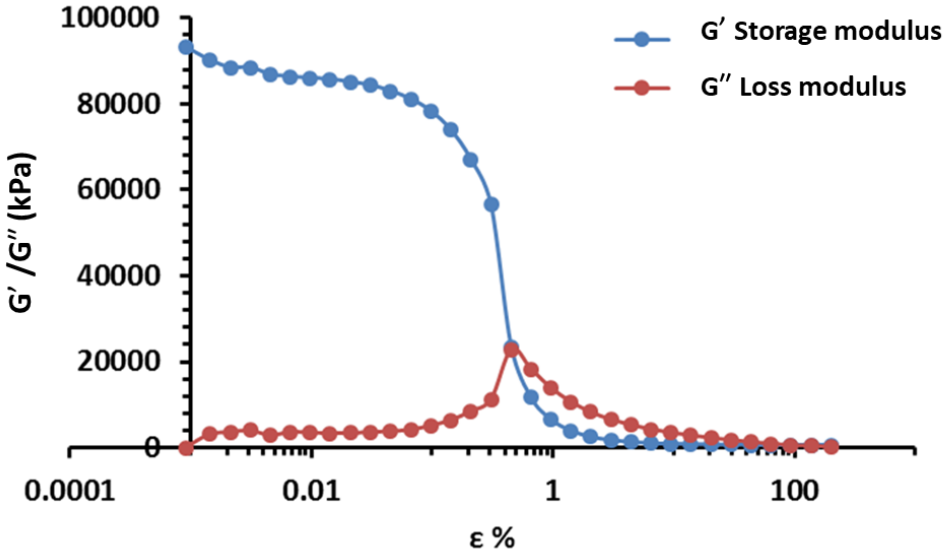

Figure (a1.42) Strain Vs Storage modulus / Loss Modulus of 0.5 M $CaCl_2$.

8. 0.7 M $CaCl_2$:

Average LVE = 95420 Pa

STDEV = 645.7553716 Pa

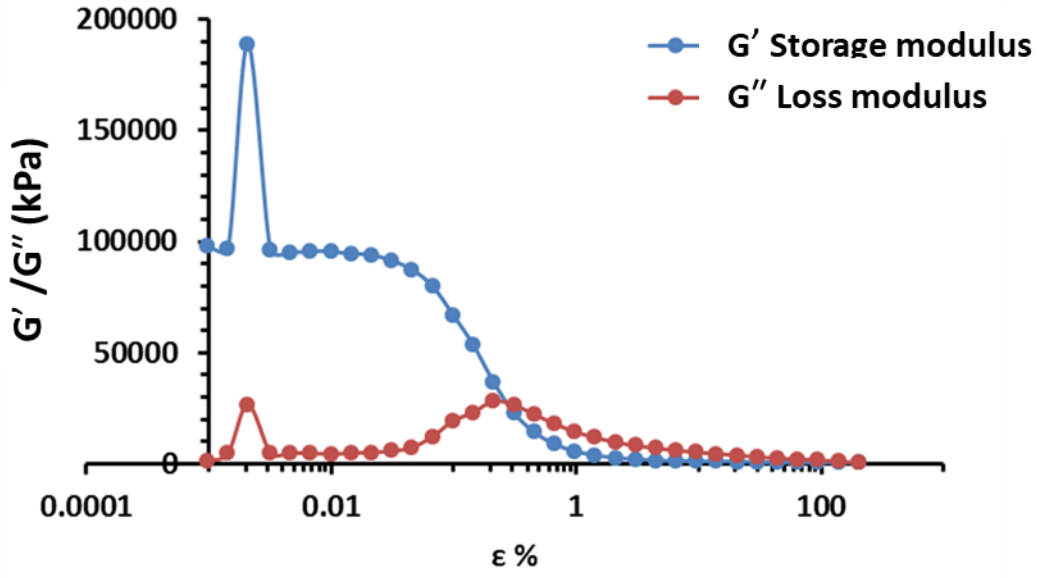

Figure (a1.43) Strain Vs Storage modulus / Loss Modulus of 0.7 M $CaCl_2$.

9. 1 M $CaCl_2$:

Average LVE = 39616.66667 Pa

STDEV = 98.31920803 Pa

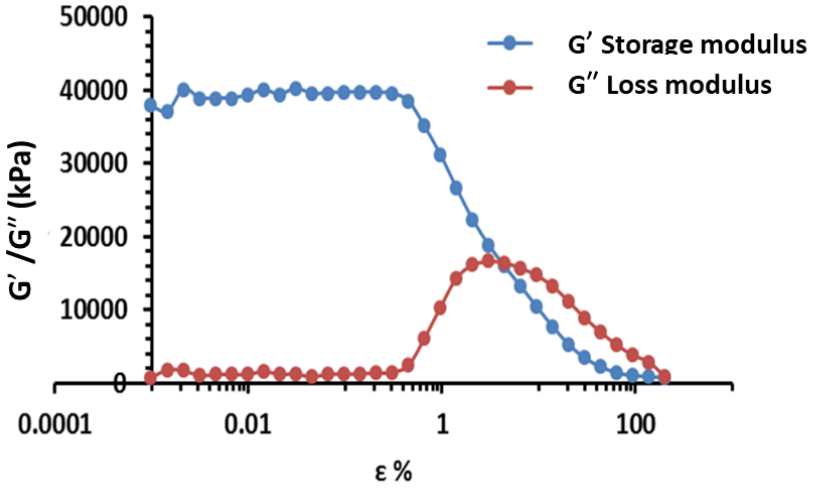

Figure (a1.44) Strain Vs Storage modulus / Loss Modulus of 1 M $CaCl_2$.

c. Studying the changing ratio of (GG/ AAM) on ICE network hydrogels:

1- 3.774 GG+1.776 AAm:

Average LVE = 12690 Pa

STDEV = 56.76462122 Pa

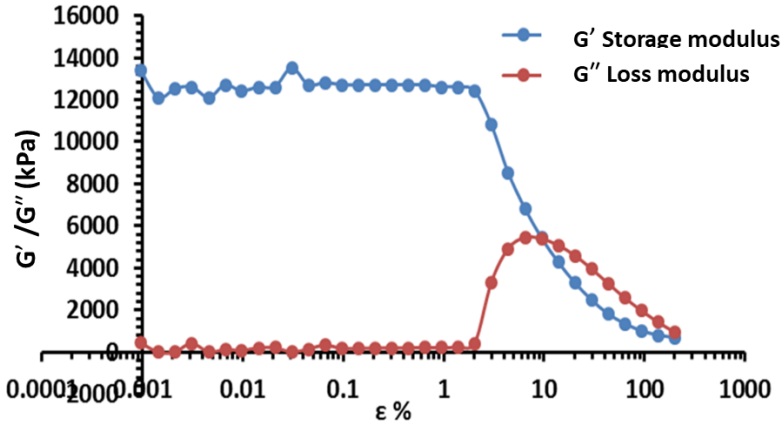

Figure (a1.45) Strain Vs Storage modulus / Loss Modulus of different ratios from GG and AAm ICE network hydrogels.

2- 3.4 GG+ 3.55 AAm:

Average LVE = 25642.85714 Pa

STDEV = 139.7276262 Pa

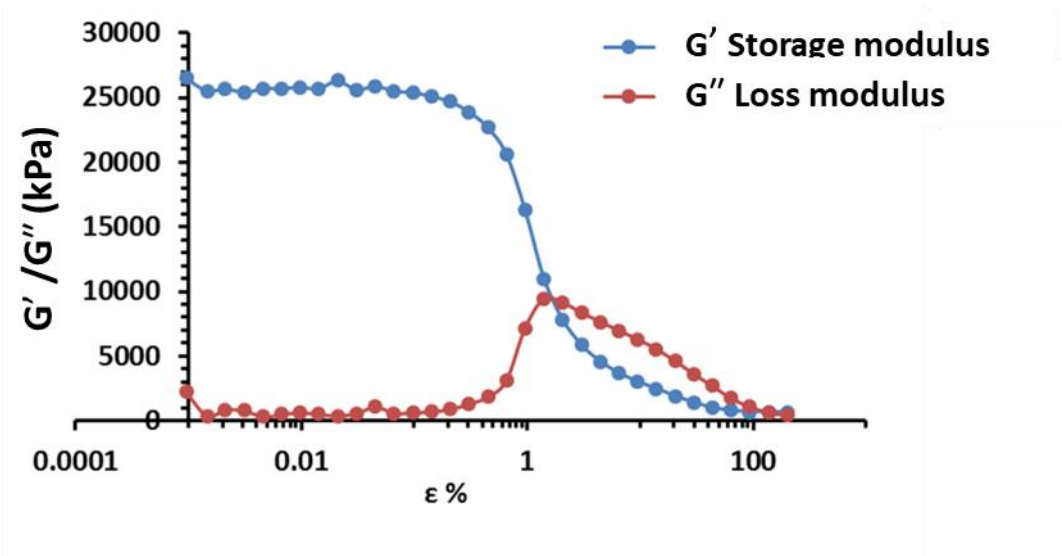

Figure (a1.46) Strain Vs Storage modulus / Loss Modulus of different ratios from GG and AAm ICE network hydrogels.

3- 1.998 GG+3.552 AAm:

Average LVE = 211083.3333

STDEV = 1641.4763

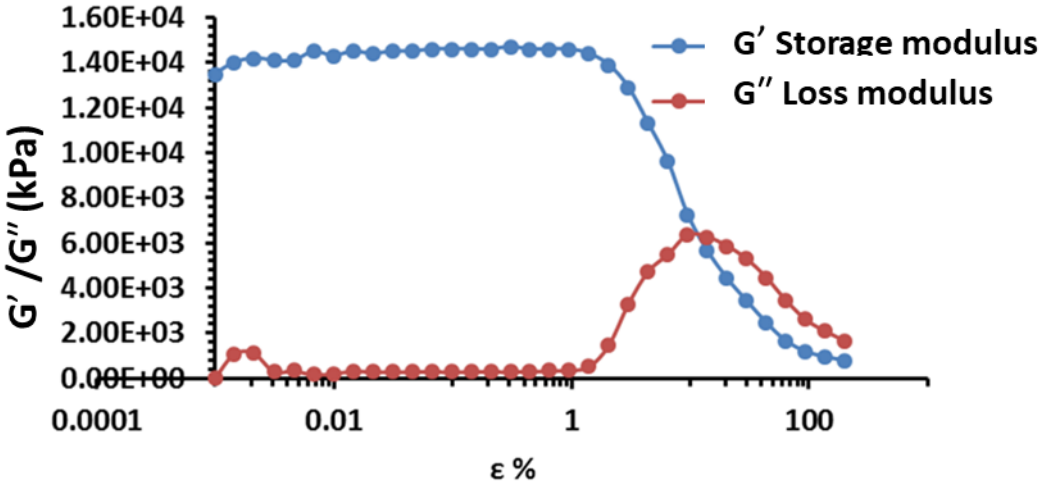

Figure (a1.47) Strain Vs Storage modulus / Loss Modulus of different ratios from GG and AAm ICE network hydrogels.

4- 1.11 GG+4.44 AAm:

Average LVE = 264333.3333 Pa

STDEV = 2943.920289 Pa

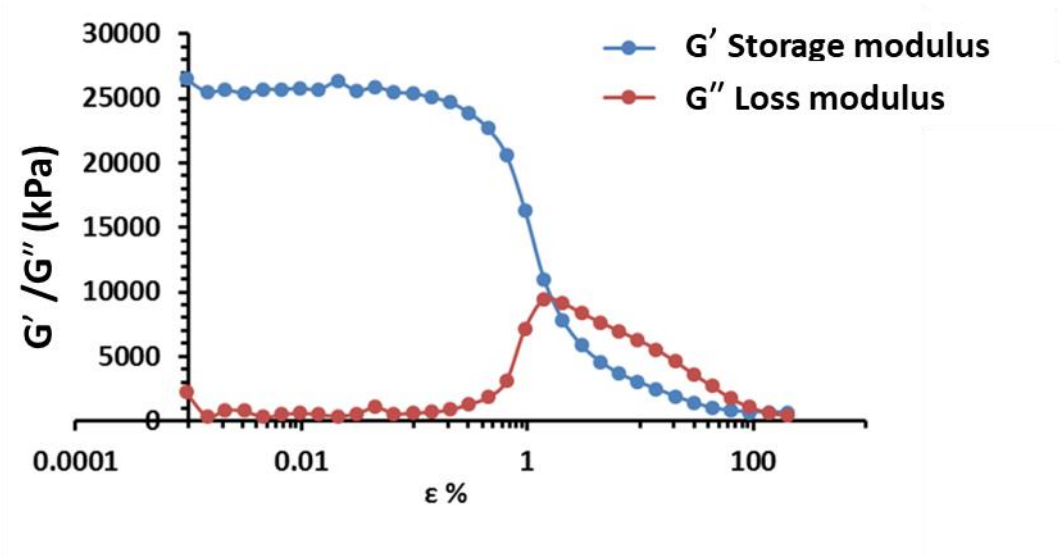

Figure (a1.48) Strain Vs Storage modulus / Loss Modulus of different ratios from GG and AAm ICE network hydrogels.

5- 0.88 AAm+ 4.66 GG:

Average LVE = 1.70E+04 Pa

STDEV = 5714.433085 Pa

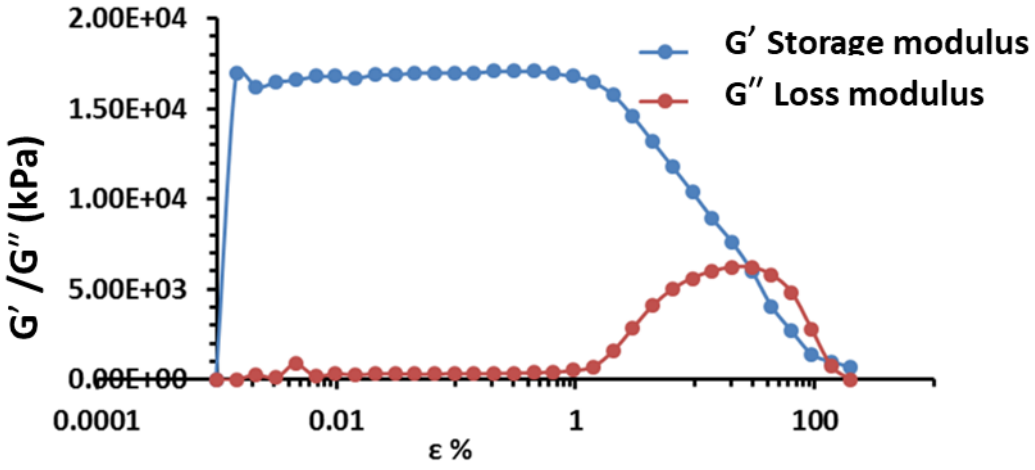

Figure (a1.49) Strain Vs Storage modulus / Loss Modulus of different ratios from GG and AAm ICE network hydrogels.

6- 0.66 GG+ 4.89 AAm:

Average LVE = 21100 Pa

STDEV = 53.45224838 Pa

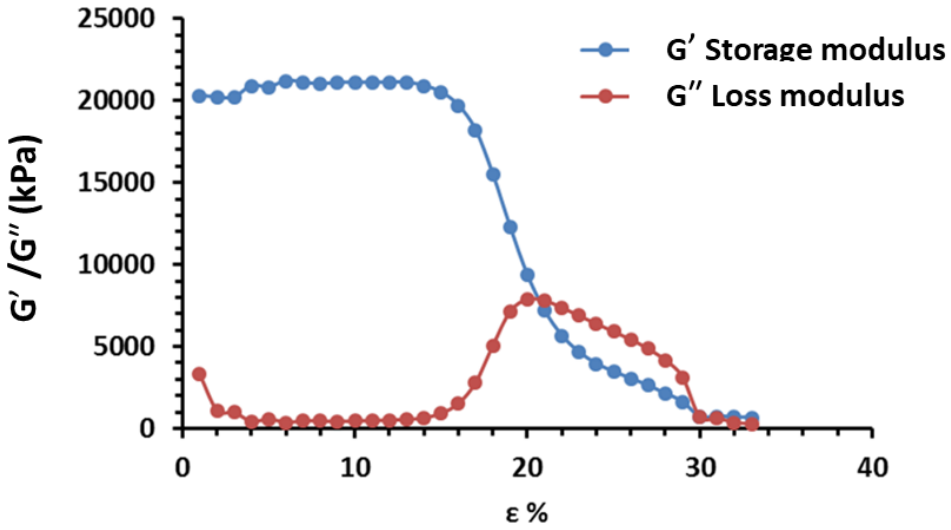

Figure (a1.50) Strain Vs Storage modulus / Loss Modulus of different ratios from GG and AAm ICE network hydrogels.

7- 0.44 GG+ 5.11 AAm:

Average LVE = 21100 Pa

STDEV = 53.45224838 Pa

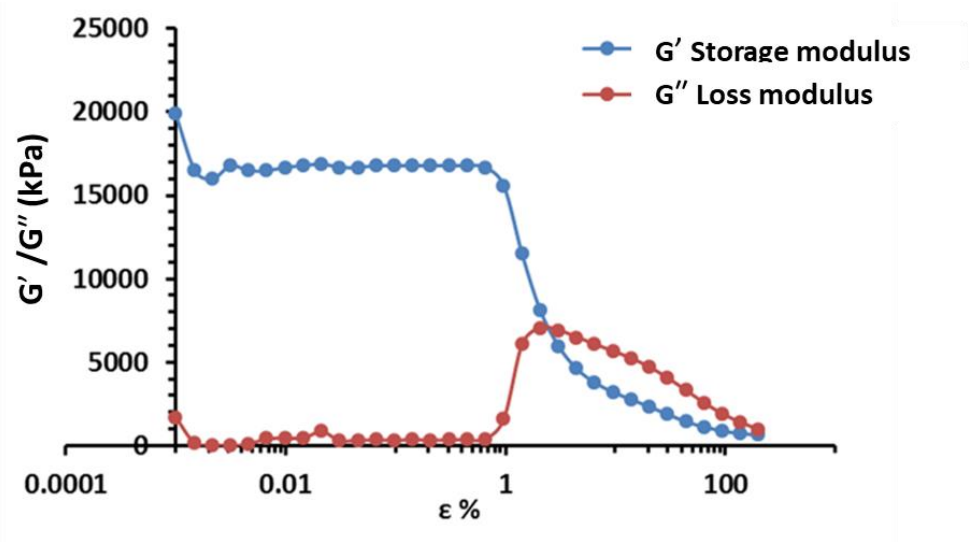

Figure (1.51) Strain Vs Storage modulus / Loss Modulus of different ratios from GG and AAm ICE network hydrogels.

8- 0.33 GG+ 5.22 AAm:

Average LVE =	2561.818182	Pa
STDEV =	28.60387768	Pa

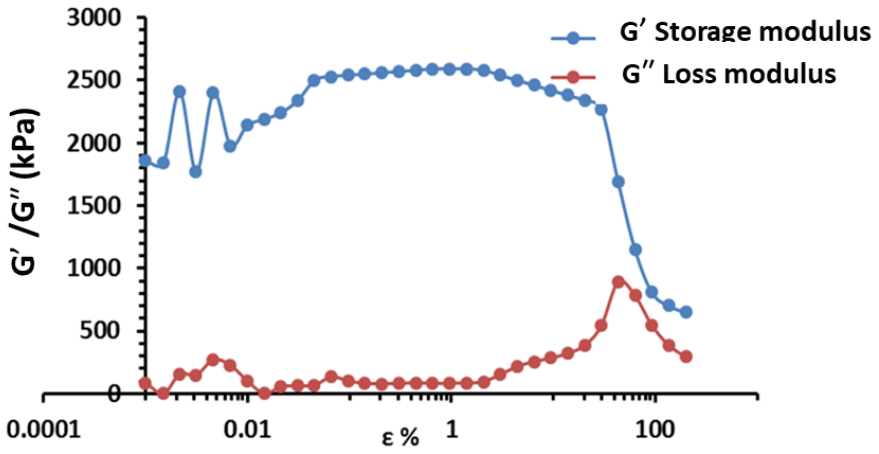

Figure (a1.52) Strain Vs Storage modulus / Loss Modulus of different ratios from GG and AAm ICE network hydrogels.

Appendix 2/ Novel hydrogel separator for spontaneous bifunctional oxygen and hydrogen evolution by composite PEDOT/nano-Ni/rGO films

This work is from the publication which is referred in chapter 8 from the manuscript "A novel hydrogel ion-bridge capable of facilitating sustained, chemically-driven oxygen and hydrogen evolution from water" which is currently under review by the journal Frontiers in Energy.

A2.1 Electrocatalytic and photoelectrocatalytic measurements

Figure 8.1(a)-(b) illustrates the PEC (photoelectrocatalytic) cell that was used in this study. The first step was to perform linear swept voltammetry (LSV) in the range 1.1-1.5 V (2-electrode cell voltage). Figure (a2.2) represents LSV of the two half-cell after 10 scans in both states with and without light illumination. As can be seen in figure (a2.2), the current density of PEDOT/nano-Ni/rGO films increased from 368 µA/cm^2 without illumination to 415 µA/cm^2 with light at 1.5 V (where both films were exposed to light illumination). In addition, it was suggested that the nano-Ni particles in the PEDOT/nano-Ni/rGO films became partially covered with NiO when the potential in the LSV scan reached the range of 1.38-143 V [390] and above. With a NiO coating, the catalyst could better respond to light due as NiO is well known to be a semiconductor that absorbs light and co-operates with PEDOT and rGO through a synergistic effect. [391-392]

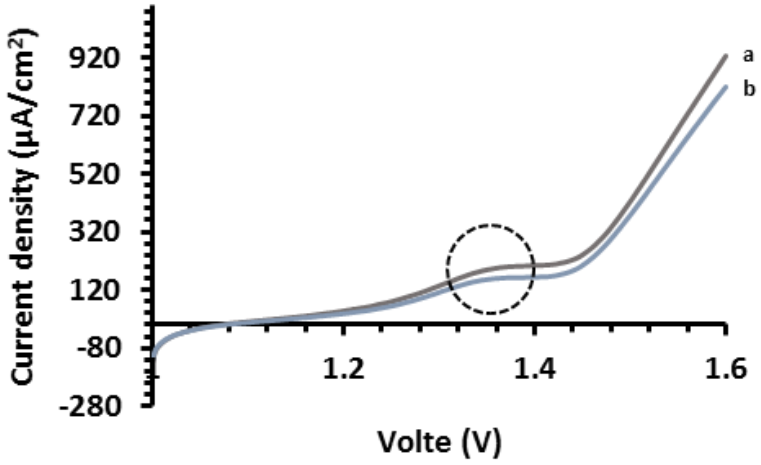

Figure (a2.1) Linear Sweep Voltammogram (LSV) of PEDOT/nano-Ni/rGO films, on FTO glass, in range (1.1-1.5 V; 2-electrode cell voltage). The anode was PEDOT/nano-Ni$_{(125\ mg)}$/rGO$_{(6\ mg)}$ film in 0.2 M Na_2SO_4 with pH 12 while the cathode was 0.1 PEDOT/nano-Ni$_{(125\ mg)}$/rGO$_{(5.4\ mg)}$ film (0.1 M H_2SO_4). Scan rate: 5 mv/s.

The second step was to examine the chronoamperometric effects at cell voltages of 1.23 V and 1.5 V respectively. The former, of course, is the minimum theoretical voltage (E^o) needed to create water splitting. The latter is just above the so-called "thermoneutral voltage" (E^{TN}), which equates to the voltage at which water electrolysis is said to be 100 % energy efficient.

As can be seen in figure (a2.2 (a)), when 1.23 V was applied, the dark current was 140 - 142 µA/ cm^2, and when the light was switched on, it has increased to 154 - 156 µA/cm^2, meaning that 14 µA/cm^2 was a photocurrent arising from light illumination (IP(i) in figure (a2.2(a)). When a bias of 1.5 V was applied, the dark current was 366 - 373 µA/cm^2, while, with light, it was raised to 386-391 µA/cm^2, producing 18-20 µA/cm^2 photocurrent (IP(ii) in figure (a2.2(b)).

In theory it is not possible to perform water-splitting at 1.23 V. However the chemical potential provided by the differing conditions at the cathode and anode, along with the influence of the light illumination, allowed the cell to readily split water at 1.23 V (albeit at a low overall current density).

The third step of this study was to perform chronoamperometry at 1.23 V and 1.5 V. The processing time was set for fourteen hours. As can be seen in figure (a2.3), when the light was turned on, the currents increased steadily at both 1.23 and 1.5 V. They stabilised after three hours of operation to exhibit current densities of 484 and 192 µA/cm^2 at 1.23 and 1.5 V respectively. The current at 1.5 V started to degrade gradually to 59 % of its stabilised current after fourteen hours of PEC operation. However, the current density was still better than that exhibited at 1.23 V, which also exhibited a high initial photocurrent density of 225 µA/cm^2. In contrast, the current density at a bias of 1.23 V was more stable over fourteen hours of operation and dropped to only 88.2 % of its stabilised current of 55 µA/cm^2.

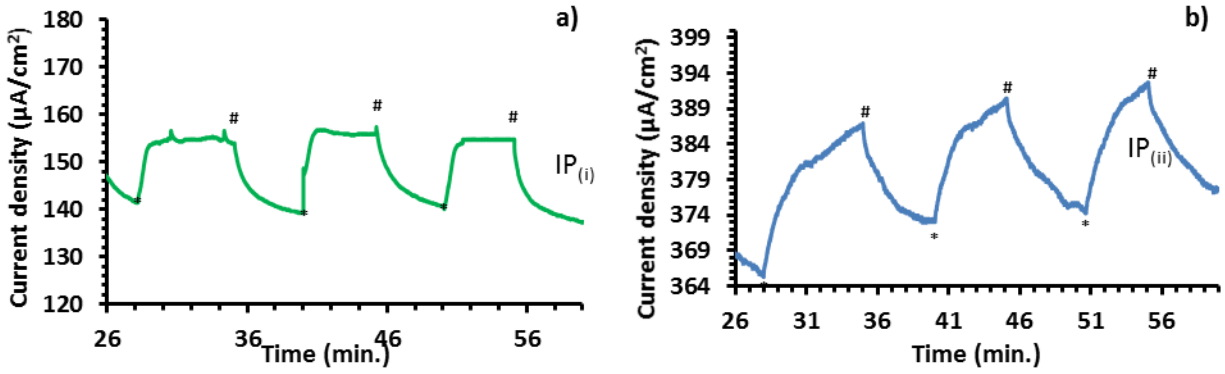

Figure (a2.2) Chronoamperogram of catalytic water-splitting with and without light illumination (ca. 0.25 sun), of FTO glass slides coated with PEDOT/nano-Ni-nano/rGO as illustrated in Figure 8.1 at a 2-electrode cell voltage of: (a) 1.23 V and (b) 1.5 V, respectively for one hour of operation.

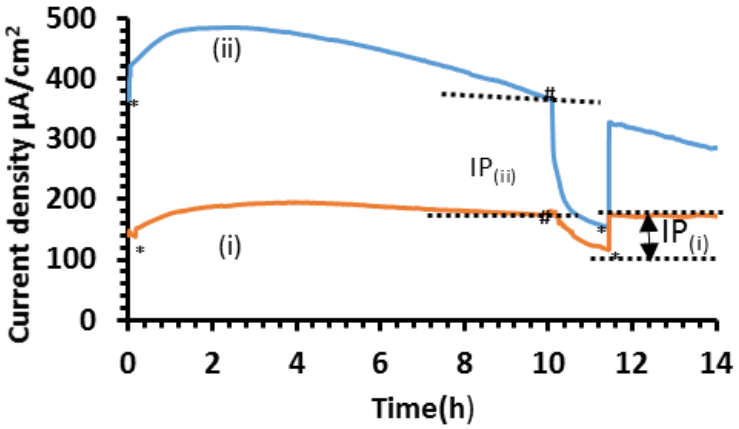

Figure (a2.3) Chronoamperogram of catalytic water-splitting with and without light illumination (ca. 0.25 sun), of FTO glass slide electrodes coated with a PEDOT/nano-Ni-nano/rGO as illustrated in Figure 8.1 at a 2-electrode cell voltage of: (a) 1.23 V and (b) 1.5 V, respectively for fourteen hours of operation. (*='light on', #='light off).

Appendix 3/ Explanation for clarification

1. Clarification for statement on Chapter 3, p98:

The MCV in table 4.3, p98 for PAAm 6 M LiCl is 810 Pa.s. This value was the MCV for PAAm +6 M LiCl measured at -6 °C. However, the MCV value for the same hydrogel in Fig. 4.5c shown below approximately 690 Pa.s measured at 20 °C.

Hydrogel	GT at 20 °C (min)	MCV at 20 °C (Pa.s)	GT at -6 °C (min)	MCV at -6 °C (Pa.s)
AAm	20	387±2	37	410±2
AAm+2.7 M NaCl	15	2250±2	20	2650±10
AAm+6 M LiCl	5	730±40	8	810±27

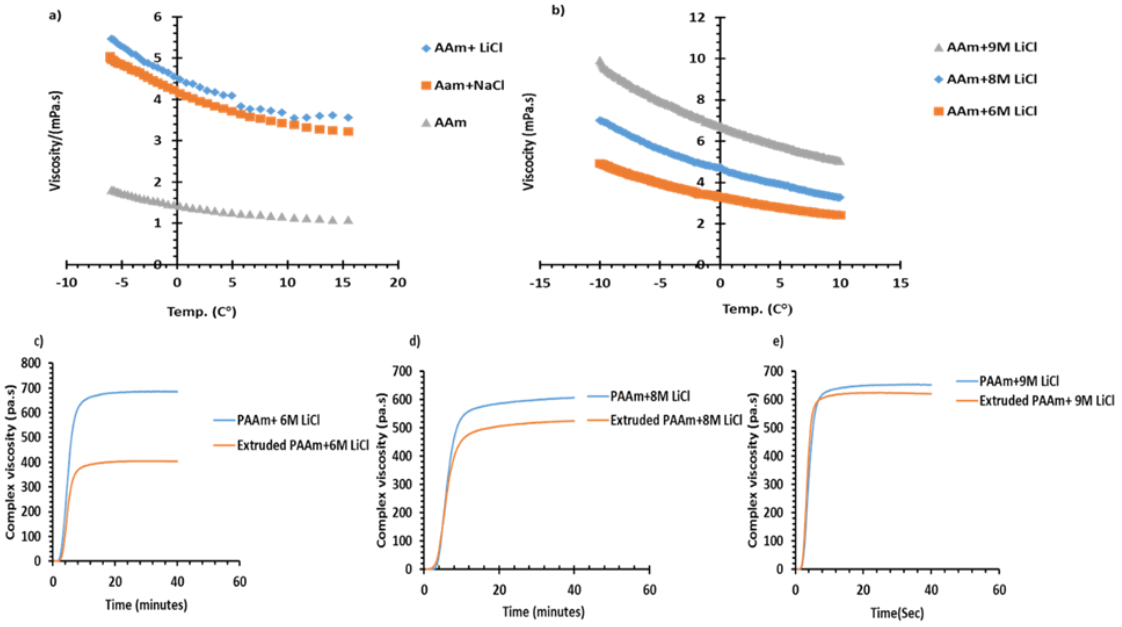

2. Clarification for statement on chapter 5, p104:

The candidate characterised the capacitance in the same way of characterising the resistance and the current as shown below:

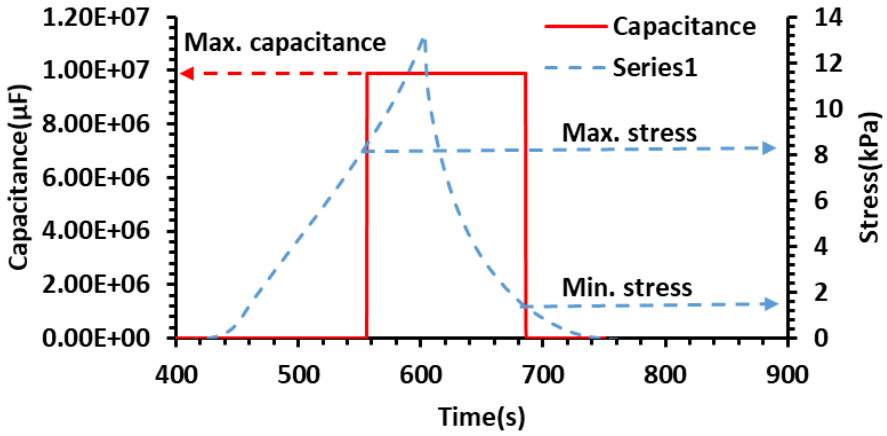

After assessing the capacitance of the SSD, the device detected a similar amplitude signal to the shape resistance of the signal generated after applying the compressive stress. Therefore, the figure was not added within the chapter because it displayed the same stress threshold and same resistance signal shape. Moreover, this study concluded that the operation of the SSD depends on the physical contact (on /off the device) between two layers of the conducting hydrogels performed through the perforated VHB layer.

3. Clarification for statement on Chapter 6, p119:

The black colour in Fig. 6.2 in page 119 represents the interface layer of the hydrogel with the VHB tape layer which is called the robust interface as shown in the following illustrated figure:

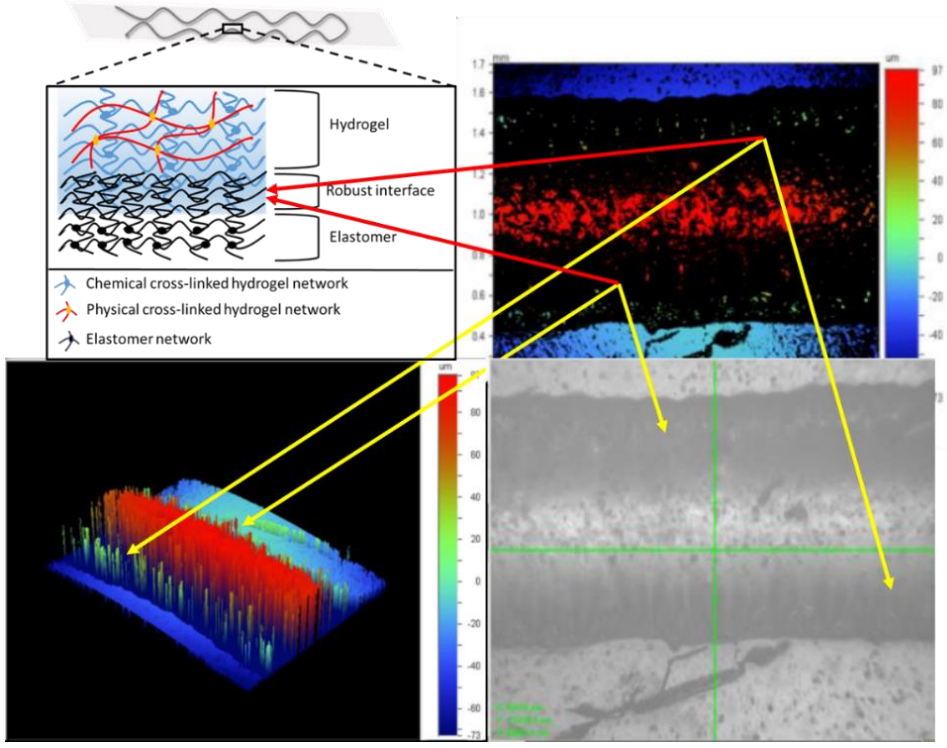

4. Clarification for statement on chapter 7, p127:

1. P127 how was surface area measured and what are the units (cm^2 per what?)

Surface area = ((2 * width (cm)* height (cm)) + (4 * length (cm) * height (cm)))= cm^2

2. Is it just based on the dimensions of the sponge in which case it should expand with water?

Yes